PLINIUS

Società Italiana di Mineralogia e Petrologia
c/o Dipartimento di Scienze della Terra
Via S. Maria 53 - 56126 PISA

ISSN 1972-1366

Rivista Annuale SIMP – Società Italiana di Mineralogia e Petrologia | Numero 51 | 2025

SOCIETÀ ITALIANA DI MINERALOGIA E PETROLOGIA
c/o Dipartimento di Scienze della Terra, Università di Pisa, Via S. Maria 53 - 56126 Pisa

www.socminpet.it | https://www.socminpet.it/344/plinius.html

Direttore Editoriale: Concetta Rispoli (concetta.rispoli@unina.it)

Comitato Editoriale: Concetta Rispoli, Virginia Marchionni, Alessandro Petroccia, Maria Verde, Andrea Maffeis, Stefania Corvò, Sara Nerone, Valeria Indelicato, Lorenza Fascio, Nadia Malaspina

FOTO COPERTINA: Matteo Chinellato | Abito lungo con cappello nero, stilista Madre Natura

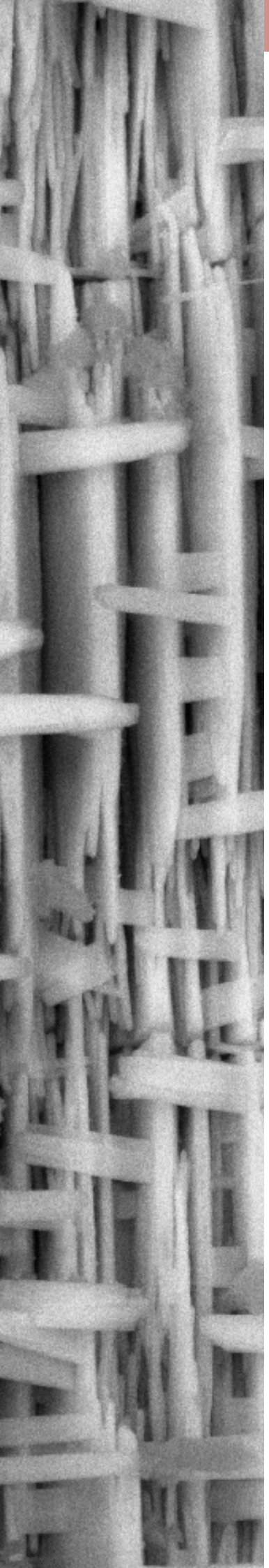

Contents

PEOPLE WHO MADE SCIENCE

1509
H. & Z. Janssen
created the first optical microscope in Holland, made by two convess lenses and wood.

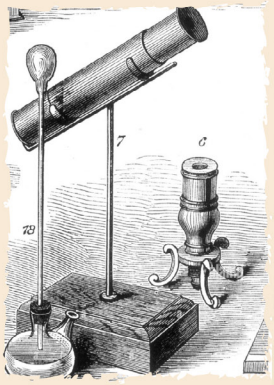

1828
W. Nicol
created the polarised optical prism in Edimburg, fundamental for the advanced polarised microscope, made in the early 1900s.

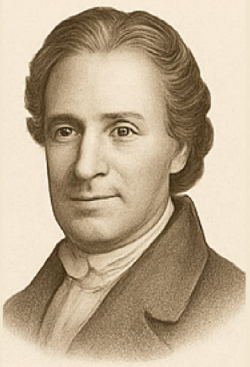

1903
M. S. Skłodowska-Curie
was the first woman to win a Nobel Prize in Physics (1903) and Chemistry (1911). Her discoveries have direct implications for isotopes and radiometric dating.

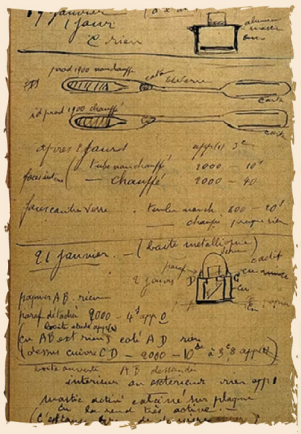

FROM LENSES TO MICROANALYSIS

1915
W. Lawrence & W.H. Bragg
received the Nobel Prize in Physics for their analysis of crystal structure by x-ray crystallography.

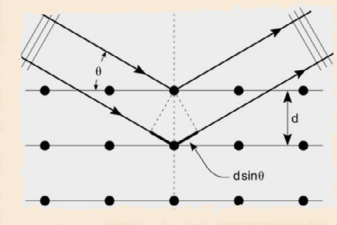

1928
C.V. Raman & K.S. Krishnan
discover the Raman Effect, fundamental for raman spectroscopy.

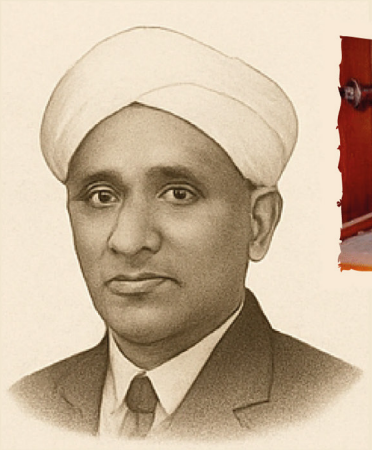

1940
M. Knoll & E. Ruska
created the first scanning electron microscope. In 1986, Ruska won the Nobel Prize in physics for the development of transmis-sion electron microscopy.

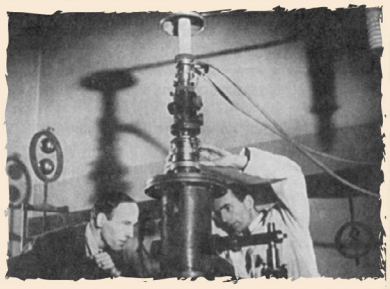

1951
R. Castaing
become the “father” of microanalysis, with the development of the electron probe microanalyzer.

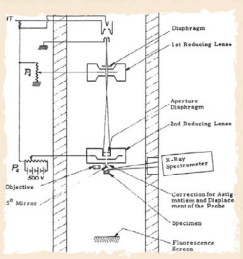

...to be continued

PLINIUS
Editorial Board

From the Editorial Board

Dear Members,

We are pleased to share with you a new issue of PLINIUS, the result of a collective effort that reflects the ongoing editorial renewal of the journal. While the core of the publication remains the Extended Abstracts of SIMP's Ph.D. students, each assigned a DOI to ensure visibility and citation, the journal continues to grow, incorporating new sections that give space to the broader cultural, educational and outreach mission of the Society.

In recent issues, we have introduced interviews with SIMP award recipients, reports from SIMP sponsored events and a refreshed graphic design aimed at making the journal more dynamic and engaging. Member participation also continues through initiatives such as the cover image contest, which highlights the creativity and diversity of our community.

This year we wish to extend our heartfelt thanks to Andrea Maffeis, Maria Verde and Valeria Indelicato, who are leaving the editorial board. Their enthusiasm and contributions have played an important role in this phase of development. They have shared a few words with us in this issue.

As always, changes bring new opportunities and new faces will soon join the editorial team. We look forward to continuing this path together with your support, ideas and active involvement.

With warm regards,
The Editorial Board

Senior's Interviews

Omar Bartoli

Omar Bartoli is associate professor in Petrology and Petrography at the University of Padova (Department of Geosciences). He completed a PhD in high-temperature metamorphism and crustal melting in 2012 at the University of Parma. He has held several research fellowships at the University of Padova and gained international experience at the Fluids Research Laboratory, Department of Geosciences, Virginia Tech (USA), and later as a visiting researcher at the Department of Earth Sciences at ETH Zurich (Switzerland).

About his interests

His main interests focus on the investigation of mechanisms and dynamics of high-temperature processes in the deep continental crust, applying innovative methodologies to the study of crustal melting and granite petrogenesis. His research has mostly been devoted to defining new analytical and experimental protocols to investigate melt inclusions, providing exciting new ways to make these small data repositories talk, and obtaining a wealth of new information on the melting of the orogenic crust.

What do GNP and SIMP represent for the scientific community, in your opinion?

I believe that the primary mission of both SIMP and GNP is to be a point of reference for the younger generations. I still remember the excitement of my first SIMP Congress in Sestri Levante in 2008, which I attended as a graduate student waiting to start my PhD a few months later. It was a great motivation for me to see that the seniors were interested in my research. At the same time, SIMP and GNP must be open to interaction with other societies. Again, this is especially important for the younger generations, because research today must be multidisciplinary.

Why did you choose science, and, in particular, geosciences? Was there anyone in particular and/or any particular experience that influenced this choice?

When I was a child, I used to spend two weeks every summer in the Dolomites, and it was from those moments that my love for the mountains was born, and my decision to study geosciences was a direct consequence. There was one pivotal moment in my path towards geosciences. When I was in high school, I was convinced that the only way to study geology was to study environmental engineering. Fortunately, one day I was in a mountain sports shop and noticed a poster advertising an event at the museum, dedicated to the discovery of a fossil whale. By attending this event, I discovered the existence of a whole degree course in geological sciences, and a few months later, I was a Bachelor's student in geological sciences at the University of Parma. So, it was serendipity. Paradoxically, I have to thank the sedimentary rocks of the Dolomites and the fossils, which, however, have never aroused my curiosity as a geoscientist in the years that followed.

As a professor in Petrology and Petrography, can you tell us about a memorable moment or experience in your career that made you particularly proud or excited?

Despite the many research projects that have been carried out over the years, the moment that has made me particularly proud has to do with my students. For a few years now I have been teaching the course on metamorphic petrology, which includes a multi-day field trip to the Ivrea Zone. When I was a Master's student, it was the Ivrea Zone that really

More recently, his research has focused on testing new approaches to dating geological processes, constraining the mobility of critical metals during high-temperature metamorphism, and reconstructing the secular evolution of tectonic styles from the Archean to the present. He is a highly active geoscientist with a lot of publications every year and extensive international collaborations. Moreover, he successfully balances his profession with his passion for the mountain and his hobbies as climbing and joining trail-running races.

Today, he is the president of Gruppo Nazionale di Petrologia (GNP) of the SIMP.

marked my path towards petrology. I had heard about this world-famous crustal section during a course on the crystalline basement and, as a reward for a successful exam, I allowed myself a few days alone to look at the rocks. I emailed a couple of professors from other universities to get some field guides of the area, and off I went. I still remember the excitement of finding outcrops that were so famous to geologists all over the world and being able to see petrological processes directly on a single outcrop. When I found myself as a professor taking my students to the same outcrops, I felt I had come full circle.

You are an innovative petrologist, who combines traditional with experimental methods, what was the most fascinated study/discover that enriched you the most?

Am I boring you by talking about the Ivrea Zone all the time? My career as a geoscientist has been closely linked to garnet. Being able to date *in situ* garnet from the Ivrea Zone has been the source of my greatest satisfaction in recent years. In fact, it was a project that I had been planning since 2019, in collaboration with the ETH in Zurich, but then the pandemic started. This study has represented an important step forward towards establishing garnet as part of the *in situ* U-Pb geochronology repertoire.

What does it mean to you to be a scientist in geosciences?

Being a very curious person who combines imagination with scientific rigour. Geoscientists have to use their imagination because most geological processes cannot be observed in real time. This makes us different from most scientists in other disciplines.

Looking at schollen dia-texites of the Ivrea Zone.

Besides being a very active scientist who participates in many initiatives, you have many hobbies including running and climbing; you have also attempted twice to climb Manaslu (8163 m, Nepal), the eighth mountain on Earth. Do these activities and experiences contribute and/or have they contributed to enriching your profession as a geoscientist? If yes, how?

Rather than having contributed, it would be better to say that they have the same common denominator: the stubbornness in pursuing our dreams. In fact, being a geoscientist in Italy today, especially if you are doing basic research, requires a lot of stubbornness to be able to carry out high-quality scientific research despite the lack of research funding, the (often oppressive) bureaucracy and the lack of modern vision at the ministerial level. Fortunately, my adventures in the mountains allow me to recharge my batteries to face even the most difficult and least satisfying part of being a geoscientist. I could not be the geoscientist I am without my experiences in the mountains. I have to admit that I also took my laptop with me to Manaslu base camp to write an article in my downtime. Of course, I never managed to switch it on.

Do you have any advice for young people who want to study geological sciences?

Cultivating both curiosity and thirst for knowledge and being passionate. In my experience, a fundamental part of my formative years was the enormous amount of time I spent reading literature, even when I was a Master's student preparing for exams. I think it's easier to do something new when you have a very solid background.

Elena Belluso

Elena Belluso is full professor in Environmental Mineralogy at the University of Torino (Department of Earth Sciences) and Director of the 'Giovanni Scansetti' Interdepartmental Centre for the study of asbestos and other harmful particulates at the same University. She obtained her PhD in Mineralogy and Crystallography in 1989. She is the referent and scientific head of the asbestos analysis laboratory, qualified by the Ministry of Health for analysis on asbestos present in various environmental matrices.

About her interests

Her research activities, mainly of an interdisciplinary nature, concern environmental studies on the interaction between the biosphere and asbestos, natural fibrous or asbestiform minerals not classified as asbestos, synthetic inorganic fibres present in air, water, rocks and soils, humans and animals (especially in relation to the respiratory system), in collaboration with physicians, veterinarians and biologists. She is a member of regional and ministerial registers, e.g., 'Technical Group Fibres in Biological Textiles

What do GNP and SIMP represent for the scientific community, in your opinion?

In my opinion, both entities are key elements in the Italian scientific panorama, contributing significantly to the advancement of knowledge, to the protection of natural and cultural heritage, to the promotion of environmental sustainability and to the advancement of knowledge in various fields, also in complementarity and collaboration with other groups. Through moments of sharing, such as conferences, dissemination and training activities, they strengthen the role of the scientific community in enhancing and protecting the resources of our country and others, promoting sustainable and informed development.

Why did you choose science, and, in particular, geosciences?

Even before adolescence, I had fallen in love with minerals, especially the shapes, colors, and shine of pyrite and vanadinite crystals.

Was there anyone in particular and/or any particular experience that influenced this choice?

My interest in geosciences, particularly in minerals, is longstanding and dates back to my elementary school years. During that time, my mother would take me on walks in nature across different seasons, encouraging me to observe plants, flowers, animals, and rocks. I was especially fascinated by the "shiny stones," which piqued my curiosity. She took me to search for pyrite in abandoned mine dumps. As my enthusiasm grew, she brought me to a mineral exhibition where I saw stunning vanadinite crystals. And from that moment on, it was truly love!

As a professor in Environmental Mineralogy, can you tell us about a memorable moment or experience in your career that made you particularly proud or excited?

A truly wonderful experience for me was when I was able, for the first time, to obtain images of intergrowths of different minerals (from the silicate family, some classified as asbestos) using a transmission electron microscope (TEM).

(BioFibres)' and has evaluated national and international scientific products and projects and industrial research projects in the field of environmental research. Finally, she organised science dissemination activities through seminars and workshop activities such as 'Girls and Children One Day at the University' and exhibitions such as 'The Pathways of Asbestos'.

Today, she is the president of Gruppo Nazionale GABeC (Georisorse, Ambiente, Beni Culturali) of the SIMP.

Which experience enriched you the most?

The most enriching experience I had, also from a human perspective, was the long period spent at a laboratory of the CNRS in Luminy (Marseille) (now the Centre Interdisciplinaire de Nanoscience de Marseille), where I learned to use a high-resolution TEM, prepare samples, collect data, and process them, guided by an extremely competent person who was scientifically very curious and in no way arrogant. I had a wonderful experience of exchanging ideas and scientific growth in an international environment.
That period also marked a deep friendship with a wonderful friend who, unfortunately, passed away a few years ago.

During your career, you have secured research grants and fellowships in Italy and abroad, leading national and international projects. In your opinion, what key skills and strengths should young researchers develop today to successfully secure funding and build a strong research career?

As for young researchers in the scientific field, I believe that first and foremost, they must acquire a solid disciplinary foundation, updated to the current state of knowledge in their field of interest.
In addition, they need to develop a wide range of skills and competencies:

- the ability to tackle complex problems using interdisciplinary approaches;
- to engage in peer-level dialogue with experts from other fields;
- to communicate scientific processes and discoveries clearly to various stakeholders (the academic community, funding bodies, policymakers, and the general public);
- to interact with the industrial sector;
- to collaborate and work without arrogance, always remaining—at least inwardly—curious and humble explorers of science;
- to make themselves available to society, taking an active part in sharing the value and impact of their research;
- to build project proposals in synergy with other specialists, with clearly defined objectives, innovation, and social impact;
- to actively participate in conferences and workshops;
- to continuously update their skills through training in new methods and technologies;
- to be willing to partially adapt their research path in response to emerging scientific and societal needs.

Looking for fibrous glaucophane in metamorphic blueschist within the Franciscan Complex (Calaveras Dam Replacement Project, 2018).

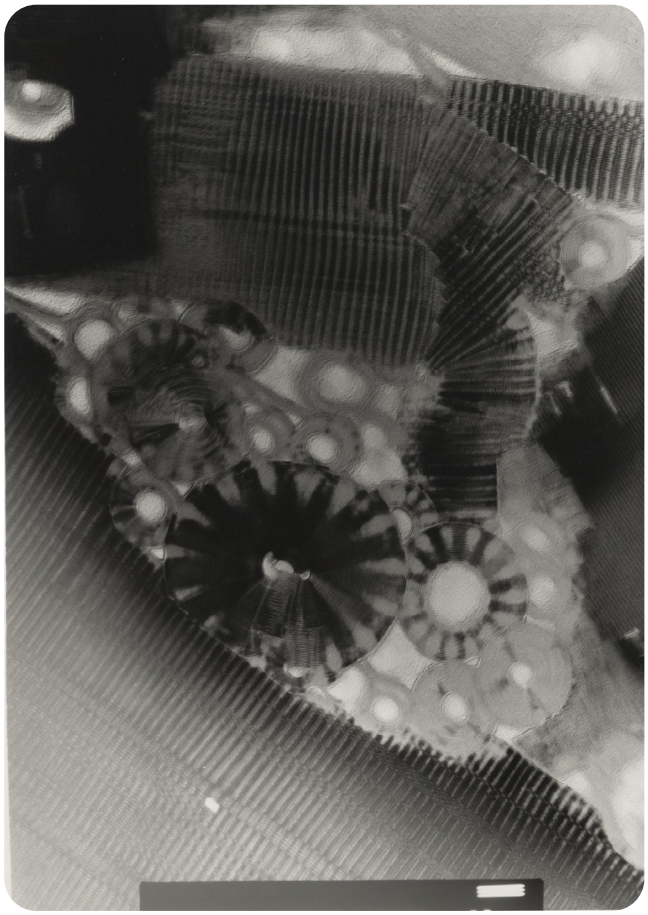

Transmission electron microscope image of a section of asbestiform and asbestos minerals.

What does it mean to you to be a female scientist in geosciences?

Today, I don't see a difference between being a female or male scientist in the field of geosciences.
It's a very different situation compared to 30 or 40 years ago, a time when there was mockery and little to no confidence in the abilities of women who wanted to enter the world of geosciences.

Can you share your experience as a female scientist in your career?

For a long phase of my career—especially in the early years, though not only then—it was truly difficult to gain recognition for my skills and abilities. Not everyone I met was hostile to the idea of supporting my path toward becoming a scientist—on the contrary, I must acknowledge that my mentor stood by me even in moments of particular vulnerability. However, many others (including peers) tried to build walls of isolation around me and, in various ways, ridiculed my research topics, methods, collaborations, and publications.
I can say it wasn't easy, and, more than once, I felt exhausted and considered stepping back entirely. But I also met people who helped keep my desire to do research alive

Did you have any difficulties in reaching your goals?

Yes, I encountered various types of difficulties – from those I mentioned earlier to the challenge of securing sufficient financial resources to maintain the equipment, and the difficulty of finding young people willing to engage in research without being able to offer them a fair or dignified compensation and a possible future in the world of academic research.

Do you have any advice for young people who want to study geological sciences?

My advice is to truly embrace an important idea: knowledge in the field of geological sciences is essential for everyone. In fact, it is fundamental for land management and urban planning; for the prevention and management of natural hazards; for the protection of natural resources; for the sourcing of critical raw materials and other natural resources (such as water); and for supporting decarbonization, the circular economy, and sustainability. If young people become aware of how important this knowledge is for their own lives and for the future of our planet, they will be more motivated to successfully pursue their studies. They will also be able to pass on to other young people –those still unsure or completely confused about their educational path– the meaning and importance of studying the Earth.

Eleonora Paris

Eleonora Paris is full professor of Mineralogy at the School of Science and Technology (University of Camerino). She obtained her PhD in 1995 from the University of Bristol in the UK. She has an extensive, internationally recognized background in experimental mineralogy. She has played a pivotal role in numerous collaborative research projects across Europe and the United States. She has held long-term affiliations with leading laboratories, including the Bayerisches Geoinstitut at Universität Bayreuth and the University of Bristol, and several major synchrotron facilities, including ESRF in France, SSRL in the USA, and LURE in France.

About her interests

Her main research interests focus on developing sustainable materials from waste for industrial and geoscientific applications. She also investigates the structural role of transition elements in minerals and glasses, as well as their impact on physical properties. During her career, she has also worked on high-pressure synthesis and in situ *analysis of oxides and silicates using diamond anvil cells. She applies XANES and EXAFS calculations to examine light and volatile elements in silicates.*

What do GNM and SIMP represent for the scientific community, in your opinion?

In many countries, there is just one scientific society dealing with all Geoscience fields. In Italy, we have several and the advantage is certainly that SIMP, over time, has helped to keep the community working in the Mineralogy-Petrology area unified, and maintained the members active and involved in the Society life, connected by common scientific interests. SIMP also helped to maintain contacts and actions in common with the other societies (SGI, AIV, SOGEI…), as is done with the annual joint conferences, which contributed to encouraging collaborations between researchers and the growth of new ideas. In fact, because the Geosciences cover a vast scientific area, interdisciplinarity must be promoted, especially for the small and scientifically disparate communities, typical of the Earth Sciences.
In this framework, GNM represents a reference point for all scientists working in the fields of mineralogy, crystallography, crystal chemistry, spectroscopy, gemology, experimental mineralogy, as well as for the many applications in industry, technology, medicine, environment, museology, and cultural heritage. GNM has a well-recognized role, also thanks to the many international successes of the members and the many activities in which the community is involved. A treasure of knowledge and competences to be transmitted to the new generations of mineralogists!

Why did you choose science and in particular geosciences? Was there anyone in particular and/or any particular experience that influenced this choice?

After the high school degree in humanities (Lyceum of classical studies) and years of Latin and Greek studies, I was attracted to Geosciences in my last year. I was fascinated by the idea to learn about plate tectonics, volcanoes, and faults: it was an incredible new world for me. More than thinking about a future job, I was interested in the challenge of this new field of studies, coupled with the study of Math, Chemistry and Physics. Surprisingly, when I decided to discuss my choice of a university degree in Geosciences with my science

Additionally, her research contributes to cultural heritage archaeometrical studies and geoscience education. She has led and contributed to several funded research projects focused on spectroscopic studies of minerals and silicate glasses and, more recently, on new materials for sustainable constructions and circular economy, including EU Life and PRIN projects, other EU programs and industrial collaborations. Since 1983, she has played an instrumental role in organising and managing the mineralogy and experimental petrology laboratories at the University of Camerino (UNICAM), thereby fostering research and education in the field. She has been the coordinator of the M.Sc. degree LM74 in UNICAM for many years.

She has been the president of Gruppo Nazionale di Mineralogia (GNM) of the SIMP from 2022 to 2024.

teacher, he tried to discourage me as much as possible! He was a geologist, maybe not satisfied with his career, but he was unable to kill my enthusiasm, and I became a geologist. Note: As many children do, I used to collect minerals and rocks in my hometown, the volcanic area of the Alban Hills… Maybe everything started then!

As a professor in Mineralogy, how has teaching evolved in recent years, both in terms of content and methodology?

Mineralogy is the building block of any Geoscience course, and it is also a very advanced area of study with many interdisciplinary connections with Physics and Chemistry. Students need time to learn and acquire practical competences, although often the compaction of courses in short periods sometimes makes it difficult at beginners' level. As a result, too often students do not consider Mineralogy as an option for interest or future specialization. However, having more time than usual, it is easy to stimulate interest in students by showing the most recent applications of mineralogy knowledge in many industrial and high technological fields or in sustainability and energy transition. By showing the advancements of experimental mineralogy in investigating minerals at non-ambient conditions for a deeper knowledge of the Earth or studying planetary materials or investigating the structure of new materials and their properties, can demonstrate the type of research mineralogists carry out and suggest how many other interesting topics are still to explore for the curious minds! Mineralogy teaching should therefore shed even more light on these fields, as well as showing how the variety of advanced analytical techniques can help in finding solutions to the many questions geoscientists are asked to answer. There is a need for young mineralogists, dealing with increasingly growing fields of applications, where they will find jobs in which their competencies will be highly appreciated.

Which project has presented the greatest challenge for you so far, and how did you overcome it?

As a young researcher, the experimental studies at high temperature and pressure on minerals and glasses have been certainly a gym from many points of view: learning to cooperate with other geoscientists from different countries or scientists from different research areas or technicians to interface with at the international labs or synchrotrons, learning new spectroscopic methods and topics, reading literature from different areas. Hard work but also very exciting work, full of new ideas, applications and challenges, which gave me a lot of enthusiasm, especially because my time was fully dedicated to research! In contrast, when coordinating a project, especially an EU project, the hard experimental work is overshadowed by bureaucratic work. Then, experimental work is not looking so hard anymore, but very, very pleasant, compared to the administrative duties! Responsibility, which comes with a large project, is not only towards reaching research goals, but it is also a responsibility towards the young people involved, who work in the project but also need to grow in research towards the next phases of their working life. However, this change of role becomes satisfying when research results are positive and appreciated, and the young people evolve in research or in new jobs.

Considering your expertise in the development of sustainable materials derived from waste, what do you consider to be the most significant and rewarding impact of integrating materials science with Earth sciences in your research?

The development of sustainable materials from waste is the most recent field I have been working on, starting just before the seismic crisis hitting Umbria-Marche in 2016. For me, living in the area, it was just automatic to dedicate some efforts to finding recycling applications for the millions of tons of rubble produced by the earthquakes, which was

hindering the reconstruction process. I developed, with my collaborators, a series of products with companies in the earthquake area, and I soon realized how these efforts were appreciated by industries, which could also apply for regional grants for R&D or develop new marketable products for these eco-sustainable materials. In that period, very difficult both economically and socially for the people trying to continue living and working in the area; it was rewarding to be useful to the companies and even, in some way, to the local inhabitants, who recognized how the University was doing something practically useful for society. For example, one time, after presenting in a dissemination seminar the new materials from earthquake rubble (Construction and Demolition Waste), a woman said: "There is a piece of my demolished house in that tile!" I almost cried but felt happy to make someone smile in a dark moment of life.

In your opinion, what role can mineralogy play in supporting the ecological and energy transition currently underway?

Mineralogy plays a crucial role in many fields by providing, for example, the knowledge and competences essential to deal with mineral deposits and critical elements necessary for clean energy technologies like solar panels, wind turbines, and electric vehicles. Lithium, nickel, cobalt, and rare earth elements are vital components in batteries and magnets. The increasing world demand and geopolitical implications, coupled with the need to find more efficient recycling processes and new technological challenges to find alternatives for critical elements, put mineralogists in key positions to deal with all these topics. Therefore, mineralogists should highlight their important role in the scientific community, society, and the industrial world, especially now that interest in these themes has increased compared to the past.

Do you have any advice for young people who want to study geological sciences?

Passion is the most important factor in every university choice! Maybe you will start with a passion for rocks and fossils as a kid and then become a mineralogist or a geomorphologist! Whether you like to climb in the mountains or look at the microscopic world, what is important is to explore and be curious. Talk to your professors as they will help you in finding your way, participate in seminars and fieldtrips, even if far away from initial interests, take any chance to increase your geological background: there are so many aspects of Geosciences that will attract your attention during your university path! So, keep your eyes and mind open to all the new topics, methods and challenges, from synchrotron-based techniques to new technological applications or environmental issues to solve. As I say to my students, if you open the same window at home, you will always see the same panorama; if you open all of them, you have a variety of horizons. The future is yours, and if there is passion, you will certainly find the field that best suits you.

Martha G. Pamato received the EMU Medal for Research Excellence 2024

Martha G. Pamato

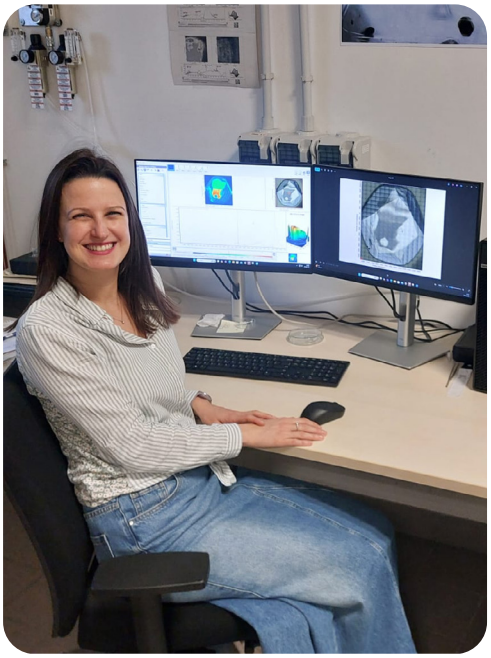

Martha G. Pamato, associate professor in Mineralogy at the University of Padova (Department of Geosciences), is the recipient of the 2024 Research Excellence Award of the European Mineralogical Union. She obtained her PhD in 2014 at Bayreuth University, Germany. After postdoctoral stays worldwide, she was awarded a Marie Skłodowska-Curie Actions fellowship, marking her return home after 11 years abroad. In 2018, she was awarded the SIMP Ugo Panichi Prize. She is currently the laureate of an ERC-Starting Grant, and the head of the single-crystal X-ray diffraction and IRMS laboratories at her department.

About her interests

Her principal interest is the crystallography of minerals composing the deep Earth and their geophysical signatures. Her latest research focuses on diamonds and how to extract reliable information on volatile elements occurrence and fate in the deep Earth from these precious witnesses. In addition to her ground-breaking experiments in mineral physics, her dedication to teaching and training the next generation of mineralogists is attested by her implication in numerous workshops,

What does SIMP represent for the scientific community, in your opinion?

SIMP brings together Mineralogists, Petrologists and solid-earth geochemists, serving as an important platform for young researchers, academics, and professionals. In my opinion, SIMP plays a crucial role in fostering scientific collaboration, promoting research, and advancing our understanding of Earth's materials and their transformations. By supporting conferences, publications, and research initiatives, the society provides a space for scientists to exchange ideas, discuss new discoveries, and address pressing geological challenges. In addition, SIMP contributes significantly to education and professional development, supporting young researchers and encouraging interdisciplinary studies that connect mineralogy and petrology with other, related disciplines, including geochemistry, volcanology and materials science. I believe SIMP plays a key role in shaping the future of mineralogical and petrological research, not only in Italy but also on an international scale.

Why did you choose science and in particular geosciences? Was there anyone in particular and/or any particular experience that influenced this choice?

Ever since I was a kid, I wanted to be a geologist. In elementary school, I had my first lessons about volcanoes and earthquakes, and I was immediately fascinated. I was eager to understand these natural phenomena, and I was captivated by the beauty of volcanic eruptions.
I was also fortunate to have a family friend who was a natural scientist, and her father happened to be a geologist. I would constantly ask her questions about volcanoes, earthquakes, and geological processes in general. Together, we would read a book about the Earth, further deepening my curiosity and passion for geosciences since I was a kid.
A particularly defining moment was when my father, who was working near Naples at the time, took me to visit Mount Vesuvius. That experience solidified my passion and set me on the path to studying geosciences.

summer schools and local events for the promotion of women in science. Martha has emerged as a new leader in the field of crystallography and mineralogy by linking cutting-edge experiments on deep Earth's materials and their primordial geophysical and geochemical consequences. Her scientific achievements, selfless cooperation at an international scale, and dedication to the next generation of mineralogists across Europe make Martha a talented recipient of the EMU Medal for Research Excellence 2024.

During your career you have received many awards and won many ambitious projects, how have these awards/grants particularly contributed to your research/career and finally to achieve the EMU Medal for Research Excellence 2024?

The awards and grants I received had a major impact on my career development. After working on several planned research projects and spending 11 years abroad, I had the opportunity to independently design and pursue my own research project, for which I was awarded a Marie Skłodowska-Curie Actions (MSCA) Individual Fellowship at the University of Padova (Italy) in 2018. Through this fellowship, I was able to address key questions in Earth Sciences, particularly by investigating the original composition of sulphide inclusions in diamonds. In addition to the scientific contributions, I acquired significant management and teaching skills, and I was able to extend my professional network. It was a critical step in strengthening my independence and leadership as a researcher, paving the way for future projects and long-term career advancement. These developments, together with the Ugo Panichi award from SIMP, allowed me to obtain the National Scientific Qualification (Abilitazione Scientifica Nazionale), a fundamental requirement for competing for University Professor positions in Italy. After completing my fellowship, I was awarded an ERC Starting grant to study diamonds to try to unravel the origin of Earth's water. This was 100% a life-changing moment. Not only did it give me the incredible opportunity to establish my own research laboratories, but it also led to my appointment as an Associate Professor. Now, I have the privilege of working with an amazing team of three great postdocs and several outstanding collaborators, from Padova and abroad.
Each of these awards and grants played a crucial role in shaping my career and have collectively contributed to the recognition of my work and ultimately to receiving the EMU Medal for Research Excellence in 2024.

During your brilliant academic career, you spent 11 years abroad before coming back to Italy. How did your PhD and postdoctoral experiences around the world shape your academic career, and what role do international research stays play in a researcher's professional development?

I completed my B.Sc. in Geological Sciences at the University of Padova, and just a week after graduation, I moved to Bayreuth, Germany to begin my M.Sc. and later on the Ph.D. in Experimental Geosciences at the Bayerisches Geoinstitut. After almost six years in Germany, I spent a year in the United States at the University of Urbana-Champaign, followed by three and a half years as a postdoctoral research associate at University College London in the UK. Right from the beginning, I was immersed in highly diverse

At work, with my son, having fun in the Isotope Ratio Mass Spectrometry Laboratory

and dynamic research environments. During my M.Sc. program, in addition to coursework and lectures, each semester required working on a new research project with a different supervisor and team. This exposed me to a wide range of analytical techniques and scientific perspectives and taught me how to approach complex problems from multiple angles. It fostered a multidisciplinary mindset that has shaped my approach ever since. As a result, although I am formally a mineralogist trained in mineral physics, my research is multidisciplinary and extends into the fields of petrology, geochemistry and material science. Overall, spending 11 years abroad was an incredibly enriching experience, both professionally and personally. Throughout this time, I had the opportunity to work in diverse research environments, collaborating with scientists from different cultural and academic backgrounds. This exposure not only broadened my scientific perspective, but also strengthened my ability to work effectively in different teams. These connections have been invaluable, fostering long-term collaborations and opening new avenues for interdisciplinary projects. My experiences abroad have shaped my academic career in profound ways and after returning to Italy, I brought back not only technical and scientific expertise but also a broader vision that continues to influence my research and mentoring approach.

What does it mean to you to be a female scientist in geosciences? Can you share your experience as a female scientist in your career? Did you have any difficulties in reaching your goals?

Being a female scientist in geosciences has been a rewarding journey. Ever since I started my studies, I have been fortunate to meet exceptional friends, colleagues and mentors, both men and women, who have guided and supported me throughout my career. Most importantly, I had two female supervisors, during my PhD and one of my postdocs, who successfully balanced their careers and family life and were role models for me. From them, I learned that it is possible to pursue research while also having a family, which is something I wanted. They always supported me and helped me believe in myself. Their example also showed me that determination, resilience, and a strong support network are key to overcoming challenges in academia. My goal now is to serve as a role model for students and postdocs, demonstrating that it is possible to successfully balance research, professional growth and personal life.
While progress has been made in creating a more inclusive scientific community, I believe challenges still exist for women in geosciences. Throughout my career, I have worked to navigate these, but to be honest, I feel encouraged by the positive changes taking place in academia, such as improved support systems for researcher parents. For example, the University of Padova now provides childcare facilities for researcher mothers, highlighting a growing awareness of the need for a more inclusive and supportive research environment. Ultimately, I believe that promoting a culture of mentorship and collaboration—among both women and men—is essential to achieving greater equity in sciences. Surrounding ourselves with inspiring and supportive individuals allows us to grow, push boundaries and contribute meaningfully to our field.

Do you have any advice for young people who want to study geological sciences?

Be curious, be passionate, be bold! And for those who want to pursue an academic career later on, particularly for the young female geoscientists, find the right balance, never give up, and always believe in yourself. Persevere—there may be setbacks along the way, but what truly matters is having the strength to rise each time you fall. If you have a dream, pursue it passionately, and if along the journey you realize it is not the right path, do not be afraid to change direction and start a new one. The road may require sacrifices, but surrounding yourself with supportive people and nurturing a healthy, open-minded environment makes all the difference.

SIMP Grants Interviews

RESEARCH GRANT FIORENZO MAZZI 2022

Enrico Cannaò

Area of Expertise:
Geochemistry, Isotope Geology, Petrology

Current position:
Researcher (RTD-B)

Current Affiliation:
Department of Earth Sciences "A. Desio", University of Milano

e-mail:
enrico.cannao@unimi.it

What were the reasons that led you to choose geology as a career? And what does geology mean to you?

Honestly, I've never been particularly interested in minerals or geology in a broader sense. But from a young age, I was drawn to science and enjoyed walking in the mountains. From there, I discovered geology. Geology combines fieldwork, lab analysis, and theory, making it an exciting and interdisciplinary science. It is more than a career, it's a continuous journey of discovery.

My scientific activity focuses on the recycling processes operating in subduction zone settings, aiming to better understand fluid-mediated mass transfer and element mobility through volcanic arcs and beyond. My research primarily relies on information obtained from the natural rock records, combining microstructural analysis with geochemical and isotopic data. In recent years, the investigation of deep element recycling has also expanded into the fascinating and powerful field of experimental petrology. Since the establishment of the new Geochemistry Laboratory in Milano, I have dedicated a significant part of my time to the analytical development of various isotope systematics, which are key to unravelling geological processes.

Currently, my research aims to simulate deep-Earth conditions to refine our understanding of element behaviour at ultrahigh pressures, specifically investigating the potential of dense hydrous magnesium silicates (DHMSs) to incorporate and transport boron, among other trace elements, to great depths through the colder parts of subducting slabs. Despite their importance in the geological water cycle, no information is currently available on the role of DHMSs as potential geochemical reservoirs in the deep mantle. Advancements in this field enhance our ability to model fluid-rock interactions, refine geochemical reservoirs, and provide new insights into trace element cycling in Earth's interior, contributing to our understanding of subduction dynamics and global geochemical cycles.

I owe a big thanks to SIMP for supporting me throughout my academic journey, providing contributions for participation in conferences, workshops, *Borsa di studio all'estero,* and, more recently, with the Fiorenzo Mazzi Research Grant. All these opportunities have been key in shaping me as a research scientist, pushing me out of my comfort zone and encouraging me to seek valuable training and formative experiences.

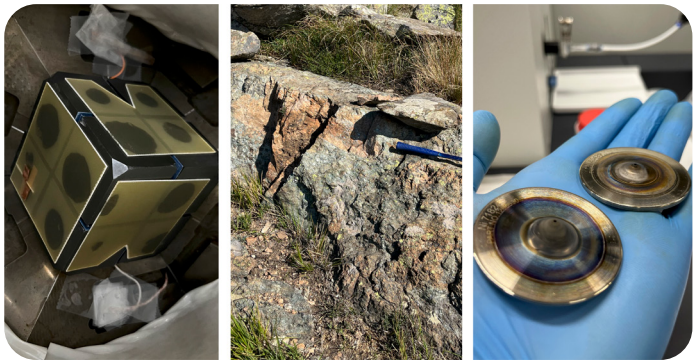

A snapshot of my current research interest: top view of a Multi-Anvil experiment (left); metasomatized high-P metarodingites from the Voltri Massif (W. Ligurian Alps, center); detail of the sample and skimmer cones of the MC-ICP-MS, in the background, the outer part of the ICP module (right).

RESEARCH GRANT FIORENZO MAZZI 2022

Luciana Mantovani

Area of Expertise:
Mineralogy

Current position:
Associate Professor

Current Affiliation:
Department of Chemistry, Life Sciences and Environmental Sustainability, University of Parma

e-mail:
luciana.mantovani@unipr.it

What were the reasons that led you to choose geology as a career? And what does geology mean to you?

Geology, for me, is about understanding a vital part of the world I live in, shaped by the interaction between nature and humans with the environment. It allows me to marvel at the complexity of natural processes daily, offering both wonder and refuge. The more I delve into geology, the more I am fascinated by how everything is intricately interconnected, and how this knowledge shapes our understanding of the Earth and our role within it.

My research spans several areas within mineralogy. During my PhD, I focused on the synthesis and characterization of Co-doped pyroxenes using high-pressure and high-temperature techniques, exploring their potential as ceramic pigments. I investigated their colour properties and behaviour when integrated into ceramic glazes. In recent years, my research has shifted toward environmental and applied mineralogy, with a particular emphasis on the mineralogical and chemical characterization of Bottom Ashes from Waste-to-Energy plants, where I try to identify their components and assess the release of potentially toxic elements. Additionally, I have explored the use of magnetic techniques to analyse atmospheric particulates and leaves, contributing to the development of environmental monitoring methods. My other areas of interest include the study of cultural heritage materials and asbestos minerals.

My research advances the field of mineralogy by investigating the potential of Bottom Ashes from Waste-to-Energy plants, transforming what traditionally is waste into a valuable resource. Achieving this requires a deep knowledge of the material, as only through detailed mineralogical and chemical characterization can critical elements be safely and efficiently extracted and the materials reused without impacting the environment. Using advanced chemical and mineralogical techniques, I can identify the mineral phases present and assess the release of potentially toxic elements. This work contributes to more sustainable waste management practices, fosters the recovery of valuable resources, reduces environmental impact, and supports the principles of the circular economy.

The SIMP grant has been of great support, allowing me to conduct advanced analyses on the materials of interest and to explore in detail their properties and potential for reuse. Additionally, it enabled me to disseminate the results within the scientific community by facilitating my participation in international conferences and the publication of my studies in relevant journals. This has contributed to raising awareness of my work among a broader audience and strengthening my position within the academic community.

My two big passions: observing and understanding how marvellous the Earth system is, and my dog.

RESEARCH GRANT FIORENZO MAZZI 2022

Azzurra Zucchini

Area of Expertise:
Mineralogy

Current position:
Associate Professor

Current Affiliation:
Department of Physics and Geology, University of Perugia

e-mail:
azzurra.zucchini@unipg.it

What inspired you to choose geology as your career path, and what does geology mean to you personally?

What to do after high school was a controversial decision, but I was sure that I wanted to do something for the Planet I lived on. I chose geology because it was a way of getting to know the Earth, learning from it and trying to mitigate the problems that today undermine the well-being of the Earth itself and its inhabitants. During my studies and early career, it was not disproven, and I still love contributing to the knowledge of our Planet and its health.

Research has focused on cation disorder and its influence on ankerite mineral physics. Piston-cylinder annealing experiments achieved the order-disorder phase transition, which was found to be dependent on temperature and Fe content. Ordered and disordered samples were studied by high-pressure synchrotron single-crystal X-ray diffraction, and disorder was found to strongly influence the stability of ankerite. The ankerite-to-ankerite-II phase transition only occurred in the ordered sample, with no clear evidence of the phase transition in disordered ankerite up to ~25 GPa. Compressibility analysis showed that ordered ankerite and ankerite-II are the most and least compressible structures, while disordered ankerite lies in between, although it becomes more compressible with increasing pressure. Research is ongoing to assess the role of disorder and Fe spin crossover in the mineral physics of differently ordered ankerite structures under non-ambient conditions.

Carbonates are important components of the lithologies involved in subducting materials from both oceanic and continental crust. The low geothermal gradient in the subduction zones allows carbonates to come across the optimal conditions for cation disordering, and, for ankerite, this scenario is easily achieved in warm subduction paths. In a cold regime, ankerite likely maintains its ordered state, encountering the ankerite-I to ankerite-II phase transition. The differences that we observed in the bulk sound velocities between the three studied polymorphs might partially contribute to deciphering the low-velocity anomalies observed in the mantle wedge. The ongoing research, devoted to studying their elasticity under non-ambient conditions, will allow us to take into account the strong anisotropic behaviour expected for both (dis)ordered ankerite and ankerite-II, likely being an additional factor that conditions the observed seismic wave anomalies.

It was an honour to receive the SIMP Grant. The funded project has allowed me to start a new research area in my career, dedicated to the study of the role of ankerite and other Fe-carbonates in the geophysical modelling of our Planet. New collaborations with Italian and foreign colleagues are starting. These will continue and form the basis for developing this project and possibly starting new ones.

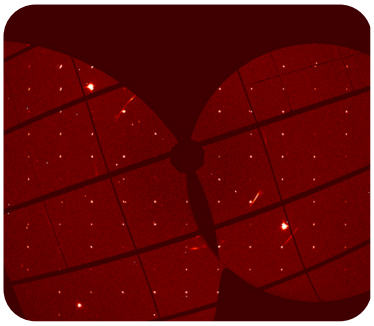

The crystal butterfly *- Precession image of a single ankerite crystal collected at ESRF synchrotron facility, during a beamtime related to the project.*

PREMIO MAZZI (EX PANICHI) 2024

Anna Barbaro

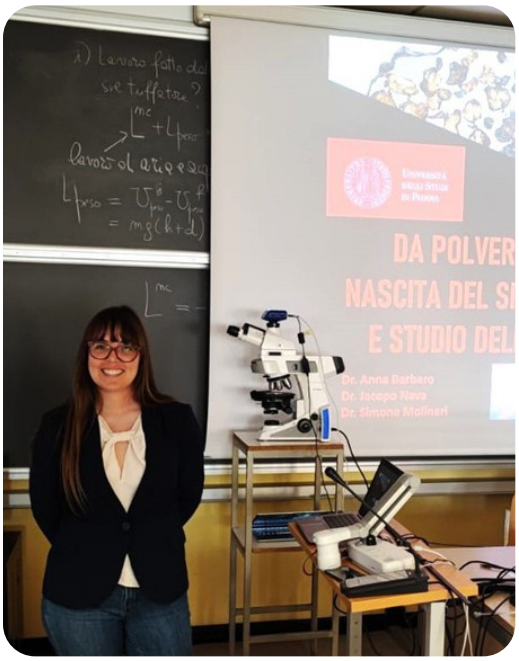

Area of Expertise:
Mineralogy, Planetary Science

Current position:
Humboldt Post-doctoral fellow

Current Affiliation:
Schwiete Cosmochemistry Laboratory, Department of Geoscience, Goethe University, Frankfurt

e-mail:
barbaro@em.uni-frankfurt.de

What inspired you to choose geology as your career path, and what does geology mean to you personally?

I have always been captivated by the mineralogy of our planet and of our solar system, a passion that began with my grandfather as we embarked on a small mineral collection together. This early interest blossomed in university and during the PhD, where my mentors guided me in linking Earth processes to planetary science, particularly by studying meteorites. To me, geology acts as a bridge between understanding our planet's history and exploring distant worlds.

I am currently investigating the intriguing world of ureilitic meteorites, where diamond and graphite offer clues about our solar system's history. My primary goal is to determine the correlation between shock events and the formation of diamonds, while revealing distinct shock-induced defects observable in both shocked graphite and diamond crystals. Utilizing Transmission Electron Microscopy (TEM), I meticulously analyse these atomic-scale defects to establish a clearer link between the extreme conditions experienced during impacts and the structural changes in carbon materials. This research not only enhances our understanding of diamond genesis but also contributes valuable insights into planetary formation and evolution. In essence, I'm piecing together the cosmic puzzle of how these remarkable materials form under pressure, all while keeping an eye on their geological significance!

These findings enhance our understanding of carbon phase transformations and provide a framework for interpreting similar processes on different planetary bodies. The implications extend to the broader geoscience community by offering new perspectives on planetary formation and evolution, potentially influencing future research on extraterrestrial materials, such as the materials from the "samples return" campaigns. My project paves the way for innovative approaches in both academic research and industrial applications related to carbon materials.

The Premio Mazzi "ex Panichi" recognition from SIMP has significantly enhanced my professional profile, making me a more competitive candidate for future opportunities. This award adds credibility to my work and opens doors to new funding and collaborations. I was truly honoured to receive it, and I will strive to uphold its significance, especially in light of the distinguished Italian scientists who have been recognized before me.

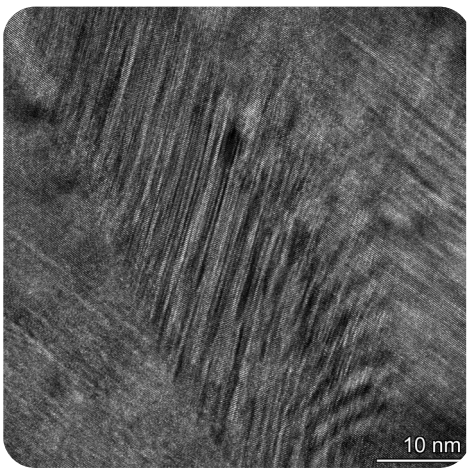

Extraterrestrial carbon at the nanoscale. HR-TEM image of stacking faults sequences in ureilitic diamond.

PREMIO MAZZI (EX PANICHI) 2024

Davide Comboni

Area of Expertise:
Mineralogy, Crystallography

Current position:
Researcher (RTD-A)

Current Affiliation:
Department of Earth Sciences "A. Desio", University of Milano

e-mail:
davide.comboni@unimi.it

What inspired you to choose geology as your career path, and what does geology mean to you personally?

I must confess that, as a freshman, I chose geology without a specific reason—it seemed interesting, but I was not entirely sure of my decision. Over the years, I have grown increasingly grateful for my (lucky) choice. Geology unravels the history and processes of our planet, studying how the georesources humanity has relied upon since the dawn of civilization formed over millions or even billions of years. Geology bridges the past and the present, helping us shape a sustainable future.

My research focuses on the study of inorganic crystalline compounds, both mineral and synthetic, under varying pressure and temperature conditions. I investigate phase transitions, stability fields, elasticity, and atomic-scale deformation mechanisms of REE-minerals and hydrated borates, as well as crystal-fluid interactions in microporous materials like zeolites. In my research, I use techniques like X-ray and neutron diffraction, optical and electron microscopy, mass spectrometry, and spectroscopic methods mainly at the Earth Science Department of the University of Milan and in large-scale facilities such as ESRF, DESY-PETRA III, and ILL.

Since my doctoral project, I have been particularly interested in the hydration kinetics of natural zeolites to explore their role as water carriers in the first kilometres of the oceanic crust. Lately, I expanded my research to hydrated borates, promising minerals for producing neutron shielding concretes and to REE-minerals, a class of minerals which is still poorly studied.

Receiving the Fiorenzo Mazzi prize is a great honour that has inspired me to pursue my research with renewed energy and dedication. This recognition reinforces my commitment to advancing my field and motivates me to strive for excellence in my scientific endeavours.

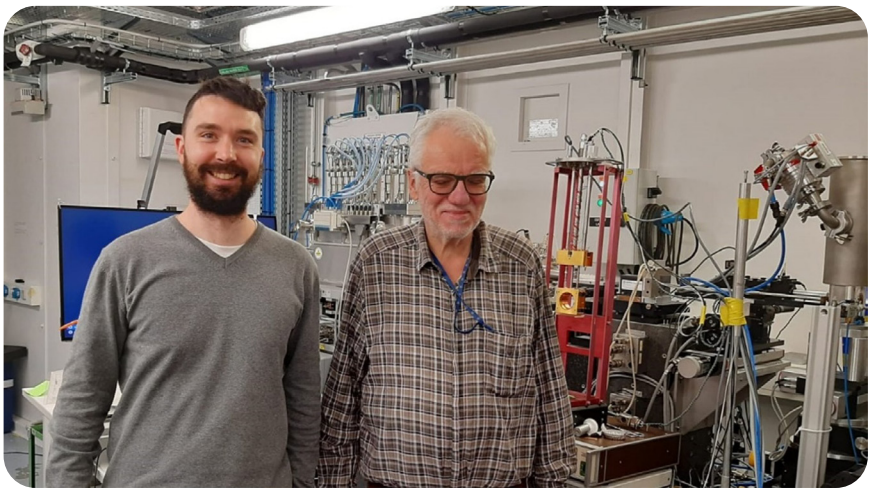

Me and my supervisor during my last day as post doc in ID15b, ESRF.

PREMIO TESI DI DOTTORATO 2024

Sumith Abeykoon

Area of Expertise:
Experimental petrology

Current position:
Post-Doc Researcher

Current Affiliation:
School of Science and Technology, Geology Division, University of Camerino

e-mail:
sumith.abeykoon@unicam.it

What inspired you to choose geology as your career path, and what does geology mean to you personally?

I was fascinated by the Earth's uniquely intricate interior structure, a foundation of its habitability. While we've explored the vastness of outer space—Voyager 1 being over 15 billion miles away and still sending data—I often wondered how we study Earth's interior. This curiosity inspired me to pursue an academic career in high-pressure, high-temperature experimental petrology, a field that uncovers the hidden mysteries deep beneath our planet's surface.

I investigated deep Earth processes using laboratory experiments with a focus on the role of sulfides and aqueous fluids in the Earth's interior. High-pressure (*P*), high-temperature (*T*) multi-anvil experiments were employed to study dissolved oxygen contents in sulfide melts, similar to the sulfide inclusions found in diamonds. From this work, a geothermometer expression was derived, yielding reliable mantle equilibrium temperatures associated with diamond formation. Moreover, high-*P-T in situ* time-of-flight neutron diffraction experiments were used to show significant hydrogen incorporation into sulfides. In another project, a novel experimental technique was developed, the 'single-crystal diamond trap (SCDT)', which can measure fluid compositions relevant to Earth's upper mantle conditions. Overall, my research contributes to understanding the role of volatiles in the Earth's interior.

My research in experimental petrology and geochemistry provides new methodologies and scientific insights into Earth's mantle processes. The new SCDT is a powerful tool for obtaining accurate high-*P-T* fluid compositions and producing essential mineral solubility data for upper mantle mineral assemblages. The novel geothermometer provides temperature constraints for the deep mantle, while revealing the behaviour of sulfide melts during diamond formation. Furthermore, significant hydrogen incorporation into sulfides at high *P-T* conditions suggests sulfide as a hydrogen reservoir within planetary interiors, which may have formed during the planet's evolution. Sulfide-hosted oxygen and hydrogen could be highly reactive, playing key roles in dynamic mantle processes even at low concentrations, with implications across various fields. These findings refine mantle geochemistry models and provide insights into planetary evolution through volatile cycles.

Assembling a high P-T, Multi-anvil experiment in Bayerisches Geoinstitut, Germany.

The SIMP award has recognized my work in experimental petrology, boosting my credibility in the field. It has opened opportunities to collaborate with experts and expand my professional network. It has enhanced my confidence and motivation to pursue innovative research. I'm grateful for the award's impact on my career growth.

PREMIO TESI DI DOTTORATO 2024

Andrea Cotellucci

Area of Expertise:
Mineralogy, Chemistry, Crystal Growth

Current position:
Laboratory technician

Current Affiliation:
COGNE ACCIAI SPECIALI, Via Paravera 16, Aosta, Italy

e-mail:
andreacotellucci94@gmail.com

What inspired you to choose geology as your career path, and what does geology mean to you personally?

My interest in geology was born by a fascination with Earth's natural processes, particularly mineral and crystal growth. Through my master's and PhD research, I gained expertise in experimental mineralogy and crystallography, applying these skills to environmental and industrial challenges. Geology, for me, is not only about understanding the Earth's history but also about using that knowledge to develop sustainable solutions.

The PhD project was mainly focused on experimental research in mineralogy and crystallography, aimed at investigating the mechanisms responsible for the genesis of Messinian evaporitic deposits in the Mediterranean basin. The topics covered include (i) providing a geometric-crystallographic background of the five twin laws of gypsum, allowing researchers to recognize the twin laws only by the measurement of their re-entrant angle value, and the extinction angle formed between the two individuals using crossed polarizers in optical microscopy; (ii) developing specific synthesis and instrumental setups for improving our understanding of different habits and twin laws of gypsum occurring, in a pure system, with and without the addition of carbonate ions in solution; in the presence and absence of sulfide oxidation.

The PhD work aims to be the key reference for those interested in recognizing gypsum twinning laws both in natural and laboratory environments. Moreover, it uniquely demonstrates that different chemical compounds in solution can lead to the selective formation of different gypsum twinning laws. This may aid in understanding the chemistry of the original brine in ancient sedimentary successions based on the observed twinning laws and habits of gypsum.

The SIMP award has been instrumental in advancing my research and career development, and I am deeply grateful for the support it has provided

How is it possible not to be fascinated by the formation mechanisms of these crystals? Giant gypsum crystals in Naica mine (Mexico). Ph. Laura Sanna.

PREMIO TESI DI DOTTORATO 2024

Francesca Innocenzi

Area of Expertise:
Petrography, Petrology, Geochemistry

Current position:
Post-Doc Researcher

Current Affiliation:
Department of Geosciences, University of Padova

e-mail:
francesca.innocenzi@unipd.it

What inspired you to choose geology as your career path, and what does geology mean to you personally?

I chose geology as my research field because I have always been captivated by the power of the Earth, which still has many secrets to human eyes. Geology is the key to reaching a better understanding of our planet, and petrology gives us the instrument to unravel the nature, the composition and the processes that characterize the inaccessible part of the Earth.

The goal of my PhD thesis was to propose a general petrogenetic model able to explain the petrogenesis of different 'ultra-' rocks (ultrabasic to basic, ultramafic and/or ultra-alkaline composition), as kamafugites, ultramafic lamprophyres, melilitites and carbonatites. A detailed comparison was carried out on exotic rocks from different geodynamic settings and with variable compositional features, to highlight similarities and differences helpful to infer the reason of such heterogeneities, but also to better constrain the relative mantle sources and the processes involved in their formation. The study was based on a multidisciplinary investigation: petrographic, mineral chemical, geochemical and isotopic data (Sr-Nd-Pb, plus conventional, as C-O, and unconventional stable isotopes, as B) were coupled with petrological experiments at different pressures (1-5 GPa) and temperatures (1000-1550°C).

Despite decades of scientific research, a full knowledge of these rare magmas and their mantle sources is far from being reached. Also, the definition of standard guidelines for the classification of these rock groups has not yet been reached. In this confused framework, my research helped to reconstruct the nature, the main features and the petrogenesis of rare and debated exotic products, which reflect peculiar and poorly constrained mantle processes. A detailed and systematic study, based on classical and innovative methods, contributed to reaching a deeper knowledge of veined and metasomatized mantle lithologies and their partial melting products, also considering that the experimental results validate the main constraints obtained from natural samples. Broader implications are related to the hot topic of deep volatile cycles (especially carbon).

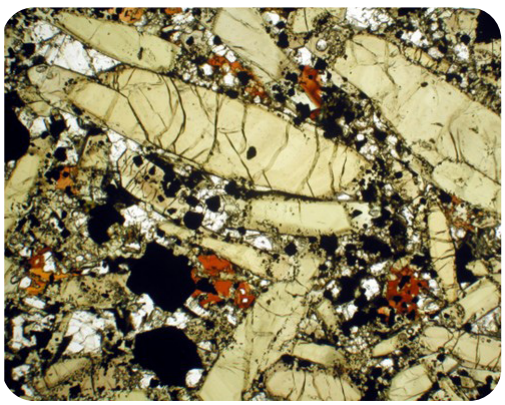

I am honoured to have won the SIMP award, as it helped in increasing the visibility of my PhD work and the related papers, acknowledging the significance of my outputs and implications. Moreover, thanks to the award, I had the opportunity to present my main results at international conferences, such as Goldschmidt.

Thin section photomicrographs of an 'ultra-' rock from my PhD thesis. Hidden beauty of nature that can be seen only by optical microscopy.

Ph.D. Thesis Extended Abstracts

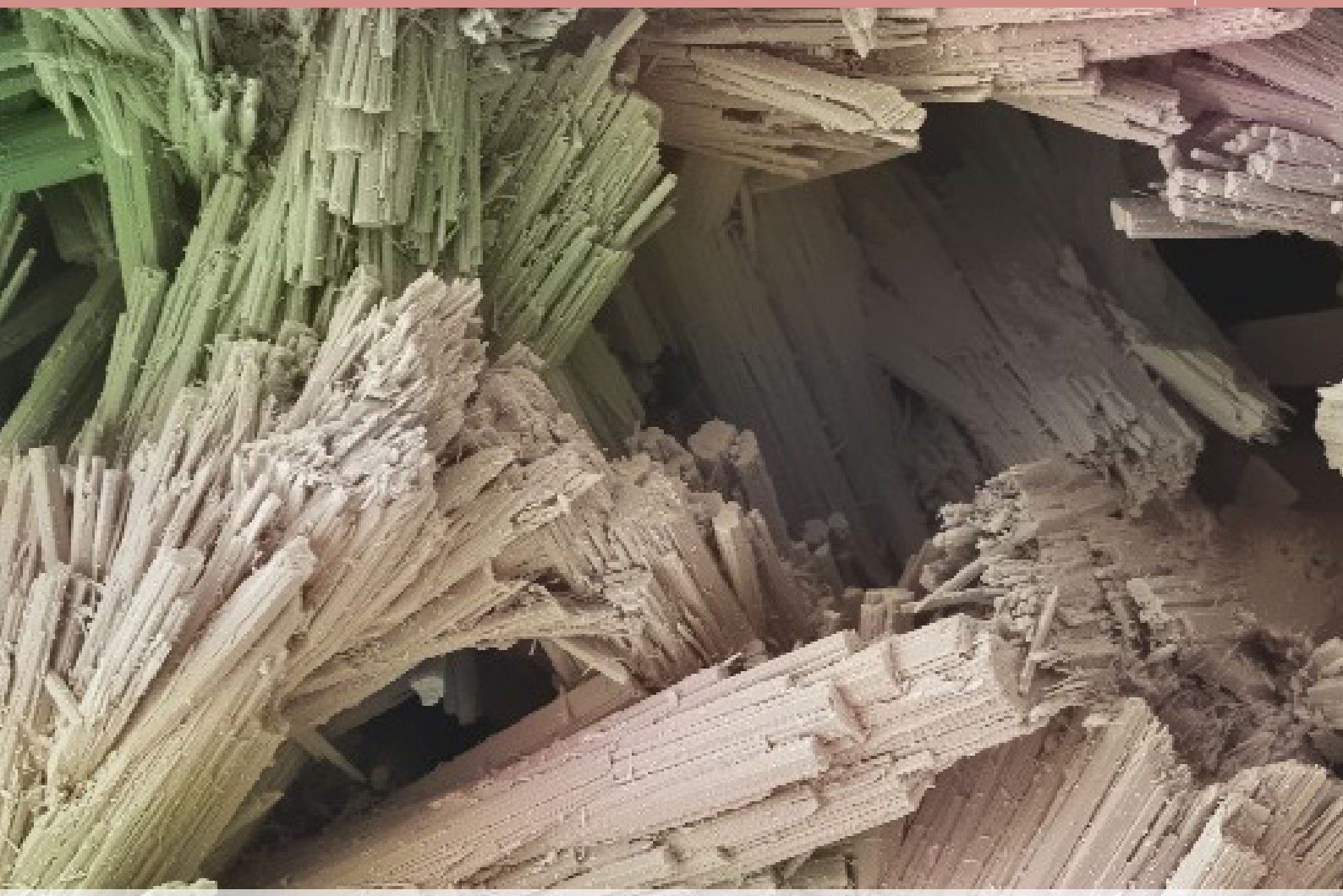

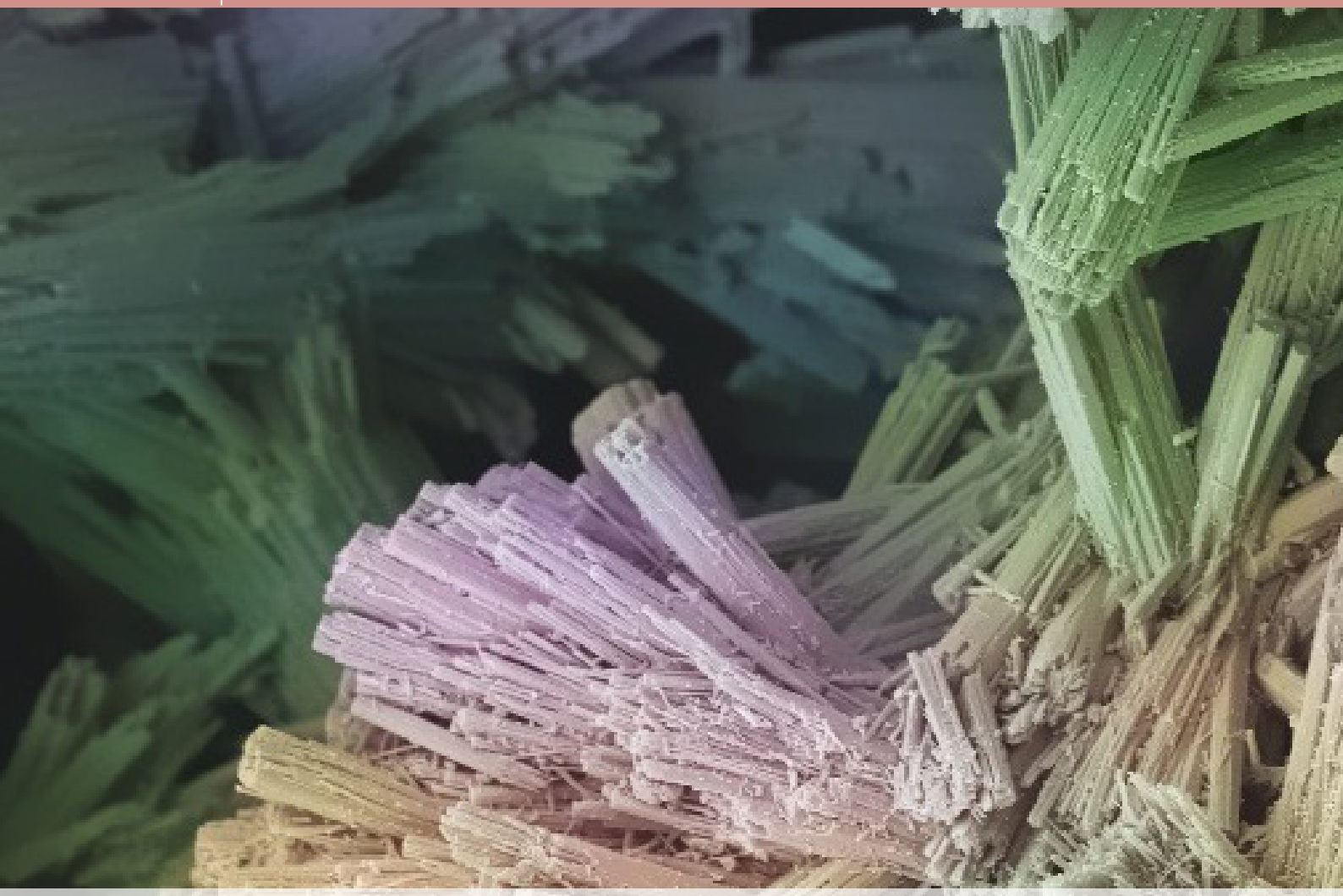

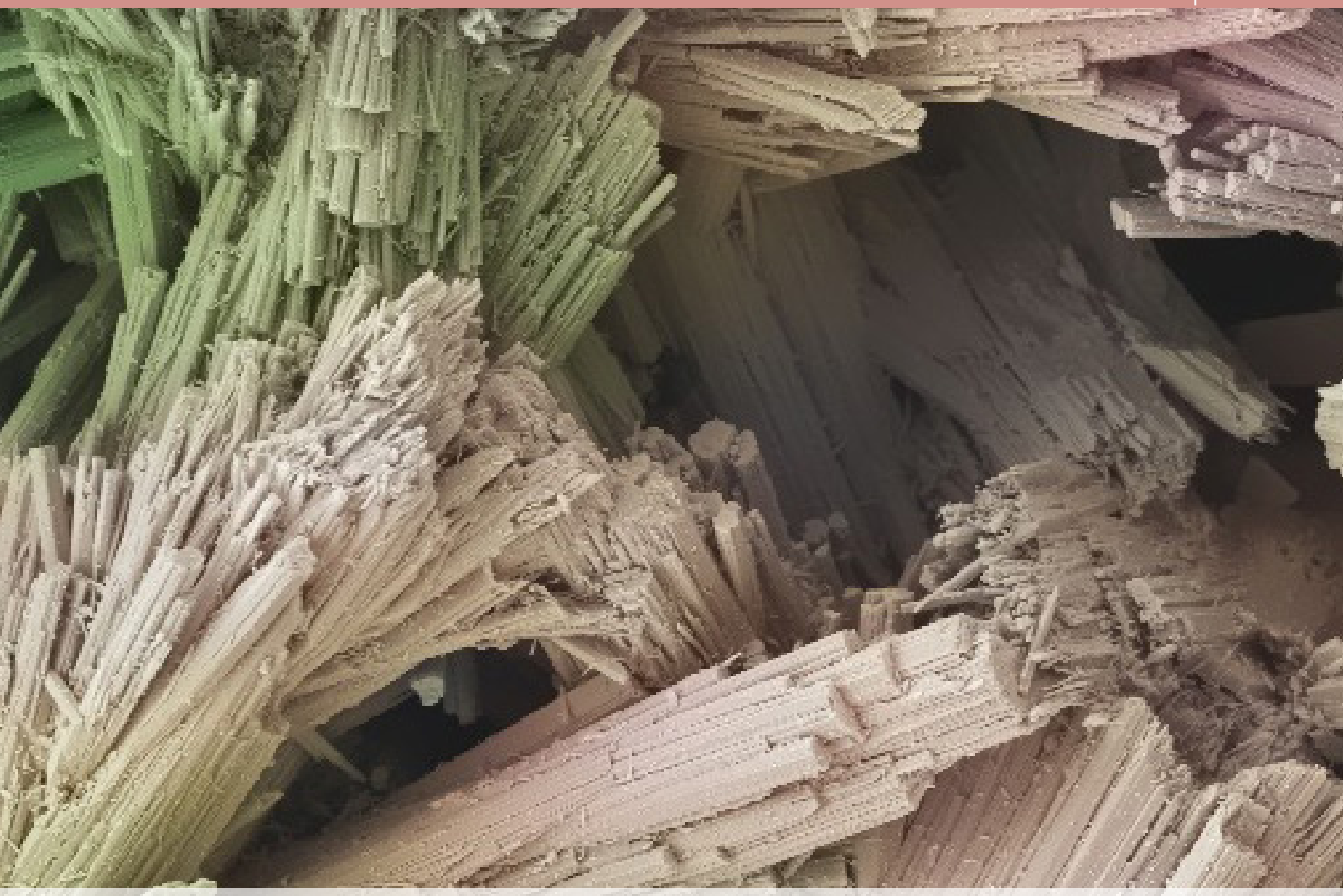

The interplay between cation ordering and elasticity of omphacites to unravel P-T-t paths of metamorphic rocks

Lisa Baratelli

Department of Earth Sciences "A. Desio", University of Milano, Via Botticelli 23, 20133, Milano

DOI: 10.19276/plinius.2025.01.001

INTRODUCTION

Clinopyroxenes (general formula $M1M2T_2O_6$) are widespread rock-forming minerals that occur in a variety of geological settings and processes. This makes them promising candidates for elastic geothermobarometry, a method that uses strain recorded by mineral inclusions to determine the pressure (*P*) and temperature (*T*) conditions of entrapment (Angel et al., 2019; Gilio et al., 2021). Among clinopyroxenes, omphacite inclusions are particularly valuable for constraining *P-T* conditions in eclogitic metabasites, where other inclusions such as quartz are absent as equilibrium phases at peak metamorphic conditions. Raman spectroscopy is one of the most used techniques to determine the pressures of inclusions for elastic geothermobarometry because it has the advantage of probing micrometer-scale regions without the need to extract the inclusion from the host. Raman scattering is highly sensitive to structural deformations, offering significant information about variations in the crystal structure caused by thermal or compressive stress. However, since omphacite is a solid solution, the positions of the Raman peaks are influenced by both the chemical composition and the degree of cation order, as well as *P*. This has so far prevented omphacites from being used for elastic geothermobarometry.

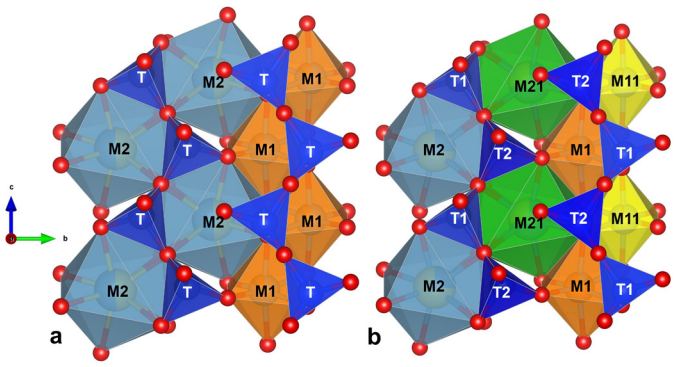

Figure 1 a) *Structural fragment of disordered (space group C2/c) and* ***b)*** *of disordered (P2/n) omphacite. SiO_4 tetrahedra are shown in dark blue, M1 sites in orange, M11 in yellow, M2 in light blue, and M21 in green. The diagrams (Baratelli et al., 2025a) were prepared using the VESTA software package (Momma & Izumi, 2008).*

The *P* and *T* conditions of the inclusion entrapment (P-T_{trap}) can be estimated knowing the inclusion *P* (P_{inc}), which affects the positions of the Raman peaks, and the elastic properties of both the host and the inclusion. These parameters define a line in *P-T* space known as isomeke, representing all possible entrapment conditions for a given host–inclusion pair. The intersection of isomekes for different inclusions in the same host can provide P-T_{trap}. Omphacite has the advantage of providing, with Raman spectroscopy, not only P_{inc} (Baratelli et al., 2024), but also the closure *T* (Baratelli et al., 2025a) through the cationic order phenomenon. As *T* decreases, omphacite undergoes a cation order process which leads to a splitting of the two sites hosting cations with six and eight coordination number, *M*1 and *M*2 (Fig. 1a), into non-symmetrically related *M*1 and *M*11, and *M*2 and *M*21, respectively (Fig. 1b). As a result, the presence of cationic order lowers the space group symmetry from *C*2/*c* to *P*2/*n*. Thus, the determination of the state of chemically ordered omphacite can constrain the closure *T* and cooling rate experienced by the host rock.

The aim of this study has been to develop the necessary tools to exploit the chemical, structural and elastic properties of omphacite to enable it to be used in elastic geothermobarometry by means of Raman spectroscopy. To achieve this goal, omphacite crystals with different degrees of cationic-site order and different chemical composition were characterised via a multi-methodological approach.

MATERIALS AND METHODS

The omphacite crystals analysed in this study are from Münchberg Mass, Bavaria (O'Brien, 1993), with compositions $Jd_{43}Di_{57}$ and $Jd_{52}Di_{48}$ (where Jd = jadeite, Di = diopside). They belong to the same omphacite samples that have been previously analysed with Infrared spectroscopy and single-crystal X-ray diffraction (SC-XRD) by Boffa Ballaran et al. (1998a, b) and by high-pressure (*HP*) SC-XRD by Pandolfo et al. (2012a, b). All of the crystals were initially analysed with SC-XRD. Fe^{3+}-rich omphacites from

Lugros and Camarate (SE Spain), and Voltri massif eclogites (Italy) (Cámara, 1995; Cámara et al., 1998), along with synthetic Fe-free omphacites (Pandolfo et al., 2015) and a Di and a Jd crystal from the Museum der Natur Hamburg - Mineralogie, were also used for the chemical calibration of omphacites using Raman spectroscopy. These samples were also chemically characterised with Electron Microprobe analysis (EMPA).

Ab initio HF/DFT (Hartree Fock/Density Functional Theory) simulations have been conducted with the CRYSTAL17 software (Dovesi et al., 2018) on a fully ordered $Jd_{50}Di_{50}$ omphacite to explore the structural and the Raman spectra evolution as a function of *P*.

Experiments at non-ambient conditions

In situ H*P* Raman spectroscopic measurements were performed using a diamond anvil cell (DAC). Two sets of experiments were performed, using omphacite crystals with two different compositions ($Jd_{43}Di_{57}$ and $Jd_{52}Di_{48}$) and various states of cation order, obtained through annealing experiments. Single crystals with a low Fe content were selected to avoid further chemical effects on the Raman spectrum. The details of the crystals used in these experiments and presented in the figures are listed in Table 1.

In addition, a H*P* SC-XRD study of a $Jd_{43}Di_{57}$ crystal, up to 10 GPa, was performed at the Xpress beamline of the Elettra Synchrotron, Trieste. The crystal was cut with a focused ion beam in two different perpendicular directions. Both slices were loaded into a DAC to maximize the available reciprocal space information. This allowed us to obtain accurate structural variations in terms of deformation of bonds and coordination polyhedra, necessary to compare these results with the H*P* Raman spectroscopy ones.

Table 1 Details of the crystals used in HP Raman spectroscopy experiments. The symbols listed here are used in the following figures. Q_{M1} and Q_{M2} are the order parameters determined from single-crystal refinements (Q = 1 for ordered and Q = 0 for disordered omphacite). T is the annealing temperature applied for time t in hours.

	Symbol	Q_{M1}	Q_{M2}	Ann. T (°C)	Ann. t (h.)
$Jd_{43}Di_{57}$	■	0.828	0.397		
	■	0.864	0.453		
	□	-	-	900	168
	□	-	-	900	168
$Jd_{52}Di_{48}$	▲	0.863	0.453		
	▲	0.751	0.419	950	1
	▲	0.624	0.318	950	5*
	▲	0.512	0.257	950	2.5
	▲	0.109	0.034	950	45
	△	-	-	950	458

* Shows a lower degree of order, corresponding approximately to an annealing time of 2 h.

RESULTS

Raman spectroscopy

According to the group theory, Raman spectra of disordered omphacites consist of 30 Raman active modes, while ordered omphacites have twice as many modes (Fig. 2). The assignment of each Raman peak to a specific atomic vibration was achieved by HF/DFT simulations. The omphacite spectrum is characterised by three regions: *i)* the bond stretching between Si-O between 1000 and 1030 cm^{-1}; *ii)* the Si–O–Si bond bending given by the most intense peak at about 681 cm^{-1}; *iii)* the lower frequency modes, between 50 and 600 cm^{-1}, related to the lattice vibrations.

The main result of this study is the calibration of the Raman peaks of omphacite as a function of 1) the chemical composition, 2) pressure, and 3) cation order degree, each of which is discussed below.

1. The chemical composition affects the wavenumber of some peaks, which increases with the increase of the Al content (Fig. 3a), allowing omphacites richer in Jd or Di component to be distinguished.
2. The wavenumbers of all Raman active modes increase with the applied *P*. The peak at 681 cm^{-1} shows a linear dependence on P (Fig. 3b); its position is not affected by the cation order but is influenced by the chemical composition.
3. The cation order causes a broadening of the Raman peaks, and it is not influenced by *P*. This is particularly visible in the Full Width at Half Maximum (FWHM) of the peak at 681 cm^{-1}, whose value increases with the increase of disorder in the *M* polyhedra (Fig. 3c).

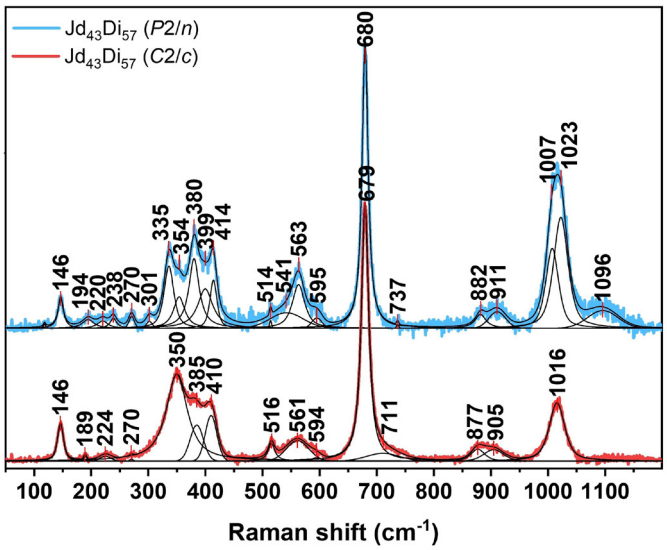

Figure 2 Measured Raman spectra of chemically ordered (light blue line) and disordered (red line) omphacite.

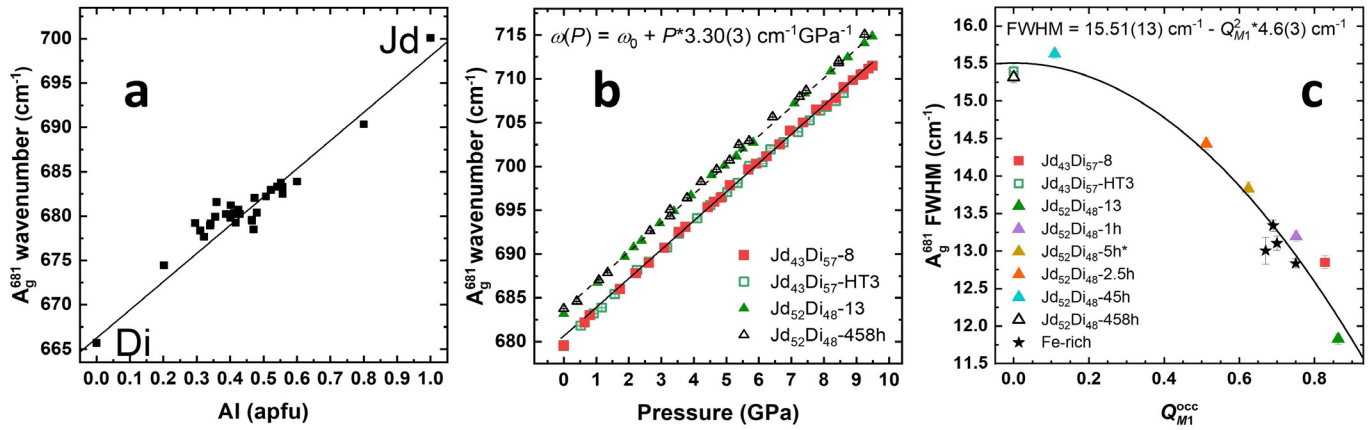

Figure 3 ***a)*** *Chemical composition and* ***b)*** *pressure dependence of the wavenumber of the peak at 681 cm^{-1}. The wavenumber increases linearly with P, but is also influenced by omphacite composition.* ***c)*** *The cation order affects the FWHM of the peak at 681 cm^{-1}, with a parabolic dependence.* ***b)*** *and* ***c)*** *are modified after Baratelli et al. (2025a). Filled symbols are related to ordered omphacites, while open symbols to disordered ones.*

The *P*-dependent behaviour of some Raman peaks exhibited a discontinuity near 5 GPa (*e.g.*, Fig. 4), suggesting a variation in the compression mechanisms occurring in the six- and eight-coordinated sites of the ordered omphacite structure.

HP SC-XRD

To explain the anomalous behaviour of the Raman peaks, H*P* SC-XRD analysis was conducted on an ordered omphacite (with composition $Jd_{43}Di_{57}$) using synchrotron radiation (Baratelli et al., 2025b). The experimental results were compared with *ab initio* simulations. A second-order Birch-Murnaghan (BM) equation of state (EoS) fit of all data yields V_0 = 422.85(15) Å^3, and K_{T0} = 121.3(11) GPa, using the EosFit7 software (Gonzalez-Platas et al., 2016). For the $Jd_{50}Di_{50}$ omphacite, calculated with hybrid HF/DFT simulations, a third-order BM EoS was employed, and the fit of all data yields V_0 = 426.52(3) Å^3, K_0 = 119(2) GPa, and K' = 4.9(5) (Fig. 5a). The results indicate a stabilisation of the *T*2 TILT angle (Fig. 5b), defined as the out-of-plane tilting of the basal face of the tetrahedron with respect to the plane (100) (Cameron et al., 1973), which correlates with distortion variation in the *M*1 octahedron around 3 GPa (Fig. 5c). This coincides with a decrease in the rate of *M*1 deformation under increasing *P*. *Ab initio* simulations indicate that the 337 cm^{-1} mode is related to tetrahedral rotation around the *c* axis, that can be related to the *T*2 TILT angle variation. Thus, both long-range (SC-XRD) and short-range (Raman spectroscopy) analysis supports the observed changes in polyhedral distortion of the *M*1 octahedra. In disordered omphacites, this behaviour cannot be observed due to symmetry constraints: in *C*2/*c* omphacite, only a single *M*1 polyhedron is present, exhibiting an average chemistry between the *M*1 and *M*11 sites of *P*2/*n* structure, resulting in a Raman spectrum that displays fewer Raman active modes.

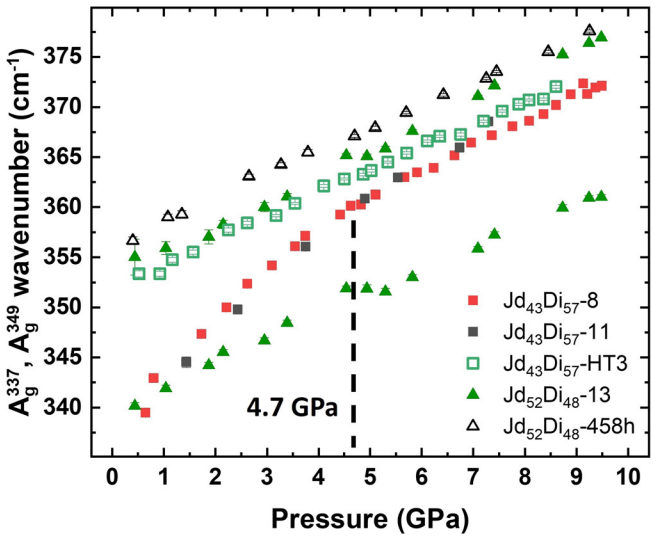

Figure 4 *Pressure dependence of the Raman peaks in the range 335-375 cm^{-1}. For sample $Jd_{43}Di_{57}$ only one peak at 337 cm^{-1} was detected experimentally, with an anomalous behaviour near 4.7 GPa in the ordered crystals. For sample $Jd_{52}Di_{48}$ two peaks were resolved, but an anomaly is still visible. Filled symbols are related to ordered omphacites, while open symbols to disordered ones.*

DISCUSSION

This study represents the first step towards using omphacite inclusions for elastic geothermobarometry via Raman spectroscopy. By knowing the EoS and the composition of the inclusion (determined by EMPA), it is possible to a first approximation to estimate its residual *P* using Raman spectroscopy. To achieve this result, it is essential to study the effects of the chemical composition, *P*, and the cation order. At the current stage, empirical calculations for selected phonon modes can be used for this purpose (see Fig. 3). Once the residual *P* of an omphacite inclusion has been measured, it is necessary to determine the entrapment isomeke. This calculation requires the EoSs of both the host and the inclusion, and the chemical composition plays a crucial role, as it influences the elastic behaviour. In the case of omphacite, for example, Pandolfo et al. (2012a) discussed the compositional dependence of the bulk modulus.

Omphacite-in-garnet is a common host-inclusion system in several geological settings. Due to the greater stiffness of garnet with respect to omphacite, the inclusion undergoes more volume relaxation, generating a

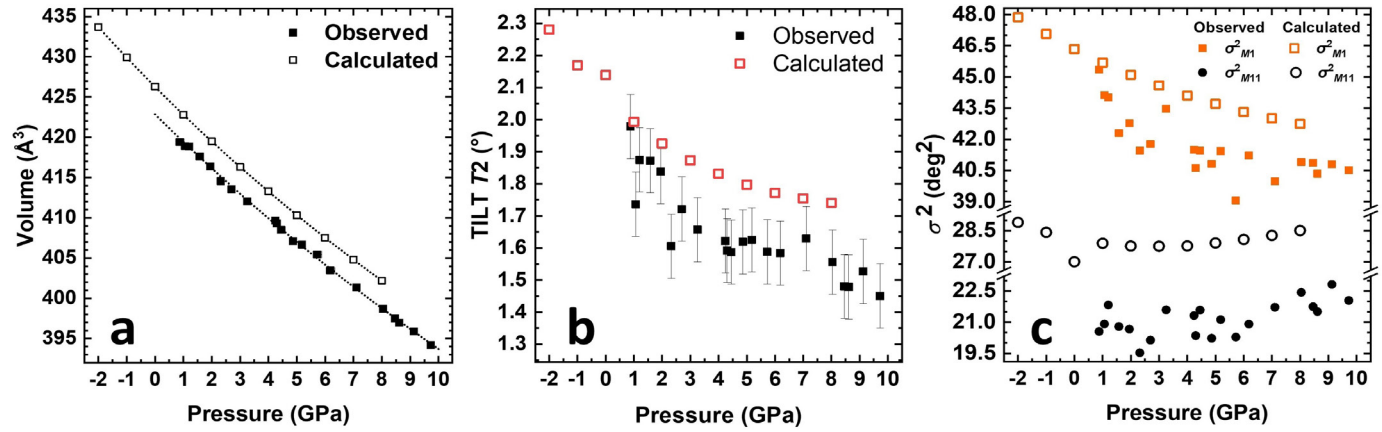

Figure 5 ***a)*** *Pressure evolution of the unit-cell volume of the analysed crystal ($Jd_{43}Di_{57}$) compared with that calculated using HF/DFT methods ($Jd_{50}Di_{50}$).* ***b)*** *Pressure dependence of the TILT angle related to T2; the angle ceases to decrease around 3 GPa.* ***c)*** *Variation of the bond angle variance (σ^2; Robinson et al., 1971) with pressure. The variation is antithetical for the M1 and M11 polyhedra: σ^2_{M1} decreases with pressure, while σ^2_{M11} remains almost constant and starts increasing gradually above 6 GPa. (Baratelli et al., 2025b).*

measurable residual P from which entrapment conditions can be calculated. The isomekes of omphacite resemble those of quartz, making it a potential barometer (Fig. 6). The slope of the isomekes and the phase transition characteristics of the omphacite-in-garnet system offer advantages over quartz- and zircon-in-garnet, expanding the *P-T* range of applicability.

CONCLUSIONS

Omphacite-in-garnet host-inclusion systems could offer important insights in low-*P* and high-*T* geological settings where both quartz and zircon inclusions (among the most used mineral phases in elastic geothermobarometry) in garnet have considerable limitations (Murri et al, 2019; Campomenosi et al., 2022). Omphacite inclusions are particularly valuable in low-silica systems such as metabasites (the main lithotype of eclogites), where quartz is not stable and omphacite becomes a suitable phase for retrieving metamorphic peak conditions.

The use of omphacite inclusions offers a double advantage: they can provide both residual *P* information, through the Raman peak position, and the closure *T*, through the cation ordering phenomenon, which affects the FWHM. The intense Raman peak near 681 cm^{-1} is particularly well-suited for this purpose, as it exhibits a strong *P* dependence, which is not affected by the cation order. Furthermore, HF/DFT calculations indicate that this mode has the highest Raman intensity, ensuring that it can be experimentally detected in any random orientation. Since garnets do not show Raman scattering in this spectral range, this peak is the best candidate to be used for elastic geothermobarometry using omphacite inclusions.

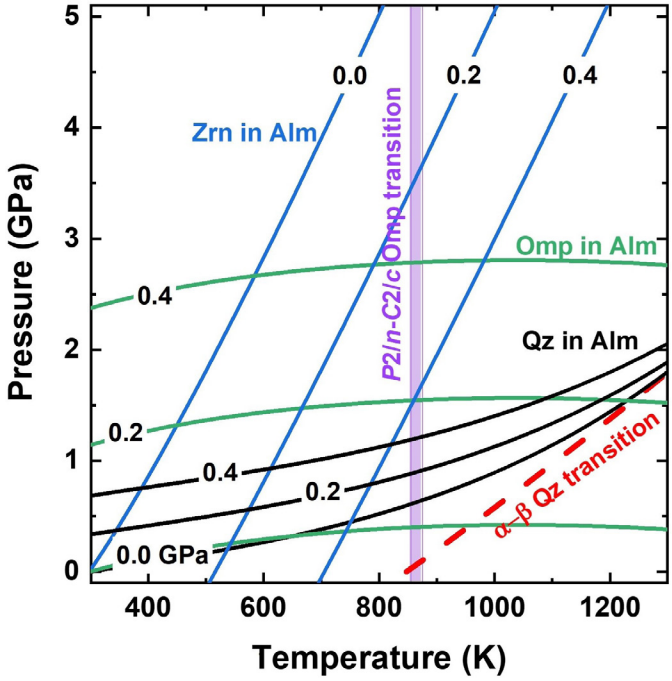

Figure 6 *Calculated isomekes for quartz (Qz), zircon (Zrn) and omphacite (Omp) inclusion in an almandine (Alm) host. The α-β quartz and the P2/n-C2/c omphacite transitions are also represented. Modified after Baratelli et al. (2024).*

REFERENCES

Angel, R.J., Murri, M., Mihailova, B., Alvaro, M. (2019) - Stress, strain and Raman shifts. Z. Krist.-Cryst. Mater., 234, 129-140.

Baratelli, L., Murri, M., Alvaro, M., Prencipe, M., Mihailova, B., Cámara, F. (2024) - Raman scattering of omphacite at high pressure: towards its possible application to elastic geothermobarometry. Am. Mineral., 109, 2105-2115.

Baratelli, L., Murri, M., Alvaro, M., Mihailova, B., Boffa Ballaran, T., Domeneghetti, M.C., Cámara, F. (2025a) - The effect of cation ordering in omphacite on the phonon compressibility: A step towards Raman elastic geothermobarometry. Chem. Geol., 678, 122650.

Baratelli, L., Merlini, M., Nestola, F., Nava, J., Joseph, B., Prencipe, M., Cámara, F. (2025b) - Determination of local geometrical distortions in an ordered omphacite under high pressure. Mineral. Mag., accepted.

Boffa Ballaran, T., Carpenter, M.A., Domeneghetti, M.C., Tazzoli, V. (1998a) – Structural mechanisms of solid solution and cation ordering in augite-jadeite py-

roxenes: I. A macroscopic perspective. Am. Mineral., 83, 419–433.

Boffa Ballaran, T., Carpenter, M.A., Domeneghetti, M.C., Salje, E.K.H., Tazzoli, V. (1998b) - Structural mechanisms of solid solution and cation ordering in augite-jadeite pyroxenes: II. A microscopic perspective. Am. Mineral., 83, 434–443.

Cámara, F. (1995) - Estudio cristalquímico de minerales metamórficos en rocas básicas del complejo Nevado-Filábride (Cordilleras Béticas). PhD thesis, Universidad de Granada, Granada.

Cámara, F., Nieto, F., Oberti, R. (1998) - Effects of Fe^{2+} and Fe^{3+} contents on cation ordering in omphacite. Eur. J. Mineral., 10, 889–906.

Cameron, M., Sueno, S., Prewitt, C.T., Papike, J.J. (1973) - High temperature crystal chemistry of acmite, diopside, hedenbergite, jadeite, spodumene, and ureyite. Am. Mineral., 58, 594–618.

Campomenosi, N., Angel, R.J., Alvaro, M., Mihailova, B. (2022) - Resetting of zircon inclusions in garnet: Implications for elastic thermobarometry. Geology, 51, 23-27.

Dovesi, R., Erba, A., Orlando, R., Zicovich-Wilson, C.M., Civalleri, B., Maschio, L., R'erat, M., Casassa, S., Baima, J., Salustro, S., Kirtman, B. (2018) - Quantum-mechanical condensed matter simulations with CRYSTAL. Wires. Comput. Mol. Sci., 8(4), e1360.

Gilio, M., Angel, R.J., Alvaro, M. (2021) - Elastic geobarometry: how to work with residual inclusion strains and pressures. Am. Mineral., 106, 1530-1533.

Gonzalez-Platas, J., Alvaro, M., Nestola, F., Angel, R.J. (2016) - EosFit7-GUI: a new graphical user interface for equation of state calculations, analyses and teaching. J. Appl. Crystallogr., 49, 1377–1382.

Momma, K. & Izumi, F. (2008) - *VESTA*: a three-dimensional visualization system for electronic and structural analysis. J. Appl. Crystallogr., 41(3), 653-658.

Murri, M., Alvaro, M., Angel, R.J., Prencipe, M., Mihailova, B.D. (2019) - The effects of non-hydrostatic stress on the structure and properties of alpha-quartz. Phys. Chem. Miner., 46, 487-499.

O'Brien, P.J. (1993) - Partially retrograded eclogites of the Munchberg Massif, Germany: records of a multi-stage Variscan uplift history in the Bohemian Massif. J. Metamorph. Geol., 11, 241-260.

Pandolfo, F., Nestola, F., Cámara, F., Domeneghetti, M.C. (2012a) - New thermoelastic parameters of natural C2/c omphacite. Phys. Chem. Miner., 39, 295–304.

Pandolfo, F., Nestola, F., Cámara, F., Domeneghetti, M.C. (2012b) - High-pressure behavior of space group P2/n omphacite. Am. Mineral., 97, 407–414.

Pandolfo, F., Cámara, F., Domeneghetti, M.C., Alvaro, M., Nestola, F., Karato, S.I., Amulele, G. (2015) - Volume thermal expansion along the jadeite–diopside join. Phys. Chem. Miner., 42, 1–14

Robinson, K., Gibbs, G.V., Ribbe, P.H. (1971) - Quadratic Elongation: A Quantitative Measure of Distortion in Coordination Polyhedra. Science, 172, 567-570.

Geochemical study of air quality in areas affected by the addition of anthropogenic and natural contaminants

Rebecca Biagi
Department of Earth Sciences, University of Firenze, Via G. La Pira 4 , 50121, Firenze
DOI: 10.19276/plinius.2025.01.002

INTRODUCTION

Air pollution can be defined as the alteration of the atmosphere's natural balance by introducing chemical, physical, or biological agents, in gaseous, liquid, or solid forms, resulting in health risks and environmental damage. The World Health Organization (WHO) reports that 99% of the global population breathes polluted air, contributing to millions of deaths annually and harming ecosystems (Grantz et al., 2003), crops (Vlachokostas et al., 2010), and biodiversity (Finizio et al., 1998). Air pollution also contributes to climate change through emissions of greenhouse gases (GHGs) and short-lived pollutants (IPCC, 2021).

Monitoring air pollution is complex due to *i)* the variety of sources, both natural (*e.g.*, volcanoes, wildfires, sea spray, wetlands) and anthropogenic activities (mainly in urban and industrial settings), with the latter causing rapid and severe changes, and *ii)* atmospheric processes that affect pollutant dispersion and transformation.

Traditional monitoring methods are accurate but expensive and limited in coverage. Recently, mobile and low-cost air quality stations have emerged as promising alternatives. Mobile stations provide high-resolution spatial data (*e.g.*, Apte et al., 2017; deSouza et al., 2020), while low-cost fixed sensors offer broader deployment (Clements et al., 2017; Spinelle et al., 2017; Sun et al., 2017), though they require careful calibration to ensure data quality (Heimann et al., 2015; Spinelle et al., 2017; Biagi et al., 2024).

This study proposes a combined monitoring strategy using high-tech mobile units and low-cost fixed stations to measure key pollutants (CO_2, CH_4, PM, H_2S, SO_2) and isotopic ratios ($\delta^{13}C$ of CO_2 and CH_4) in areas with overlapping natural and human sources. The method was tested in volcanic, wetland, and urban-industrial environments, demonstrating its potential for improving air quality assessments and supporting climate-related research.

CASE STUDIES: FROM NATURAL TO ANTHROPOGENIC SOURCES

Volcanic-hydrothermal areas

Vulcano Island (hereafter VU) stands as the southernmost subaerial active volcano in the Aeolian Archipelago (Southern Italy). Following the last eruption in 1888–1890 (De Astis et al., 1997) VU has been marked by intense degassing activity with *i)* high-temperature fumaroles (< 400°C after 2016) in the northern part of the La Fossa crater, with the typical composition from active volcanic systems (Nuccio et al., 1999), and *ii)* low-temperature fumaroles (< 100°C) and boiling and bubbling pools in the Baia di Levante area, reflecting the typical compositions of hydrothermal systems (Chiodini et al., 1995; Randazzo et al., 2024).

In September 2021, a new episode of volcanic unrest occurred, peaking at the end of October-early November 2021. The volcanic gas hazard on the island caused some health concerns and led to the interdiction of the crater, as well as that of the Baia di Levante beach (Mayor's ordinance n. 46/2022).

Pozzuoli (Southern Italy; hereafter PZ), located within the Campi Flegrei caldera, is a notable example of dense human settlements coexisting with an active volcanic system. The most recent eruptive activity occurred in 1538 A.D. (Monte Nuovo eruption; Orsi et al., 1996), while bradyseismic crises occurred in 1970–72 and 1982–84, when PZ was affected by a rapid ground inflation, causing uplifts up to 3.5 m (De Vivo et al., 2001). A new phase of unrest and inflation started in 2005 and is still ongoing.

The Campi Flegrei caldera is currently showing intense hydrothermal activity (Caliro et al., 2007), mostly affecting two sites: *i)* the Solfatara Crater, a 1.4 km^2-wide tuff cone produced about 4 ka from a low-magnitude eruption (Isaia et al., 2009), that hosts prominent hydrothermal discharges; *ii)* Pisciarelli, a 0.03 km^2 fault-related hydrothermal area located at the base of the Solfatara cone (approximately 400 m eastward), characterized by

high-flow fumaroles and boiling pools. Weak fumaroles and hydrothermal diffuse emissions also occur along Antiniana Street, a densely urbanized sector of the Campi Flegrei caldera located 1 km south of Pisciarelli, in the Agnano crater, where two wells were drilled for geothermal prospection.

Wetland: Padule di Fucecchio

The Padule di Fucecchio (Central Italy; hereafter FU) is the largest inner wetland (1,800 hectares) in Italy and is included in the list of wetlands of international importance under the Ramsar Convention (Ministerial Decree 303/2013). During the last centuries, the area has undergone significant hydrological changes, mainly due to anthropogenic activities, which modified the natural outflow of water for reclamation purposes (De Martin Mazzalon, 2017) and degraded the quality of the water bodies (ARPAT, 2014).

A ring of small nuclei and rural villages surrounds the FU shores, which are dominated by agricultural practices. Moving northward, the plain exhibits dense urbanization and industrialization characteristics. FU bears the impact of this anthropogenic pressure: among the critical issues are the scarce quantity and quality of water resources in spring and summer seasons, and the hunting management of marsh vegetation, which lead to a frequent manifestation of eutrophication phenomena that negatively influence the maintenance of the wetland (*e.g.*, ARPAT, 2014).

Anthropogenic sources in urban and industrial areas: a CO_2 production plant

A CO_2 production plant was selected near Sant'Albino village (hereafter SA), a residential area of approximately 2,000 inhabitants in southern Tuscany (Central Italy). The area is characterized by the emergence of bubbling pools rich in CO_2, which are fed by the deepest carbonate units hosting water and CO_2 reservoirs (Hernández-Rodríguez et al., 2017). The CO_2 discharges from these bubbling pools have been estimated at up to 100 tons day^{-1} of CO_2, while the rate of CO_2 extracted by the facility is 96 tons day^{-1} (Frondini et al., 2008; Hernández-Rodríguez et al., 2017).

From February 21 to March 12, 2023, an extraordinarily high-flux discharge activity of unfiltered CO_2 and H_2S-dominated gas was released from two chimneys of the plant, during exceptional maintenance of the waste gas cleaning apparatus, to assess the potential impact of unusual emissions on the local inhabitants.

MATERIALS AND METHODS

Mobile monitoring

CO_2, CH_4, H_2S, and SO_2 concentrations, and $\delta^{13}C_{CO_2}$ and $\delta^{13}C_{CH_4}$ values, were measured along transects within the study areas using a mobile station hosting high-tech instruments (S-volatile species were not measured at FU), following a well-established strategy to evaluate the spatial distribution of air contaminants in areas with natural (Cabassi et al., 2017) and/or anthropogenic (Vaselli et al., 2013) emissions.

The CO_2 and CH_4 concentrations, and the $\delta^{13}C_{CO_2}$ and $\delta^{13}C_{CH_4}$ values, were measured by Wavelength-Scanned Cavity Ring-Down Spectroscopy using a Picarro G2201-i analyzer. The operating interval ranged from 380 to 2,000 ppm for CO_2, and from 1.80 to 15.0 ppm for CH_4. Calibration was performed at the beginning of each measuring period. The precision was within 0.2 ppm (CO_2), 0.05 ppm (CH_4), 0.16‰ vs. V-PDB ($\delta^{13}C_{CO_2}$), and 1.15‰ vs. V-PDB ($\delta^{13}C_{CH_4}$). A copper-shavings trap was installed at the analyzer inlet port when H_2S concentrations above background values were expected (*i.e.*, VU, PZ, and SA) to minimize spectral interferences, which may result in significant depletion in ^{13}C (Malowany et al., 2015).

The H_2S and SO_2 concentrations were measured by Pulsed Fluorescence using a Thermo 450i analyzer. The instrument, which operates in the range 1-15,000 ppb, was calibrated at the beginning of the measuring periods. The precision was within ±1%.

Both instruments were housed in the back of a car moving at an average speed of ~30 km h^{-1}. Air was drawn through vacuum pumps with sampling rates of 25 mL min^{-1} and 70 mL min^{-1} for the Picarro and the Thermo devices, respectively, through 1.5 m long silicon tubes (3 mm diameters) installed on the top of the vehicle (ca. 1.80 m from the ground) to avoid the interference of exhausting gases. The Geo Tracker application, available for Android devices, was used to relate the measured parameters to the location.

The transects were selected by considering the nature and location of potential contaminant sources.

Fixed monitoring

Monitoring surveys at fixed sites were performed using low-cost multiparametric stations developed by the Department of Earth Sciences of the University of Florence (Biagi et al., 2024).

At VU, PZ, and SA, they were equipped with: *i)* a non-dispersive infrared CO_2 sensor (Sensirion SCD30); *ii)* an optical laser counting sensor for $PM_{2.5}$ and PM_{10} (Nova Fitness SDS011); and *iii)* a thermistor and a capacitive humidity sensor for T and RH, respectively (Adafruit DHT22). At FU, metal oxide semiconductor sensors for CH_4 (Figaro NGM2611-E13) were integrated, as CH_4 is one of the primary GHGs emitted by wetlands.

The CO_2 and CH_4 sensors were calibrated with a machine-learning algorithm, according to the procedure

described by Biagi et al. (2024), providing measurements with mean absolute errors < 4 ppm and < 0.03 ppm for CO_2 and CH_4, respectively. Regarding PM concentrations, several studies demonstrated generally reliable performances of this sensor compared to reference instruments (*e.g.*, Božilov et al., 2022), with very low inter-unit variability (Brugnone et al., 2024; Tagle et al., 2020). To assess the repeatability of the $PM_{2.5}$ and PM_{10} measurements across sensors, an Intraclass Correlation Coefficient (ICC) analysis was performed, obtaining excellent sensor concordance with values of 0.983 for $PM_{2.5}$ and 0.966 for PM_{10}.

The low-cost multiparametric stations were fixed at 1.5 m height, corresponding to the average breathing height of standing humans. The number of monitoring sites and their location were commensurate with the extension of the study areas and the presence of potential sources.

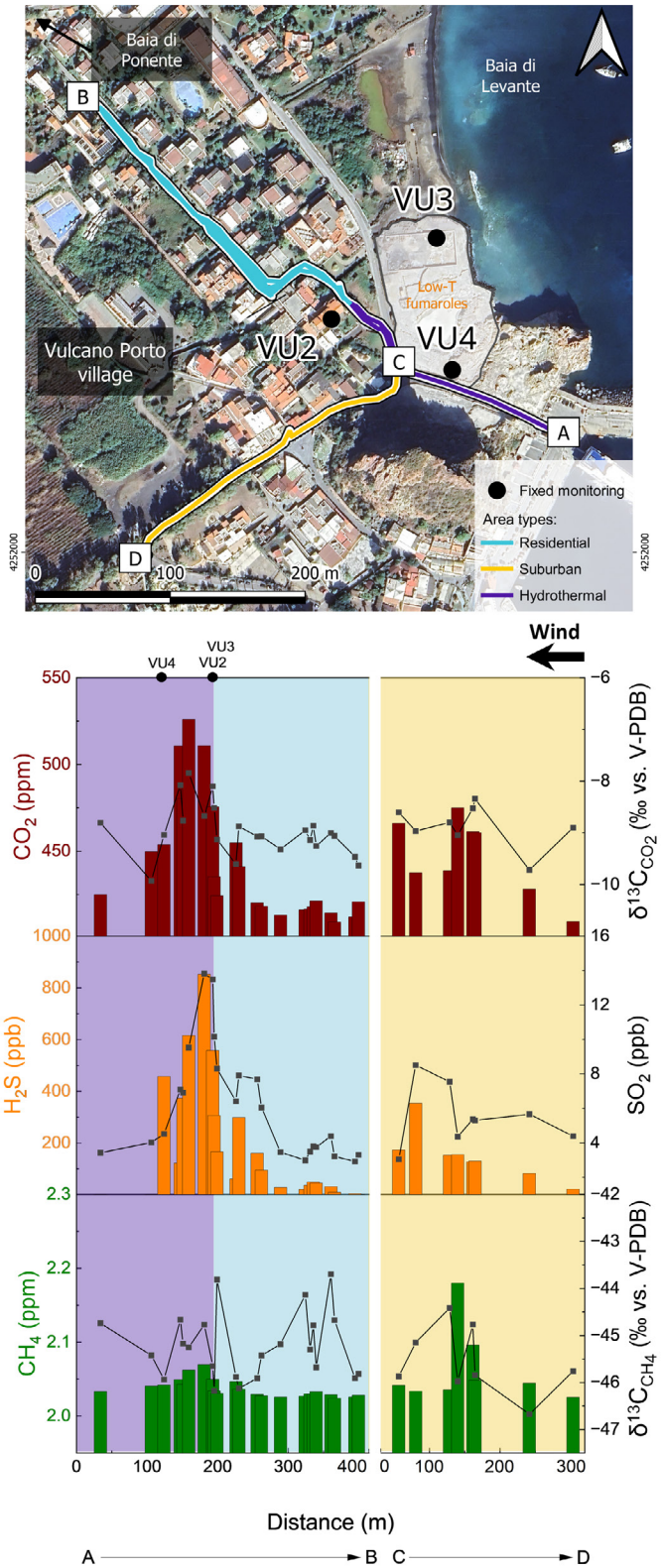

*Figure 1 Spatial distribution of CO_2, H_2S, and CH_4 concentrations (bars) and $\delta^{13}C_{CO_2}$, SO_2, and $\delta^{13}C_{CH_4}$ values (line + scatter) along the VU study area (**a,b** and **c,d**), plotted against the distance from the starting point (x-axis). Colored sections on the map and plot represent different area types (i.e., residential, suburban, and hydrothermal). Fixed monitoring sites (VU2-4), wind direction, and low-T fumaroles are also shown.*

RESULTS AND DISCUSSION

The proposed monitoring strategy yielded a high-resolution dataset (1 data point per minute), comprising approximately 1,150,000 data points from fixed monitoring and 1,100 data points from mobile monitoring.

Vulcano Island (VU)

At VU, mobile monitoring revealed significant short-distance variations in atmospheric CO_2 concentrations, reaching up to 536 ppm near the hydrothermal emissions in the Baia di Levante (Fig. 1). None of the measured CO_2 levels posed health risks based on short-term (NIOSH, 2014), occupational (OSHA, 2024), or chronic exposure standards (Martrette et al., 2017).

H_2S levels peaked at 882 ppb along the same transect, following a similar trend as CO_2 (Fig. 1). Though H_2S concentrations decreased away from the source, they remained above the 10-ppb odor threshold (WHO, 2003). However, they were well below levels associated with health impacts (≥ 90 ppb) (Batterman et al., 2023).

Isotopic analysis and theoretical mixing models (Keeling plot; Keeling, 1961) confirmed that the primary source of CO_2 and H_2S was related to the hydrothermal emissions of the Baia di Levante, although some CO_2 enrichment suggested minor anthropogenic contributions, likely from fossil fuel combustion (Fig. 2a, b). A strong correlation between H_2S and SO_2 supported oxidation-driven transformations in the air (Pearson's r: 0.84).

CH_4 concentrations (2.02–2.18 ppm) mirrored the spatial patterns of CO_2 and H_2S, likely indicating their common hydrothermal origin (Fig. 1). However, isotopic data did not clearly identify the signature of the CH_4 source (Fig. 2c), and a few CH_4 anomalies indicated possible unidentified anthropogenic contributions (Fig. 2d).

Fixed-site monitoring, combined with wind direction data, further helped in identifying the main sources of CO_2 and PM in the monitored sites. At Baia di Levante (VU2, VU3, VU4; Fig. 1), CO_2 concentrations (up to 835 ppm) were linked to specific wind patterns from the hydrothermal emissions. $PM_{2.5}$ and PM_{10} data exhibited complex behaviors, indicating both hydrothermal and

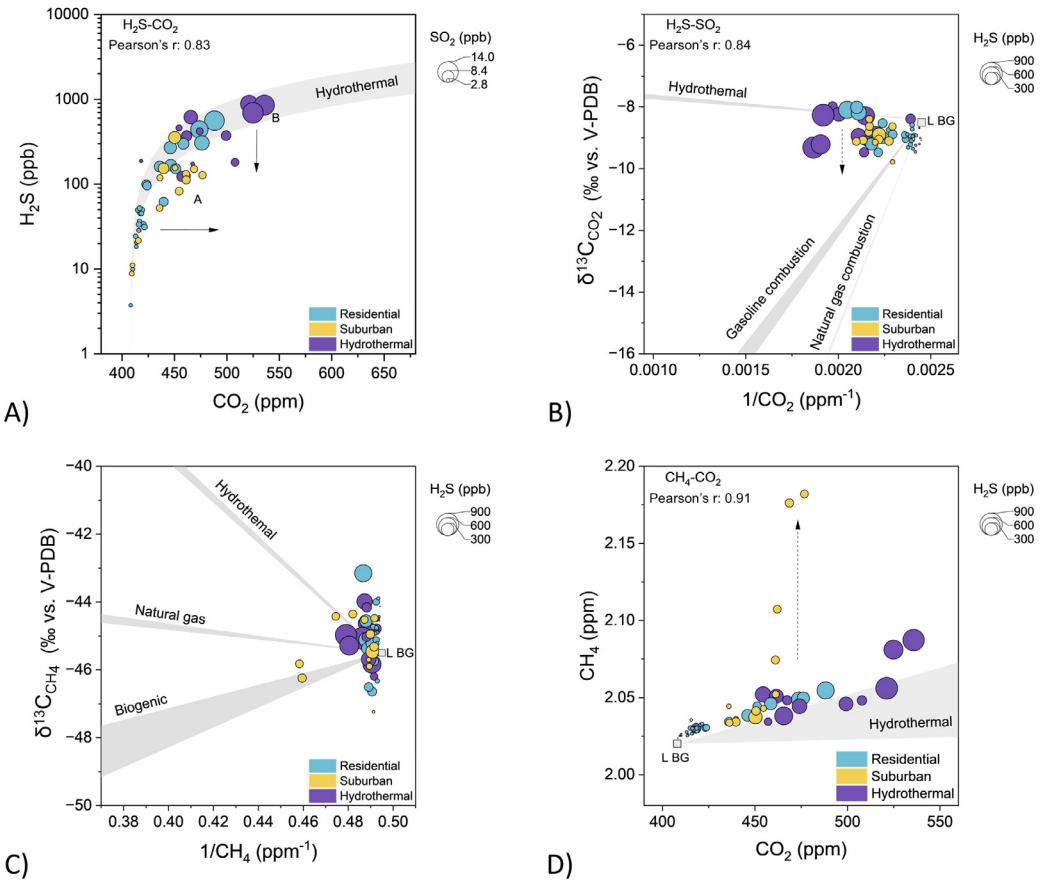

Figure 2 a) *H_2S vs. CO_2 diagram.* ***b)*** *CO_2 and* ***c)*** *CH_4 Keeling plots.* ***d)*** *CH_4 vs. CO_2 diagram. Symbol size is proportional to* ***(a)*** *SO_2 concentration and* ***(b-d)*** *H_2S concentration. Symbol colors represent the area types (i.e., residential, suburban, and hydrothermal). Gray fields represent mixing trends with theoretical sources. L BG is the chemical and isotopic composition of the local background.*

anthropogenic origins. Particularly, $PM_{2.5}$ was more often associated with hydrothermal sources, while PM_{10} appeared to be influenced by local human activities in Vulcano Porto.

Pozzuoli (PZ)

Mobile monitoring in the PZ study area revealed higher CO_2 concentrations in hydrothermal (up to 798 ppm) and urban/industrial sectors (up to 546 ppm), while values in suburban and residential zones remained closer to the 2022 global background average (~418 ppm).

H_2S concentrations were higher in hydrothermal areas (up to 364 ppb), but NE winds occasionally transported it into suburban (up to 29 ppb) and residential (up to 82 ppb) sectors. These findings indicate that hydrothermal gases can affect air quality over distances greater than 2 km from the major emission sites of La Solfatara, Pisciarelli, and Antiniana Street.

A common hydrothermal origin for CO_2 and H_2S was confirmed by mixing trends consistent with emissions from La Solfatara and Pisciarelli. However, observed CO_2 enrichments resulted from *i)* anthropogenic input (which led to lighter $\delta^{13}C_{CO_2}$ without a corresponding increase in H_2S concentrations), and/or *ii)* depletion of H_2S due to oxidation to SO_2, supported by a strong correlation between the two S-species (Pearson's r = 0.85).

CH_4 showed modest spatial variability with peaks up to 2.25 ppm, particularly in suburban areas, but lacked a clear spatial pattern. Isotopic signatures ($\delta^{13}C_{CH_4}$) and bivariate analyses suggest multiple sources (including hydrothermal, natural gas, and biogenic inputs), as well as the influence of atmospheric oxidation.

At fixed monitoring sites, CO_2 accumulation occurred primarily under low wind conditions, with directional wind analyses indicating both hydrothermal and anthropogenic influences depending on location. Particulate matter (PM) levels varied across sites, with $PM_{2.5}$ occasionally exceeding long-term WHO exposure limits (5 $\mu g\ m^{-3}$), particularly under stable atmospheric conditions and traffic influence.

While CO_2 and PM levels did not indicate immediate health risks, H_2S concentrations in a car dealership and a nursing home warrant concern due to chronic exposure risks. Estimated H_2S levels, based on H_2S/CO_2 ratios measured during the mobile monitoring, reached 49 ppb and 292 ppb, respectively, the latter representing a potential health risk for vulnerable populations.

Padule di Fucecchio (FU)

Mobile monitoring in FU showed nearly constant CO_2 concentrations (~420 ppm), while CH_4 levels decreased along the transect. The $\delta^{13}C_{CO_2}$ and $\delta^{13}C_{CH_4}$ values of a potential end-member computed using the Keeling plots analysis indicated a common biogenic source for both CO_2 (-25.5‰ vs. V-PDB) and CH_4 (-67.7‰ vs. V-PDB), consistent with microbial activity in anaerobic soil and wetland environments.

At nine fixed monitoring sites, clear diurnal cycles related to the Planetary Boundary Layer dynamics were observed: higher concentrations at night/morning un-

der stable conditions and lower values in the afternoon. Wetland sites showed greater CO_2 and CH_4 due to biogenic emissions, while upstream rural sites had lower and more stable levels. Notably, constantly higher CH_4 concentrations (2.60 ppm on average) were observed at one site inside the wetland across nearly all wind directions, likely due to the presence of several canals where eutrophic conditions may have enhanced CH_4 production.

Particulate matter showed a different distribution: $PM_{2.5}$ was higher in urban zones and transported upstream by wind, while PM_{10} was higher in the downstream wetland sites. Notably, long-term exposure thresholds for $PM_{2.5}$ were consistently exceeded at two sites, indicating a need for continued monitoring in these areas.

The CO_2 production plant (SA)

At SA, three monitoring campaigns evaluated air quality impacts from the CO_2 production plant under different operational conditions: FLD (filtered low-discharge) and UHD (unfiltered high-discharge).

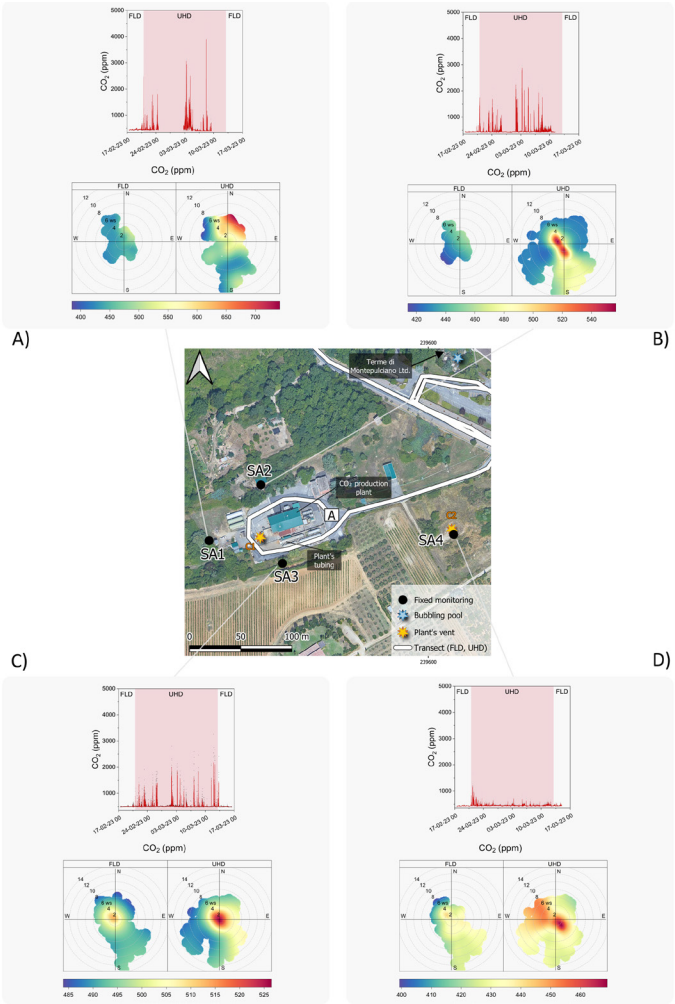

*Figure 3 Time series of CO_2 concentrations (1-minute average black point; 5-minute rolling mean red line), along with polar plots of CO_2 10-minute averaged concentrations (represented by different colors) at SA1 **(a)**, SA2 **(b)**, SA3 **(c)**, and SA4 **(d)**, divided into FLD and UHD conditions. The pink areas in the time series are the periods under UHD conditions. Fixed monitoring sites, bubbling pools, and the main plant's emitting vents (C1 and C2) are also shown.*

Under FLD conditions, CO_2 and CH_4 concentrations were generally higher in suburban and residential areas of SA, rather than near the plant, with peaks up to 495 ppm (CO_2) and 2.33 ppm (CH_4). Near the plant, levels were close to background (404 ppm CO_2, 2.02 ppm CH_4), suggesting minimal plant influence under standard operations. Instead, vehicular traffic and domestic heating in the village were likely the main contributors of CO_2 and CH_4 based on their $\delta^{13}C$ values, with a minor geogenic signal near a local bubbling pool. H_2S levels were negligible, indicating no detectable emissions from the plant under normal operation.

Under UHD conditions, a strong, localized gas anomaly was detected near the plant, with concentrations of CO_2 up to 2,000 ppm, CH_4 up to 10.5 ppm, H_2S up to 95.3 ppb, and SO_2 up to 3.44 ppb, with $\delta^{13}C$ values indicating a geogenic gas source. However, these values rapidly decreased with distance due to dilution and H_2S oxidation. Outside the immediate area, gas levels remained low with $\delta^{13}C$ values compatible with anthropogenic emissions.

At fixed sites, the three closest to the plant (SA1–SA3; Fig. 3a-c) showed CO_2 peaks under UHD conditions, especially in the early morning, matching reported gas discharge times. Site SA3 (Fig. 3c) showed elevated CO_2 even under FLD, possibly due to a local leak from plant tubing. Conversely, more distant sites (SA4 and SA5; Figs. 3d and 4, respectively) had stable CO_2 levels (~440 ppm).

$PM_{2.5}$ and PM_{10} concentrations were higher under UHD, especially near the plant, likely due to secondary particle formation from geogenic emissions. However, PM was often higher in the village (SA5) than near the plant, suggesting a stronger influence from domestic and traffic-related sources. WHO thresholds for $PM_{2.5}$ and PM_{10} were exceeded in both periods at certain sites, especially SA5.

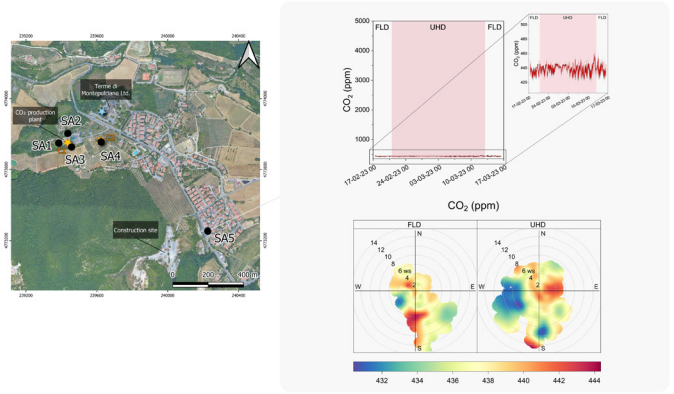

Figure 4 Time series of CO_2 concentrations (1-minute average black point; 5-minute rolling mean red line), along with polar plots of CO_2 10-minute averaged concentrations (represented by different colors) at SA5 divided into FLD and UHD conditions. The pink areas in the time series are the periods under UHD conditions. Fixed monitoring sites, bubbling pools, and the main plant's emitting vents (C1 and C2) are also shown.

Wind analysis showed that high CO_2 and PM concentrations at SA1–SA4 under UHD were associated with low wind speeds and downwind conditions from the plant, confirming plant emissions. However, at SA5, CO_2 and PM patterns did not differ between UHD and FLD, confirming local non-plant sources (*e.g.*, traffic, domestic heating, and a nearby construction site).

CONCLUSIONS

This study demonstrates that combining low-cost fixed stations with high-tech mobile systems offers an effective, adaptable, and affordable approach to air quality monitoring across diverse environments, including volcanic, wetland, urban, and industrial areas.

Fixed stations enabled continuous tracking of pollutants like CO_2, CH_4, $PM_{2.5}$, and PM_{10}, capturing variability due to weather and emission sources. Their affordability and improved calibration allowed for denser networks and better spatial resolution, especially in underserved regions. Mobile systems complemented this with broader spatial coverage and detailed source identification using isotopic analysis.

While challenges remain, such as limited long-term sensor calibration and the labor-intensive nature of mobile surveys, the integrated approach enhances monitoring capabilities, supports research and policy, and is suitable for citizen science. Its scalability makes it ideal for at-risk areas, with future potential for drone integration to access hazardous or hard-to-reach sites.

REFERENCES

Apte, J.S., Messier, K.P., Gani, S., Brauer, M., Kirchstetter, T.W., Lunden, M.M., Marshall, J.D., Portier, C.J., Vermeulen, R.C.H., Hamburg, S.P. (2017) - High-Resolution Air Pollution Mapping with Google Street View Cars: Exploiting Big Data. Environ. Sci. Technol., 51, 6999–7008.

ARPAT (2014) - Valutazione della qualità ambientale del Padule di Fucecchio Aggiornamento 2013 Report ARPAT Dipartimento provinciale ARPAT di Pistoia.

Avnery, S., Mauzerall, D.L., Liu, J., Horowitz, L.W. (2011) - Global crop yield reductions due to surface ozone exposure: 1. Year 2000 crop production losses and economic damage. Atmos. Environ., 45, 2284–2296.

Batterman, S., Grant-Alfieri, A., Seo, S.-H. (2023) - Low level exposure to hydrogen sulfide: a review of emissions, community exposure, health effects, and exposure guidelines. Crit. Rev. Toxicol., 53, 244–295.

Biagi, R., Ferrari, M., Venturi, S., Sacco, M., Montegrossi, G., Tassi, F. (2024) - Development and machine learning-based calibration of low-cost multiparametric stations for the measurement of CO_2 and CH_4 in air. Heliyon, 10.

Božilov, A., Tasić, V., Živković, N., Lazović, I., Blagojević, M., Mišić, N., Topalović, D. (2022) - Performance assessment of NOVA SDS011 low-cost PM sensor in various microenvironments. Environ. Monit. Assess., 194, 595.

Brugnone, F., Randazzo, L., Calabrese, S. (2024) - Use of Low-Cost Sensors to Study Atmospheric Particulate Matter Concentrations: Limitations and Benefits Discussed through the Analysis of Three Case Studies in Palermo, Sicily. Sensors, 24, 6621.

Cabassi, J., Tassi, F., Venturi, S., Calabrese, S., Capecchiacci, F., D'Alessandro, W., Vaselli, O. (2017) - A new approach for the measurement of gaseous elemental mercury (GEM) and H_2S in air from anthropogenic and natural sources: Examples from Mt. Amiata (Siena, Central Italy) and Solfatara Crater (Campi Flegrei, Southern Italy). J. Geochem. Explor., 175, 48–58.

Caliro, S., Chiodini, G., Moretti, R., Avino, R., Granieri, D., Russo, M., Fiebig, J. (2007) - The origin of the fumaroles of La Solfatara (Campi Flegrei, South Italy). Geochim. Cosmochim. Acta, 71, 3040–3055.

Chiodini, G., Cioni, R., Marini, L., Panichi, C. (1995) - Origin of the fumarolic fluids of Vulcano Island, Italy and implications for volcanic surveillance. Bull. Volcanol., 57, 99–110.

Clements, A.L., Griswold, W.G., Abhijit, R.S., Johnston, J.E., Herting, M.M., Thorson, J., Collier-Oxandale, A., Hannigan, M. (2017) - Low-cost air quality monitoring tools: From research to practice (A workshop summary). Sensors (Switzerland).

De Astis, G., La Volpe, L., Peccerillo, A., Civetta, L. (1997) - Volcanological and petrological evolution of Vulcano island (Aeolian Arc, southern Tyrrhenian Sea). J. Geophys. Res. Solid Earth, 102, 8021–8050.

De Martin Mazzalon, M. (2017) - Inquadramento idrogeologico del Padule di Fucecchio. In: "Guida del Padule di Fucecchio. Natura, storia, tradizioni, itinerari. Quaderni del Padule di Fucecchio N.8.", A. Bartolini, G. Calvetti, L. Candiani, M. De Martin Mazzalon, A. Lucci, A. Malvolti, E. Zarri, eds. Centro di Ricerca, Documentazione e Promozione del Padule di Fucecchio.

De Vivo, B., Rolandi, G., Gans, P.B., Calvert, A., Bohrson, W.A., Spera, F.J., Belkin, H.E. (2001) - New constraints on the pyroclastic eruptive history of the Campanian volcanic Plain (Italy). Miner. Petrol., 73, 47-65.

deSouza, P., Anjomshoaa, A., Duarte, F., Kahn, R., Kumar, P., Ratti, C. (2020) - Air quality monitoring using mobile low-cost sensors mounted on trash-trucks: Methods development and lessons learned. Sustain. Cities Soc., 60, 102239.

Finizio, A., Di Guardo, A., Cartmale, L. (1998) - Hazardous Air Pollutants (HAPs) and their Effects on Biodiversity: An Overview of the Atmospheric Pathways of Persistent Organic Pollutants (POPs) and Suggestions for Future Studies. Environ. Monit. Assess., 49, 327–336.

Frondini, F., Caliro, S., Cardellini, C., Chiodini, G., Morgantini, N., Parello, F. (2008) - Carbon dioxide degassing from Tuscany and Northern Latium (Italy). Global Planet. Change, 61, 89–102.

Grantz, D.A., Garner, J.H.B., Johnson, D.W. (2003) - Ecological effects of particulate matter. Environ. Int., 29, 213-239.

Heimann, I., Bright, V.B., McLeod, M.W., Mead, M.I., Popoola, O.A.M., Stewart, G.B., Jones, R.L. (2015) - Source attribution of air pollution by spatial scale separation using high spatial density networks of low cost air quality sensors. Atmos. Environ., 113, 10–19.

Hernández-Rodríguez, A., Montegrossi, G., Huet, B., Vaselli, O., Virgili, G. (2017) - A study of wellbore cement alteration controlled by CO_2 leakage in a natural analogue for geological CO_2 storage. Appl. Geochem., 86, 13–25.

IPCC (2021) - Climate Change 2021: The Physical Science Basis. Cambridge University Press.

Isaia, R., Marianelli, P., Sbrana, A. (2009) - Caldera unrest prior to intense volcanism in Campi Flegrei (Italy) at 4.0 ka B.P.: Implications for caldera dynamics and future eruptive scenarios. Geophys. Res. Lett., 36.

Keeling, C.D. (1961) - The concentration and isotopic abundances of carbon dioxide in rural and marine air. Geochim. Cosmochim. Acta, 24, 277–298.

Malowany, K., Stix, J., Van Pelt, A., Lucic, G. (2015) - H_2S interference on CO_2 isotopic measurements using a Picarro G1101-i cavity ring-down spectrometer. Atmos. Meas. Tech., 8, 4075–4082.

Martrette, J.M., Egloff, C., Clément, C., Yasukawa, K., Thornton, S.N., Trabalon, M. (2017) - Effects of prolonged exposure to CO_2 on behaviour, hormone secretion and respiratory muscles in young female rats. Physiol. Behav., 177, 257–262.

NIOSH (2014) - Carbon dioxide [WWW Document]. URL: https://www.cdc.gov/niosh/idlh/124389.html#print (accessed 1.8.25).

Nuccio, P.M., Paonita, A., Sortino, F. (1999) - Geochemical modeling of mixing between magmatic and hydrothermal gases: the case of Vulcano Island, Italy. Earth Planet. Sci. Lett., 167, 321–333.

Orsi, G., De Vita, S., Di Vito, M. (1996) - The restless, resurgent Campi Flegrei nested caldera (Italy): constraints on its evolution and configuration. J. Volcanol. Geoth. Res., 74, 179-214.

OSHA (2024) - CARBON DIOXIDE [WWW Document]. URL: https://www.osha.gov/chemicaldata/183 (accessed 11.15.24).

Randazzo, A., Venturi, S., Tassi, F. (2024) - Soil processes modify the composition of volatile organic compounds (VOCs) from CO_2- and CH_4-dominated geogenic and landfill gases: A comprehensive study. Sci. Total Environ., 923.

Schulze, E.-D. (1989) - Air Pollution and Forest Decline in a Spruce (Picea abies) Forest. Science, 244, 776–783.

Spinelle, L., Gerboles, M., Villani, M.G., Aleixandre, M., Bonavitacola, F. (2017) - Field calibration of a cluster of low-cost commercially available sensors for air quality monitoring. Part B: NO, CO and CO_2. Sens. Actuators B Chem., 238, 706–715.

Sun, L., Westerdahl, D., Ning, Z. (2017) - Development and evaluation of a novel and cost-effective approach for low-cost NO2 sensor drift correction. Sensors (Switzerland), 17.

Tagle, M., Rojas, F., Reyes, F., Vásquez, Y., Hallgren, F., Lindén, J., Kolev, D., Watne, Å.K., Oyola, P. (2020) - Field performance of a low-cost sensor in the monitoring of particulate matter in Santiago, Chile. Environ. Monit. Assess., 192.

Van Dingenen, R., Dentener, F.J., Raes, F., Krol, M.C., Emberson, L., Cofala, J. (2009) - The global impact of ozone on agricultural crop yields under current and future air quality legislation. Atmos. Environ., 43, 604–618.

Vaselli, O., Higueras, P., Nisi, B., María Esbrí, J., Cabassi, J., Martínez-Coronado, A., Tassi, F., Rappuoli, D. (2013) - Distribution of gaseous Hg in the Mercury mining district of Mt. Amiata (Central Italy): A geochemical survey prior the reclamation project. Environ. Res., 125, 179–187.

Vlachokostas, Ch., Nastis, S.A., Achillas, Ch., Kalogeropoulos, K., Karmiris, I., Moussiopoulos, N., Chourdakis, E., Banias, G., Limperi, N. (2010) - Economic damages of ozone air pollution to crops using combined air quality and GIS modelling. Atmos. Environ., 44, 3352–3361.

WHO (2003) - Hydrogen sulfide: human health aspects. World Health Organization, Geneva.

Quantitative Mineralogy: novel approaches for sorting and recycling Construction and Demolition Waste (CDW)

Andrea Bisciotti
Department of Physics and Earth Science, University of Ferrara, Via Giuseppe Saragat 1, 44121, Ferrara
DOI: 10.19276/plinius.2025.01.003

INTRODUCTION

Globally, the building and construction sector represents the single most important source of mineral resource consumption. After drinkable water, concrete is the most used material worldwide, with three tons used annually per person on earth (Gagg, 2014). The primary source of angular sand for concrete production is river deposits and quarry mining, accounting for the largest share of globally extracted mineral resources, ranging from 32 to 50 Gt annually, surpassing even fossil fuel extraction (Torres et al., 2017). Additionally, at the end of their life cycle, construction and demolition waste (CDW) continues to represent a burden to the environment, accounting for 35% of global waste disposed of in landfills (Caro et al., 2024). The average CDW composition includes mainly natural sand and rocks, cement and concrete, metal, plastic, wood, ceramic and glass, all materials with high potential recycling rate.

The most common and simplest way to reuse CDW is to convert the inorganic mineral fraction into recycled aggregates, which could replace natural aggregates in the production of concrete, mortars, and plasters. In this recycling process, the first stage is the acceptance and pre-sorting audit, in which the CDW is weighed and visually inspected upon arrival. Only specific waste types are accepted, based on their composition according to the European Waste Code classification (CER). Large and unwanted items, such as hazardous materials or oversized debris, are removed manually to avoid damaging the processing equipment. Afterwards, industrial magnets are commonly adopted together with clamshell buckets in order to separate metal components, mostly resulting from the concrete rebars. The second and most crucial recycling step is the crushing stage using either jaw or impact crushers, which is typically followed by sieving.

The size reduction and sieving are focused on maximizing the yield of the coarse fraction (< 40 mm) to decrease the production of fines (> 4 mm) that are later difficult to valorize (Whittaker et al., 2021). Afterwards, in the Italian framework, each produced batch of secondary raw material (3000 m^3) must undergo leaching tests to evaluate compliance with the "End of Waste" decree no. 127/2024. The UNI 20802 standard and the method specified by the UNI EN 12457-2 are used for the determination of these values.

Nowadays, recycled aggregates are mostly devoted to sub-bases and bases of pavements of roads and highways, employed in unbound layers, often deemed as down-cycling. As a matter of fact, the lack of their recycling in high-grade applications, called up-cycling, comes from the composite and mixed composition that results from poor sorting practices (Wu et al., 2019).

To overcome this challenge, this work, which summarizes the outcomes of a doctoral thesis, introduces a pipeline for the 4.0 green transition of the sector, starting from an automated "End-of-Waste" certification protocol powered by machine learning predictions. Additionally, it explores CDW sorting using optical sensors and computer vision. Then, a novel method for quality control of recycled aggregates using X-ray Powder Diffraction is presented. The aim is to introduce cutting-edge innovations that could be upscale to support the circularity of the construction sector, minimizing its environmental impact.

MATERIALS AND METHODS

The samples of CDW are collected from stockpiles of landfilled materials in authorized recycling facilities in Ferrara (Italy). The procedure follows the guidelines in standard UNI-EN 932–1, 1997. For each material, 20 kg are collected, homogenized and decreased using a quartering process according to UNI-EN 932–2, 1999. Samples are labeled and divided into three main groups: ceramic (CER), which includes samples of brick, porcelain, tile, stoneware and roof tile. Concrete (CON), and lastly, mixed waste (MRA), comprise the CER samples mixed with the CON sample in a 1:1 ratio.

Geochemical analysis

Bulk major and trace (Ba, Co, Cr, Cu, Ga, Ni, Sc, V, and Zn) element concentrations are determined by wavelength-dispersive X-ray fluorescence spectrometry (XRF) on pressed powder pellets using an ARL Advant-XP+ spectrometer. The leaching test follows the protocol modified from UNI EN 12457-Part 2 (2004) and reported in Bianchini et al. (2020).

Mineralogical analysis

The X-ray Powder Diffraction (XRPD) are collected in the 2θ range of 3-90° at room temperature at each 0.02 step (θ) for a time of 2 or 3 seconds, depending on the expected resolution. The setting used is a fixed irradiated length mode, where the slit width is automatically adjusted to maintain a constant irradiated length of 15 mm. The instrument used within the present thesis is a Bruker D8 Advance Da Vinci. Phase identification was carried out with DIFFRACT.EVA v. 6.0 suite utilizing the Powder Diffraction File (PDF-2) database maintained by the International Centre for Diffraction Data (ICDD).

Machine learning

The leaching prediction modeling is executed using the PyTorch library (version 2.0.0) in the Python environment (version 3.10.10). The pipeline follows those of previous neural network-based studies (Song et al., 2020). A simple neural network architecture with a single hidden layer of four neurons is adopted for modeling. Functional layers—batch normalization followed by rectified linear unit nonlinear activation are added before and after the hidden layer (Bisciotti et al., 2025).

The advanced-sorting of CDW based on optical sensors and computer vision instead relies on convolutional neural networks using ResNet-18. The model training is driven by minimizing the mean squared error (MSE) loss between the predicted values and measured ones. A transfer learning approach is then followed (Bisciotti et al., 2024).

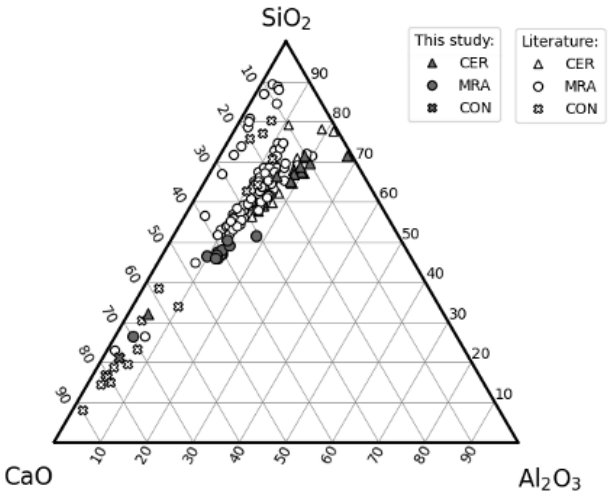

Figure 1 Triplot for the XRF major oxides composition (reproduced from Bisciotti et al., 2025).

RESULTS

Automated Prediction of Leaching Concentrations

The XRF analysis of the CDW of this study displays a considerable degree of variability in major oxides composition. Positive or negative correlations between oxides in binary diagrams indicate the dominant mineralogy of the CDW materials (Bisciotti et al., 2023). The CER samples are primarily silicate-based (SiO_2: 50–70 wt.%), whereas the CON samples have a calcium-based chemical structure (CaO: 35–50 wt.%), resulting from Portland cement binders, lime, and gypsum. The MRA samples are clustered between these two end-members (Fig. 1).

It is known that the release of potential contaminant elements is inversely proportional to the granulometry of materials. Therefore, the worst-case scenario is taken to assess the maximum potential release of chemical species. Fine powder (< 100 μm) of CDW samples is subjected to 24-h leaching tests while pH and temperature are monitored.

The results for CER samples show the highest levels of V and SO_4, whereas CON samples have high Cr. A different scenario occurs in the MRA compared to the pure CER environment. Due to higher alkaline pH (from CON interaction), the mobility of the leachates is influenced and the actual release of these elements is lower.

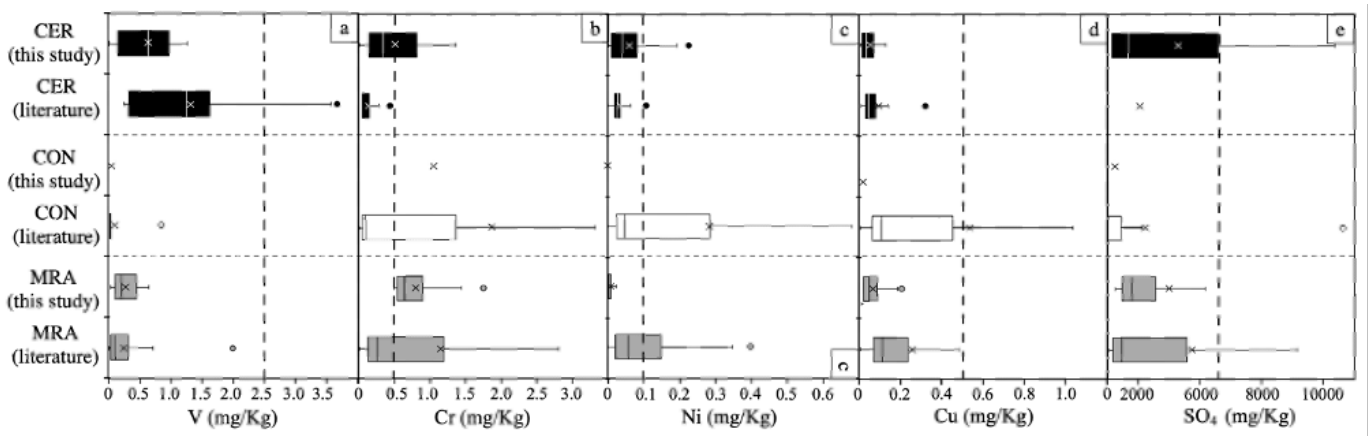

Figure 2 Leaching values (mg/Kg) of selected chemical elements and species (reproduced from Bisciotti et al., 2025).

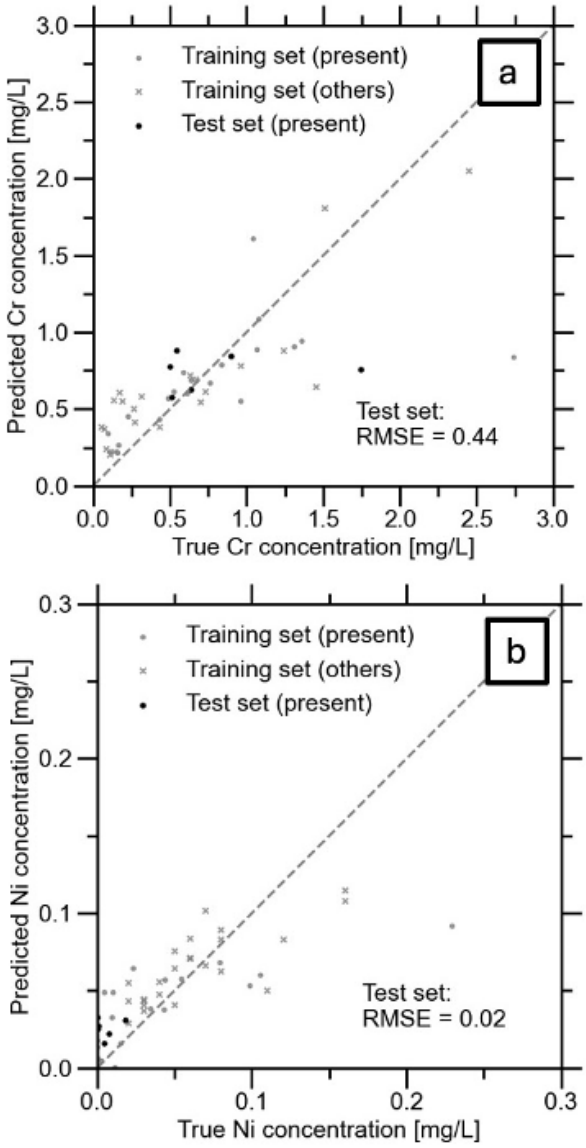

Figure 3 Machine Learning model prediction accuracy (reproduced from Bisciotti et al., 2025).

However, most of the concentrations are below the limits established by the Italian "End-of-Waste" criteria (D.M. n. 127/2024) thresholds.

With the aim of providing a faster approach for assessing the release of contaminants from CDW, a prediction of the same values is conducted directly from the bulk XRF composition using machine learning (Bisciotti et al., 2025).

The results obtained reflect varying levels of model accuracy based on their respective Root Mean Square Errors (RMSEs). The highest RMSE (0.44) is observed for Cr, indicating that the model struggles to accurately predict leaching. Indeed, Cr mobility is linked to the pH of the environment, making it hard to predict. In contrast, Ni shows the highest predictive levels (RMSE ~0.02), indicating that the model effectively captures the variables influencing Ni leaching (Fig. 3).

The development of non-supervised real-time risk-assessment tools for CDW management is supported by machine learning tools that can be effectively implemented to predict the concentrations of key leachates directly from the bulk chemical composition of the input waste. In such a way, if the predictions don't exceed the threshold values set by the D.M. 127/2024, the process of "End-of-Waste" declaration could be completed without any significant concern. Instead, if the predictions show signs of risk of exceeding such threshold values, an accurate analysis must be conducted according to the protocol defined by the UNI-EN 1245-7.

Machine learning algorithms and computer vision systems can automate waste classification, predict contaminant leaching behavior, and optimize recycling processes. By analyzing large datasets of waste composition, leaching test results, and regulatory thresholds, AI models support decision-making for safe material reuse, hazard assessment, and compliance with circular economy targets. This integration accelerates sustainable practices in the construction sector while reducing landfill dependency.

Eventually, by speeding up this procedure, a higher volume of materials can be recycled in a circular economy, achieving a more effective recycling of CDW (Bisciotti et al., 2025).

Automated Sorting based on the Leftover Cement content

In the Italian framework, following "End-of-Waste" acceptance (D.M. n. 127/2024), the recycled aggregates produced can be formally re-introduced in the circular pathways of new building materials. However, especially when obtained from CDW crushed concrete (CON samples), these materials are typically composed of the original natural sand and gravel and of a variable amount of leftover cement paste (LCP), clinging to their surface (Fig. 4).

It is known that the quality of recycled aggregates is directly influenced by the total amount of LCP (Dinh et al., 2022). Therefore, implementing an industrial separation based on this characteristic could significantly advance the circular economy within the sector. Ultimately, it would enable the sorting of high-quality raw materials from lower-quality fractions.

To this aim, an extensive database of more than 300 individual images of CON samples has been collected. An image analysis procedure is then performed based

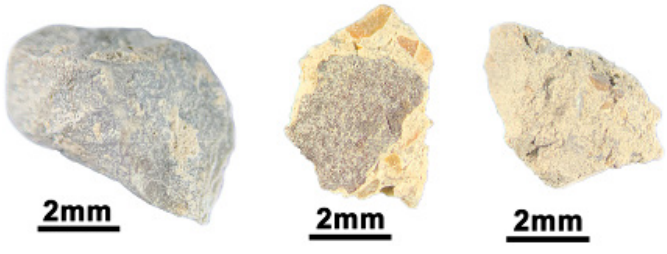

Figure 4 Recycled aggregates with variable amounts of LCP (reproduced from Bisciotti et al., 2024).

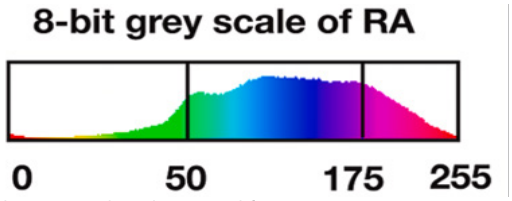

Figure 5 8-bit grayscale values used for segmentation.

on the grayscale 8-bit transformation of the original RGB database. The grayscale values have been therefore divided into three selected intervals (0–50, 50–175, and 175–255) that cover the characteristic pixel values associated with the background, aggregates, and LCP, respectively (Fig. 5).

To overcome the bottleneck associated with the manual image analysis procedure, a deep learning model is further incorporated to automate the determination of the LCP, which enables high-throughput screening of CDW in real production.

The Convolution Neural Network approach is selected because it is well-recognized for visual imagery with its dominant superiority in accuracy and efficiency among all algorithms for computer vision developing (Song et al., 2020).

Following common practice, 80% of the images are used (i.e., training set) to train the model, while the remaining 20% of images (i.e., test set) are kept hidden for testing the prediction accuracy of the model trained. The model accuracy is again evaluated by the MSE loss. The results show that as the training proceeds, the model loss decreases exponentially and plateaus at around 60 epochs. After that, model performance gradually converges to a steady stage where a small divergence between training and test sets is observed.

Eventually, the model reached an impressive 90% recall rate in correctly predicting the clean materials and LCP cover aggregates, distinguishing the two categories

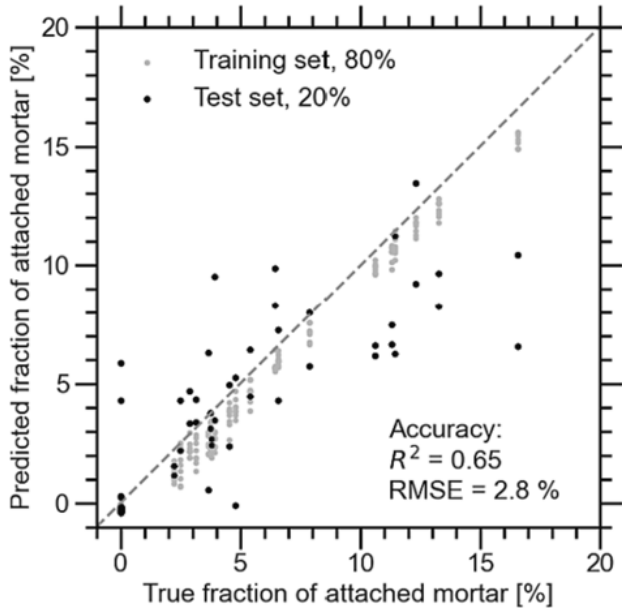

Figure 6 Machine Learning prediction accuracy (reproduced from Bisciotti et al., 2024).

from the predicted values (Fig. 6). This result shows that a portion of high-quality secondary raw materials can be exploited from the CDW unsorted waste stream using an optical-based sorting facility that employs machine learning.

These recycled aggregates, free from LCP, can be fully reused in the production of concrete without compromising the overall engineering properties of building materials, making them perfectly comparable to those derived from mineral resources extraction, like river sand and quarry mining (Bisciotti et al., 2024).

Upcycling of CDW based on the amount of Leftover Cement content

The introduction of advanced optical sorting equipment is not always feasible, and still some time will be needed to achieve a full-scale development of similar technologies. However, the proportion of LCP to natural sand and gravel remains the most significant parameter to establish the quality of recycled aggregates, prior to their reuse.

Different studies propose multiple approaches to measure LCP ranging from wet chemical tests to more advanced spectroscopy, microscopy, and image analysis. However, many of these methods are time-consuming, unsuitable for laboratory routine quality control, or prone to inaccuracies (Ulsen et al., 2022). For example, wet methods may overestimate LCP in aggregates containing acid-soluble minerals, absorption tests are influenced by cement porosity, physical methods lack reproducibility, and microscopy is operator-dependent. At the same time, an estimation based on the chemical composition, such as X-ray fluorescence, cannot distinguish LCP from limestone. In this scenario, XRPD coupled with Rietveld quantitative phase analysis may provide a valuable solution. XRPD opens enormous possibilities for in-situ monitoring of process and quality control, even in the field of continuous in-line measurements during industrial production, like CDW sorting and recycling. This method has grown beyond its roots in the world of laboratory research and is regarded as one of the most powerful industrial process-control tools in the field of building materials and minerals.

To test this approach, CON samples are collected and ground into a fine powder using a jaw crusher, followed by compaction with a mechanical press. The obr powder obtained is directly analyzed through XRPD. An accurate quantitative phase analysis is then performed by the Rietveld profile fitting using the Bruker TOPAS 5.0 software. The results provide a direct weighted (wt.%) quantification of the crystalline assemblage of the natural sand and gravel and of the LCP's minerals (*i.e.*, clinker constituents, hydration phases and carbonation products).

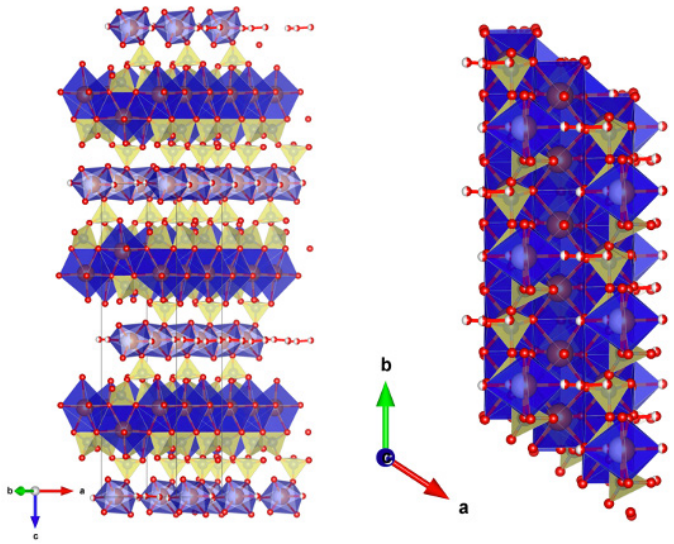

Figure 7 Tobermorite structure (natural analogues of C-S-H).

The majority of the LCP is composed of cement hydration products (namely C-S-H, ettringite, portlandite and hydrated calcium aluminates). For the C-S-H gel component, a tobermorite-like structure can be used to mimic C-S-H chemical and semi-crystalline composition (Fig. 7). To this aim, the crystallite size was fixed at 1.5 nm to achieve a profile fitting that follows the LCP amorphous content.

During the Rietveld calculation, the individual peak shape functions of the crystalline constituents are summed and combined with a background function. The background is modeled using a three-term Chebyshev polynomial equation over the entire 2θ range to maintain an almost linear profile. This approach allows for the visualization and quantification of the semi-amorphous C-S-H peak, which overlaps with the background and lies beneath the bases of the more crystalline peaks. The goodness of fit is evaluated using the Residual Weighted Profile (Rwp) value and by visually assessing the difference between the observed and calculated profiles on the same scale.

The same batch of recycled aggregates tested is afterwards used in the manufacturing of concrete specimens. The mix-design of the concrete is done according to the British Department of the Environment (DOE) standard method. Cement type, water-to-cement ratio, and mixing and curing procedures are kept constant. This consistency helps highlight the effects of the LCP itself on the concrete microstructure.

The investigation of the concrete microstructure is conducted by adopting lab-based X-ray computed tomography (X-ray micro-CT). The analyses are done using a Zeiss XRadia MicroXCT-400 at ZAG's Materials Department (Slovenia) with an 80 kV voltage, 10 W power, and LE2 filtering. Each sample underwent 1600 projections over 360°, with a 3-second exposure per projection and a 17.6 µm pixel size. Tomographic reconstruction was performed using Zeiss XRM software, which includes beam hardening correction. The resulting 16-bit TIFF axial slices were processed and analyzed using DragonFly software.

The pore characteristics in the concrete specimens are strongly influenced by the usage of recycled aggregates and specifically by the LCP content (Fig. 8). Therefore, various statistical attributes were computed for each specimen, including pore volume, pore sphericity and connected pores skeletonization (Skeleton Euclidean Length).

When natural aggregates are replaced with recycled aggregates, the average pore volume decreases by 75%, from 0.08 mm³ to 0.002 mm³. Sphericity index shows minor variations, whereas the highest impact is seen in pore network connectivity. When recycled fines replace natural aggregates, the number of connected pores increases tenfold and the skeleton Euclidean length decreases.

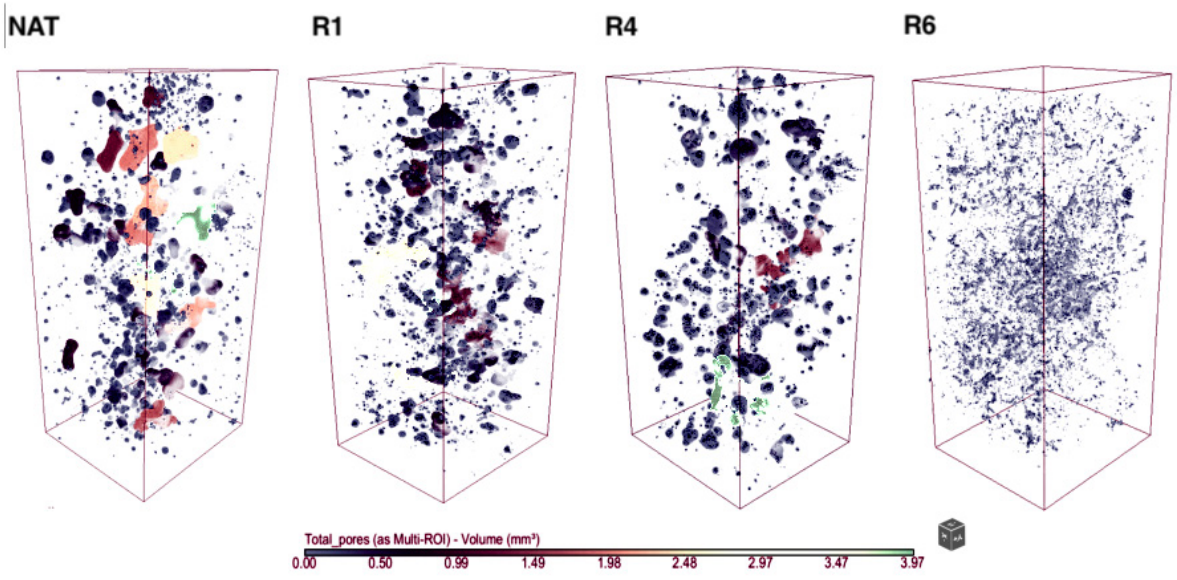

Figure 8 3D rendering of concrete specimens produced with recycled aggregates highlighting their internal porosity, NAT is concrete made with natural aggregates R1 with 10-4 mm recycled agg., R4 with 4-0.6 mm and R6 with 0.6-0 mm.

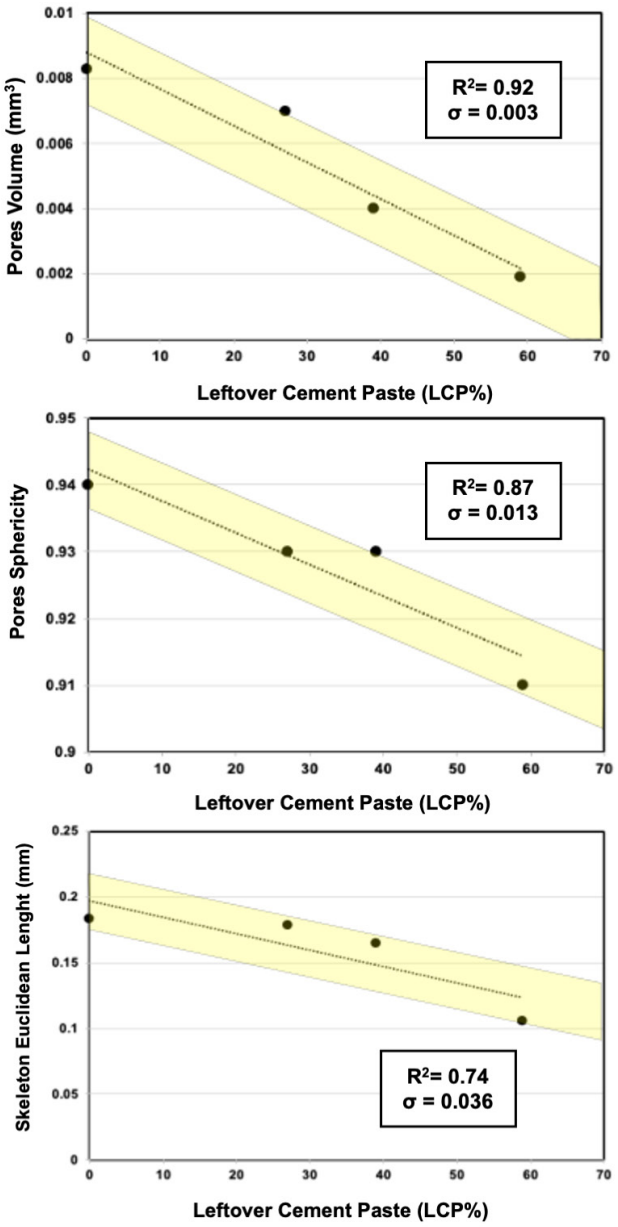

Figure 9 Comparison of LCP% and concrete microstructure.

All these features of the concrete porosity appear to be linked with the LCP values obtained from XRPD, which span from 0% (for natural aggregates) to 59% (recycled aggregates fines) with intermediate values for coarse and medium size aggregates (Fig. 9).

The impact of the LCP content in concrete microstructure is shown, highlighting the importance of monitoring such features prior to their reuse, while supporting the validity of the protocol described based on XRPD and Rietveld quantitative phase analysis

DISCUSSION

Selective demolition of old constructions remains the most effective practice for maximizing the recycling potential of Construction and Demolition Waste (CDW) into high-grade applications. However, this approach is often deemed excessively time-consuming and cost-inefficient, leading to its limited adoption. As a result, CDW is frequently found in a mixed, unsorted state after demolition and prior to its recycling.

The findings of this research indicate that the bulk chemical composition of CDW reflects its mineralogical and material composition. Significant variations arise due to the fluctuating content of concrete (CON) in relation to ceramics (CER) and other minor constituents. These variations directly impact the leaching behavior of CDW, as different constituent ratios lead to varying pH levels, influencing pollutant release.

By integrating machine learning methods, leaching values can be predicted solely on the bulk chemical composition of CDW. This capability presents significant potential for environmental hazard monitoring and the development of rapid, accurate auditing technologies preceding the final End-of-Waste declaration. If this declaration serves as the passport for recycled CDW, the adoption of such predictive models could function as a digital tracking system, enabling rapid screening to immediately identify potentially hazardous compositions.

It is clear that achieving a circular construction sector presents considerable challenges. Even when homogenous CON-based CDW is available, its upcycling may be hindered by various factors, with the presence of leftover cement paste (LCP) being a primary concern. The LCP content significantly affects the quality of recycled aggregates, limiting their applications in high-grade structural concrete. One potential solution is the implementation of advanced sorting machines equipped with optical sensors. The development of such facilities is becoming increasingly common, particularly in Europe, where they are being introduced for sorting CDW based on the material composition and also adopting robotic arms. These optical sensors for waste separation range from standard RGB cameras to more complex Hyperspectral Imaging (HSI) devices.

This research demonstrates that accurate sorting of CDW can be achieved using standard RGB cameras. Deep learning techniques enable robust and high-speed image analysis of screened materials. LCP can be distinguished from natural clasts through differences in grayscale values, as well as other distinguishing characteristics such as roughness, texture, and morphology, which are recognized through computer vision. While these features may seem negligible to the human eye, they are crucial for computer-based analysis in determining whether a recycled aggregate is coated with LCP or is comparable to newly extracted quarry materials. Efficient separation of high-quality recycled aggregates from mixed CDW streams can result in the recovery of substantial quantities of valuable minerals.

Nevertheless, additional laboratory-based quality evaluation protocols are essential for determining LCP content, especially in a batch of materials that might come from standard sorting facilities. The LCP presence in recycled aggregates significantly affects the mechanical

properties of concrete, raising concerns about structural safety, durability, and sustainability. Therefore, prior to precasting and on-site concrete production, the assessment of this feature must be verified. However, currently available methods often have limitations and may yield low-accuracy measurements.

To address this issue, X-ray Powder Diffraction (XRPD) has been tested as a rapid and efficient tool for monitoring the quality of recycled aggregates. Using Rietveld refinement and quantitative phase analysis, LCP content can be accurately measured, providing a volume reconstruction. However, this method may be unfamiliar or complex for laboratory technicians who are not specialized in XRPD applications. To mitigate this challenge, machine learning can be integrated to develop automated software capable of estimating LCP content from XRPD patterns. While this advancement is still in development, it represents one of the most critical future directions for this research.

CONCLUSIONS

The construction sector must transition towards sustainability, as traditional building materials production remains highly polluting despite 200 years of technological progress. This research presents a focus on circular economy approaches in Construction and Demolition Waste (CDW) management, emphasizing recycling, sorting, and environmental risk assessment using AI-driven models. Key advancements include predicting contaminant leaching, improving recycled aggregates for high-value applications, and implementing automated material characterization with XRPD and AI. Standardized methods and advanced sorting technologies are needed to enhance CDW recycling, reduce environmental impact, and achieve End-of-Waste certification. The circular economy in construction is essential for sustainability, resource efficiency, and climate change mitigation.

REFERENCES

Bianchini, G., Ristovski, I., Milcov, I., Zupac, A., Natali, C., Salani, G.M., Marchina, C., Brombin, V., Ferraboschi, A. (2020) - Chemical characterisation of construction and demolitionwaste in Skopje city and its surroundings (Republic of Macedonia). Sustainability, 12(5).

Bisciotti, A., Cruciani, G., Brombin, V., Bianchini, G. (2023) - Tracing different Construction and Demolition Waste (CDW) environmental impacts through mineralogical and geochemical analyses. Goldschmidt Abstract.

Bisciotti, A., Jiang, D., Song, Y., Cruciani, G. (2024) - Estimating attached mortar paste on the surface of recycled aggregates based on deep learning and mineralogical models. Clean. Mater., 11, 100215.

Bisciotti, A., Brombin, V., Song, Y., Bianchini, G., Cruciani, G. (2025) - Classification and predictive leaching risk assessment of construction and demolition waste using multivariate statistical and machine learning analyses. Waste Manag., 196, 60–70.

Caro, D., Lodato, C., Damgaard, A., Cristóbal, J., Foster, G., Flachenecker, F., Tonini, D. (2024) - Environmental and socio-economic effects of construction and demolition waste recycling in the European Union. Sci. Total Environ., 908.

Dinh, H.L., Liu, J., Ong, D.E.L., Doh, J.H. (2022) - A sustainable solution to excessive river sand mining by utilizing by-products in concrete manufacturing: A state-of-the-art review. Clean. Mater., 6, 100140.

Gagg, C.R. (2014) - Cement and concrete as an engineering material: An historic appraisal and case study analysis. Eng. Fail. Anal., 40, 114–140.

Song, Y., Huang, Z., Shen, C., Shi, H., Lange, D.A. (2020) - Deep learning-based automated image segmentation for concrete petrographic analysis. Cem. Concr. Res., 135, 106118.

Torres, A., Brandt, J., Lear, K., Liu, J. (2017) - A looming tragedy of the sand commons. Sci. 357, 6355, 970–971.

Ulsen, C., Contessotto, R., dos Santos Macedo, R., Kahn, H. (2022) - Quantification of the cement paste and phase's association in fine recycled aggregates by SEM-based image analysis. Constr. Build. Mater., 320.

Whittaker, M.J., Grigoriadis, K., Soutsos, M., Sha, W., Klinge, A., Paganoni, S., Casado, M., Brander, L., Mousavi, M., Scullin, M., Correia, R., Zerbi, T., Staiano, G., Merli, I., Ingrosso, I., Attanasio, A., Largo, A. (2021) - Novel construction and demolition waste (CDW) treatment and uses to maximize reuse and recycling. ABER, 15(2), 253–269.

Wu, H., Zuo, J., Zillante, G., Wang, J., Yuan, H. (2019) - Status quo and future directions of construction and demolition waste research: A critical review. J. Clean. Prod., 240.

Into the structure of the Permian deep continental crust

Multiscale reconstruction of migmatization in the Valpelline Series (Dent Blanche Tectonic System, Western Italian Alps)

Fabiola Caso

Department of Earth Sciences "A. Desio", University of Milano, Via Luigi Mangiagalli 34, 20133, Milano

DOI: 10.19276/plinius.2025.01.004

INTRODUCTION

The deep continental crust is the lowest part of the crust above the lithospheric mantle, mainly composed of rocks associated with partial melting, such as migmatites and granulites (Bohlen, 1987; Hacker et al., 2015). In extensional geodynamic frameworks, lithospheric thinning causes asthenospheric upwelling, enhancing partial melting of the lithospheric mantle and deep crust. In these contexts, deformation plays a fundamental role in melanosome-leucosome differentiation by facilitating the movement and segregation of melt within the crust. Foliation and shear zones provide pathways for melt migration, which allow melt to move and accumulate into discrete leucosome bands, reacting with the host rock, enhancing the differentiation of the crust.

During the Permian, the Variscan lithosphere was affected by extension due to the Pangea breakup, followed by the Tethys opening. Among the preserved Permian basements across the Alps, the Valpelline Series in the Dent Blanche Tectonic System in the Western Alps represents an exceptionally preserved exposure of granulite and migmatite, showing high-temperature structures and mineral assemblages despite being involved in the subsequent Alpine collision (Manzotti & Zucali, 2013). This contribution provides a multiscale description that focuses on understanding the effects of deformation and metamorphism in shaping the deep continental crust structure of the Valpelline Series during the Permian time.

GEOLOGICAL SETTING

The Valpelline Series lies in the Dent Blanche Tectonic System of the Western Italian Alps, which is a continental klippe belonging to the Adriatic paleomargin and overlying the oceanic units of the Liguro-Piemonte ocean (Fig. 1a). Together with the neighbouring Arolla Series it has been involved in Alpine subduction-collision events (Compagnoni et al., 1977; Manzotti et al., 2014), still preserving pre-Alpine amphibolite- to granulite-facies mineral assemblages and structures (Manzotti & Zucali, 2013) or magmatic textures like those within the Arolla Series Permian granitoids (Baletti et al., 2012). The Valpelline Series is a deep continental crust section composed of migmatitic gneiss, amphibolites and marbles enclosing lenses of mafic granulites, crosscutted by different systems of pegmatitic dykes (Manzotti & Zucali, 2013; Caso et al., 2024a, b). The regional foliation S_2 in the Valpelline Series is related to the partial melting of both metapelites and amphibolites and is folded and locally transposed at different scales, developing a sillimanite-rich foliation S_3. The pressure (*P*) – temperature (*T*) conditions of partial melting and regional foliation development are 810±40°C and 0.7±0.01 GPa (Manzotti & Zucali, 2013). Metamorphism and partial melting of the Valpelline Series are Permian in age (Kunz et al., 2018) and are related to the crustal thinning and magmatism during the Pangea breakup (Lardeaux & Spalla, 1991).

RESULTS

Rock types of the deep continental crust

The Valpelline Series is mostly made of migmatitic gneiss (pink colour in Fig. 1b) whose outcrops can extend up to hundreds of metres and host the regional structures (S_2 foliation traces in Fig. 1b). Migmatitic gneiss are made of a stromatic structure made of dark-coloured layers (melanosomes) consisting of biotite, sillimanite and garnet and light-coloured layers (leucosomes) of plagioclase, K-feldspar and quartz (Fig. 2a). Leucosomes, assumed to represent the melt, highlight folds with different geometries. In localised outcrops, migmatitic gneiss contains cordierite or orthopyroxene along with garnet. Sillimanite-gneiss occurs as centimetric to hectometric domains that overprint the pervasive foliation of migmatitic gneiss. They show a foliation extremely rich in sillimanite (and locally biotite) wrapping garnet and, when present, cordierite porphyroblast (Fig. 2b). Leucosomes in sillimanite-gneiss are thinner, discontinuous and locally even absent. Felsic granulite

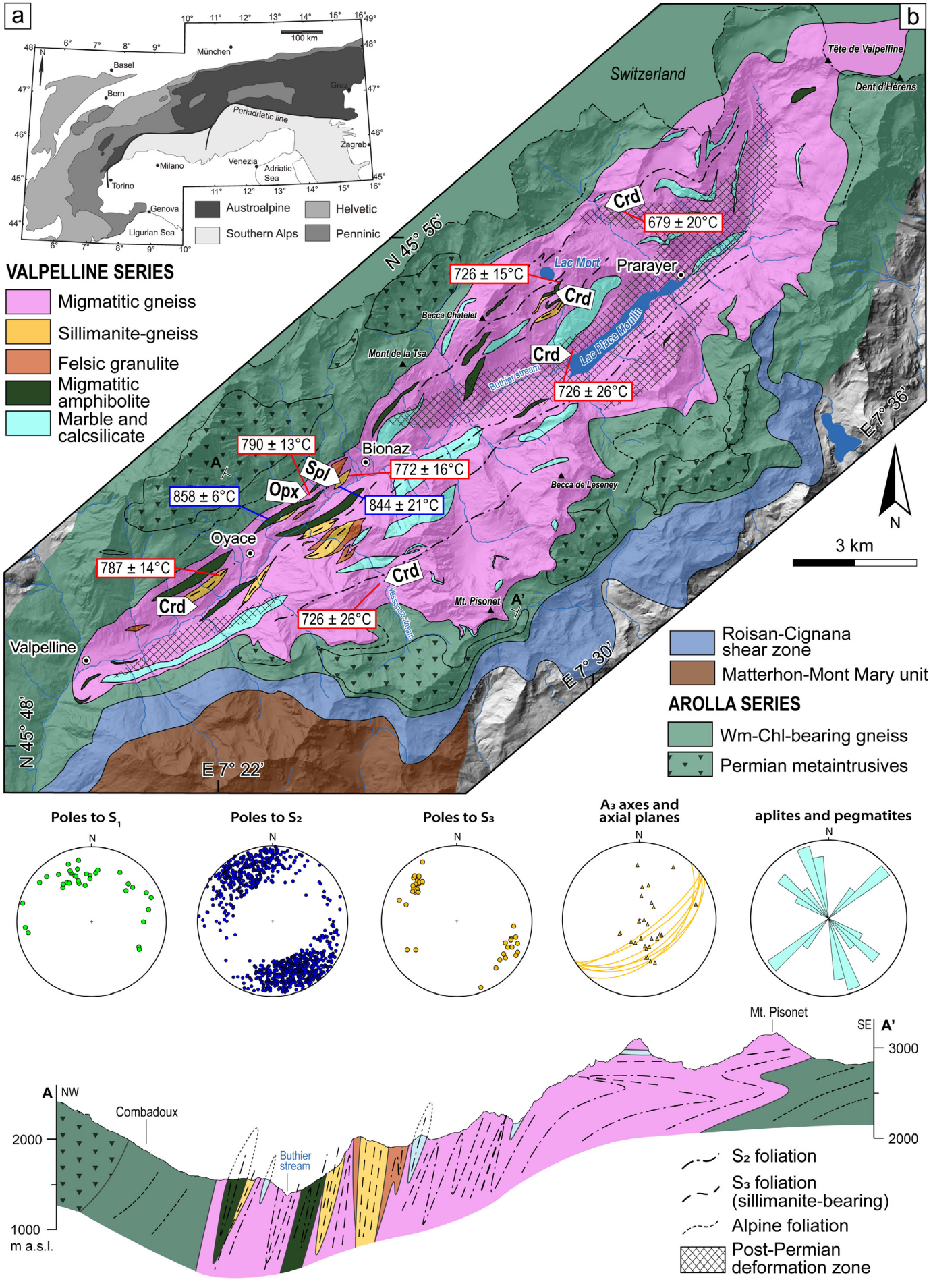

Figure 1 a) *Tectonic sketch map of the Alps.* ***b)*** *Geological maps of the Valpelline and Arolla Series with temperatures estimations, stereoplots of the main structural elements and geological cross section on the bottom (modified after Caso et al., 2024a).*

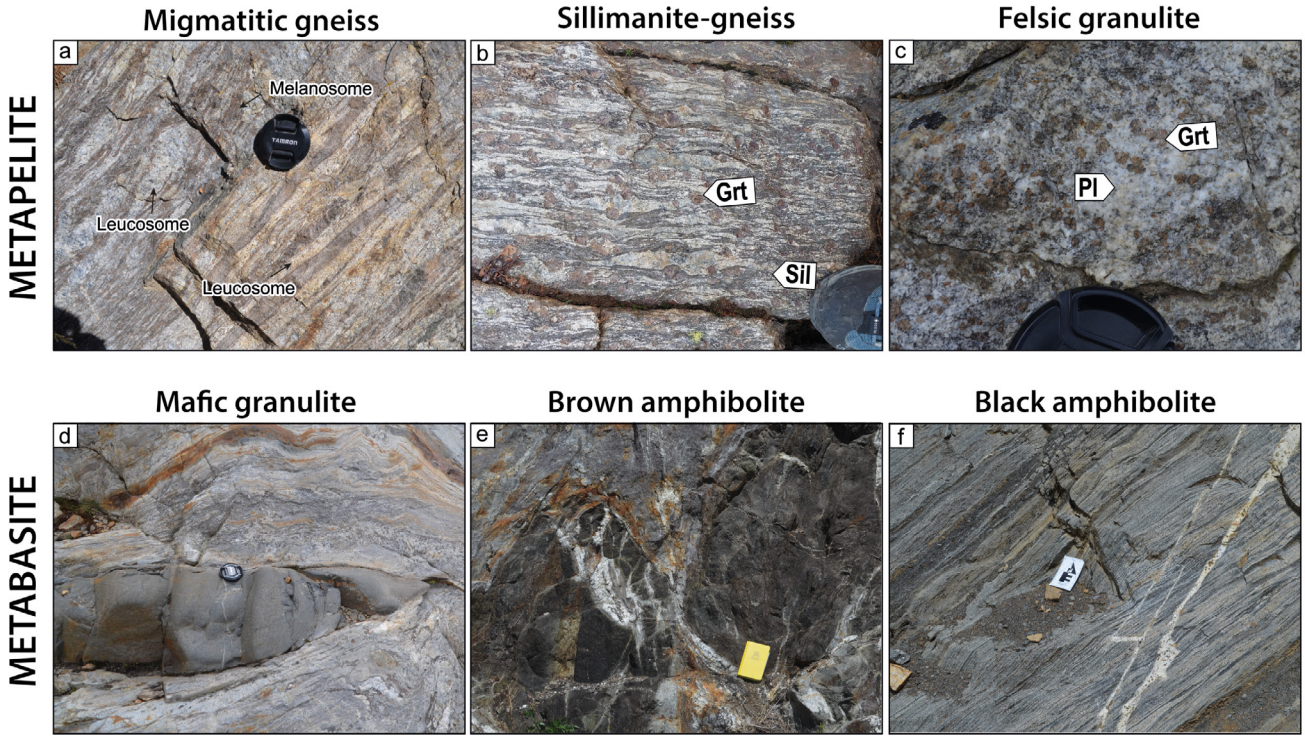

Figure 2 a) Migmatitic gneiss outcrop with leucosome and melanosome layers indicated. b) Sillimanite-gneiss made of Sil-rich layer wrapping around large Grt porphyroblasts (mineral abbreviations after Warr, 2021). c) Felsic granulite with a granoblastic structure made of Pl and Grt. d) Lense of mafic granulite within migmatitic gneiss. e) Lenses of brown amphibolite within migmatitic gneiss. f) Outcrop of black amphibolite whose foliation is cut by a pegmatite.

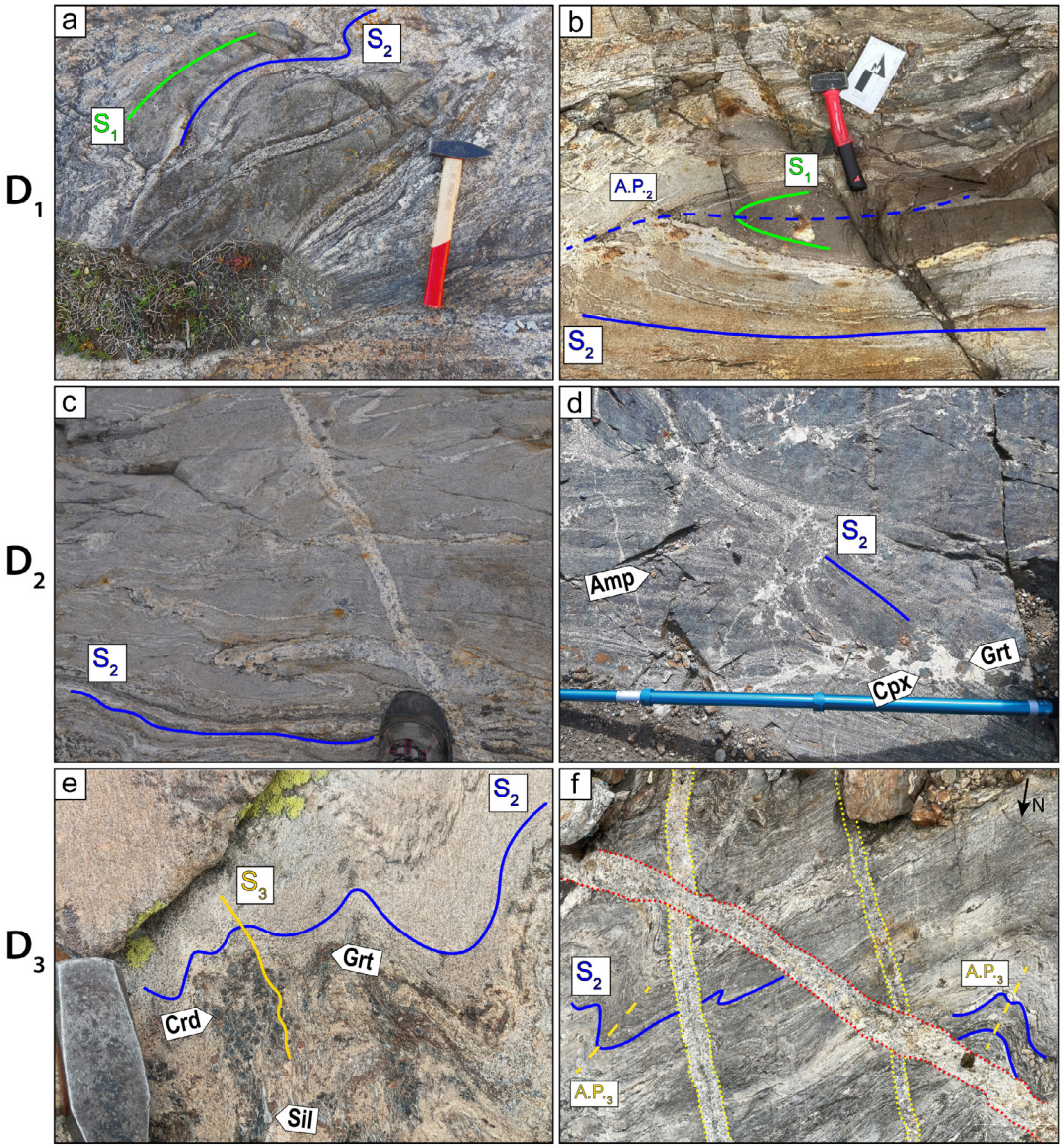

Figure 3 a) Mafic granulite lenses hosting S_1 foliation, wrapped by the S_2 pervasive in migmatitic gneiss. b) Folded brown amphibolite layer withi Crd-migmatitic gneiss, highlighting the S_1 foliation. c) S_2 foliation in Crd-migmatitic gneiss cut by leucosomes and pegmatite. d) S_2 in black amphibolite made of dark-green amphibole; the S_2 fabric is cut by Pl+Cpx+Grt leucosomes. e) D_3 folds in Crd-migmatitic gneiss with S_3 axial plane foliation made of Sil, wrapping Crd and Grt porphyroblasts. f) D_3 folds in migmatitic gneiss crosscut by two different systems of pegmatitic dykes.

occurs as lenses and layers within migmatitic gneiss. It displays garnet, plagioclase and quartz with granoblastic texture (Fig. 2c).

Metabasite in the Valpelline Series comprises mafic granulite and brown amphibolite cropping out as metric lenses or boudins (Fig. 2d, e) and black amphibolite cropping out as hectometric outcrops (Fig. 2f). Mafic granulite has a granoblastic structure made of orthopyroxene, plagioclase, amphibole and locally biotite. Brown amphibolite is made of brown hornblende and plagioclase, marking a foliation. Black amphibolites are banded, with alternating levels of dark-green amphibole and whiteish plagioclase-rich levels. Their main fabric is locally crosscut by leucosomes made of plagioclase, garnet and clinopyroxene.

Structural evolution

The deformation evolution of the Valpelline Series related to the migmatization history can be summarised in three deformation stages: D_1, D_2 and D_3 recognised at meso- and microscale.

The D_1 stage is testified by the S_1 foliation, which is localised in the metric boudins of mafic granulite and brown amphibolite. This foliation has various orientations to the regional S_2 foliation and elongation of main lithological boundaries (see stereonets in Fig. 1b). In most cases, the S_1 is geometrically discordant to the long axis of the boudins and to the penetrative foliation that wraps them (Fig. 3a). At microscale, the S_1 is marked by Amp I + Pl I + Cpx I + Opx I in mafic granulites and brown amphibolites (Fig. 4a, b). In metapelites, there is no clear evidence of S_1 but rounded inclusions of Bt I, Pl I and Qz I within peritectic Grt/Crd or Opx and relict Bt I and Sil I may be attributed to this stage (Fig. 4c).

During the D_2 the S_1 is folded (Fig. 3b), and the main regional foliation S_2 develops. The S_2 and the lithological boundaries tend to strike NE–SW and dip vertically toward NW or SE (see stereonets in Fig. 1b). The S_2 is pervasive in migmatitic gneiss and black amphibolite (Figs. 3c, d). In migmatitic gneiss, S_2 is marked by leucosome-melanosome alternation (Fig. 3c). At microscale, the S_2 is marked by Bt II + Grt + Opx in + Qz II Opx-migmatitic gneiss and by Bt II + Sil II + Qz II + Pl II + Grt + Crd in Crd-migmatitic gneiss (Fig. 4d, e). In black amphibolite is marked by the isorientation of Amp II and Pl II. Locally, the Pl-rich levels contain Grt and Cpx interpreted as peritectic phases (Fig. 4f).

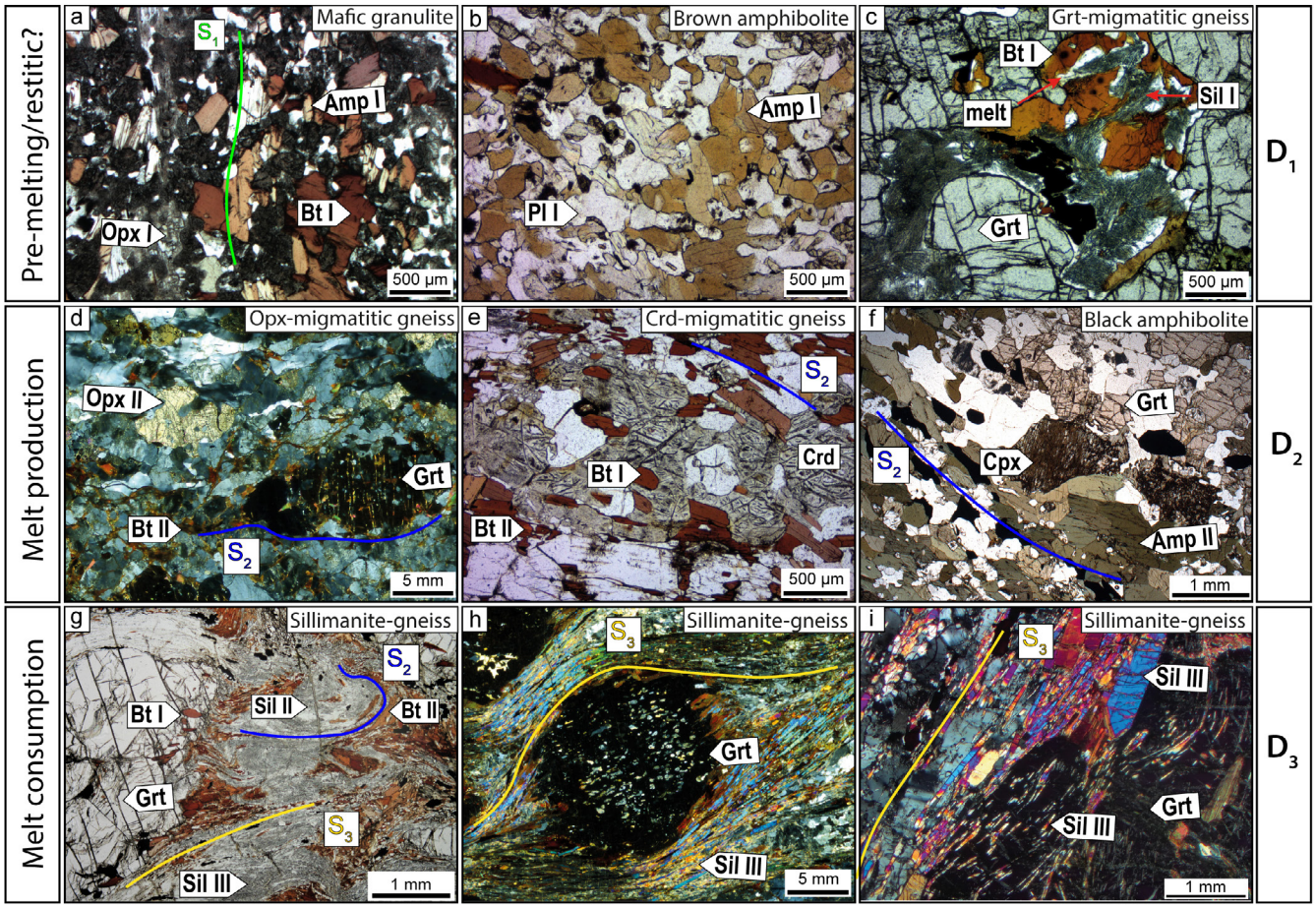

Figure 4 a) *Opx I, Bt I and Amp I in mafic granulite boudin (XPL: crossed-polarised light).* ***b)*** *Amp I and Pl I in brown amphibolite (PPL: plane-polarised light).* ***c)*** *Relict deformed Bt I and fibrous Sil I reacting to produce melt and Grt II in migmatitic gneiss (PPL).* ***d)*** *Microscale view of Opx and Grt porphyroblasts marking S_2 foliation in Opx-migmatitic gneiss (XPL).* ***e)*** *Rounded Bt I blasts included in Crd in a migmatitic gneiss and Bt II marking S_2 foliation (PPL).* ***f)*** *S_2 foliation in black amphibolite marked by Amp II + Cpx + Grt (PPL).* ***g)*** *S_2 microfold preserved within microlithon in sillimanite-gneiss, whose limbs are parallel to S_3 foliation marked by Sil III and Bt III (PPL).* ***h)*** *Sillimanite-gneiss whose foliation is defined by prismatic Sil III blasts wrapping around centimetric Grt porphyroblasts (XPL).* ***i)*** *Garnet rim with fine-grained needles of sillimanite marking an internal foliation in continuity with respect to the external one (XPL).*

During the D_3, the S_3 is deformed and folded in different ways. In migmatitic gneiss, the folds affecting S_2, highlighted by leucosomes, are mainly close to open and only locally isoclinal. In domains where the folding is more intense, the S_2 is transposed and overprinted by the Sil-rich axial plane S_3 foliation (Fig. 3e), which wraps around Grt and Crd (Fig. 4g, h, i). Locally, at microscale in sillimanite-gneiss is still possible to observe in microlithons the overprinting relationships between S_2 and S_3, where S_2 is preserved as relict microfolds marked by Sil II and Bt II (Fig. 4g). Peritectic garnet, grown during D_2, locally continues to grow also during D_3 stage, as testified by thin garnet rims with an internal foliation made of Sil III needles parallel the external S_3 (Fig. 4i).

These domains of high-strain D_3-related deformation correspond to sillimanite-gneiss, domains that can range from the cm- up to hectometric scale, where leucosomes are deformed and sometimes completely transposed.

Temperature and pressure estimations

The *P-T* conditions related to the D_1-D_2-D_3 stages have been retrieved by combining different geothermobarometers on metapelites and metabasite of the Valpelline Series.

Temperatures have been obtained using the Zr-in-rutile (Tomkins et al., 2007) and the Ti-in-biotite (Henry et al., 2005) thermometers on metapelites and the Ti-in-amphibole thermometer (Liao et al., 2021) applied on black and brown amphibolites. Since the Zr-in-rutile thermometer is P-dependent, a value of 0.7 GPa has been used as input for the calculations (value from Manzotti & Zucali, 2013). We have analysed rutile crystals from different microstructural positions, like those included within garnet or marking S_2 or S_3 fabrics. Rutile from sillimanite-gneiss yielded temperatures ranging from 691 to 818°C, while Grt-migmatite gneiss temperatures vary between 683 and 773°C (Fig. 5a). In felsic granulite, temperatures range between 667 and 843°C (Fig. 5a). The Ti-in-Bt thermometer has been applied to biotites from three different microstructural domains (Bt I, Bt II and Bt III). Temperatures from Grt-bearing migmatitic gneiss range from 676 and 784°C. There is a slight difference in temperatures between Opx- and Crd-migmatitic gneiss: in the former, temperatures range from 750 to 810°C, while in the latter are lower, from 654 to 789°C. Temperatures from sillimanite-gneiss range from 721 and 812°C (Fig. 5b).

The Ti-in-amphibole thermometer yielded higher temperatures with respect to those from metapelite: *i)* in brown amphibolite (Amp I marking the S_1), they range from 750 to 900°C, *ii)* in black amphibolites (Amp II marking S_2) temperatures are between 746 and 880°C with two main clusters at 767 ± 19°C and 844 ± 21°C (Fig. 5c).

Pressures have been obtained applying two geobarometers, *i.e.*, the Grt–Crd (Bhattacharya, 1986) and the Pl–Amp barometer (Molina et al., 2015). Pressures from Crd-migmatitic gneiss are at 0.55-0.58 GPa (orange ellipse in Fig. 5d) while those from black-amphibolite are much higher. Obtained *P* ranges between 0.8 ± 0.08 GPa (at 767°C) and 1.1 ± 0.10 GPa (at 879°C; green ellipse in Fig. 5d).

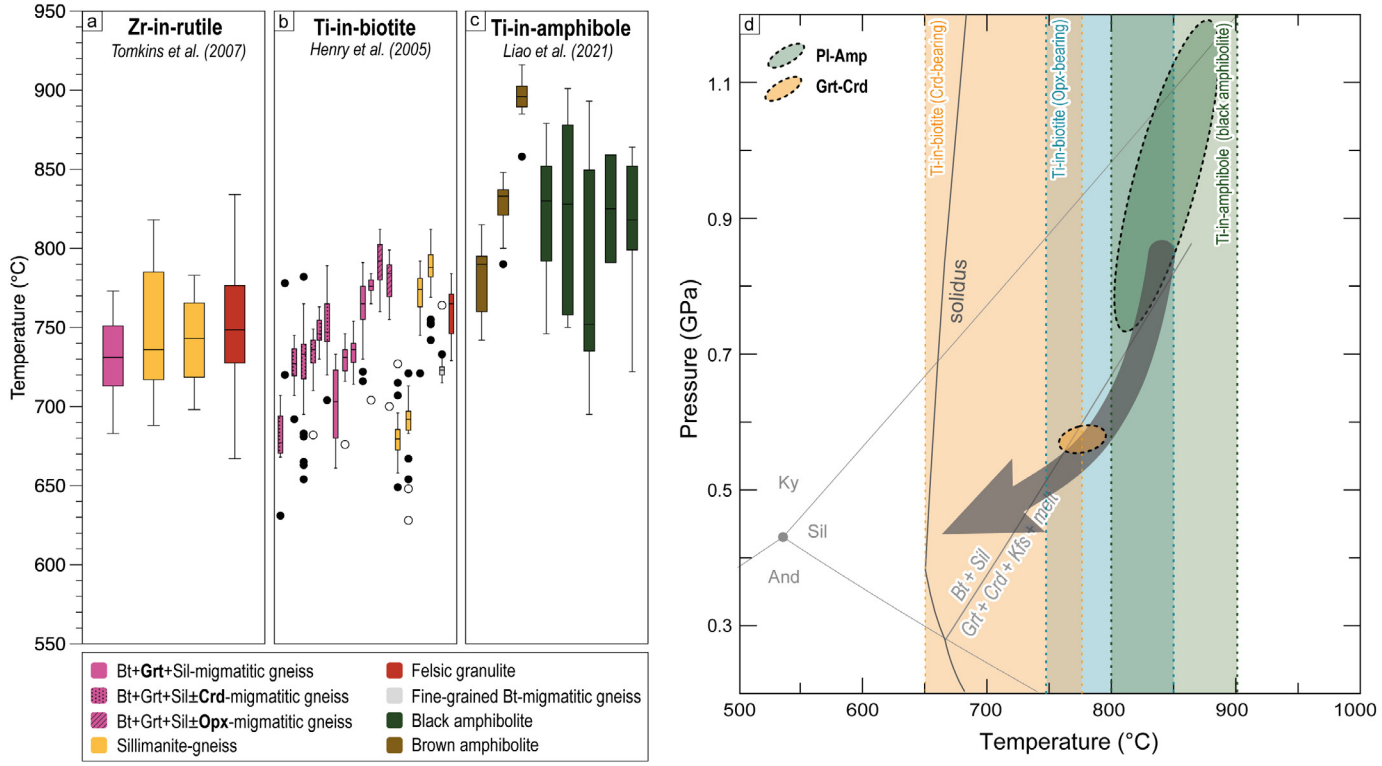

Figure 5 *Summary of the T°C ranges of each analysed sample for different applied methods.* ***a)*** *Zr-in-rutile thermometer of Tomkins et al. (2007).* ***b)*** *Ti-in-biotite thermometer of Henry et al. (2005).* ***c)*** *Ti-in-amphibole thermometer of Liao et al. (2021).* ***d)*** *Summary of the P-T conditions of the Valpelline Series (modified from Caso et al., 2024a).*

DISCUSSION AND FINAL REMARKS

The Valpelline Series represents a well-suited case study that exhibits diagnostic features and structures revealing information about different stages of the continental crust evolution and partial melting processes.

The oldest structures related to the D_1 stage are found in the mafic granulite and brown amphibolite meter-scale boudins, as an S_1 foliation. It is not easy to state whether these rocks have melted during this stage or not. However, the temperatures obtained, reaching ~850–900°C, may have been high enough to induce partial melting.

The regional S_2 foliation in the Valpelline Series is marked by leucosomes in migmatitic gneiss and locally in black amphibolite, testifying partial melting during the D_2. Temperatures obtained for this stage span from ~700 to ~900°C, with higher values in Opx-migmatitic gneiss (Ti-in-biotite; ~850°C) and black amphibolite (Ti-in-amphibole; ~800–900°C), agreeing with Bt-dehydration melting reaction (Fig. 5d). Temperatures are ~50–100°C lower in Crd-migmatitic gneiss than in Opx-migmatitic gneiss. Pressure estimates for the D_2 stage also change, being much higher in black amphibolite (up to 1.1 GPa) and lower in Crd-migmatitic gneiss (~0.58 GPa). Partial melting and S_2 development in migmatitic gneiss occurred at slightly different *P-T* conditions. Despite these differences in the *P-T* conditions, the presence of granulite-facies relicts related to the D_1 stage (mafic boudins with S_1 foliation) both in Opx- and Crd-bearing migmatites, and the common development of sillimanite-rich S_3, support that these portions were part of the same unit.

The S_3 foliation, marked by abundant sillimanite that wraps peritectic minerals as garnet and cordierite, can be the product of a back-reaction between peritectic phases and the melt that has migrated into these domains during D_3 stage deformation (Kriegsman & Alvarez-Valero, 2010). Moreover, *T* retrieved from biotite marking S_3 foliation in different samples across the valley yielded values from ~750 to 850°C, testifying that the conditions during this later stage were still at high temperature. The S_3 foliation can be used to trace the domains in which melt has migrated and reacted with the host rock during D_3 folding and axial plane foliation development.

The pervasive distribution of migmatite-bearing structures in the Valpelline Series rocks testifies that this unit was part of a km-scale migmatitic terrane involved in high-grade metamorphism during Permian lithospheric extension and asthenosphere rising, linked with abundant melt production.

REFERENCES

Baletti, L., Zanoni, D., Spalla, M.I., Gosso, G. (2012) - Structural and petrographic map of the Sassa gabbro complex (Dent Blanche nappe, Austroalpine tectonic system, Western Alps, Italy). J. Maps, 8(4), 413-430.

Bhattacharya, A. (1986) - Some geobarometers involving cordierite in the $FeO–Al_2O_3–SiO_2(+H_2O)$ system: refinements, thermodynamic calibration, and applicability in granulite facies rocks. Contrib. Mineral. Petr., 94, 387–394.

Bohlen, S.R. (1987) - Pressure-temperature-time paths and a tectonic model for the evolution of granulites. J. Geol., 95, 617–32.

Caso, F., Strambini, A., Zucali, M. (2024a) - Structural, lithostratigraphic and thermal features of a Permian lower crust from the Western Italian Alps (Valpelline Series, Valle d'Aosta). Geol. Mag., 160(11), 1983-2009.

Caso, F., Piloni, C.B., Filippi, M., Pezzotta, A., Fazio, E., Visalli, R., Ortolano G., Roda M., Zucali, M. (2024b) - Combining traditional and quantitative multiscale structural analysis to reconstruct the tectono-metamorphic evolution of migmatitic basements: the case of the Valpelline Series, Dent-Blanche Tectonic System, Western Alps. J. Struct. Geol., 182, 105099.

Compagnoni, R. (1977) - The Sesia-Lanzo Zone, a slice of continental crust with Alpine high-pressure-low temperature assemblages in the western Italian Alps. Rend. Soc. Ital. Mineral. Petrol., 33, 281-334.

Hacker, B.R., Kelemen, P.B., Behn, M.D. (2015) - Continental lower crust. Annu. Rev. Earth Pl. Sc., 43, 167–205.

Henry, B., Guidotti, C.V., Thomson, J.A. (2005) - The Ti-saturation surface for low-to-medium pressure metapelitic biotite: implications for geothermometry and Ti-substitution mechanisms. Am. Mineral., 90, 316–28.

Kriegsman, L.M. & Alvarez-Valero, A.M. (2010) - Melt-producing versus melt-consuming reactions in pelitic xenoliths and migmatites. Lithos, 116, 310–320,

Kunz, B.E., Manzotti, P., von Niederhäusern, B., Engi, M., Darling, J.R., Giuntoli, F., Lanari, P. (2018) - Permian high-temperature metamorphism in the Western Alps (NW Italy). Int. J. Earth Sci., 107, 203–229.

Lardeaux, J.M. & Spalla, M.I. (1991) - From granulites to eclogites in the Sesia Zone (Italian Western Alps) – a record of the opening and closure of the Piedmont Ocean. J. Metamorph. Geol., 9, 35–59.

Liao, Y., Wei, C., Rehman, H.U. (2021) - Titanium in calcium amphibole: Behavior and thermometry. Am. Mineral., 106(2), 180–191.

Manzotti, P. & Zucali, M. (2013) - The pre-Alpine tectonic history of the Austroalpine continental basement in the Valpelline unit (Western Italian Alps). Geol. Mag., 150, 153–172.

Manzotti, P., Ballèvre, M., Zucali, M., Robyr, M., Engi, M. (2014) - The tectonometamorphic evolution of the Sesia–Dent Blanche nappes (internal Western Alps): review and synthesis. Swiss J. Geosci., 107(2), 309–336.

Molina, J.F., Moreno, J.A., Castro, A., Rodríguez, C., Fershtater, G.B. (2015) - Calcic amphibole thermobarometry in metamorphic and igneous rocks: New calibrations based on plagioclase/amphibole Al-Si partitioning and amphibole/liquid Mg partitioning. Lithos, 232, 286–305.

Tomkins, H.S., Powell, R., Ellis, D.J. (2007) - The pressure dependence of the zirconium-in-rutile thermometer. J. Metamorph. Geol., 25(6), 703–713.

Warr, L.N. (2021) - IMA–CNMNC approved mineral symbols. Mineral. Mag., 85(3), 291-320.

Development of a water monitoring network in the Pesaro-Urbino province (northern Marche, central Italy) aimed at seismic precursors

Lorenzo Chemeri
Department of Pure and Applied Sciences, University of Urbino Carlo Bo, Via Ca Le Suore 2/4, 61029, Urbino
DOI: 10.19276/plinius.2025.01.005

INTRODUCTION

In the last decades, several studies stated that earthquakes of moderate to large magnitude (M_w > 4) are able to produce detectable changes in the geochemical composition of the waters circulating close to the epicentral area and/or in hydrogeological features of the aquifers involved (Cicerone et al., 2009; Wang & Manga, 2021). These variations, also called "seismic tracers" (Martinelli, 2020), may be of different nature and are generally observed before (from months to days), concurrently, or immediately after the seismic event (Thomas, 1998; Cicerone et al., 2009). Notable changes were related to discharges of springs, piezometric levels in wells, chemical and isotopic composition of waters and dissolved gases and groundwater physico-chemical parameters (Cicerone et al., 2009; Wang & Manga, 2021). These modifications are considered to be produced by the earthquake and its preparation process (*i.e.*, the seismic cycle), since several chemical and physical processes may be triggered (Doglioni et al., 2014). Precursory changes were observed in different geological and geodynamic settings characterized by intense seismic activity worldwide. However, due to the fact that these changes are often transitory and strictly site-sensitive, the identification of possible and suitable seismic precursors represents one of the major challenges for geoscientists (Franchini et al., 2021). Consequently, to improve scientific knowledge on this topic, the development of multi-parametric water monitoring networks located in seismic-prone areas is a fundamental step towards a better understanding of the underlying relationship between the seismic cycles and the seismic tracers (Franchini et al., 2021; Chemeri et al., 2024). Therefore, the aim of this research was to characterize the geochemistry of the waters (springs and wells) discharging in the Pesaro-Urbino (hereafter, PU) province, which was characterized in both past and recent history by an intense seismic activity, to define the main processes controlling the waters (and dissolved gases) composition and, later, to develop a hydrogeochemical monitoring network by applying a three-step hydrogeochemical approach: *i*) characterization, *ii*) detailed isotopic analysis and *iii*) monitoring. The outcomes can be summarized in to: (a) define the acting geochemical processes and the hydrogeological pathways, (b) investigate the possible interplay between deep-originated fluids and shallow aquifers, (c) evaluate the possible use of selected geochemical parameters as seismic tracers for this specific study area and (d) select sampling sites that should be included in a continuous water-monitoring network aimed at seismic surveillance (Franchini et al., 2021; Chemeri et al., 2024).

GEOLOGICAL AND GEODYNAMIC SETTING

The PU province is located in the northern Marche (Central Italy) within the Umbria-Marche Apennines, which represent the external part of the Northern Apennines, developed during the Miocene. The study area was recently interested by a moderate seismicity (up to 6.4 M_w), in terms of both frequency of events and magnitudes, related to the presence of two major composite seismogenic structures (DISS Working Group, 2021), located in the Umbria-Marche Apennines, along the Mt. Catria-Mt. Nerone Ridge, and on the Adriatic coast and off-shore areas, respectively (Fig. 1). The activity on the Adriatic coast and offshore is characterized by events with magnitudes usually lower than 6 (*e.g.*, the 1916 Rimini – M_w: 5.8 -, the 1930 Senigallia – M_w: 5.8 –, and the recent Marche offshore – M_w: 5.5 – seismic sequences) and related with transpressive and compressive structures. Contrarily, along the Apennine chain, the most destructive and strongest events are generally associated with extensional movements, such as the 1781 Cagli earthquake (M_w = 6.4) (Chemeri et al., 2025a and reference therein).

The study area features a variable topography and a complex geological-structural setting, with the outcropping geological formations spanning from Lower Jurassic to north-west to Miocene-Pleistocene deposits covered by Quaternary alluvial deposits in the coastal

area, to the east (Conti et al., 2020 and therein references). Moreover, it must be remarked that the Burano Fm, which is not outcropping in the study area, occurs at the bottom of the succession (Capaccioni et al., 2001; Conti et al., 2020), and was reached at 620 and 1550 m depth at the Nerone-Catria and Cesane Ridges areas (Fig. 1), respectively, during hydrocarbon exploration drillings.

Hydrogeological features

In the study area, three superimposed aquifers are present (Capaccioni et al., 2001). The upper aquifer is hosted in the limestone and marly-limestones belonging to the Scaglia Rossa and Scaglia Bianca Fms (*i.e.*, the Scaglia Calcarea aquifer), whilst the intermediate system is within the Maiolica Fm (Maiolica Aquifer). Eventually, the deepest is in the Calcare Massiccio and Corniola Fms (Basal Aquifer). The latter is the major hydrogeological unit in the area, being characterized by high infiltration rates and high permeability due to extensive karstification. The Basal Aquifer is confined, at the bottom, by the Burano Fm, which acts as a regional aquiclude. Marlstones and clayey-marlstones pertaining to the Marne a Fucoidi Fm represent an aquiclude between the Scaglia Calcarea and Maiolica aquifers, whilst the Calcare Massiccio and Maiolica aquifers are separated by the Rosso Ammonitico, Calcari Diasprini, and Bugarone Fms (Capaccioni et al., 2001). Furthermore, minor and shallow aquifers can also be recognized, and they are hosted in the *i*) siliciclastic Bisciaro and Marnoso Arenacea Fms and *ii*) Quaternary and alluvial deposits.

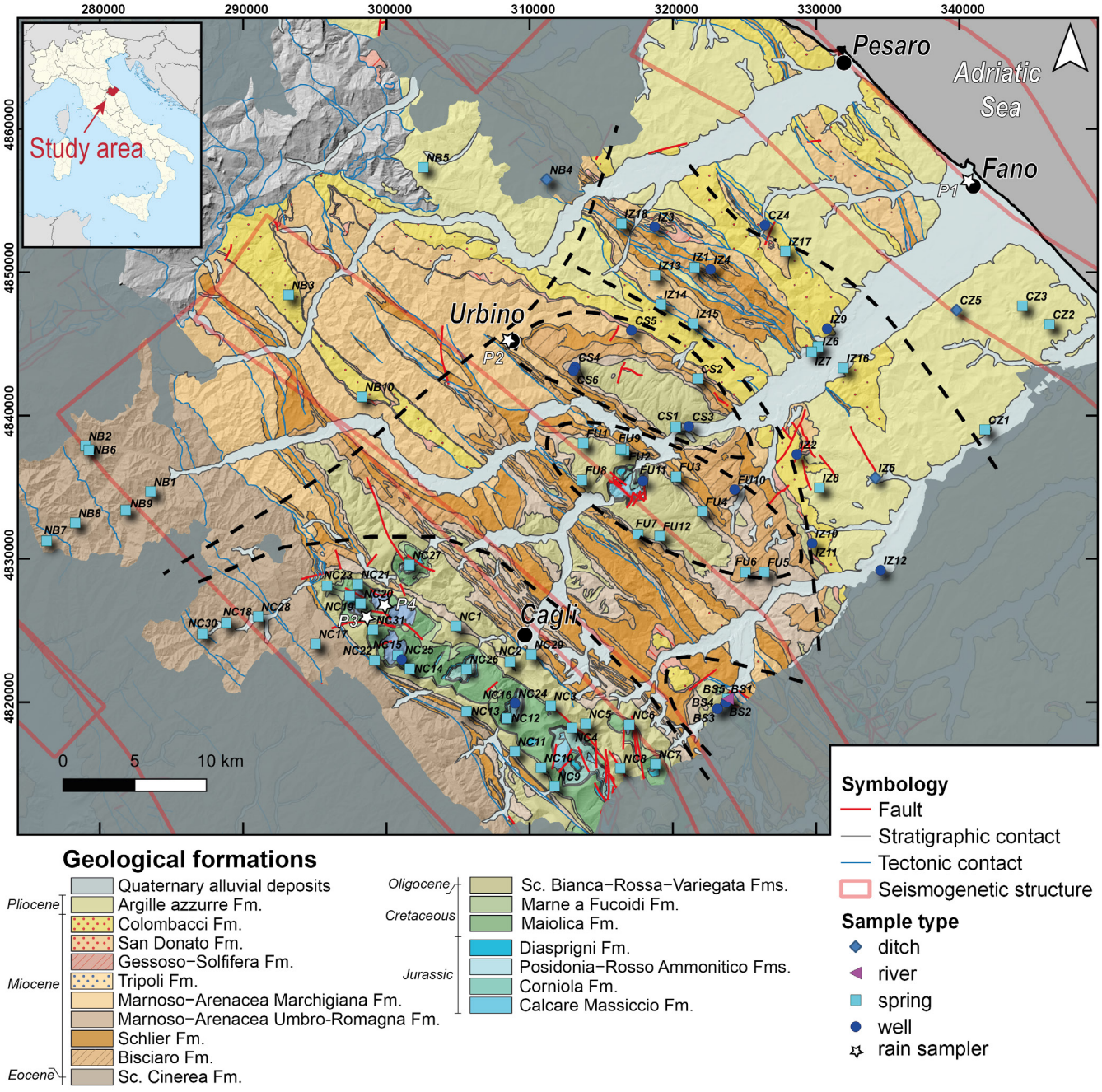

Figure 1 *Geological map of the Pesaro-Urbino (Conti et al., 2020) and location of the sampling points. Major seismogenetic structures are reported after Diss Working Group (2021). Black dashed lines represent the borders of the sampling areas: NC (Nerone-Catria Ridge), FU (Furlo Gorge), CS (Cesano-Ridge), BS (Bellisio Solfare), IZ (Internal Zone), CZ (Coastal Zone), and NB (Northern Border). For further details, please refer to Chemeri et al. (2024).*

SAMPLING STRATEGY AND ANALYTICAL METHODS

During the first step of the project, a large-scale sampling survey was performed, covering as much as possible the entire study area and its geological and topographic variability, collecting a total of 87 water samples from springs, wells and ditches, to define the main geochemical processes acting in the PU province. The survey was performed twice, during Spring and Winter 2022 (for a total of 145 analyses), in order to evaluate any possible influence related to seasonality. At each sampling sites, physico-chemical parameters were measured in situ and different aliquots were collected to determine *i*) major and minor components, *ii*) trace elements, *iii*) water stable isotopes and *iv*) the $\delta^{13}C$ in dissolved CO_2 and CH_4, this latter analysis was performed on a restricted number of sampling sites. For a detailed description of the sampling procedures and of the analytical methods deployed, I refer to Chemeri et al. (2024).

For the second step, a multi-isotopic approach was carried out, during February and November 2023, to deepen the understanding on water-rock interaction processes, reconstruct the hydrological pathways and assess sampling sites' suitability for the inclusion in a water monitoring network aimed at seismic surveillance (Chemeri et al., 2025b). A restricted number of sampling sites was selected following the results obtained from the large-scale geochemical characterization (Chemeri et al., 2024). The multi-isotopic approach involved the determination of *i*) the $\delta^{13}C$ in the total dissolved inorganic carbon (TDIC), *ii*) the $\delta^{34}S$ and $\delta^{18}O$ in the dissolved sulfate (SO_4), *iii*) the boron isotopic ratios ($\delta^{11}B$) and *iv*) those of strontium ($^{87}Sr/^{86}Sr$). Together with the isotopic determinations, major and trace components as well as water stable isotopes were also determined. The detailed description of the sampling strategy and of the different chemical and isotopic methodologies applied for the second step of the project are widely discussed and presented in Chemeri et al. (2025b).

RESULTS AND DISCUSSION

Hydrogeochemical characterization

The PU waters showed a wide compositional variability and a large variation of TDS values (230 mg/L < TDS < 4930 mg/L), thus reflecting multiple water-rock interaction processes acting at different extents and different hydrological pathways within shallow and deeper aquifers. The complete results are reported in Chemeri et al. (2024). Hence, the PU groundwaters can be classified into 5 compositional groups (Fig. 2a): (a) Ca-HCO_3 waters, including most of the samples, *i.e.*, those collected from springs and wells characterized by TDS values < 750 mg/L; (b) Ca-HCO_3(SO_4) waters, which showed significant enrichment in SO_4^{2-} (up to 200 mg/L); (c) Ca-SO_4 waters, including high-TDS (>1500 mg/L) springs; (d) Na-HCO_3 waters, pertaining to waters collected from "sulfur springs" which were also characterized by alkaline pH (> 8.8) and negative Eh (< -180 meV); and (e) Na-Cl waters, those collected from ditches (Chemeri et al., 2024). The water stable isotope composition did not show any relevant correlation with the compositional groups and setting aside for Ca-SO_4 and/or Na-HCO_3 discharges (showing anomalous values in a few trace elements such as Li, B, As, Sr), most of the waters were characterized by extremely low contents in trace metals. Referring to major dissolved gases, two compositional clusters were identified: (a) N_2-dominated gases with N_2/Ar ratios similar to those of air and ASW (Air Saturated Water), mainly pertaining to Ca-HCO_3 discharges; (b) CO_2- and/or CH_4-rich gases related to Ca-SO_4 and Na-HCO_3 springs.

Based on the geochemical evidence, the Ca-HCO_3 hydrofacies includes most of the waters characterized by low-to-medium TDS values (< 1200 mg/L) and does not show any anomaly in terms of pH values and trace element contents. Therefore, the origin of Ca-HCO_3 waters results by the congruent dissolution of carbonate-bearing (*i.e.*, calcite, dolomite) rocks, in accordance with the geology of the area (Fig. 1). However, slight enrichments in Na^+ may be associated with silicate weathering. Ca-HCO_3(SO_4) waters, characterized by moderate to strong enrichments in sulfate (up to 240 mg/L), are related to the dissolution of gypsum and anhydrite minerals hosted within deeper layers (i.e., Burano Fm) since these waters emerge from carbonate formations linked to the Basal Aquifer. The variable contents of sulfate likely depend on the different degrees of interaction with the anhydrite formations or dilution processes with shallower aquifers (Capaccioni et al., 2001; Chemeri et al., 2024). The Ca-SO_4-type are characterized by TDS values up to 4,900 mg/L. Their origin is related to interaction with gypsum-anhydrite lithologies, i.e., the Burano Fm or the Gessoso-Solfifera Fm, according to their geographical location and local geology (Fig. 1). The enrichments in chloride and sodium shown by a few of these waters indicate halite dissolution as another major process governing their geochemistry, which is also consistent with their Br, B, and Li contents (Chemeri et al., 2024; 2025b). These waters emerge in areas where Messinian evaporites or Triassic anhydrites do not outcrop, thus suggesting that they are related to long flow paths in deeper layers (Capaccioni et al., 2021; Chemeri et al., 2024; 2025b). The Na-HCO_3 waters show strong Na and (HCO_3+CO_3) excess relative to the stoichiometric ratio with Cl and Ca+Mg, respectively. Among minor and trace elements, these waters display high contents in F, NH_4, Li and B and relatively low values of Sr and Ba.

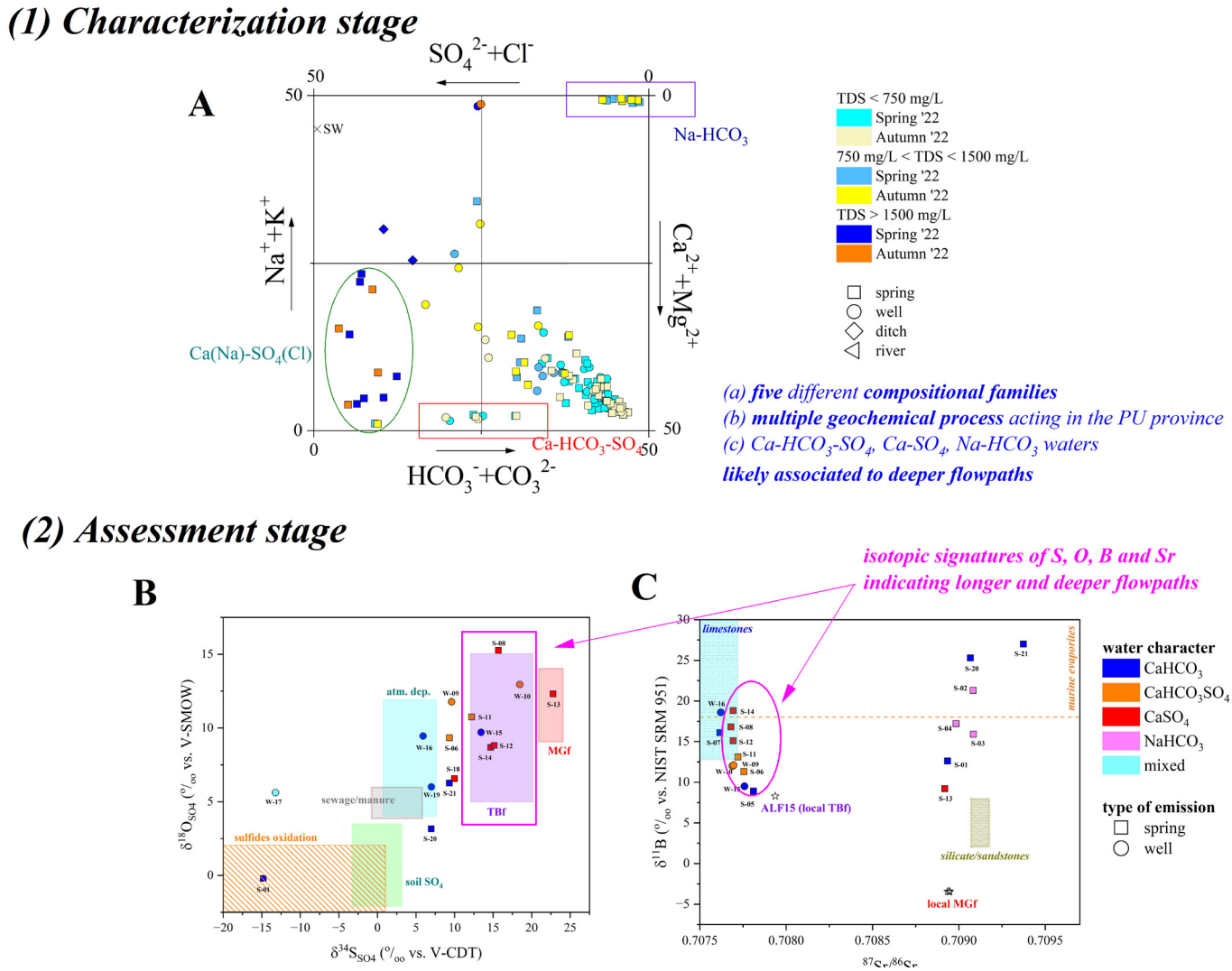

Figure 2 Summary of the results obtained during the characterization and assessment stages. **a)** Langellier-Ludwig square diagram for the waters circulating within the Pesaro-Urbino province (from Chemeri et al., 2024). **b)** $\delta^{18}O_{SO_4}$ (in ‰ vs. V-SMOW) vs. $\delta^{34}S_{SO_4}$ (in ‰ vs. V-CDT) binary diagram. **c)** $\delta^{11}B$ (in ‰ vs. NIST SRM 951) vs. $^{87}Sr/^{86}Sr$. In plot **(b)**, the isotopic ranges for different potential sources of sulfate are also drawn according to Gori et al. (2023) and Chemeri et al. (2025b). Acronyms are: TBf (Triassic Burano Fm), MGf (Messian Gessoso Solfifera Fm), oS (organic sulfur) and ps (sulfides). In plot **(c)**, the isotopic ranges for both B and Sr in limestones and siliciclastic sediments/sandstones are reported according to Chemeri et al. (2025b). The stars indicate the $\delta^{11}B$ and $^{87}Sr/^{86}Sr$ ratios measured in local rocks TBf (Triassic Burano formation: ALF15) and MGf (Messinian Gessoso Solfifera formation). IDs as reported in Chemeri et al. (2025b).

Moreover, the B/Cl and Li/Cl ratios in these waters are higher than those recorded in Ca(Na)-SO_4(Cl) discharges, indicating that the Na-HCO_3 waters are enriched in B and Li and Cl-poor when compared to those detected in the Ca(Na)-SO_4(Cl) springs. Their composition is likely acquired following prolonged weathering of Na-rich silicate rocks, thus allowing the release of sodium in solution, along with B, Li and F, due to their marked affinity with the former. This hypothesis agrees with the fact that these waters emerge from the siliciclastic Marnoso Arenacea Fm (Fig. 1), whose interaction with the circulating waters produces alkaline hydrolysis, as supported by the high pH values detected in these samples. The excess in bicarbonate species is likely associated with the $CO_{2(aq)}$ produced by the decay of organic matter trapped in the foredeep sediments, boosted by a reducing environment (negative Eh values). Eventually, Na-Cl waters were only pertaining to those samples collected from ditches, and they are likely deriving from a mixing process involving meteoric-sourced solutions and highly saline (Na-Cl) connate waters, whose presence within the Adriatic foredeep clayey deposits has widely been reported (Chemeri et al., 2024 and references therein).

As far as the origin of dissolved gases is concerned, the N_2, Ar and O_2 contents in both N_2- and CO_2(CH_4)-dominated samples are related to the dissolution of atmospheric gases whereas CO_2 and CH_4 are biogenically derived, as confirmed by their $\delta^{13}C$ values, are probably formed following plant-root respiration processes and decay of organic matter (Chemeri et al., 2024).

Consequently, the results obtained from the first step of the project allowed to understand that Ca-HCO_3(SO_4), Ca(Na)-SO_4(Cl) and Na-HCO_3 water discharges are likely related to relatively deeper hydrogeological pathways and their emergence at surface is probably favoured by the local structures and might be interesting to monitor for seismic precursors. Following these results, these sampling sites were carefully investigated during the second phase (*i.e.*, multi-isotopic approach).

Multi-isotopic approach

Stable and radiogenic isotope composition of groundwaters has been proven to be highly effective in interpreting geochemical and hydrogeological processes in natural environments. In the present study, isotope (H, O, C, S, B, Sr) systematics were explored to disentangle different information and constraints on the characteristics of the groundwater circulating in the seismically active area of the PU province and evaluate the sampling sites' hydro sensitivity for their inclusion in a water monitoring network aimed at seismic surveillance and hazard mitigation. The full results are reported In Chemeri et al. (2025b).

The investigated waters are characterized by δ^{13}C-TDIC values < -1.67 ‰ vs. V-PDB, with less negative δ^{13}C values associated with the Na-HCO_3 and Ca(Na)-SO_4(-Cl) waters. These values are consistent with the dissolution of calcite and the interaction with biogenic soil CO_2 as the primary sources for the origin of dissolved carbon species (Bottrell et al., 2019) and are consistent with those of $\delta^{13}C_{CO_2}$ and $\delta^{13}C_{CH_4}$, which were previously mentioned (Chemeri et al., 2024; 2025b). These results clearly indicate a predominant biogenic origin for carbonate species produced at relatively shallow depths with absent or negligible contributions from deep-seated fluids. The use of sulfur and oxygen isotope systematics in the PU waters is of notable importance since some of them are characterized by either a Ca-SO_4 composition or a strong sulfate enrichment (Capaccioni et al., 2001; Chemeri et al., 2024). In both cases, sulfate can be derived by the interaction with the anhydrite-bearing Triassic Burano (TBf) or the gypsum-bearing Messinian Gessoso Solfifera (MGf) Fms, which lie at the bottom and the top of the Umbro-Marche succession, respectively (Conti et al., 2020 and references therein). Thus, if the chemical contribution of SO_4^{2-} is isotopically different, it is possible to define and constrain the hydrological circuits. Indeed, the $\delta^{34}S_{SO4}$ and $\delta^{18}O_{SO4}$ values from TBf and MGf are characterized by different isotopic ranges (Fig. 2b). In the PU waters, the more positive δ^{34}S values (> 10 ‰ vs. V-CDT) are usually associated with those waters where the gypsum-anhydrite dissolution is predominant compared to that of carbonate-bearing minerals ($SO_4 \gg HCO_3 + CO_3$) (Fig. 2b). Among the sulfate-enriched sampled, most of them are discharged from the Basal aquifer (setting aside for samples VLZ and PGL in Fig. 2b, c) with their sulfate isotopic values falling close, or within, the *TBf* field, indicating a likely interaction with the Burano Fm (Fig. 2b). Nevertheless, the influence of secondary processes, like "microbially-mediated" sulfate reduction, cannot be ruled out, at least for those waters characterized by strongly negative Eh values. On the other hand, the PGL water discharges from a hill where the Gessoso Solfifera Fm is largely outcropping (Fig. 1), and falls within the MGf field, pointing that the sole source of sulfate is related to the Messinian gypsum. Moreover, the location of VLZ contrasts with the SO_4 isotopic signature (Fig. 2b). This spring is located far from the carbonate anticline, where the TBf have been identified at > 1500 m depth in a deep well), thus suggesting that the interaction with TBf is unlikely. The Ca-HCO_3 waters tend to be positioned between or within the TBf, atmospheric deposition and soil SO_4 fields, therefore suggesting a mixed origin related to multiple sources contributing to different extents.

While the application of B isotopes may present some limitations since different sources are characterized by similar and overlapping ranges, the Sr isotopes provided useful clues. In fact, two groups of samples can be identified according to their $^{87}Sr/^{86}Sr$ ratios: *i*) $^{87}Sr/^{86}Sr$ ranging from 0.70762 and 0.70781 (including also Ca-SO_4 and Ca-SO_4-HCO_3) and falling within the TBf and limestones (*i.e.*, Calcare Massiccio and Corniola Fms) isotopic ranges; *ii*) $^{87}Sr/^{86}Sr$ ratios included between 0.70892 and 0.70937 (including also Na-HCO_3 and PGL waters), approaching the reference values of MGf and the carbonate fraction of the Marnoso Arenacea Fm. Taking into account the δ^{11}B, the distribution of the first group of samples in Figure 2c suggests that the primary source of Sr (and consequently of Ca) is represented by TBf and/or limestones, which is consistent with the main geochemical processes occurring in these waters and with the hydrogeological features of the areas where they circulate. Additionally, Sr and B values confirmed that the PGL sample is interacting with the MGf and that the origin of Na-HCO_3 waters is associated with the interaction with silicate lithologies, since they all show isotopic values consistent with the weathering of the local Marnoso Arenacea Fm (Fig. 2c). As previously discussed, the different contributions in Ca-HCO_3 may be multiple and influenced by the surroundings lithology and hydrogeology. Further details on the data discussion are reported in Chemeri et al. (2025b).

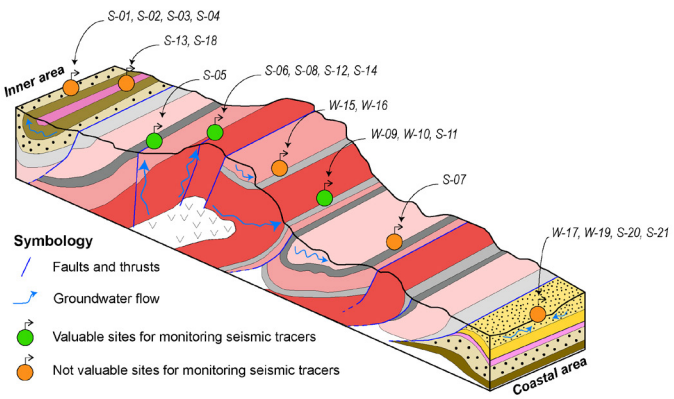

Figure 3 *Conceptual model summarizing the hydrogeological circuits of the investigated sites, which helps to define the most valuable setting to be monitored for possible seismic tracers' recognition in the investigated area of the Pesaro-Urbino Province. The sketch follows and modifies the schematic model of Nanni and Vivalda (2005). For sample IDs and colours, refer to Chemeri et al. (2025b).*

CONCLUDING REMARKS

In deploying a water geochemical monitoring network to identify possible seismic tracers, selecting the most suitable sampling sites, *i.e.*, those related to longer circulation paths and fed by deep aquifers, is a fundamental and necessary step. For this purpose, a detailed hydrogeochemical and isotopic characterization of the groundwaters circulating in the seismically active PU province was carried out. A conceptual model of the main hydrogeological, geochemical, and isotopic findings of the present work are summarized in Figure 3. In conclusion, our results suggest that (most of) the Ca-SO_4 and Ca-HCO_3-SO_4 waters are discharged by the Basal aquifer after long and deep flow paths that lead to water–rock interactions with the local deep-seated TBf (Fig. 3), maintaining the isotopic signature of the primary source (almost) unchanged and thus less affected by secondary processes; notably, faults can play a critical role in facilitating groundwater circulation from deep layers to the surface, especially during seismic periods, when they can act as preferential flow features (Fig. 3). Indeed, these kinds of water have been widely found to be sensitive to possible geochemical and isotopic variations in similar geological-tectonic contexts such as the Sibillini Mts. (Marche Region) or the Gran Sasso Mt. area (Abruzzo Region) (*e.g.*, Barberio et al., 2017). The results of this work make our approach applicable to other geological contexts where seismic activity is well-documented, thus taking a step further to mitigate the seismic hazard.

REFERENCES

Barberio, M.D., Barbieri, M., Billi, A., Doglioni, C., Petitta, M. (2017) - Hydrogeochemical changes before and during the 2016 Amatrice-Norcia seismic sequence (central Italy). Sci. Rep., 7(1), 11735.

Capaccioni, B., Didero, M., Paletta, C., Salvadori, P. (2001) - Hydrogeochemistry of groundwaters from carbonate formations with basal gypsiferous layers: an example from the Mt. Catria-Mt. Nerone ridge (Northern Apennines, Italy). J. Hydrol., 253, 14-26.

Chemeri, L., Taussi, M., Cabassi, J., Capecchiacci, F., Randazzo, A., Tassi, F., Renzulli, A., Vaselli, O. (2024) - Groundwater and dissolved gases geochemistry in the Pesaro-Urbino province (northern Marche, central Italy) as a tool for seismic surveillance and sustainability. Sustainability, 16, 5178.

Chemeri, L., Taussi, M., Fronzi, D., Cabassi, J., Mazzoli, S., Tazioli, A., Renzulli, A., Vaselli, O. (2025a) - Groundwater hydrogeochemical changes predating and following the November 9, 2022 Mw 5.5 Adriatic Offshore earthquake. J. Hydrol., 653, 132792.

Chemeri, L., Taussi, M., Cabassi, J., Venturi, S., Huertas, A. D., Granados, A., Agostini, S., Fronzi, D., Renzulli, A., Vaselli, O. (2025b) - Water-rock interaction processes and hydrogeological pathways in seismically active areas as revealed by a multi-isotopic (C, S, O, H, B, Sr) approach. J. Hydrol., 661, 133533.

Cicerone, R. D., Ebel, J. E., Britton, J. (2009) - A systematic compilation of earthquake precursors. Tectonophysics, 476, 371-396.

Conti, P., Cornamusini, G., Carmignani, L. (2020) - An outline of the geology of the Northern Apennines (Italy), with geological map 1:250.000 scale. Ital. J. Geosci., 139, 149-194.

DISS Working Group (2021) - Database of Individual Seismogenic Sources (DISS), Version 3.3.0: a compilation of potential sources for earthquakes than M 5.5 in Italy and surrounding areas. Istituto Nazionale di Geofisica e Vulcanologia (INGV).

Doglioni, C., Barba, S., Carminati, E., Riguzzi, F. (2014) - Fault on-off versus coseismic fluid reactions. Geosci. Front., 5(6), 767-780.

Franchini, F., Agostini, S., Barberio, M. D., Barbieri, M., Billi, A., Boschetti, T., Pennisi, M., Petitta, M. (2021) - HydroQuakes, central Apennines: towards a hydrogeochemical monitoring network for seismic precursors and the hydro-seismo-sensitivity of boron. J. Hydrol., 598, 125754.

Gori, F., Paternoster, M., Barbieri, M., Buttitta, D., Caracausi, A., Parente, F., Sulli, A., Petitta, M. (2023) - Hydrogeochemical multi-component approach to assess fluids upwelling and mixing in shallow carbonate-evaporitic aquifers (Contursi area, southern Apennines, Italy). J. Hydrol., 619, 129258.

Nanni, T. & Vivalda, P. (2005) - The aquifers of the Umbria-Marche Adriatic region: relationships between structural setting and groundwater chemistry. Boll. Soc. Geol. It., 124, 523-542.

Thomas, D. (1988) - Geochemical precursors to seismic activity. Pure Appl. Geophys., 126, 241-266.

Wang, C-Y. & Manga, M. (2021) - Water and earthquakes. Springer Nature.

Unravelling the Ancient (> 46 ka) Volcanostratigraphy of Pantelleria Island (Sicily Strait, Italy) by Single-Grain $^{40}Ar/^{39}Ar$ Dating

Alessandra Cinquegrani
Department of Earth and Marine Sciences, University of Palermo, Via Archirafi 22, 90123, Palermo
DOI: 10.19276/plinius.2025.01.006

INTRODUCTION

Peralkaline magmatism is frequently associated with highly explosive activity (*e.g.*, Parker & White, 2008; Claessens et al., 2016; Wallace et al., 2025), making the precise reconstruction of eruptive cycles essential for volcanic hazard assessment, particularly in densely populated magmatic districts such as Pantelleria Island.

Located within the Sicily Strait Rift Zone (Italy), Pantelleria represents the subaerial portion of a large, active, composite Quaternary volcanic complex, distinguished as the type locality for pantellerite, an iron-rich, peralkaline (Na+K/Al > 1; Macdonald, 1974) rhyolite. Peralkaline magmatism has primarily driven the subaerial eruptive history of the island, accounting for ~ 95% of the exposed lithology (Fig. 1), emplaced as ignimbrites, fallout deposits, and lava flows. Basaltic lava flows and cinder cones constitute only ~ 5% of the total volcanic products, and together they represent the typical bimodal alkaline rock suite (the 'Daly Gap') characteristic of certain intraplate settings (*e.g.*, Scaillet & Macdonald, 2001; White et al., 2009; Romengo et al., 2012; Macdonald et al., 2022).

Pantelleria boasts a subaerial eruptive history spanning over 320 kyr (Mahood & Hildreth, 1986), characterised by the emplacement of nine recognised ignimbrite deposits (ignimbrite periods), linked to at least two caldera collapse events (*e.g.*, Mahood & Hildreth, 1986; Rotolo et al., 2013; Scaillet et al., 2013; Jordan et al., 2018). While the last seven ignimbrites have been geochronologically well-constrained by the $^{40}Ar/^{39}Ar$ method within the range of 187-46 ka (Rotolo et al., 2013; Scaillet et al., 2013; Jordan et al., 2018), the earliest two have remained poorly constrained or undated. Specifically, the Zinedi Fm. was dated by the K/Ar method at ~ 189 ka (Mahood & Hildreth, 1986) but with large analytical errors (± 6 ka; 1σ) and poor internal systematics, whereas the Pozzolana Fm. was broadly constrained between 189 and 128 ka based on field

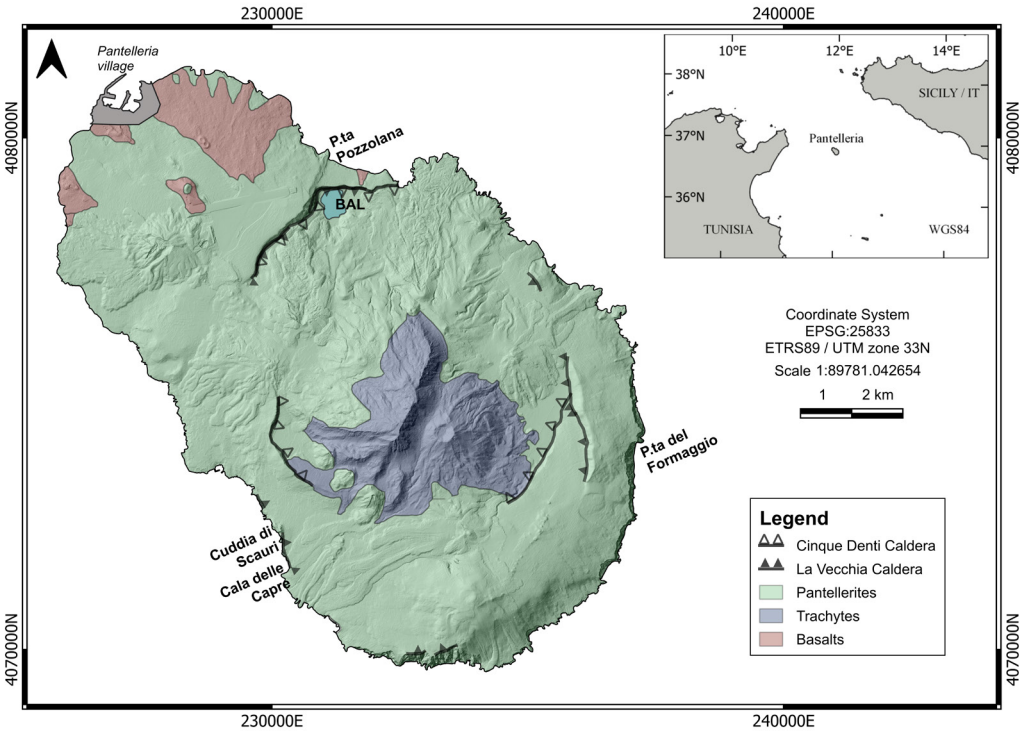

Figure 1 *Digital Elevation Model (DEM) of Pantelleria Island with a simplified geological extent. The location of Pantelleria within the Sicily Strait (Italy) is indicated in the top right box. BAL = Bagno dell'Acqua Lake.*

relationships (Mahood & Hildreth, 1986; Jordan et al., 2018).

The ignimbrite-forming eruptions were interspersed with several less explosive to effusive activity (inter-ignimbrite periods) from minor, locally distributed eruptive centres (*e.g.*, Civetta et al., 1984, 1988; Mahood & Hildreth, 1986; Rotolo et al., 2007; Scaillet et al., 2011; Romano et al., 2022). The more recent eruptive history, following the emplacement of the last ignimbrite deposit, the Green Tuff Formation (GT Fm.) (~ 46 ka; Scaillet et al., 2013), has been widely investigated by the scientific community (*e.g.*, Civetta et al., 1984, 1988; Mahood & Hildreth, 1986; Rotolo et al., 2007; Scaillet et al., 2011; Romano et al., 2022). In contrast, the older (pre-GT) eruptive cycles had remained poorly constrained. The existing geochronological framework for the pre-GT deposits had mostly relied on 24 K/Ar ages, all dating back to the 1980s (Civetta et al., 1984; Mahood & Hildreth, 1986), affected by large analytical uncertainties (up to ± 72 ka; 1σ), with some representing duplicate dates from the same eruptive centres.

This study focused on $^{40}Ar/^{39}Ar$ geochronology as a tool to refine the island's stratigraphy by dating previously unknown rock formations and enabling reliable field correlations. We conducted radiometric analyses on single anorthoclase crystals, a ubiquitous phase within the peralkaline eruptive units (*e.g.*, Scaillet & Macdonald, 2001; White et al., 2009; Scaillet et al., 2011, 2013). We targeted the earliest recognised ignimbrite units and associated lava and breccia deposits to establish the stratigraphic sequence of the major eruptions. Additionally, we dated some of the earliest eruptive units, mostly located in a few discontinuous, southern coastal sections, in order to assess the subaerial eruptive onset and early eruptive cyclicity. This approach has provided improved constraints on the subaerial eruptive history of Pantelleria, enabling the evaluation of eruptive timescales and associated volcanic hazards.

SAMPLE PREPARATION AND ANALYTICAL TECHNIQUES

Samples for $^{40}Ar/^{39}Ar$ dating were collected based on their freshness on site and further examined under a petrographic microscope. After dry-crushing and sieving into 0.5-1 mm and 1-2 mm, feldspar phenocrysts were separated using an isodynamic magnetic separator and etched with 5 mol% HF for ~ 5 min in an ultrasonic bath to remove adhering glass (if any). Feldspars were then carefully hand-picked under a binocular microscope for final concentrations, discarding crystals with incipient alteration or hosting inclusions.

Samples were wrapped in Al foils and stacked in a cylindrical sample holder (10 mm diameter) with 7 grains of a known age fluence monitor (Fish Canyon Tuff, 28.305 ± 0.036 Ma; Renne et al., 2010, 2011) interspersed every five sample packets, and sent for neutron irradiation into the Cadmium-Lined in-Core position CLICIT of Corvallis Nuclear Reactor (Oregon State University, United States).

$^{40}Ar/^{39}Ar$ analyses were conducted at the Institut des Sciences de la Terre d'Orléans (CNRS-ISTO) using a Thermo Fisher Helix mass spectrometer. After loading, samples were baked at ~ 200°C for approximately 48 hours. A minimum of 27 single-grain analyses were carried out for each sample using one-step laser ablation at high temperature with a CO_2 laser operated at 20% full power for about 40 seconds and equipped with a focusing lens.

Ages are reported as Weighted Mean Age (WMA), determined on the analyses sorted by increasing age, as long as the Mean Square Weighted Deviates (MSWD) remained within the fiducial interval (review in Schaen et al., 2021). Age calculations used an initial atmospheric $^{40}Ar/^{36}Ar$ ratio of 295.5 (Nier, 1950) and a total decay constant for ^{40}K of 5.543×10^{-10} y^{-1} (Steiger & Jäger, 1977). Ages are reported with uncertainties of 1σ.

DISCUSSION

A total of 25 new eruptive ages are provided, covering 2 ignimbrites, 12 lava flows, 8 fallout deposits, 1 dyke, and 1 welded breccia, resulting in a substantial revision of the previously accepted stratigraphy (Fig. 2). These new eruptive ages have enabled more robust stratigraphic correlations between isolated volcanic units, refining the temporal and stratigraphic framework of Pantelleria Island. In particular, the revised chronology allows for a clearer temporal ordering of eruptive cycles, improves the identification of stratigraphic gaps, and facilitates more accurate correlation of dispersed outcrops across the island.

Refinement of the Ignimbrite Stratigraphy

Previously considered the oldest ignimbrite units of Pantelleria, the Zinedi and Pozzolana Fms. yielded WMAs of 178.1 ± 0.8 ka (1σ) and 156.5 ± 1.1 ka (1σ), respectively. These new data have led to a revised stratigraphy of the island's highly explosive volcanic events, significantly modifying the previously accepted chronological framework (Fig. 3). The oldest ignimbrite deposit is now recognised as the Polacca Fm. (~ 187 ka; Jordan et al., 2018), slightly younger than or subcoeval with the lava flow (Punta Pozzolana lava; Fig. 1) set at the base of the stratigraphic sequence (beneath the Zinedi Fm.) in the northeast sector, which yielded a WMA of 188.9 ± 1.6 ka (1σ). This raises the possibility that the Polacca Fm. may extend below the present-day sea level, as it is improbable that it is exposed only in the southern sector of the island, despite being the most voluminous ignimbrite (DRE of ~ 0.64 km^3; Jordan et al., 2018).

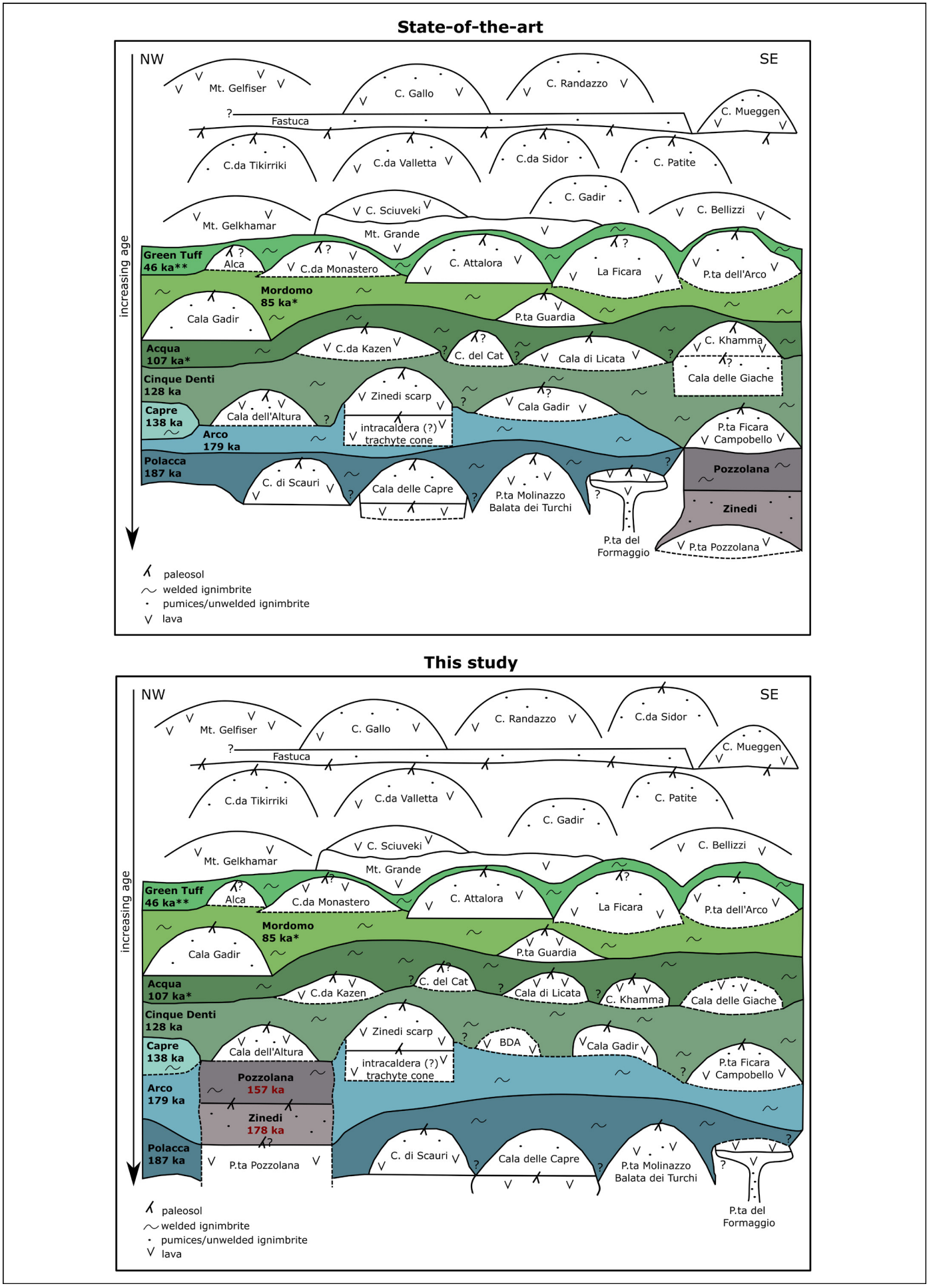

Figure 2 Schematic stratigraphic schemes of Pantelleria (modified after Rotolo et al., 2021), according to the state-of-the-art (above) and after this study (below). Coloured levels represent ignimbrite deposits, with eruptive ages from Jordan et al. (2018), except for: *ages from Rotolo et al. (2013); **age from Scaillet et al. (2013). New eruptive ages from this study are in red.

Earlier (> 46 ka) eruptive cycles

The earliest deposit has been recorded in the southwestern sector of the island, at Cala delle Capre (Fig. 1), where the lava flow at the base of the stratigraphic sequence provided a WMA of 326.5 ± 0.9 ka (1σ). The volcanic activity then migrated less than 1 km to the northwest, at Cuddia di Scauri (Fig. 1), where the dating of a fallout deposit provided a WMA of 323.1 ± 1.6 ka (1σ), suggesting the early development of a complex eruptive system along a narrow coastal corridor. Subsequently, volcanism progressed to the southeast up to Punta del Formaggio (≤ 200 ka; Fig. 1), likely being active simultaneously with the previously mentioned Pozzolana centre to the northeast, as no older deposits have been recorded to the north. Evolved, peralkaline magmas primarily drove the emplacement of multiple lava flows and fallout deposits from localised, short-lived eruptive centres, which preceded the earliest Polacca ignimbrite (~ 187 ka; Jordan et al., 2018). After this initial stage and the emplacement of the nine known ignimbrite deposits, the intervening (inter-ignimbrite) periods were dominated by effusive to mildly explosive eruptions, more widely distributed across the island. We particularly constrained fallout deposits in the range of 154-60 ka, and lava flows between 151 and 47 ka, sometimes considerably refining previous K/Ar ages affected by large analytical uncertainties (up to ± 72 ka; 1σ).

CONCLUSIONS

Pantelleria Island has been characterised by vigorous volcanic activity, punctuated by several explosive to effusive eruptions mainly fed by peralkaline magmas. The subaerial activity preceding the emplacement of the earliest ignimbrite-forming eruption, currently set as the Polacca Fm. (~ 187 ka; Jordan et al., 2018), is now accurately assessed at ~ 327 ka in the southwestern coastal section. The Polacca Fm. predates the Zinedi (~ 178 ka) and Pozzolana (~ 157 ka) Fms., which had previously been considered the earliest major explosive events. An average ignimbrite eruption frequency of ~ 0.064 events/kyr (one ignimbrite every ~ 15.7 ka) was calculated between 186.9 and 45.7 ka (Rotolo et al., 2013; Scaillet et al., 2013; Jordan et al., 2018; this study). However, significant temporal variability is observed, including the earliest three ignimbrite events within ~ 9 kyr and a prolonged quiescence of ~ 39 kyr prior to the latest GT eruption.

The inter-ignimbrite periods were characterised by the emplacement of several lava flows and fallout deposits, which occurred simultaneously along the entire volcanic history of the island, as several local eruptive centres produced both explosive and effusive activities. The eruptive activity involved various sectors of the island from north to south, potentially influenced

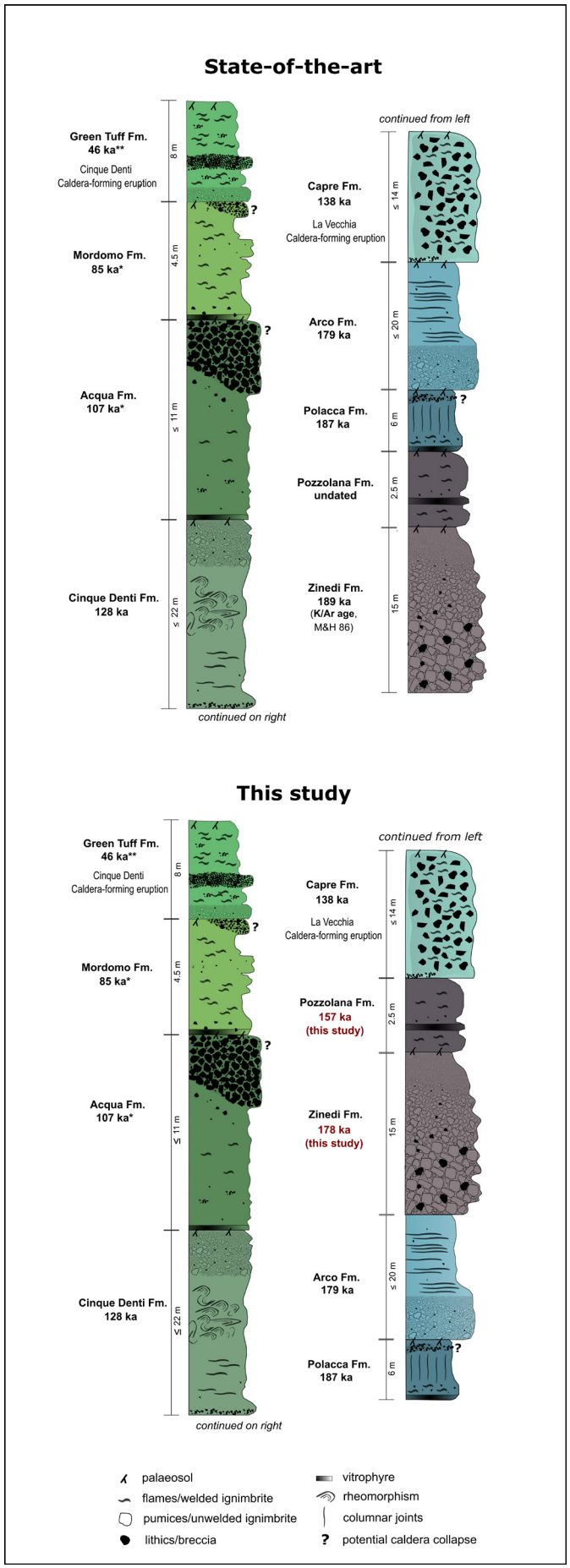

Figure 3 Synthetic logs of the ignimbrite stratigraphy of Pantelleria (modified after Jordan et al., 2018), according to the state-of-the-art (above) and after this study (below). $^{40}Ar/^{39}Ar$ ages are from Jordan et al. (2018), except for: *ages from Rotolo et al. (2013); **age from Scaillet et al. (2013). New eruptive ages from this study in red. M&H 86 refers to Mahood & Hildreth (1986). Question marks indicate welded breccias associated with potential caldera collapses.

by the emplacement of ignimbrite-forming eruptions and associated caldera collapses, which repeatedly modified the geological and structural setting of the island. The post-GT eruptive activity appears to have migrated from the south to the north, with the last inland eruption occurring ~ 7 ka (Scaillet et al., 2011) and the 1891 submarine eruption (Foerstner volcano) ~ 4 km northwest of Pantelleria (Kelly et al., 2014), consistent with the tectonic alignment of the Sicily Strait (*e.g.*, Civile et al., 2010).

The obtained results have several scientific implications and will offer valuable insights for ongoing and future research. Defining the entire subaerial eruptive history of the island and integrating it with the geochemical and geophysical data acquired by the active monitoring networks will permit us to define the true state of activity of the volcanic system. In this way, it may be possible to investigate any long and short-term volcanic cyclicity, with implications for possible volcanic unrest. It is important to consider that the diffusive volcanism that followed the latest GT ignimbrite (~ 46 ka; Scaillet et al., 2013), with a multitude of volcanic centres up to the latest inland eruption (~ 7 ka; Scaillet et al., 2011), may itself represent an inter-ignimbrite period. The age data, coupled with macro- and micro-scale petrological observations and whole-rock analyses, will enable the evaluation of the degree of magma evolution over time. This will lead to a deeper understanding of the plumbing system dynamics, particularly the productivity of pantellerite magmas, given its propensity to originate highly explosive eruptions on the island. Moreover, a refined stratigraphy will allow correlations with distal tephra deposits, enabling the assessment of the true dispersal of major eruption deposits and the quantitative determination of their magnitude. The obtained ages will also serve as a valuable constraint for the ongoing compilation of the geological map "Torretta Granitola – Pantelleria" at the scale 1:50.000 by the Geological Survey of Italy-ISPRA (CARG-Project). Finally, a comparison with Linosa Island, for which $^{40}Ar/^{39}Ar$ dating is still in progress, will provide deeper insights into the volcanic and magmatic dynamics of the Sicily Strait district, which can then be applied to similar highly productive Quaternary volcanic centres worldwide, particularly in terms of volcanic hazard assessment.

REFERENCES

Barberio, M.D., Barbieri, M., Billi, A., Doglioni, C., Petitta, M. (2017) - Hydrogeochemical changes before and during the 2016 Amatrice-Norcia seismic sequence (central Italy). Sci. Rep., 7(1), 11735.

Civetta, L., Cornette, Y., Crisci, G., Gillot, P.Y., Orsi, G., Requejo, C.S. (1984) - Geology, geochronology and chemical evolution of the island of Pantelleria. Geol. Mag., 121(6), 541–562.

Civetta, L., Cornette, Y., Gillot, P.Y., Orsi, G. (1988) - The eruptive history of Pantelleria (Sicily channel) in the last 50 ka. B. Volcanol., 50, 47-57.

Civile, D., Lodolo, E., Accettella, D., Geletti, R., Ben-Avraham, Z., Deponte, M., Facchin, L., Ramella, R., Romeo, R. (2010) - The Pantelleria graben (Sicily Channel, Central Mediterranean): An example of intraplate 'passive' rift. Tectonophysics, 490(3–4), 173–183.

Claessens, L., Veldkamp, A., Schoorl, J.M., Wijbrans, J. R., Van Gorp, W., Macdonald, R. (2016) - Large scale pantelleritic ash flow eruptions during the Late Miocene in central Kenya and evidence for significant environmental impact. Glob. Planet. Change, 145, 30-41.

Jordan, N.J., Rotolo, S.G., Williams, R., Speranza, F., McIntosh, W.C., Branney, M.J., Scaillet, S. (2018) - Explosive eruptive history of Pantelleria, Italy: Repeated caldera collapse and ignimbrite emplacement at a peralkaline volcano. J. Volcanol. Geoth. Res., 349, 47–73.

Kelly, J.T., Carey, S., Pistolesi, M., Rosi, M., Croff-Bell, K.L., Roman, C., Marani, M. (2014) - Exploration of the 1891 Foerstner submarine vent site (Pantelleria, Italy): Insights into the formation of basaltic balloons. B. Volcanol., 76(7), 844.

Macdonald, R. (1974) - Nomenclature and petrochemistry of the peralkaline oversaturated extrusive rocks. B. Volcanol., 38(2), 498–516.

Macdonald, R., White, J.C., Belkin, H.E. (2022) - Peralkaline silicic extrusive rocks: Magma genesis, evolution, plumbing systems and eruption. C. R. Geosci., 353(S2), 7–59.

Mahood, G.A. & Hildreth, W. (1986) - Geology of the peralkaline volcano at Pantelleria, Strait of Sicily. B. Volcanol., 48(2–3), 143–172.

Nier, A.O. (1950) - A Redetermination of the Relative Abundances of the Isotopes of Carbon, Nitrogen, Oxygen, Argon, and Potassium. Phys. Rev., 77(6), 789–793.

Parker, D.F. & White, J.C. (2008) - Large-scale silicic alkalic magmatism associated with the Buckhorn Caldera, Trans-Pecos Texas, USA: comparison with Pantelleria, Italy. B. Volcanol., 70, 403-415.

Renne, P.R., Balco, G., Ludwig, K.R., Mundil, R., Min, K. (2011) - Response to the comment by W.H. Schwarz et al. On "Joint determination of ^{40}K decay constants and $^{40}Ar^*/^{40}K$ for the Fish Canyon sanidine standard, and improved accuracy for $^{40}Ar/^{39}Ar$ geochronology" by P. R. Renne et al. (2010). Geochim. Cosmochim. Ac., 75(17), 5097–5100.

Renne, P.R., Mundil, R., Balco, G., Min, K., Ludwig, K. R. (2010) - Joint determination of ^{40}K decay constants and $^{40}Ar^*/^{40}K$ for the Fish Canyon sanidine standard, and improved accuracy for $^{40}Ar/^{39}Ar$ geochronology. Geochim. Cosmochim. Ac., 74(18), 5349–5367.

Romano, P., White, J., Rotolo, S., Jordan, N., Cirrincione, R., De Giorgio, G., Fiannacca, P., Vaccaro, E.

(2022) - Contrasting Styles of Inter-Caldera Volcanism in a Peralkaline System: Case Studies from Pantelleria (Sicily Channel, Italy). Minerals, 12, 406.

Romengo, N., Landi, P., Rotolo, S.G. (2012) - Evidence of basaltic magma intrusions in a trachytic magma chamber at Pantelleria (Italy). Period. Mineral., 81(2), 163–178.

Rotolo, S.G., La Felice, S., Mangalaviti, A., Landi, P. (2007) - Geology and petrochemistry of the recent (< 25 ka) silicic volcanism at Pantelleria island. Boll. Soc. Geol. Ital., 126, 191-208.

Rotolo, S.G., Scaillet, S., La Felice, S., Vita-Scaillet, G. (2013) - A revision of the structure and stratigraphy of pre-Green Tuff ignimbrites at Pantelleria (Strait of Sicily). J. Volcanol. Geoth. Res., 250, 61–74.

Rotolo, S.G., Scaillet, S., Speranza, F., White, J.C., Williams, R., Jordan, N.J. (2021) - Volcanological evolution of Pantelleria Island (Strait of Sicily) peralkaline volcano: a review. C. R. Geosci., 353, 111-132.

Scaillet, B. & Macdonald, R. (2001) - Phase Relations of Peralkaline Silicic Magmas and Petrogenetic Implications. J. Petrol., 42(4), 825–845.

Scaillet, S., Rotolo, S.G., La Felice, S., Vita-Scaillet, G. (2011) - High-resolution $^{40}Ar/^{39}Ar$ chronostratigraphy of the post-caldera (<20ka) volcanic activity at Pantelleria, Sicily Strait. Earth Planet. Sc. Lett., 309(3–4), 280–290.

Scaillet, S., Vita-Scaillet, G., Rotolo, S.G. (2013) - Millennial-scale phase relationships between ice-core and Mediterranean marine records: Insights from high-precision $^{40}Ar/^{39}Ar$ dating of the Green Tuff of Pantelleria, Sicily Strait. Quaternary Sc. Rev., 78, 141–154.

Schaen, A.J., Jicha, B.R., Hodges, K.V., Vermeesch, P., Stelten, M.E., Mercer, C.M., Phillips, D., Rivera, T. A., Jourdan, F., Matchan, E.L., Hemming, S.R., Morgan, L.E., Kelley, S.P., Cassata, W.S., Heizler, M.T., Vasconcelos, P.M., Benowitz, J.A., Koppers, A.A.P., Mark, D.F., Niespolo, E.M., Sprain, C.J., Hames, W.E., Kuiper, K.F., Turrin, B.D., Renne, P.R., Ross, J., Nomade, S., Guillou, H., Webb, L.E., Cohen, B.A., Calvert, A.T., Joyce, N., Ganerod, M., Wijbrans, J., Ishizuka, O., He, H., Ramirez, A., Pfänder, J.A., Lopez-Martínez, M., Qiu, H., Singer, B.S. (2021) - Interpreting and reporting $^{40}Ar/^{39}Ar$ geochronologic data. Geol. Soc. Am. Bull., 133(3–4), 461–487.

Steiger, R.H. & Jäger, E. (1977) - Subcommission on geochronology: Convention on the use of decay constants in geo- and cosmochronology. Earth Planet. Sc. Lett., 36(3), 359–362.

Wallace, P.A., Otieno, V., Godec, P., Njoroge, R.W., Tubula, M.S., Cappelli, L., Kamau, P.M., Nomade, S., Mariita, N.O., Fontijn, K. (2025) - Temporal and spatial evolution of explosive silicic peralkaline eruptions at the Olkaria Volcanic Complex and Longonot volcano in the Southern Kenya Rift. J. Volcanol. Geoth. Res., 460, 108275.

White, J.C., Parker, D.F., Ren, M. (2009) - The origin of trachyte and pantellerite from Pantelleria, Italy: Insights from major element, trace element, and thermodynamic modelling. J. Volcanol. Geoth. Res., 179(1–2), 33–55.

Moving towards circular economy: REE recovery from secondary sources exploiting zeolites cation exchange properties

Francesco Colombo
Department of Chemical and Geological Sciences, University of Modena and Reggio Emilia, Via G. Campi 103, 41125, Modena
DOI: 10.19276/plinius.2025.01.007

INTRODUCTION

Rare Earth Elements (REEs) comprise a group of 17 elements, including the 15 lanthanides (atomic numbers 57-71) plus scandium (Sc) and yttrium (Y). These elements are typically divided into light rare earth elements (LREEs: La-Gd) and heavy rare earth elements (HREEs: Tb-Lu) based on their electron configurations and atomic masses. Most REEs predominantly form trivalent ions (RE^{3+}), though cerium can also exist as Ce^{4+} and europium as Eu^{2+} under specific conditions. The most economically significant REE deposits include the Bayan Obo deposit in China, considered the world's largest REE deposit (Huang et al., 2015; Smith et al., 2016; Song et al., 2018; Dushyantha et al., 2020), the Mountain Pass deposit (USA), a carbonatite-hosted deposit rich in bastnäsite (Castor, 2008), Mount Weld (Australia), notable for its high-grade REE concentrations (Lottermoser et al., 1988; Lottermoser, 1990; Jaireth et al., 2014) and Ion Adsorption Clays (Southern China), formed from weathered granites, particularly important for HREE production due to their ease of extraction (Borst et al., 2020; Feng et al., 2021). Other significant deposits exist in Brazil, Russia, and Africa, often associated with alkaline complexes or carbonatites. Global REE production in 2023 reached approximately 350,000 metric tons, with China responsible for ~68.5% of the output. The U.S. (Mountain Pass) and Myanmar have also become key producers. Total global reserves are estimated at ~110 million tonnes of REO, with major deposits in China, Vietnam, and Brazil (U.S. Geological Survey, 2024). REE mining and processing pose significant environmental challenges. Among the others, the mining process generates dust, habitat destruction, and acid mine drainage; the processing requires strong acids (H_2SO_4, HCl) and produces toxic byproducts (*e.g.*, thorium in Baotou tailings). Extraction from Ion Adsorption Clays, while less damaging, still requires ammonium sulphate leaching, which can contaminate groundwater. The European Union classifies REEs as critical raw materials due to their economic importance and supply risks, as the region currently imports nearly all its REEs (Grohol & Veeh, 2023). The importance of these elements is strongly related to their indispensable role in numerous advanced technological applications that define modern life. Their unique magnetic and luminescent properties make them particularly valuable in clean energy technologies, such as high-performance permanent magnets used in electric vehicle motors and wind turbine generators. With the global transition toward renewable energy and electrified transportation, demand for these strategically important elements has been growing exponentially. This surge in demand underscores both the critical importance of rare earth elements in modern technology and the need for secure, responsible supply chains to meet future requirements. Recycling REEs from end-of-life products (*e.g.*, magnets, batteries), or from other typologies of wastes (*e.g.*, WEEE) is becoming increasingly important to supplement primary production and reduce environmental impacts. Potential secondary sources include industrial mining byproducts like phosphogypsum, red mud and coal ash, and electronic waste (WEEE) such as NdFeB magnets, NiMH batteries and fluorescent lamp phosphors. Effective separation of Rare Earth Elements (REEs) from leachates - deriving from waste materials - employs several possible methods such as selective precipitation, solvent extraction, selective adsorption (*e.g.*, with activated carbon, biochar, or functionalized resins), ion exchange exploiting resins or Metal-Organic Frameworks (MOFs). Zeolites–particularly faujasite-types (X and Y, differing in Si/Al ratio)– can be exploited for their cation exchange property for REE recovery. Recent studies highlight zeolites' potential in REE separation from waste streams, leveraging their pore structure and exchange properties. This work is a feasibility study aimed at evaluating the efficiency of recovery of REEs from waste solutions, exploiting the cation exchange property of zeolites. These materials have the potential to be a reusable and selective method for the separation of REEs. In particular, a NH_4-exchanged zeolite 13X was prepared to facilitate the further recovery of REEs from the zeolite. In

fact, the procedure we propose is a two-step exchange: *i)* NH_4-exchanged 13X is contacted with REE solution to promote the extraction of selected REE from the solution through a REE-NH_4 exchange; *ii)* the REE-exchanged zeolites are then contacted with an NH_4 solution to extract the REE. The presence of only NH_4 in the zeolites, in fact, simplifies the final REE recovery, allowing a selective precipitation as nitrates. The waste solutions used in this work are lab-made solutions mimicking the products obtained from the leaching of spent fluorescent lamps, a complex secondary source of rare earth elements (REEs), containing valuable metals such as yttrium, europium, terbium, cerium, and lanthanum.

MATERIALS AND METHODS

13X zeolite

Faujasite-type zeolites (FAU) have a highly porous cubic structure composed of sodalite cages and double 6-rings, forming large supercages with ~7.5 Å openings. Variants X and Y differ by Si/Al ratio: faujasite X, with a lower Si/Al ratio, offers higher cation-exchange capacity but lower acid stability. For this work, the starting material NaX zeolite was selected for its ion-exchange potential. The zeolites were then NH_4-exchanged. The presence of NH_4 as the only extra-framework cation would help in the further exchange required for the REE recovery, enabling separation of REEs via pH-controlled precipitation, as NH_4^+ remains soluble while REEs form insoluble hydroxides. Full sodium substitution was nevertheless not achieved.

Mono- and bi-elemental exchanges

Mono- and bi-elemental exchange tests were carried out using NH_4-exchanged 13X zeolite and REE solutions mimicking concentrations found in leachates of spent fluorescent lamps (Eduafo et al. 2015): Ce (0.03 M), La (0.04 M), Eu (0.006 M), and Y (0.17 M). Mono-elemental tests involved contacting the zeolite with individual REE solutions at three different liquid-to-solid (L/S) ratios (10:1, 50:1, and 100:1 mL/g) for 24 h under stirring at room temperature. Bi-elemental tests were performed using Ce-La and Y-Eu mixed solutions at the same concentrations of the mono-elemental solutions, with a fixed L/S ratio and a shorter contact time of 3 h, as the first REE exchange allowed to understand that the equilibrium was quickly achieved. Buffered pH conditions (~4.4–4.8) were maintained to avoid zeolite degradation and REE precipitation. Elemental analysis, thermogravimetric analysis, SEM-EDS, XRPD and ICP-MS analyses were performed on the sample obtained. Selected samples after mono-elemental exchanges were analysed by high-resolution XRPD at ESRF for phase and structural characterization.

REEs recovery from zeolite

REEs were recovered from the exchanged 13X zeolites through a secondary exchange with NH_4Cl solutions. Zeolites from mono-elemental tests were treated with 0.8 M NH_4Cl for 24 h (L/S = 1/125 g/mL), while those from bi-elemental tests were treated with 1 M NH_4Cl for 3 h (L/S = 1/100 g/mL), both under stirring at room temperature. The higher NH_4Cl concentration for bi-elemental samples was chosen to improve REE recovery. Elemental analysis, thermogravimetric analysis, SEM-EDS, XRPD and ICP-MS analyses were performed on the sample obtained. Selected samples after mono-elemental exchanges were analysed by high-resolution XRPD at ESRF for phase and structural characterization.

RESULTS AND DISCUSSION

Mono- and bi-elemental exchanges

REE uptake from mono-elemental solutions is shown in Figure 1a. At low liquid-to-solid ratios (10 mL/g), Ce, La, and Eu are nearly fully extracted, while Y shows lower uptake (~60%). Increasing the solution volume reduces extraction efficiency for Ce, La, and Y, but not for Eu. REE loading on the zeolite (Fig. 1b) increases with the increase in the liquid/solid ratio, reaching 150–160 mg/g for Ce and La, and ~75 mg/g for Y. For all the systems at liquid/solid ratio higher than 50 a plateau is achieved, indicating the approaching of cation exchange saturation. Y uptake plateaus at values inferior to the other REEs tested, despite being the most concentrated in the starting solution, suggesting lower affinity. The zeolite Si/Al

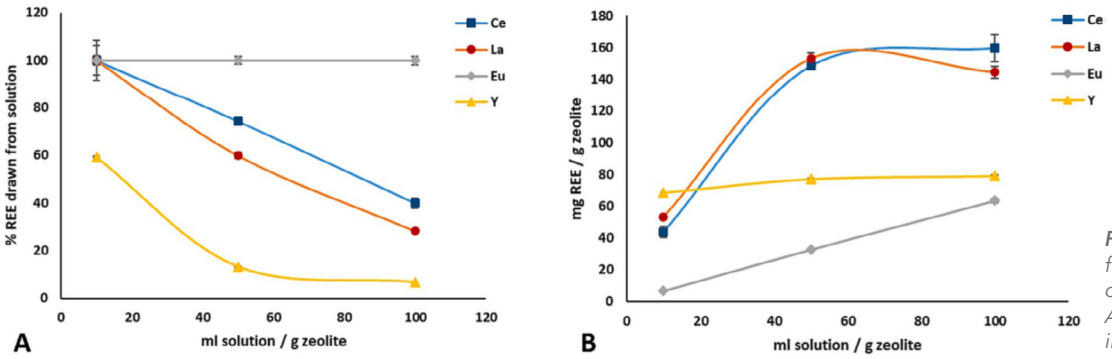

Figure 1 a) *REE fraction drawn from solution as a function of the solid/liquid ratio.* ***b)*** *Amount of REE incorporated in the zeolite as a function of the solid/liquid ratio.*

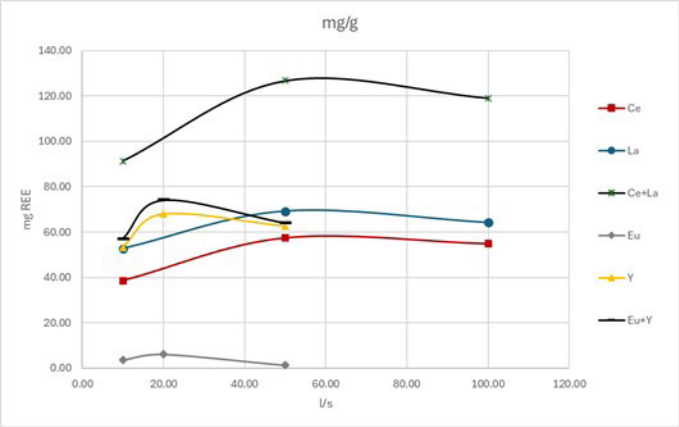

Figure 2 *Amount of REE incorporated in the zeolite as a function of the solid/liquid ratio. REEs are also reported in the graph individually, to allow a clearer view of the exchange behaviours of the bi-elemental exchanges. The lines are guides for the eye.*

ratio (1.23) remains stable post-exchange. The extent of extra-framework aluminium (EFAL) correlates inversely with REE content; high REE loading stabilizes the framework, echoing behavior seen in REE-Y catalysts in FCC applications (Vogt & Weckhuysen, 2015). Exchange data show that REEs preferentially replace NH_4^+ rather than Na^+ left in the channels, as a demonstration that Na^+ is hardly exchangeable. NH_4^+ content decreases linearly with REE loading, while Na^+ remains constant until high REE exchange levels are reached. The results of bi-elemental REE exchange experiments reveal behaviours consistent with mono-elemental tests, while highlighting the influence of inter-element competition and solution concentration (Fig. 2). At low liquid-to-solid (l/s) ratios (*e.g.*, 10), Ce and La are almost fully extracted from solution (~100%), but efficiency decreases with increasing l/s, dropping to ~30% at l/s = 50 and below 20% at l/s = 100. This suggests optimal exchange occurs between l/s = 10–50. La is exchanged more efficiently than Ce (70 vs. 60 mg/g), in line with its higher starting concentration. For the Eu+Y system, REE uptake is limited regardless of l/s ratio: more than 50% of Y remains unexchanged at l/s = 10, and over 90% at l/s = 50. Eu uptake drops to ~60% at l/s = 10 and falls below 5% at higher l/s ratios. Nevertheless, Y dominates the exchange process due to its higher concentration in the starting solution (0.17 M vs. 0.006 M Eu). The total REE exchange capacity remains consistent with mono-elemental data, reaching ~130 mg/g (Ce+La) and ~80 mg/g (Y+Eu). Starting concentration appears to be the dominant factor in competitive uptake.

REEs recovery after mono- and bi-elemental exchanges

Two consistent trends emerge from both mono- and bi-elemental exchange tests: Y is partially recovered (45%), while Ce, La and Eu show significantly lower recoveries (10–18%), indicating a stronger retention of the latter in the 13X framework. This behaviour is linked to charge balance variation; greater imbalance after recovery of Y suggests weaker stabilization and easier displacement, while Ce La and Eu induce minimal charge variation, pointing to stronger binding. Y consistently displays the highest exchangeability, confirming its distinct behaviour and easier removal.

XRPD analyses

The structural behaviour of selected REE-bearing zeolites after mono-elemental exchanges was investigated via Rietveld structural refinement and compared with the literature. Diffraction data reveal significant differences in peak intensity ratios among the REE-exchanged samples, indicating different electronic densities in relation to the cations exchanged. Ce and La preferentially occupy site II* (after Frising & Leflaive, 2008) (in the supercage), near the hexagonal window of the sodalite cage (see Fig. 3), and partially share site I' (in the sodalite cage) with Na^+. These cations coordinate both framework oxygens and water molecules. Eu exhibits similar site preferences but with lower incorporation, likely due to its lower starting concentration. Y shows distinct behavior, predominantly occupying site IV in the supercage and the sodalite cage in site I', coordinating mainly with water and showing weaker interaction with the framework. The data indicate that exchange efficiency and site selectivity depend on cation size and on its hydration shell. After NH_4^+ further exchange Y, which vacates in site IV while retaining a minor presence in I', appears more labile and poorly retained compared to the other REEs, highlighting the importance of the hydration shell of Y in the exchange mechanism, in fact, in site IV Y was bonded only with water molecules and not directly with the zeolite framework as the other REEs. Electron balance analyses from XRPD, SEM-EDS, TG, and EA indicate consistency in most samples. Discrepancies in site occupancies are largely compensated by water molecules, suggesting mixed occupancies for the sites.

CONCLUSIONS

This research demonstrated the potential of NH_4-exchanged zeolite 13X for selectively recovering REEs (Ce, La, Eu, Y). The zeolite maintained its exchange capacity under mildly acidic conditions and showed high affinity for Ce and La, and low for Y. Further tests are required for Eu since the behaviour seems influenced by starting concentrations mono-elemental exchange tests revealed Ce and La reached exchange plateaus at moderate liquid-to-solid ratios, while Y, despite its higher concentration, exchanged less efficiently. Structural analysis confirmed Ce, La, and Eu cations directly bond to the framework at defined sites, whereas Y resides in the supercage, weakly bound to water, explaining its easier recovery upon NH_4^+ counter-exchange and less overall

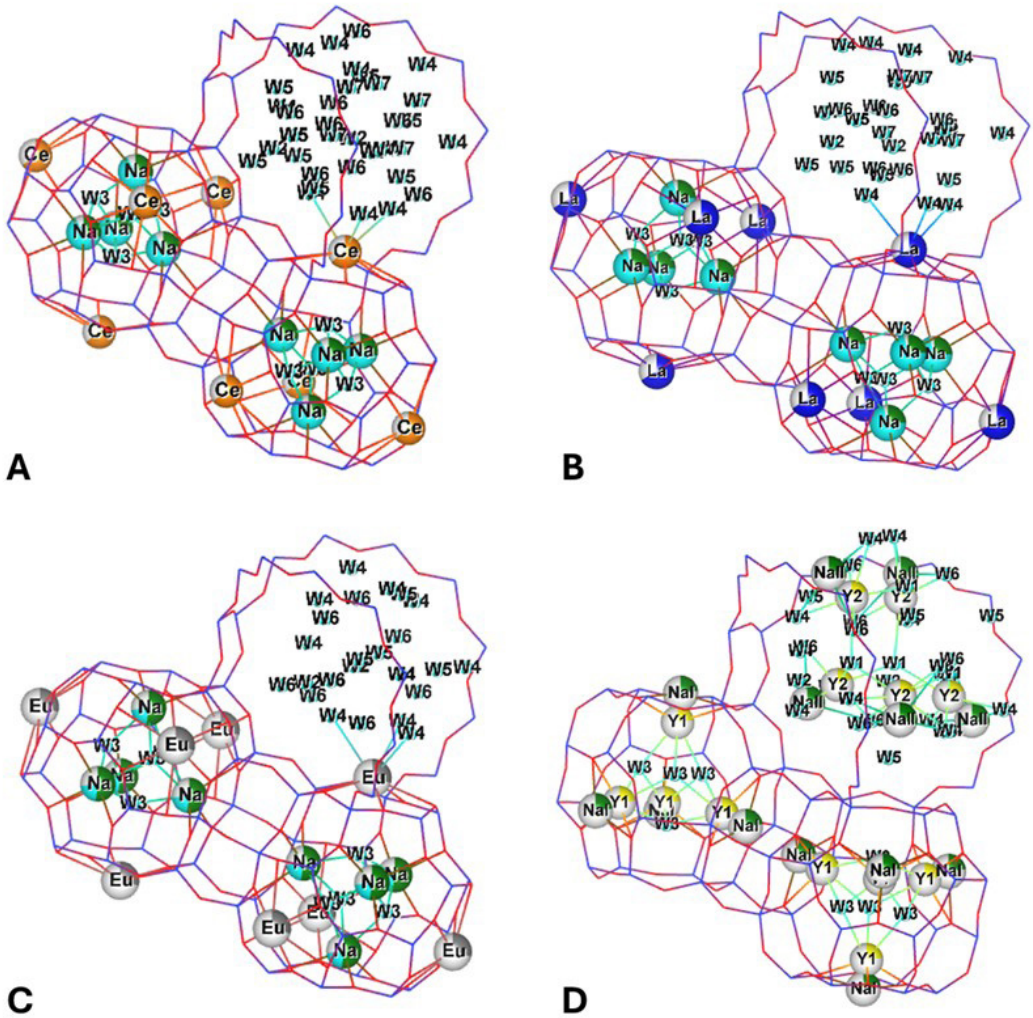

Figure 3 ***a)*** *graphical representation of the zeolite framework, with cations (Ce in orange, Na in green) and water molecules (in light blue).* ***b)*** *graphical representation of the zeolite framework, with cations (La in blue, Na in green) and water molecules (in light blue).* ***c)*** *graphical representation of the zeolite framework, with cations (Eu in grey, Na in green) and water molecules (in light blue).* ***d)*** *graphical representation of the zeolite framework, with cations (Y in yellow, Na in green) and water molecules (in light blue).*

exchange capacity. Bi-elemental tests further highlighted the zeolite's selectivity, particularly in separating Y from Eu. Only Y was significantly recovered in these tests, while Ce, La, and Eu remained strongly retained. The presence of residual Na may have influenced exchange behaviours, suggesting future work should focus on full NH_4 substitution. Overall, NH_4-13X shows promise for REE separation, especially Y, and selective retention of Ce and La, with potential implications for REE recycling and recovery from complex waste streams.

REFERENCES

Borst, A., Smith, M.P., Finch, A., Estrade, G., Villanova-de-Benavent, C., Nason, P., Marquis, E., Horsburgh, N.J., Goodenough, K., Xu, C., Kyniky, J., Geraki, K. (2020) - Adsorption of rare earth elements in regolith-hosted clay deposits. Nat. Commun., 11, 4386.

Castor, S.B. (2008) - Rare Earth Deposits of North America. Resour. Geol., 58(4), 337–47.

Dushyantha, N., Batapola, N., Ilankoon, I.M.S.K., Rohitha, S., Premasiri, R., Abeysinghe, B., Ratnayake, N., Dissanayake, K. (2020) - The story of rare earth elements (REEs): Occurrences, global distribution, genesis, geology, mineralogy and global production. Ore Geol. Rev., 122, 103521.

Eduafo P.M., Strauss M.L., Mishra B. (2015) - Experimental investigation of recycling rare earth metals from waste fluorescent lamp phosphors. In: "Rare Metal Technology 2015", N. R. Neelameggham, S. Alam, H. Oosterhof, A. Jha, D. Dreisinger, S. Wang, eds. Springer, Cham, 253–259.

Feng, X., Onel, O., Council-Troche, M., Noble, A., Yoon, R., Morris, J.R. (2021) - A study of rare earth ion-adsorption clays: The speciation of rare earth elements on kaolinite at basic pH. Appl. Clay Sci., 201.

Frising, T. & Leflaive, P. (2008) - Extraframework cation distributions in X and Y faujasite zeolites: A review. Micropor. Mesopor. Mat., 114(1), 27–63.

Grohol, M. & Veeh, C. (2023) - Study on the critical raw materials for the EU 2023, Final report.

U. S. Geological Survey (2024) - Mineral commodity summaries 2024, Report: 212 pp.

Huang, X. W., Zhou, M. F., Qiu, Y. Z., Qi, L. (2015) - In-situ LA-ICP-MS trace elemental analyses of magnetite: The Bayan Obo Fe-REE-Nb deposit, North China. Ore Geol. Rev., 65, 884–99.

Jaireth, S., Hoatson, D. M., Miezitis, Y. (2014) - Geological setting and resources of the major rare-earth-element deposits in Australia. Ore Geol. Rev., 62, 72–128.

Lottermoser, B.G. & England, B.M. (1988) - Compositional variation in pyrochlores from the Mt Weld carbonatite laterite, Western Australia. Mineral. Petrol., 38(1), 37–51.

Lottermoser B.G. (1990) - Rare-earth element mineralisation within the Mt. Weld carbonatite laterite, Western Australia. Lithos, 24(2), 151–67.

Smith, M.P., Moore, K., Kavecsánszki, D., Finch, A.A., Kynicky, J., Wall, F. (2016) - From mantle to critical zone: A review of large and giant sized deposits of the rare earth elements. Geosci. Front., 7(3), 315–34.

Song, W., Xu, C., Smith, M.P., Chakhmouradian, A.R., Brenna, M., Kynický, J., Chen, W., Yang, Y., Deng, M., Tang H. (2018) - Genesis of the world's largest rare earth element deposit, Bayan Obo, China: Protracted mineralization evolution over ~1 b.y. Geology, 46(4), 323–6.

Vogt, E.T.C. & Weckhuysen, B.M. (2015) - Fluid catalytic cracking: recent developments on the grand old lady of zeolite catalysis. Chem. Soc. Rev., 44(20), 7342–70.

Micro and Nanoscale Study of Calcium and Rare Earth Element Fluorcarbonates

Establishing a Link Between Mineral Structure and Genesis

Roberto Conconi
Department of Earth and Environmental Sciences, University of Milano-Bicocca, Piazza della Scienza 4, 20126, Milano
DOI: 10.19276/plinius.2025.01.008

INTRODUCTION

The development of green technologies to establish the basis for a low-carbon future is leading to an increase in the demand for critical raw materials (CRMs) (Vidal et al., 2013). Indeed, green and renewable technologies such as wind turbines, electric vehicles and solar panels require a large quantity of CRM, including rare earth elements (REE), platinum group metals (PGMs), Li and Co, among others.

For these reasons and because it is estimated that the demand for REE will constantly grow in the next decades, innovative methods for extracting REE are envisaged. There are over 200 mineral species containing REE, but only a few contain enough REE to have the potential for forming economic ore deposits (Kanazawa & Kamitani, 2006). The primary ore minerals for REE are: REE-carbonates, -fluorcarbonates and -phosphates like bastnäsite, parisite, synchysite, monazite, and xenotime. However, despite the economic importance of REE and their bearing minerals, a lot of unanswered questions about the mechanisms that govern the REE transport and deposition in natural systems, as well as the crystallization of REE-bearing phases, remain. These challenges arise from the difficulty of replicating the complex natural conditions in the laboratory and the inherent challenge of separating different REE. In this regard, it is universally recognized, as well as often forgotten, that fundamental research is the nourishment of applied research. Indeed, mineralogical and crystallographic studies on REE-bearing minerals may shed light on their nature and genesis, eventually suggesting more successful prospection routes, enhanced metallurgical processes and recycling strategies. For these reasons, (Ca-REE) fluorcarbonates (hereafter CRFC) have been identified as the ideal mineral group for conducting mineralogical and crystallographic studies. The interesting characteristic of CRFC is that they form a polysomatic series (Donnay & Donnay, 1953; Conconi et al., 2023, 2025a, b), where bastnäsite and synchysite are the end members, and different intermediate polysomes, such as parisite and röntgenite, have been identified over the years. The study of polysomatism is particularly significant, as the intergrowths of different polysomes may indicate changes in crystallization conditions or fluid composition (Gysi & Williams-Jones, 2015).

In this work, various CRFC samples from different localities and geological settings were studied using multiple techniques such as scanning electron microscopy (SEM) coupled with energy dispersive spectroscopy (EDS) and electron backscattered diffraction (EBSD), Raman spectroscopy, transmission electron microscopy (TEM), precession-assisted three-dimensional electron diffraction (3DED) and single-crystal X-ray diffraction (SCXRD). The goal was to link their micro- and nanostructures to the large-scale processes responsible for their formation. Indeed, micro- and nanoscale observations proved fundamental in fully characterizing these minerals and provided important insights into the possible crystallization mechanisms of CRFC. These findings aim to contribute valuable knowledge to the understanding of the complex processes behind the crystallization of these minerals.

SAMPLES

The samples studied in this work come from two different localities: Mount Malosa (Malawi, Africa) and Cuasso al Monte (Varese, Italy). The CRFC from Mount Malosa were previously described by Guastoni et al. (2009, 2010) and Capitani (2019). They are polycrystals made of stacking different CRFC (Fig. 1a). They typically exhibit a yellowish-reddish colour and are associated with aegirine. In contrast, the CRFCs from Cuasso al Monte occur in three distinct morphologies, all of which are micrometer-sized: rosette-like aggregates, hexagonal prisms, and blocky subhedral shape (Fig. 1b, c, d).

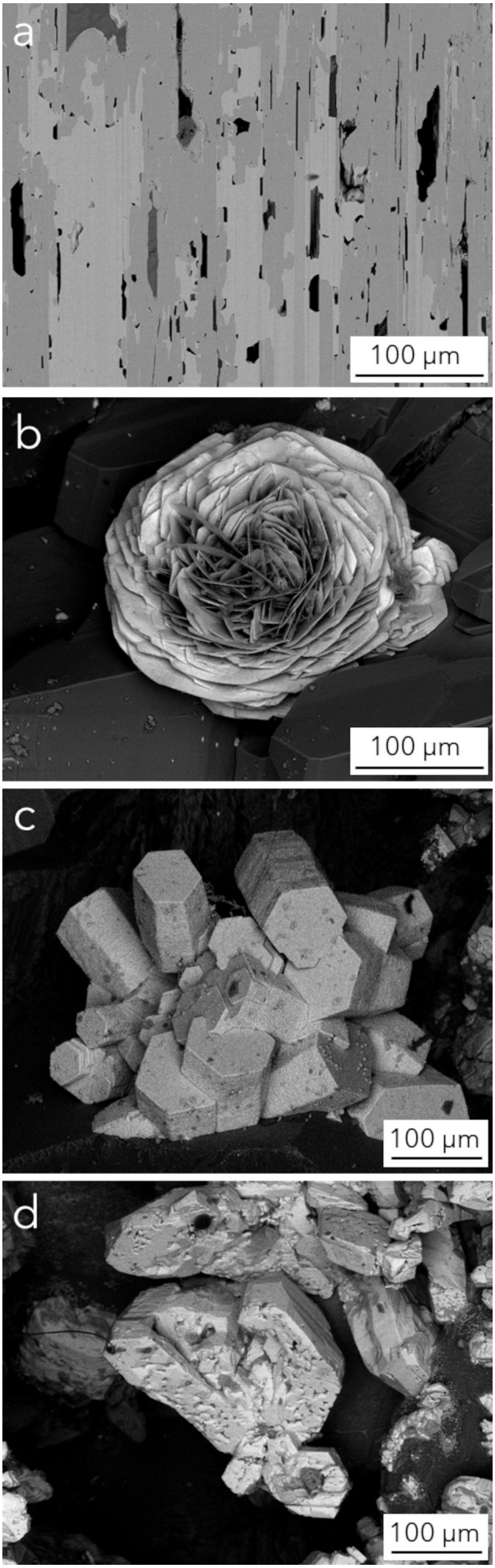

Figure 1 SEM images showing: ***a)*** *CRFC from Mount Malosa showing syntactic intergrowths.* ***b, c, d)*** *CRFCs from Cuasso al Monte displaying three different morphologies (Conconi et al., 2023; 2025a).*

A MULTI-METHODOLOGICAL IDENTIFICATION OF CRFC

The CRFCs from Mount Malosa were studied using a multimethodological approach to provide a roadmap for the correct identification of these minerals. First, the samples were analysed using SEM-EDS to gain an initial understanding of their microstructure and chemical variability at a microscopic scale. As expected, the samples display the parallel banding typical of CRFC syntactic intergrowths (Fig. 1a). EDS spot analyses revealed the presence of different CRFC polysomes such as bastnäsite, parisite, röntgenite, synchysite, and several unnamed intermediate terms.

Subsequently, EBSD analyses were conducted to: (1) establish the initial orientation of the samples; and (2) evaluate the method's capability to distinguish different polysomes. EBSD successfully established sample orientation, but it failed to discriminate between the various polysomes. This limitation can be understood considering that electron diffraction is dominated by heavy atoms, and in CRFC the stacking of heavy atoms (Ca and REE) is hexagonal for all the terms of the series.

Raman spectroscopy was performed on samples with different crystal orientations. Generally, different polysomes can be identified by analysing the $v_1(CO_3)$ symmetric stretching vibration of the carbonate group. Bastnäsite shows a single band; synchysite displays two bands; and the intermediate terms exhibit three bands, with intensity ratios that vary depending on orientation (Fig. 2a).

TEM observations revealed nanoscale disorder characterized by intergrowths of different stacking faults. At the TEM scale, the Mount Malosa samples appear to consist mostly of bastnäsite–parisite intergrowths, with minor areas containing more ordered polysomes (Fig. 2b, c).

This suggests that while SEM and Raman spectroscopy provide an overview of the sample composition, TEM remains the most effective technique for the detailed characterization of CRFCs.

These observations indicate that the most common microstructure in Mount Malosa CRFCs consists of rhythmic parisite–bastnäsite intergrowths, along with several more or less ordered intermediate polysomes. The observed microstructure supports a primary growth mechanism in which fluorcarbonates crystallize from a fluid near thermodynamic equilibrium, with conditions rapidly and repeatedly crossing the parisite–bastnäsite stability boundary, rather than following a stepwise progression toward equilibrium (for more details, see Conconi et al., 2023).

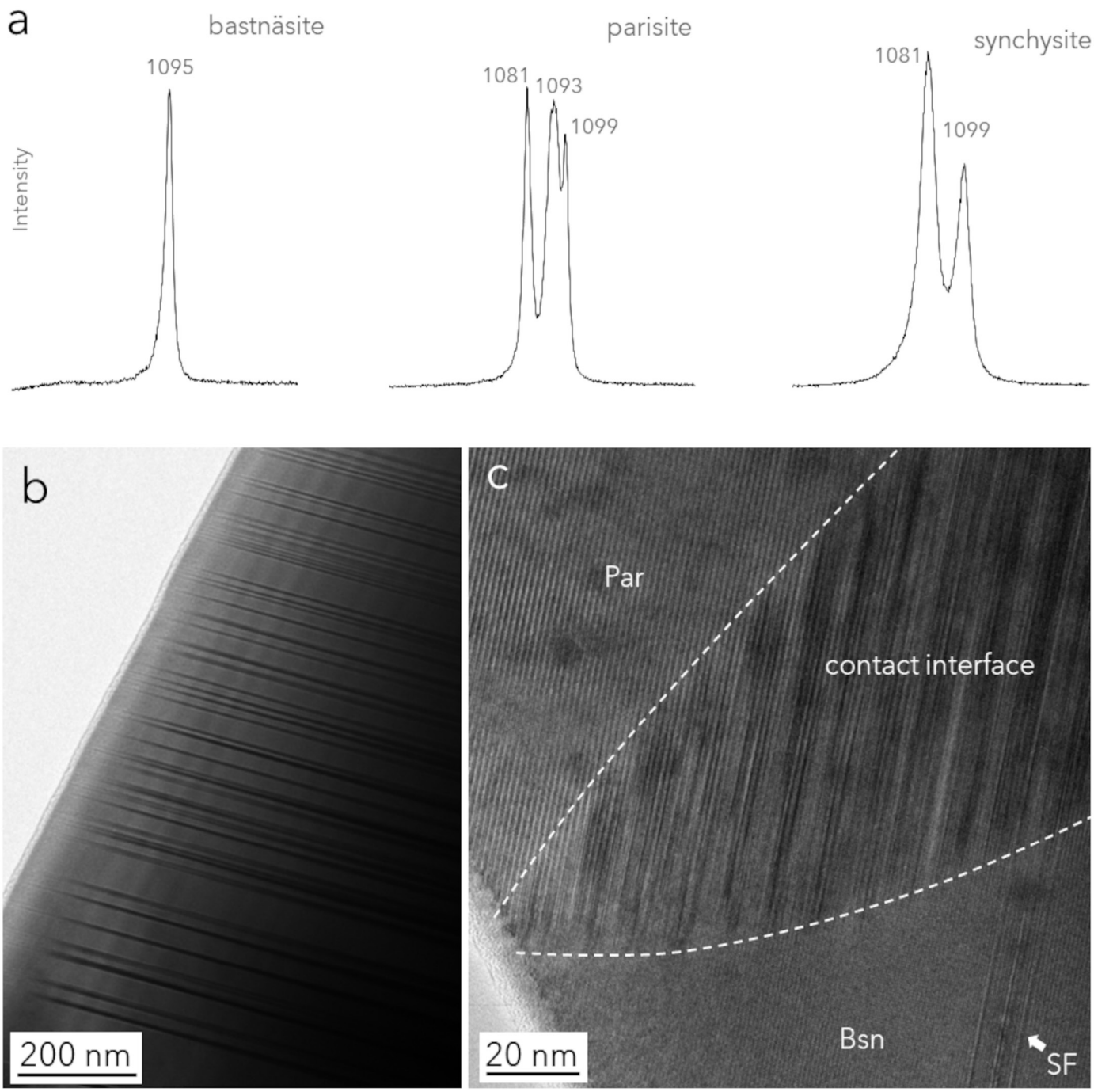

Figure 2 a) *Raman spectra of bastnäsite, parisite and synchysite, showing the different numbers of bands associated with the $v_1(CO_3)$ symmetric stretching vibration of the carbonate group.* ***b)*** *TEM image showing the typical nanostructures of CRFC from Mount Malosa, made of dense stacking faults.* ***c)*** *Contact interface between parisite (Par) and bastnäsite (Bsn); stacking faults (SF) are visible within the bastnäsite.*

A VARIETY OF MORPHOLOGIES, COMPOSITIONS AND NANO-STRUCTURES: INSIGHTS INTO REE PARTITIONING AND MOBILITY

At Cuasso al Monte, CRFCs exhibit a wide variety of morphologies and compositions. Three main types have been identified: *i)* synchysite-(Ce) occurring as hexagonal prisms (Fig. 1c) and rosette-like aggregates (Fig. 1a); *ii)* bastnäsite-(Ce) forming blocky aggregates (Fig. 1d); and *iii)* bastnäsite-(Nd) forming desert rose-like intergrowths (Fig. 3e). Among these, hexagonal prism synchysite-(Ce), rosette-like synchysite-(Ce), and desert rose-like bastnäsite-(Nd) have been studied in greater detail.

The hexagonal prisms synchysite-(Ce) show a core-rim chemical zoning with three different areas: *i)* a core enriched in Ce, La and Nd; *ii)* a rim enriched in Y and *iii)* an outer rim enriched in Th (Fig. 3a). TEM analysis reveals the presence of hematite nanocrystal inclusions (Fig. 3b), while selected area electron diffraction (SAED) patterns show a superstructural order in synchysite with a periodicity of approximately 93 Å, a value that is commensurate with the quarter-cell of synchysite (~4.6 Å), moreover its structure has been refined using both SCXRD and 3DED. This superstructure suggests that the hexagonal prism synchysite-(Ce) may represent a long-range polytype, which likely lacks a distinct thermodynamic stability field and may have formed via a screw dislocation

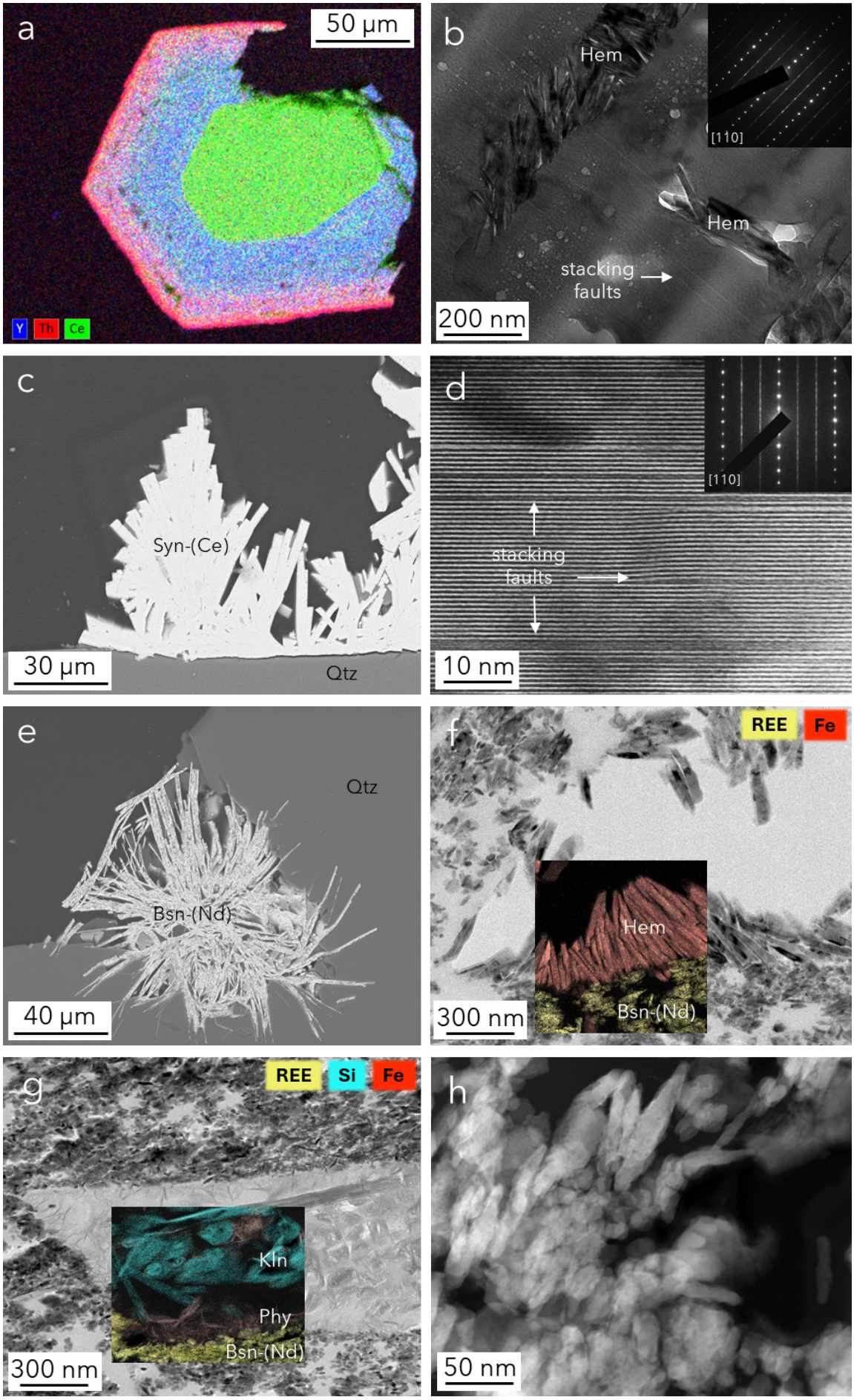

Figure 3 a) *SEM-EDS map of the hexagonal prism synchysite-(Ce) showing the chemical zoning.* ***b)*** *TEM image and corresponding SAED pattern of the hexagonal prism synchysite-(Ce), showing the presence of hematite nanocrystals and stacking faults within the crystal.* ***c)*** *SEM image showing the rosette-like synchysite-(Ce).* ***d)*** *High resolution TEM image and corresponding SAED pattern of* ***(c)*** *showing the presence of stacking faults.* ***e)*** *SEM image showing the desert rose-like bastnäsite-(Nd).* ***f, g)*** *TEM images showing the intergrowth of bastnäsite-(Nd) with hematite (Hem), phyllosilicates (Phy) and a kaolinite-like phase (Kln).* ***h)*** *TEM image showing the rod shape morphology of bastnäsite-(Nd) nanocrystals, (images taken and modified from Conconi et al., 2025a, b).*

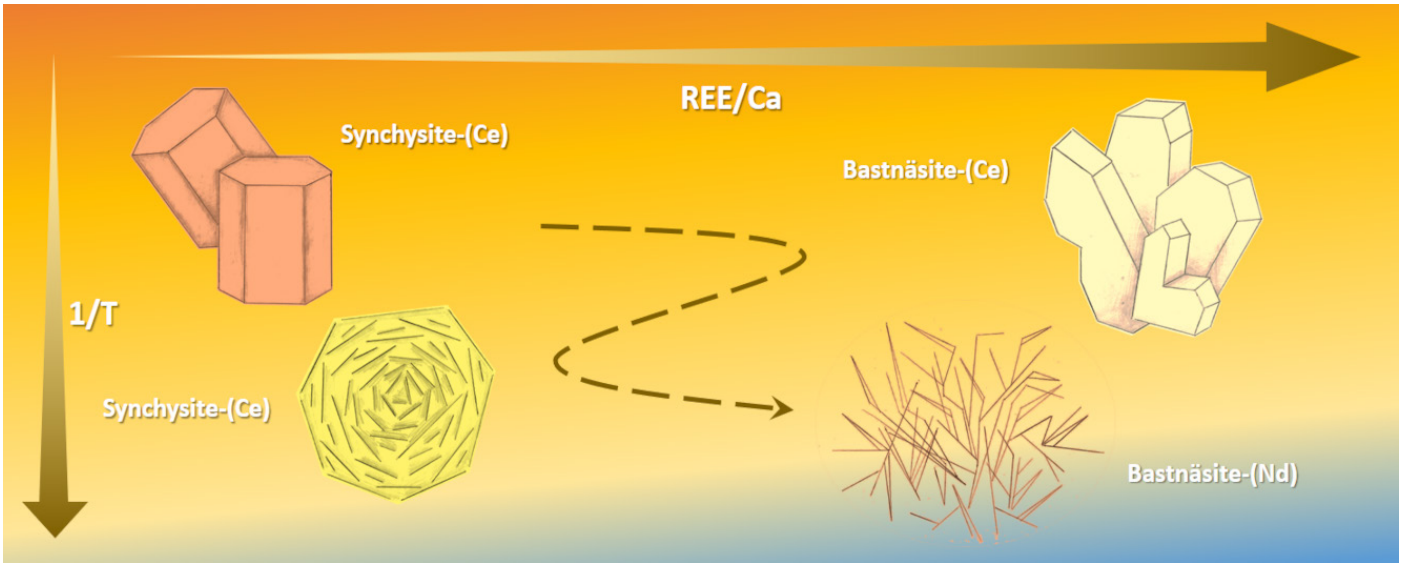

Figure 4 *Schematic drawing of the possible crystallization pathway for the CRFCs of Cuasso al Monte (Conconi et al., 2025a).*

growth mechanism. However, this mechanism appears incompatible with the sharp core–rim chemical zoning. It is therefore plausible that the core initially formed via screw dislocation, followed by a second stage of growth on the crystal's outer faces from a Y-enriched liquid. The outermost rim, enriched in Th, likely formed through diffusive exchange or REE substitution by Th (Conconi et al., 2025b).

Rosette-like synchysite-(Ce) forms thick, flat, and compact lamellae (Fig. 3c). TEM-EDS analysis reveals that these lamellae have a nanostructure in which the rosette-like "petals" are single crystals, with their shortest dimension oriented parallel to **c***, the stacking direction of Ca, CeF, and (CO_3) layers. Each petal can thus be interpreted as a stubby prism. SAED patterns and lattice fringe images indicate the presence of polysomatic and polytypic disorder, reflecting structural complexity at the nanoscale (Fig. 3d).

In contrast, desert rose-like bastnäsite-(Nd) forms thinner and slightly bent lamellae with a widespread porosity (Fig. 3e). At the nanoscale, bastnäsite-(Nd) shows a complex nanostructure recalling the gypsum or calcite "desert rose" (although at a smaller scale), made of an intergrowth of bastnäsite and hematite nanocrystals, with also phyllosilicates, including a kaolinite-like phase (Fig. 3f, g). The CRFC nanocrystals generally appear as nanorods less than 50 nm in length (Fig. 3h). Hematite was observed both as nanorods up to 200 nm in length and as irregular nanoparticles, generally dispersed within bastnäsite, but sometimes forming clusters. Phyllosilicates are present either along the rim of the rosette-like "petals" or within interstices left by bastnäsite-hematite intergrowths. Overall, lattice fringe images and the SAED patterns of the bastnäsite-(Nd) show an ordered structure. Furthermore, a distinctive feature of this phase is the REE distribution, with Nd as the dominant REE, followed by La and Ce.

At Cuasso al Monte, the CRFC were among the latest phases to crystallize from a F-rich hydrothermal fluid (Capitani et al., 2018). Based on our observations, a possible crystallization pathway for CRFCs has been proposed (Fig. 4): *i)* synchysite-(Ce) prisms formed early in the crystallization sequence from a Ca- and F-rich fluid, at relatively low cooling rate; *ii)* the Ca-depleted fluid then reached the condition to form blocky bastnäsite-(Ce), still at relatively low cooling rates; *iii)* the fluid reached again, at slightly lower temperatures, supersaturation conditions for Ca and Ce, crystallizing rosette-like synchysite-(Ce). Indeed, so many "petals" of synchysite-(Ce) may represent fast nucleation events under a relatively high cooling rate that resulted into undeveloped prisms; *iv)* the remaining fluid, at that point depleted in Ca and Ce and at low temperature, crystallized rosette-like bastnäsite-(Nd) (Conconi et al., 2025a).

CONCLUSIONS

In the present study, CRFCs belonging to the bastnäsite-synchysite series were investigated to establish a relationship between their micro- and nano-structure and the genetic mechanisms driving their crystallization. A multimethodological approach was employed, using various analytical techniques, including SEM-EDS, EBSD, Raman spectroscopy, TEM-EDS, 3DED, and SCXRD. Initially, a roadmap for identifying CRFC polysomes was developed. The results demonstrate that Raman spectroscopy effectively distinguishes CRFC members based on the symmetric $v_1(CO_3)$ stretching vibration of the carbonate group. Although Raman spectroscopy can effectively determine the Ca/(Ca+REE) ratio in CRFC, it may not be suitable for distinguishing between ordered and disordered intergrowths with similar composition. For this reason, TEM-EDS remains the ultimate technique for polysome identification. However, TEM also has its own intricacies. Since most high-resolution TEMs have a

limited tilt range, the sample needs to be pre-oriented before preparation; for this purpose, EBSD can be very useful. Indeed, EBSD can easily distinguish CRFC among other phases and correctly provides their orientation relationship, but under routine application, it fails to distinguish among different polysomes.

The micro- and nano-scale analysis revealed diverse structures among the CRFC samples, which can provide insights into the mechanisms responsible for their crystallization. In Mount Malosa CRFCs, the most common microstructure is rhythmic parisite-bastnäsite intergrowths alongside a number of more or less ordered intermediate polysomes. The observed microstructure indicates a primary growth mechanism where CRFCs crystallized from a fluid near thermodynamic equilibrium, with conditions repeatedly crossing the parisite–bastnäsite stability boundary.

In contrast, CRFCs from Cuasso al Monte exhibit a wider variety of morphologies, compositions, and nanostructures. From these observations, it was possible to infer a crystallization pathway involving an initial F-rich fluid that, upon cooling, sequentially precipitated different CRFC phases under evolving physicochemical conditions.

In conclusion, this study highlights that advancements in imaging and analytical techniques have enabled the acquisition of chemical and structural information with exceptional spatial resolution, which is crucial for fully characterizing the material under analysis. Indeed, information obtained from the micro- to the nano-scale has proven important in explaining macro-scale processes, such as crystallization and elements partitioning. Understanding these processes is of paramount importance, especially considering that CRFC are the primary ore for REE.

REFERENCES

Capitani, G. (2019) - HRTEM investigation of bastnäsite–parisite intergrowths from Mount Malosa (Malawi): ordered sequences, polysomatic faults, polytypic disorder, and a new parisite-(Ce) polymorph. Eur. J. Mineral., 31, 429–442.

Capitani, G., Mugnaioli, E., Gentile, P. (2018) - Submicrometer yttrian zircon coating and arborescent aeschynite microcrystals on truncated bipyramidal anatase: An electron microscopy study of miarolitic cavities in the Cuasso al Monte granophyre (Varese, Italy). Am. Mineral., 103, 480–488.

Conconi, R., Fumagalli, P., Capitani, G. (2023) - A multimethodological study of the bastnäsite-synchysite polysomatic series: Tips and tricks of polysome identification and the origin of syntactic intergrowths. Am. Mineral., 108, 1658–1668.

Conconi, R., Gentile, P., Fumagalli, P., Nieto, F., Capitani, G. (2025a) - CaREE-fluorcarbonates: A variety of morphologies, compositions and nanostructures with insights into REE partitioning and mobility. Lithos, 108033, 504–505.

Conconi, R., Merlini, M., Fumagalli, P., Mugnaioli, E., Folco, L., Capitani, G. (2025b) - Average Structure and Microstructure of Synchysite-(Ce) from Cuasso al Monte (Varese, Italy). Eur. J. Mineral., 37, 233–247.

Donnay, G. & Donnay, J.D.H. (1953) - The crystallography of bastnäsite, parisite, röntgenite and synchysite. Am. Mineral., 38, 932–963.

Guastoni, A., Nestola, F., Giaretta, A. (2009) - Mineral chemistry and alteration of rare earth element (REE) carbonates from alkaline pegmatites of Mount Malosa, Malawi. Am. Mineral., 94, 1216–1222.

Guastoni, A., Kondo, D., Nestola, F. (2010) - Bastnäsite-(Ce) and Parisite-(Ce) From Mt. Malosa, Malawi. Gems Gemol., 46, 42–47.

Gysi, A.P. & Williams-Jones, A.E. (2015) - The thermodynamic properties of bastnäsite-(Ce) and parisite-(Ce). Chem. Geol., 392, 87–101.

Kanazawa, Y. & Kamitani, M. (2006) - Rare earth minerals and resources in the world. J. Alloys Compd., 408–412, 1339-1343.

Vidal, O., Goffé, B., Arndt, N. (2013) - Metals for a low-carbon society. Nat. Geosci., 6, 894–896.

Constraining the chemical and mineralogical composition of Earth's lower mantle through high-pressure crystallography and mineral elasticity

Giacomo Criniti
Bayerisches Geoinstitut, University of Bayreuth, Universitätsstraße 30, 95447, Bayreuth, Germany
DOI: 10.19276/plinius.2025.01.009

THE EARTH'S DEEP INTERIOR

The Earth's lower mantle, spanning from approximately 660 to 2890 km depth, comprises more than half of the total volume of the Earth. Due to its inaccessibility and the lack of pristine natural samples reaching the surface from such great depths, some of its key properties, such as bulk chemical composition and temperature, need to be inferred from the interpretation of geophysical observations. It is the role of high-pressure experiments to provide the tools necessary to retrieve this information by investigating the phase equilibria, mineral transformations, and physicochemical properties of candidate lower mantle phases.

Seismic models and laboratory experiments

On first approximation, the geophysical properties of the Earth's deep interior, such as its density and seismic velocities, have been approximated as spherically symmetrical. One-dimensional (1D) seismic models, such as the preliminary reference Earth model (Dziewonski & Anderson, 1981), have therefore been used by experimentalists to infer the average chemical composition of the deep Earth, including the lower mantle. Phase equilibrium experiments on bulk rock compositions ranging from harzburgite to basalt at lower mantle pressure and temperatures have revealed bridgmanite, $(Mg,Fe,Al)(Si,Al)O_3$ with a distorted perovskite-type structure, to be the most abundant mineral phase down to at least 2700 km depth. Its abundance relative to (Mg,Fe)O ferropericlase, the second most abundant mineral, remains, however, controversial. For the past several decades, extensive efforts have been put into measuring the density and wave propagation velocities of candidate lower mantle phases. The most utilized technique has been Brillouin scattering, which can be coupled to diamond anvil cells (DACs) to measure velocities up to conditions of the deep lower mantle. Technological and experimental challenges, however, have often limited the effective pressure and temperature range in which such properties can be measured. For instance, the Brillouin signal from the diamond anvils tends to mask the compressional velocities of minerals at lower mantle pressures, limiting observations to only the shear velocities. It follows that the accuracy and precision of mineral physical models used to interpret 1D seismic models has not allowed us to apply robust constraints on the average lower mantle composition and temperature yet.

Water in the deep Earth

Hydrogen, often expressed as its oxide component H_2O and simply referred to as "water", is a minor, yet crucial component of mantle rocks. It can significantly lower their solidus temperature, enhance their thermal and electrical conductivity, as well as reduce their viscosity.

Dense hydrous magnesium silicates (DHMS) are synthetic phases that appear in high-pressure-temperature experiments on hydrous mafic and ultramafic compositions from upper to lower mantle conditions. They are believed to be the primary water carriers within subducted oceanic plates down to the mantle transition zone but are believed to dehydrate in the shallow lower mantle due to their limited thermal stability (Frost, 2006). Owing to a coupled substitution of Mg^{2+} and Si^{4+} by Al^{3+}, super-aluminous equivalents of phase D ($MgSi_2O_6H_2$) and phase H ($MgSiO_4H_2$) were found to survive up to temperatures approaching or even exceeding those of the ambient mantle geotherm (Pamato et al., 2015). Constraining their physical properties can therefore improve our understanding of the seismic signature of water within rocks deep inside the Earth.

Out of the nominally anhydrous minerals that have been studied so far, stishovite, a high-pressure polymorph of SiO_2 and major component of meta-basaltic rocks at lower-mantle conditions, was shown to have the highest water storage capacity, exceeding 1 wt.% H_2O (*e.g.*, Ishii et al., 2022). The coupled substitution of Si^{4+} by Al^{3+} and H^+ has recently drawn significant attention as

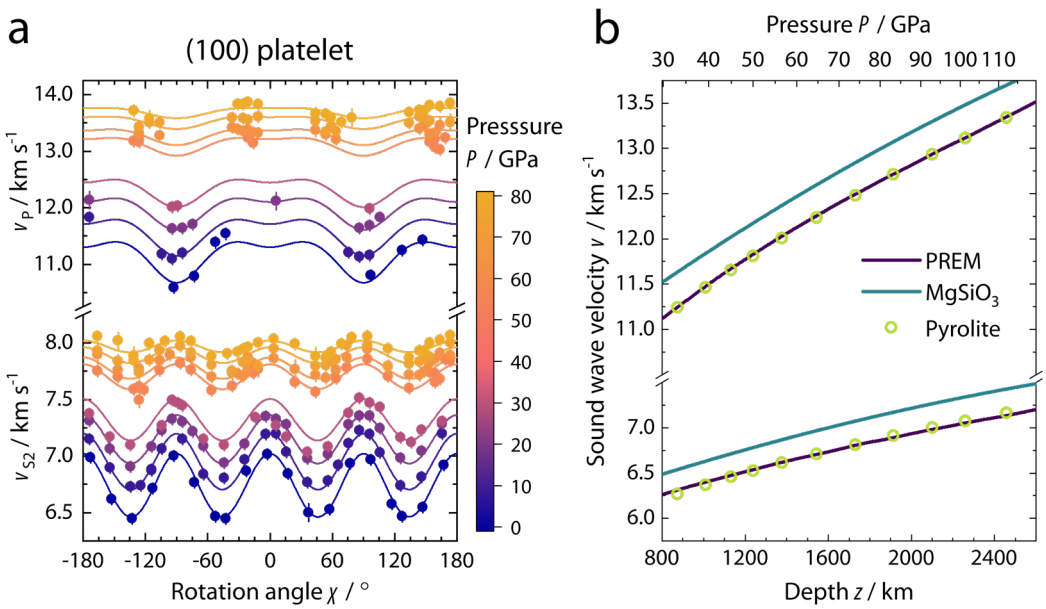

Figure 1 a) *Measured shear (v_{S2}) and compressional (v_P) velocities of a platelet of $MgSiO_3$ bridgmanite (symbols) and calculated dispersion curves calculated from the global inversion (lines) as a function of pressure (color scale) in the (100) crystal platelet.* ***b)*** *Seismic velocities in the lower mantle according to PREM and calculated velocities of $MgSiO_3$ bridgmanite (teal line) from this thesis and of a pyrolite phase assemblage (green symbols) as a function of depth along an adiabatic temperature profile.*

it was found to also affect the stability and elastic properties of stishovite. In fact, it reduces the pressure at which stishovite undergoes a structural phase transition to so-called post-stishovite, or $CaCl_2$-type SiO_2, where both phases experience extensive shear elastic softening. These elastic anomalies in silica phases with different Al and H contents could explain a series of seismic scatterers detected in the shallow- to mid-lower mantle in the proximity of subducted slabs (Kaneshima, 2019).

Aim of this thesis

The scope of this thesis is twofold: *i)* to improve our understanding of the composition of the ambient mantle by accurately determining the thermoelastic properties of bridgmanite, its most abundant mineral; and *ii)* to seek potential "water signatures" in the seismic properties of water-bearing silicates in lower-mantle basaltic phase assemblages. To this end, diamond anvil cell experiments were conducted to determine the high-pressure single-crystal elasticity of $MgSiO_3$ bridgmanite, the thermal equation of state of Al-bearing bridgmanite, the pressure-induced phase transformation of H,Al-bearing SiO_2 stishovite, and the compressibility of Mg-free Al-phase D.

ACOUSTIC VELOCITIES OF $MgSiO_3$ BRIDGMANITE IN THE MID-LOWER MANTLE

High-pressure measurements of the sound velocities of mantle minerals by Brillouin scattering in diamond anvil cell (DAC) are often impeded by the overlap of the compressional velocities (v_P) of the sample with the much more intense shear velocity (v_S) of diamond anvils (Kurnosov et al., 2017; Murakami et al., 2012). Because sound velocities vary depending on propagation and polarization directions in single-crystalline materials, it is possible to tune the reciprocal orientation of diamond anvils and single-crystal bridgmanite samples to minimize the overlap between the two peaks in Brillouin spectra. To this end, I developed a protocol to prepare bridgmanite samples for Brillouin scattering measurements in the DAC that allowed me to determine for the first time the full elastic tensor of $MgSiO_3$ bridgmanite up to ~80 GPa (Fig. 1a), corresponding to pressures of the mid-lower mantle. While at pressures below 30 GPa the bridgmanite v_P was observed in a few directions, at the diamond v_S maxima, above 50 GPa a crossover was observed at the diamond v_S minima, thus providing us with the first experimental constraints on the v_P of any bridgmanite composition at such high pressures.

Finite-strain equations of state describing how the elastic coefficients of bridgmanite (c_{ij}) vary with volume were employed in a simultaneous inversion of all diffraction and Brillouin data. This allowed gaps in the high-pressure data to be filled by using constraints from the low-pressure data, and vice versa. It also allowed the c_{ij}, as well as the bulk (K) and shear (G) moduli, to be calculated throughout the entire pressure range investigated by just refining a set of fit parameters for each c_{ij} equation of state (c_{ij0}, c'_{ij0}) instead of a set of 9 c_{ij} at each pressure.

The high-pressure sound velocity data obtained here were subsequently combined with previously published velocity data sets collected at high pressure and temperature by ultrasonic interferometry in the multi-anvil press to reassess the thermoelastic parameters of the $MgSiO_3$ bridgmanite end member (Fig. 1b). Together with experimental and theoretical results from previous studies on other lower mantle minerals (*e.g.*, Stixrude & Lithgow-Bertelloni, 2005) and thermodynamic data on the Fe^{2+}-Mg partitioning between bridgmanite and ferropericlase (Nakajima et al., 2012), an internally consistent mineral physical model was built. This model was used

to calculate the sound wave velocities of a simplified pyrolite composition along an adiabatic temperature profile at lower mantle depths and compare them with 1D seismic models of the lower mantle. Although simplified, the model is in excellent agreement with seismic data (Fig. 1b), suggesting that the chemical compositions of the upper and lower mantle may not be as dissimilar as previously proposed (Murakami et al. 2012).

EFFECT OF AL SUBSTITUTIONS ON THE THERMOELASTICITY OF BRIDGMANITE

The occurrence of vacancies in the oxygen sublattice of bridgmanite has been known for decades (Navrotsky et al., 2003). To accurately quantify the effect of the oxygen-vacancy (OV) $MgAlO_{2.5}$ substitution mechanism against that of the charged-couple (CC) $AlAlO_3$ mechanism, measurements of well-characterized, high-quality single crystals are critical. Here, we synthesized four aluminous bridgmanite samples at shallow lower mantle conditions in a multi-anvil press and characterized them *in-house* by electron microprobe and single-crystal X-ray diffraction at ambient conditions. Al contents ranged from 0.10 to 0.18 per formula unit, with molar fractions of the OV component from 2% to 5%.

Three of the four samples were subsequently loaded in resistive-heated DAC and single-crystal X-ray diffraction measurements were carried out at the synchrotron beamline P02.2 of Petra-III (Hamburg, Germany) up to 80 GPa at room temperature and up to 30 GPa and 1000 K at combined high pressure and temperature. A 3rd-order Birch-Murnaghan equation of state with the thermal pressure model formulated by Stixrude & Lithgow-Bertelloni (2005) was employed to fit the experimental pressure-volume-temperature data sets (Fig. 2a).

From the analysis of the molar volumes and bulk moduli of Al-bearing bridgmanite samples reported in this and previous studies, no apparent divergence between trends described along the CC and OV joins were found (Fig. 2b), despite previous studies reporting significantly larger molar volume and smaller bulk modulus for the $MgAlO_{2.5}$ component. Therefore, the presence of 5 mol.% OV component in bridgmanite, compatible with the concentrations expected in a pyrolitic lower mantle (Huang et al., 2021), likely has a negligible effect on the seismic properties of bridgmanite. By comparing the compression behavior of the whole structure and that of its individual crystallographic sites, it further appears that the main factor influencing the compressibility of aluminous bridgmanite is the Al content in the octahedral site.

The experimental results obtained here were then used to extrapolate previously determined phase equilibria in the MgO-$AlO_{1.5}$-SiO_2 system to explore how pressure and temperature affect the concentration of the OV component in bridgmanite down to mid-lower mantle

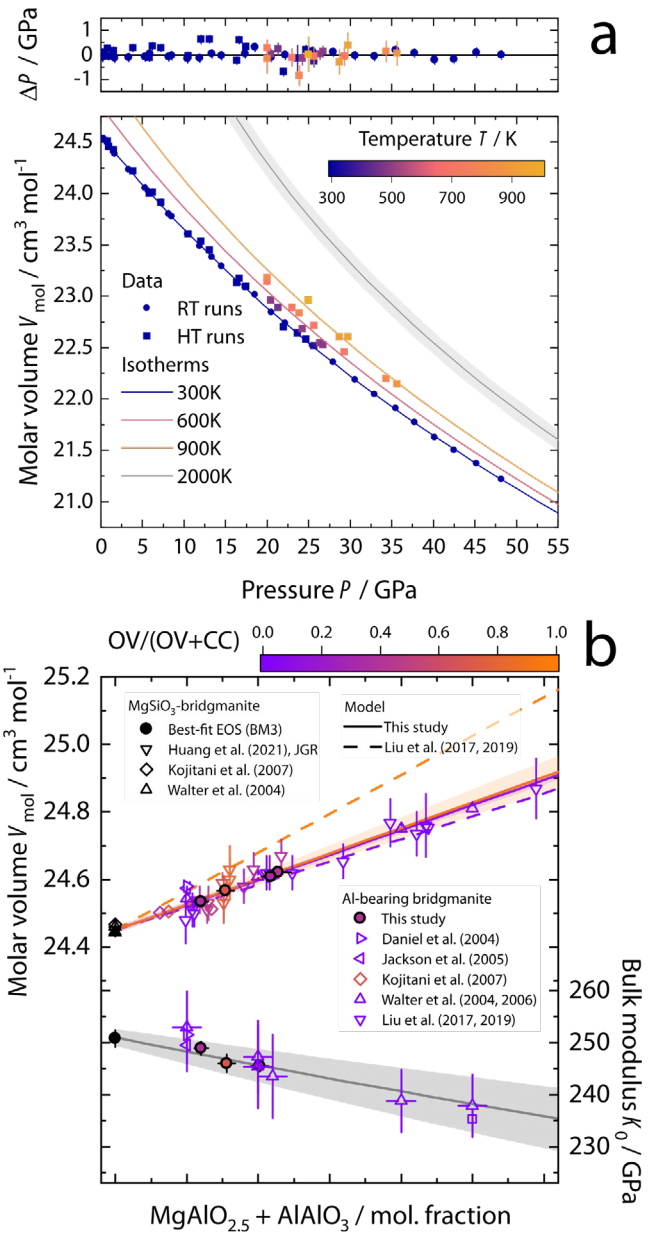

Figure 2 a) *Measured volumes for bridgmanite sample CC2-OV5 as a function of pressure and temperature (color scale), and calculated isotherm at selected temperatures. The 2000 K isotherm also displays the propagated uncertainty from the fit parameters. At the top, the difference between the measured and calculated pressures (ΔP).* ***b)*** *Measured and modelled molar volume (top) and bulk modulus (bottom) of bridgmanite along the $MgSiO_3$-$AlAlO_3$ and $MgSiO_3$-$MgAlO_{2.5}$ joins. Ratios of CC and OV components are expressed by the color scale. At the bottom, the two Al-end members were assumed to have the same bulk modulus, and the fitted curve is represented in gray instead of the purple-orange color coding. Shaded areas represent propagated uncertainties from a three- (top) or two-end-member model (bottom).*

conditions. From a reanalysis of literature data at 27 GPa and 2000 K, the standard-state Gibbs free energy (ΔG^0) and interaction parameter of Si and Al in the B-site of bridgmanite (W_{SiAl}^{B}) were refined. Extrapolation to higher pressures using the newly determined thermoelastic parameters of aluminous bridgmanite produced a much better agreement with the few available literature data than previous computational estimates (Brodholt, 2000). When included in more complete models, considering the effects of Fe and oxygen fugacity, the thermoelas-

tic and thermodynamic parameters reported here will enable more reliable estimates for the composition of bridgmanite and coexisting ferropericlase at shallow- to mid-lower mantle conditions to be obtained.

ANOMALOUS BEHAVIOR OF H,AL-BEARING SILICA PHASES UNDER PRESSURE

Although H and Al are known to expand the stability field of post-stishovite at the expense of that of stishovite, their individual and combined effects have not yet been disentangled. Recently, we found Al-bearing silica synthesized at 2200 K and 28 GPa not only to incorporate more than 1 wt.% H_2O but also to retain the $CaCl_2$-type structural modification of post-stishovite upon decompression to ambient conditions (Ishii et al., 2022), suggesting H plays a crucial role in stabilizing post-stishovite. To better understand the relation between Al and H incorporation, phase stability and physical properties, single-crystal synchrotron X-ray diffraction, structural refinements, and Raman spectroscopy measurements were conducted in the DAC up to 50 GPa on two samples of tetragonal $Al_{0.05}Si_{0.95}O_{1.98}H_{0.02}$ (Al5) and orthorhombic $Al_{0.11}Si_{0.89}O_{1.97}H_{0.07}$ (Al11).

Upon compression to about 16 GPa, the symmetry of Al5 changed from tetragonal to orthorhombic, whereas the Al11 sample preserved its orthorhombic symmetry throughout the entire pressure range investigated. The structure of the two samples was refined at every pressure point, and the amplitude of the symmetry-breaking structural mode Γ_2^+, related to the octahedral tilt angle, was calculated. In a pseudo-proper ferroelastic transition, as in SiO_2 stishovite, the tilt angle increases linearly with pressure (Zhang et al., 2023). Our results, however, highlight a concave rather than linear evolution (Fig. 3a), suggesting that another mechanism could also be involved in the transition. Additionally, the evolution of the Raman active soft mode associated with the post-stishovite transition displayed a different behavior from previously studied SiO_2 and aluminous stishovite samples (*e.g.*, Zhang et al., 2021). When the squared wavenumber (ω^2) is plotted against pressure, instead of changing abruptly at the transition pressure, ω^2 of the Al5 sample was found to decrease up to 20 GPa (*i.e.*, past the crystallographic transition pressure), then remain constant for approximately 10 GPa, and finally increase only above 30 GPa (Fig. 3b). An interval with weak-to-no pressure dependence of the soft mode was also found in the Al11 sample, whose symmetry is orthorhombic already from room pressure (Fig. 3b). Given the higher hydrogen content of our samples with respect to samples described in previous studies, and the fact that a symmetrization of the hydrogen (H-) bonds follows the Γ_2^+ symmetry-breaking structural mode, we concluded that the coupled substitution $Si^{4+} = Al^{3+} + H^+$ is much more efficient in decreasing the transition pressure of stishovite to post-stishovite than the oxygen vacancy substitution $Si^{4+} = Al^{3+} + 1/2OV^{2-}$.

It is still unclear at what pressure elastic anomalies are expected to occur in H,Al-bearing silica, whether at the onset of the crystallographic phase transition from or throughout the Raman soft mode plateau. Depending on which scenario is considered, and assuming the phase transition has a Clapeyron slope of 89 K/GPa (Nomura et al., 2010), the calculated transition pressures and temperatures for Al5 (*i.e.*, 2700 ppm wt. H_2O) match those expected for seismic scatterers detected at 720 or 860 km depth, for instance, underneath the Fiji-Tonga and South American subduction zones. The shallower occurrence of seismic scatterers in deep subduction settings seems, therefore, compatible with the presence of reservoirs of hydrous basaltic crust being recycled into the deep lower mantle.

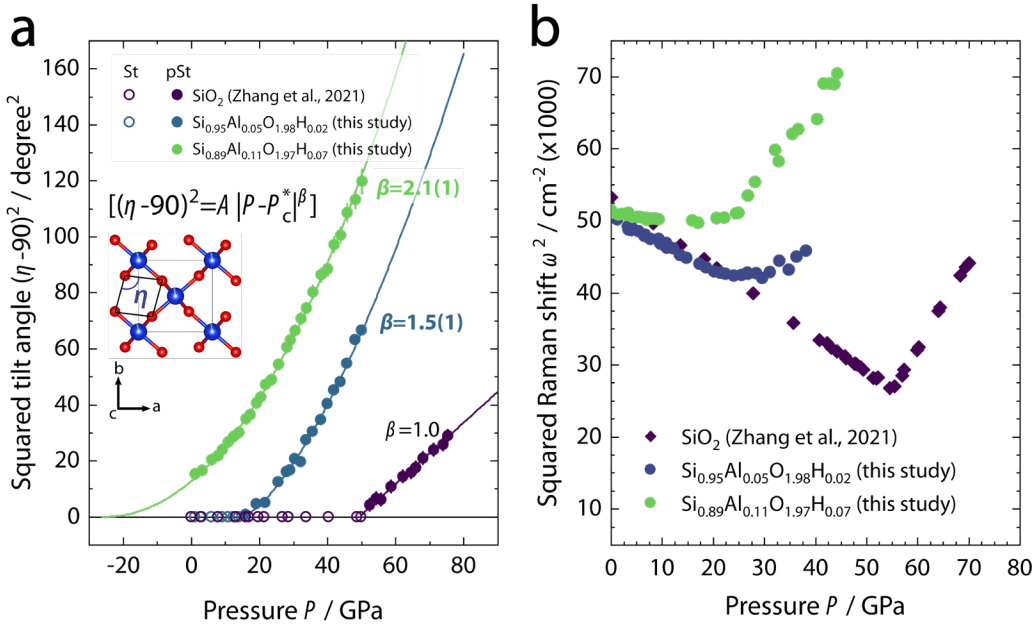

Figure 3 a) Pressure evolution of the squared octahedral tilt angle [(η – 90)²] in SiO_2 and H,Al-bearing stishovite (St) and post-stishovite (pSt), and power law fits to the experimental data. The exponent β is reported next to each curve. In the inset, crystal structure of post-stishovite highlighting the tilting of the octahedra. ***b)*** *Pressure dependence of the squared Raman mode in SiO_2 and H,Al-bearing stishovite.*

COMPRESSIBILITY OF DENSE HYDROUS SILICATE AL-PHASE D

Out of the hydrous phases that have been proposed to carry water in the mantle transition zone and topmost lower mantle, the Al-rich end member of DHMS phase D, nominally $Al_2SiO_6H_2$, was found to be the most resilient to the high temperatures of the ambient mantle, possibly due to its strong H-bonds (Pamato et al., 2015). The effect of Al substitution on the elastic properties of phase D samples remains, however, controversial.

Here, the first experimental constraints on the crystal structure and compressibility of a synthetic $Al_{1.53(2)}Fe^{3+}_{0.22(1)}Si_{0.86(1)}O_6H_{3.33(9)}$ Al-phase D sample are presented. Single-crystal X-ray diffraction measurements in the DAC were conducted at the ECB P02.2 (Petra-III, Hamburg, Germany) over two runs between room pressure and 52 GPa. A fit of the experimental data up to 38 GPa yielded a K_0 value that falls toward the higher range of previously proposed parameters for Mg-phase D. No evidence for elastic stiffening due to the symmetrization of H-bonds was found in this pressure interval, suggesting that the strength of H-bonds and their symmetrization do not affect the compressibility of Al-phase D.

Above 38 GPa, a change in the compression behavior was observed because of a high-to-low spin crossover of octahedrally coordinated Fe^{3+}, as reported by previous studies (*e.g.*, Wu et al. 2016). Despite the limited number of data points at these pressures, a recently proposed formalism was adopted, which makes use of crystal field parameters and their volume-dependency to calculate the energy associated with the high-spin and low-spin electronic states, from which the electronic energy and its derivatives can be calculated (Buchen, 2021). An inversion of all data from room pressure to 52 GPa shows excellent agreement with the experimental data points and suggests that the spin crossover region extends between approximately 35 and 65 GPa (Fig. 4), in good agreement with some previous studies.

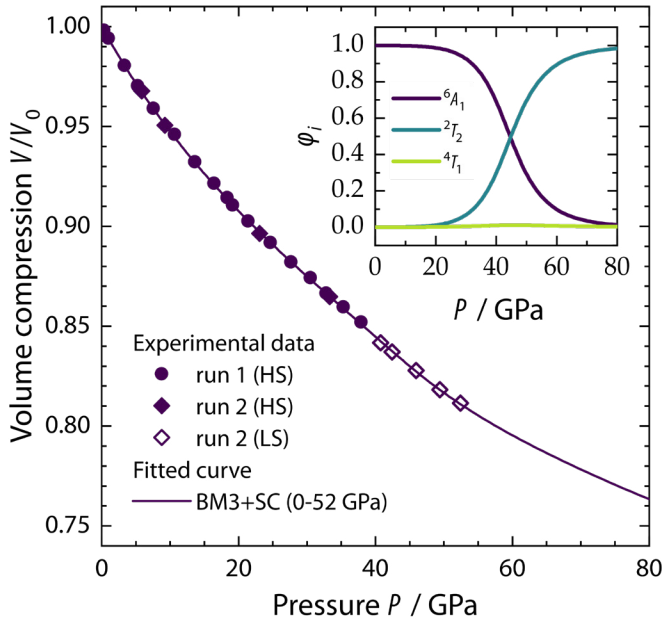

Figure 4 *Volume compression data of Fe-bearing Al-phase D and fitted spin-crossover (SC) 3rd-order Birch-Murnaghan (BM3) equation of state across the Fe^{3+} high-spin (HS) to low-spin (LS) crossover region. In the inset, the fraction (φ) of electrons in the HS ($^6A_1$) and LS ($^2T_2$, $^4T_1$) states is modelled as a function of pressure using the same BM3+SC fit parameters used to model the equation of state.*

Despite phase D solid solution displaying a wide range of K_0 and K'_0 values at room pressure, such a variability vanishes almost completely at ~20 GPa, where phase D is expected to be stable, due to the anti-correlation of the proposed K_0 and K'_0. Therefore, at the mantle transition zone and topmost lower mantle pressures, the bulk modulus of phase D solid solution is expected to be weakly affected by crystal chemical substitutions.

REFERENCES

Brodholt, J.P. (2000) - Pressure-induced changes in the compression mechanism of aluminous perovskite in the Earth's mantle. Nature, 407, 620–622.

Buchen, J. (2021) - Seismic Wave Velocities in Earth's Mantle from Mineral Elasticity. In: "Mantle Convection and Surface Expressions", H. Marquardt, M. Ballmer, S. Cottaar, J. Konter, eds. American Geophysical Union, 51-95.

Dziewonski, A.M. & Anderson, D.L. (1981) - Preliminary reference Earth model. Phys. Earth Planet. In., 25, 297–356.

Frost, D.J. (2006) - The Stability of Hydrous Mantle Phases. Rev. Mineral. Geochem., 62, 243–271.

Huang, R., Boffa Ballaran, T., McCammon, C.A., Miyajima, N., Dolejš, D., Frost, D.J. (2021) - The composition and redox state of bridgmanite in the lower mantle as a function of oxygen fugacity. Geochim. Cosmochim. Ac., 303, 110–136.

Ishii, T., Criniti, G., Ohtani, E., Purevjav, N., Fei, H., Katsura, T., Mao, H.K. (2022) - Superhydrous aluminous silica phases as major water hosts in high-temperature lower mantle. P. Natl. Acad. Sci. USA, 119, 1–6.

Kaneshima, S. (2019) - Seismic scatterers in the lower mantle near subduction zones. Geophys. J. Int., 218, 1873–1891.

Kurnosov, A., Marquardt, H., Frost, D.J., Boffa Ballaran, T., Ziberna, L. (2017) - Evidence for a Fe3+-rich pyrolitic lower mantle from (Al,Fe)-bearing bridgmanite elasticity data. Nature, 543, 543–546.

Murakami, M., Ohishi, Y., Hirao, N., Hirose, K. (2012) - A perovskitic lower mantle inferred from high-pressure, high-temperature sound velocity data. Nature, 485, 90–94.

Nakajima, Y., Frost, D.J., Rubie, D.C. (2012) - Ferrous iron partitioning between magnesium silicate perovskite and ferropericlase and the composition of perovskite in the Earth's lower mantle. J. Geophys. Res.-Solid, 117.

Navrotsky, A., Schoenitz, M., Kojitani, H., Xu, H., Zhang, J., Weidner, D.J., Jeanloz, R. (2003) - Aluminum in magnesium silicate perovskite: Formation, structure, and energetics of magnesium-rich defect solid solutions. J. Geophys. Res.-Solid, 108.

Nomura, R., Hirose, K., Sata, N., Ohishi, Y., Suetsugu, D., Bina, C., Inoue, T., Wiens, D., Jellinek, M. (2010) - Precise determination of post-stishovite phase transition boundary and implications for seismic heterogeneities in the mid-lower mantle. Phys. Earth Planet. In., 183, 104–109.

Pamato, M.G., Myhill, R., Boffa Ballaran, T., Frost, D.J., Heidelbach, F., Miyajima, N. (2015) - Lower-mantle water reservoir implied by the extreme stability of a hydrous aluminosilicate. Nat. Geosci., 8, 75–79.

Stixrude, L. & Lithgow-Bertelloni, C. (2005) - Thermodynamics of mantle minerals - I. Physical properties. Geophys. J. Int., 162, 610–632.

Wu, X., Wu, Y., Lin, J.-F., Liu, J., Mao, Z., Guo, X., Takashi, Y., McCammon, C., Prakapenka, V.B., Xiao, Y. (2016) - Two-stage spin transition of iron in FeAl-bearing phase D at lower mantle. J. Geophys. Res.-Solid, 121, 6411–6420.

Zhang, Y., Fu, S., Wang, B., Lin, J.F. (2021) - Elasticity of a Pseudoproper Ferroelastic Transition from Stishovite to Post-Stishovite at High Pressure. Phys. Rev. Lett., 126, 25701.

Zhang, Y., Chariton, S., He, J., Fu, S., Xu, F., Prakapenka, V.B., Lin, J.F. (2023) - Atomistic insight into the ferroelastic post-stishovite transition by high-pressure single-crystal X-ray diffraction. Am. Mineral., 108, 110–119.

Tectono-metamorphic evolution and petrogenesis of a medium-grade fragment of the Variscan orogen: the Zicavo Metamorphic Complex, Corsica (France)

Lorenzo Dulcetta
Department of Chemical and Geological Sciences, University of Cagliari, Cittadella Universitaria, 09042, Monserrato (CA)
DOI: 10.19276/plinius.2025.01.010

INTRODUCTION

The Corsica-Sardinia block (CSb) represents one of the many preserved Variscan domains across Europe. Even though hundreds of articles were published regarding both the orogenic and pre-orogenic features of the Sardinian part of the CSb, studies on the Variscan Corsica are still fragmented. This lack of detailed information on the Corsica transept led to the usual interpretation that Corsica and Sardinia represented a coherent crustal block throughout the entire Palaeozoic. However, recent data (Faure & Ferrière, 2022) may have shed light on a possible different tectonic and paleogeographic interpretation. In order to put new constraints on the tectono-metamorphic evolution and the petrogenesis within the disjointed Variscan basement of Corsica, the Zicavo Metamorphic Complex (ZMC) has been chosen as the study area due to the absence of detailed pressure (*P*) - temperature (*T*) and geochemical data. As such, a combination of field geology, petrography, geochemistry, and thermodynamic modelling has been employed, and the results have been interpreted in the view of the ZMC evolution and the more regional-scale CSb one, giving a possible new description of the pre-Variscan and Variscan evolution of this segment of the orogen.

FIELD GEOLOGY AND DEFORMATION

The ZMC (Fig. 1a) is a highly heterogeneous metamorphic complex consisting of three tectonic units, from bottom to top: the Orthogneiss Unit, the Leptyno-Amphibolite Unit, and the Micaschist Unit (Dulcetta et al., 2023). They are separated by two NE-dipping, dextral, ductile shear zones (Fig. 1b), characterized by a top-to-the-SE sense of shear.

The Orthogneiss Unit is made up of an ultramylonitic orthogneiss, a mylonitic augen gneiss, and garnet-bearing paragneisses on top of the unit. The ultramylonitic orthogneiss is a leucocratic, banded rock consisting of quartz- and feldspar-rich bands which are oriented following the main foliation. The augen gneiss is a coarse-grained rock with K-feldspar and plagioclase porphyroclasts that evidence a top-to-the-SE sense of shear. On top of both orthogneisses, a thin sequence of garnet-bearing paragneisses, which pass to greyish feldspar-rich paragneisses, occurs. The Leptyno-Amphibolite Unit is a thick metavolcanic sequence formed by interlayered amphibolites and meta-rhyolites. Amphibolites can be massive to banded, wherein banding is evidenced by different plagioclase content. The meta-rhyolites are whiteish foliated rocks with feldspars visible by the naked eye. Within the metavolcanics, lenses of garnet-staurolite micaschists, metaconglomerates and serpentinites can be observed. Finally, the Micaschist Unit is formed by garnet-staurolite and garnet-biotite schists, and garnet-bearing phyllites on top.

The ZMC recorded four deformation phases. The D_1 phase is characterized by the development of a metamorphic foliation whose orientation is now impossible to determine due to the strong overprinting and transposition by the subsequent phases. In the Leptyno-Amphibolite and Micaschist Units, the S_1 is highlighted by transposed metamorphic layers of quartz- and/or phyllosilicate-rich composition. In the Orthogneiss Unit, the D_1 deformation was not preserved/recorded. The D_2 deformation is the main deformation at the scale of the complex. It developed a NE-dipping S_2 axial plane foliation associated with F_2 isoclinal folds and an L_2 object lineation; the S_2 is often associated with a top-to-the-SE sense of shear. Furthermore, the mylonitic foliation on the two tectonic contacts is parallel to the regional S_2. The D_3 deformation was responsible for the development of upright open F_3 folds with rarely associated an S_3 crenulation cleavage, while the D_4 phase locally formed sub-horizontal F_4 folds.

METHODS

More than 200 samples were collected and analysed through the use of *i)* electron microscopy and electron microprobe, and *ii)* Raman spectroscopy. Among them, five samples from the three tectonic units were select-

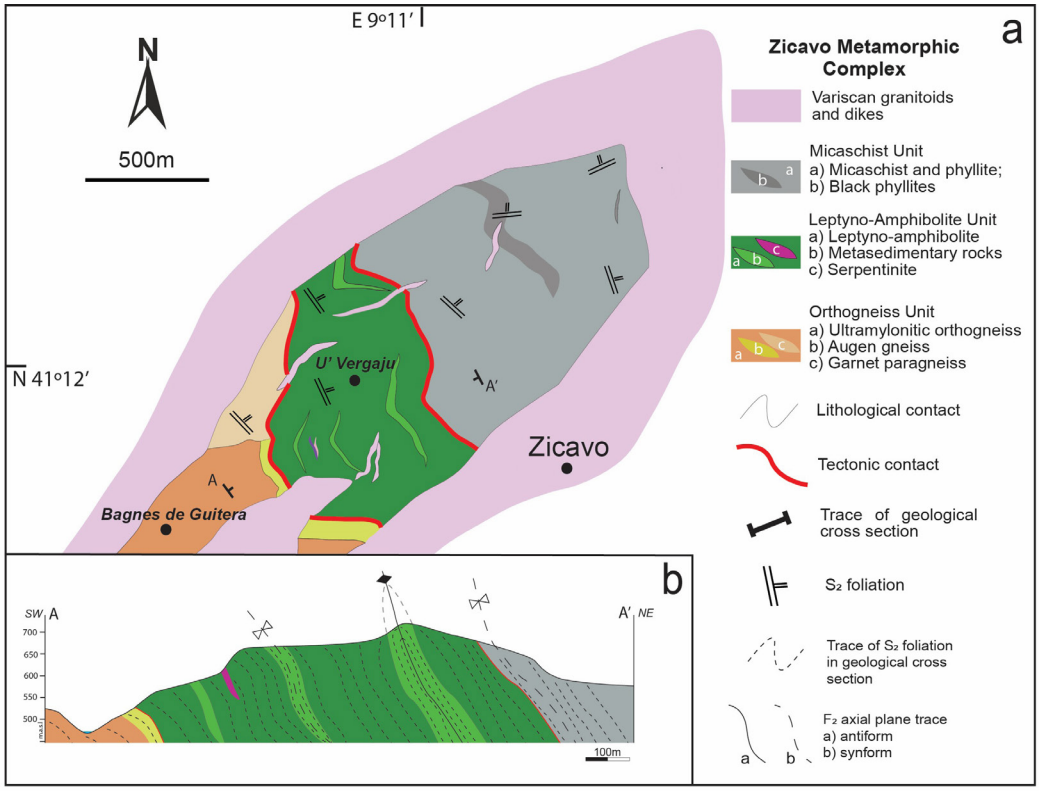

Figure 1 a) *Schematic geological map of the Zicavo Metamorphic Complex.* ***b)*** *Geological cross section of the Zicavo Metamorphic Complex. Modified from Dulcetta et al. (2023).*

ed for detailed thermodynamic modelling and elastic barometry to unravel the metamorphic *P-T* evolution of the ZMC: an augen gneiss from the Orthogneiss Unit, a garnet-staurolite micaschist from the Leptyno-Amphibolite Unit, and three garnet-rich micaschists from the Micaschist Unit. For each modelled sample, T-X^{Fe3+} phase diagrams were calculated first to infer a possible amount of ferric iron to be used in the *P-T* phase diagrams' calculations, following petrographic and mineral chemistry information. All diagrams were calculated using the 6.9.1 version of the Perple_X package (Connolly, 1990). The Holland & Powell (2011) internally consistent thermodynamic dataset (the tds633 version), with the Holland et al. (2018) integrated newest *a-X* (activity-composition) solution models, has been used. H_2O-saturation was assumed for all the pelitic samples.

Lastly, 19 selected samples from the Orthogneiss and Leptyno-Amphibolite Units were analysed for their major and trace/REE whole rock compositions by X-ray fluorescence and LA-ICPMS for palaeotectonic inferences.

RESULTS AND DISCUSSION

Petrography and microstructures of selected samples

The selected augen gneiss (sample ZIC-139) consists of mm- to cm-sized porphyroclasts of K-feldspar and (rarer) albitic plagioclase floating in a mylonitic matrix. The porphyroclasts are deformed by a top-to-the-SE sense of shear evidenced by asymmetric mantles and pressure shadows. The matrix is formed by Qz + Kfs + Ab + K-rich Wmca (abbreviations from Warr, 2021) oriented following the S_2 foliation.

Sample ZIC-157 from the Leptyno-Amphibolite Unit is a garnet-staurolite micaschist (Fig. 2a). It consists of Qz + Wmca + Grt + St + Bt + Ilm + And (±Pl±Ap±Mnz). Garnet forms subhedral porphyroblasts which can reach millimetric dimensions; it contains S_1-oriented mineral inclusions of Chl + Wmca + Ilm (±Ap±Qz±Mnz±Zrn±Als). In the matrix, white mica, biotite, ilmenite and staurolite are present. White mica forms very thin prismatic and/or acicular crystals, which are cross-cut by later, coarser mica grains; in between the white mica bundles, trails of biotite are also identified, often retrogressed in chlorite. Moreover, relict paragonite has sometimes been observed together with oriented muscovite, or statically overgrowing the matrix. Staurolite forms subhedral to euhedral prismatic crystals, showing white mica and ilmenite inclusions. Staurolite grows in clusters or single crystals around large garnet porphyroblasts in correspondence with resorption gulfs, in turn with overgrowths of andalusite or chlorite. The matrix is extensively overgrown by post-kinematic, subhedral andalusite, associated with newly formed, highly chloritized, biotite aggregates. Andalusite porphyroblasts grew at the expense of staurolite, muscovite and chlorite, which can sometimes be observed as relict inclusions, while margarite is observed growing along polygonal fractures.

The three samples from the Micaschist Unit (ZIC-3, 10, 11) are, respectively, a garnet phyllite, a garnet-biotite schist and a garnet-staurolite micaschist. The phyllite is a fine-grained rock consisting of Qz + Bt + Wmca + Chl + Grt + Ilm (±Pl±Ap±Zrn±Mnz). Garnet is the main porphyroblast, even though it has sub-millimetric size. It is anhedral to subhedral with pre- to inter-kinematic

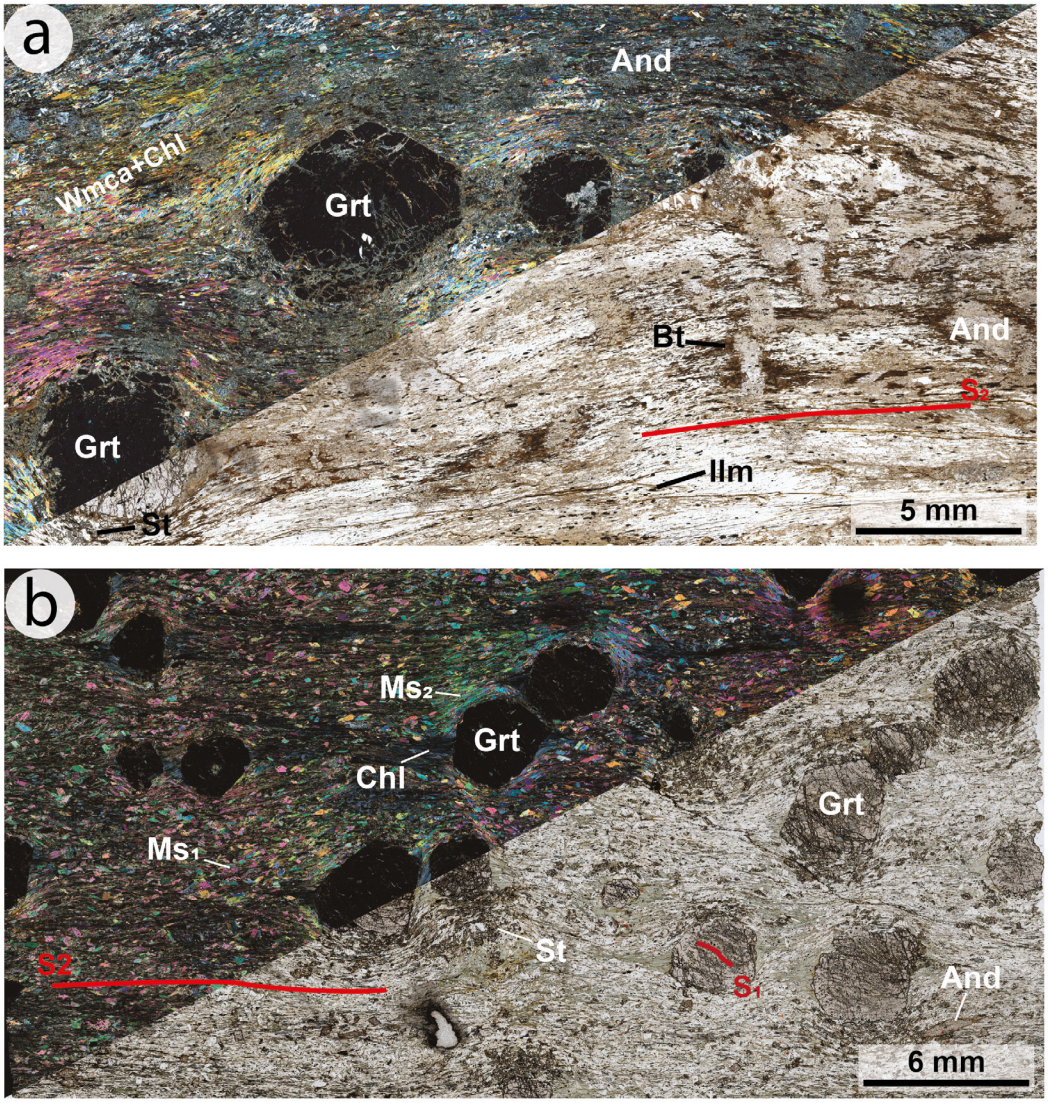

*Figure 2 a,b) Crossed polarized (upper left) and plane-polarized (lower right) photomicrographs for the garnet-staurolite mica-schists ZIC-157 **(a)** and ZIC-11b **(b)**.*

Chl + Qz + Ilm mineral inclusions, and is wrapped by a mica-rich matrix formed by muscovite, chlorite, biotite, quartz and rare plagioclase. The Grt-Bt schist consists of Qz + Pl + Bt + Wmca + Grt + Ilm (±Chl±Ap±Mnz±Zrn). The schists are texturally arranged in alternated layers and/or boudins made up of recrystallized quartz and layers consisting of phyllosilicates, plagioclase, garnet and quartz. Plagioclase represents the main porphyroblast, reaching millimetric size and showing a well-developed compositional zoning. The second main porphyroblast is garnet, which grows as millimetric crystals with equidimensional to elongated shape. It has S_1-oriented mineral inclusions of Qz + Chl + Ilm (±Ep±Zrn). The garnet inclusions' patterns are witnesses of the previous S_1 foliation, which can also be observed in microlithons outside porphyroblasts. Both plagioclase and garnet are wrapped by the S_2-oriented matrix consisting of Bt + Wmca + Ilm ± Chl. In the matrix, biotite has a coarse-grained size and is arranged in trails or aggregates, while white mica is organized either in trails or in mm-thick bundles. Chlorite is mostly a late phase growing on biotite or observed as an inclusion in garnet and plagioclase. The Grt-St micaschist (Fig. 2b) is a coarse-grained, strongly foliated rock made up of Qz + Pl + Grt + Wmca + Chl + St + Bt + Ilm. They are arranged in an oriented matrix, made up of Wmca + Bt + Chl + Ilm, which wraps mm-sized porphyroblasts and quartz-rich boudins. Garnet occurs as poikiloblasts reaching up to 5 mm in diameter. It shows inclusion-rich cores and mantles, and inclusion-poor rims. Inclusions are mainly represented by low amounts of rutile and chloritoid. Ilmenite is abundant in the mantle. In fact, rare rutile in the mantle has been observed overgrown by newly formed ilmenite. White mica is less abundant within garnet. Staurolite is the second main porphyroblast and can reach millimetric sizes, growing at the expense of chloritoid. Clusters of staurolite can also be observed close to the garnet boundaries. The matrix mainly consists of white mica, chloritoid, chlorite, ilmenite, and subordinate quartz, plagioclase, biotite, apatite and monazite.

P-T estimates

Figure 3a shows the *P-T* paths obtained for the five selected samples after detailed *T-X*$^{Fe3+}$ and *P-T* phase equilibrium modelling. Overall, the reported *P-T* conditions show a wide range of pressure and temperature values, especially for the high-pressure (HP) stage, both considering the samples' single *P-T* ellipses and/or those of different samples from the same unit.

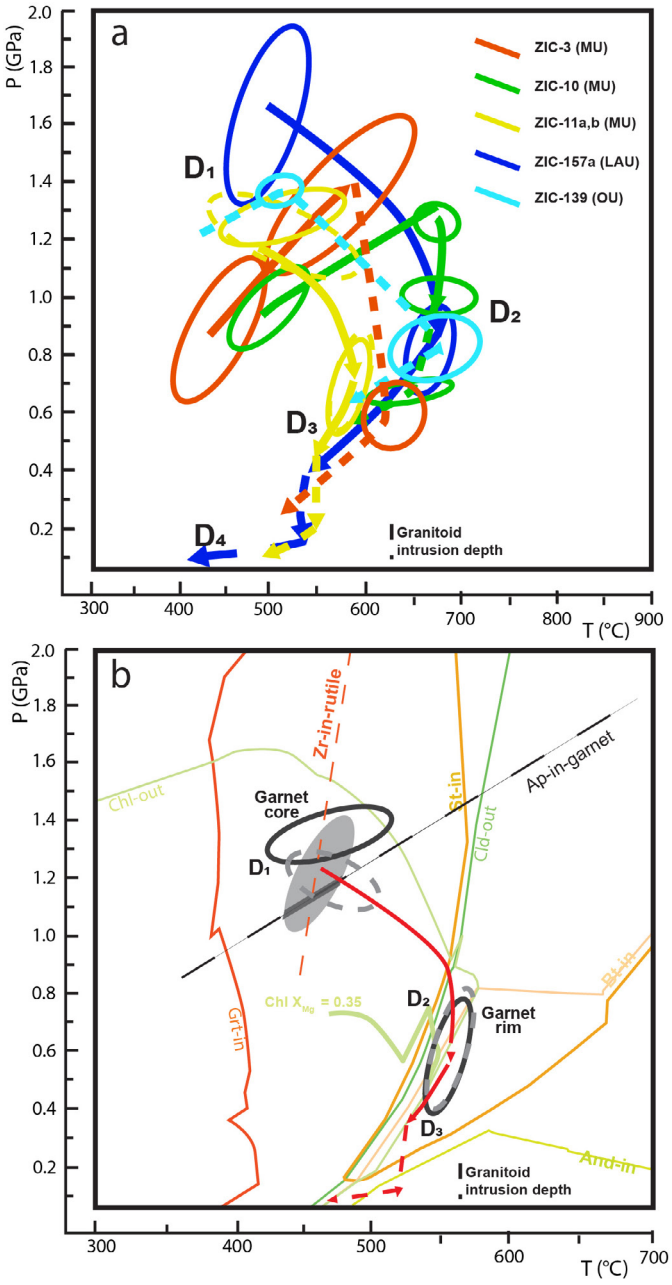

Figure 3 a) *obtained P-T-D metamorphic paths for the selected samples from the Zicavo Metamorphic Complex.* ***b)*** *P-T path for sample ZIC-11 from the Micaschist Unit refined using Zr-in-ritile thermometry and apatite-in-garnet elastic barometry.*

Regarding errors within the single ellipses, this is due to *i)* the propagated errors derived from the thermodynamic modelling, *i.e.*, those errors associated with activity composition models and the thermodynamic database, or *ii)* chemical re-equilibration and component diffusion, which lead to isopleths' scattering. Altogether, the presented *P-T* paths have a similar evolutionary trend. All the modelled rocks underwent a (relatively) high-pressure/low- to medium-temperature metamorphic stage, followed by a rather strong decompression characterized either by heating or isothermal conditions. The pressure and temperature range for the first metamorphic stage falls in the range 0.65-1.9 GPa/400-700°C. The H*P* stage can be said to be coeval to the first deformation phase D_1, which is retained as inclusions' patterns in garnet cores and mantles.

As a whole, the H*P* metamorphic stage in the ZMC, coeval (at least for the pelitic samples) with the first documented D_1 deformation, occurred at relatively high pressures and low to medium temperatures, in a tectonic regime characterized by low geothermal gradients ranging from 9 (ZIC-157a) to 16 (ZIC-10) °C/km. According to the reported *P-T* conditions, the studied samples were buried (assuming a geobaric gradient of 0.03 GPa/km) to depths of 30 (ZIC-3), 40 (ZIC-10), 43 (ZIC-11a,b), and 56 (ZIC-157a) kilometres during the D_1 deformation. These depths, related to the low geothermal gradients, are characteristic of cold subduction environments, or perhaps of the deepest portion of an accretionary prism close to the subducting, cold lithosphere. The inferred *P-T* conditions increase from the shallowest to the deepest rock units. The high-pressure D_1 stage was followed by a rather strong decompression, which indistinctly affected all three units to various degrees. This medium-pressure/medium-temperature (M*P*/M*T*) metamorphic stage has been constrained using the garnet rim and the matrix minerals' isopleths. The matrix minerals are oriented following the main S_2 foliation, which, in the ZMC, is related to a strong, dextral, top-to-the-SE shear deformation. Therefore, this stage was probably coeval with the progressive and composite D_2 deformation phase. The *P-T* conditions for this phase range between 0.65-1.1 GPa/560-720°C. Respectively, the Leptyno-Amphibolite Unit's micaschist, the Micaschist Unit's Grt-St and Grt-Pl micaschists and the Orthogneiss Unit's augen gneiss underwent 25 km, 15 km, 10 km and 18 km of exhumation. The maximum heating was experienced by sample ZIC-157a, which passed from 500 to 650-700°C, just a bit higher than sample ZIC-139 (530-700°C). Samples ZIC-11a,b underwent only ~100°C of heating. Summing up, the M*P*/M*T* metamorphic stage (coeval to the progressive D_2 shear deformation) developed during a heating-decompression trajectory, from high pressure (greenschist/low pressure blueschist facies) to the lower to upper amphibolite facies. The thermal peak occurred in a high geothermal gradient environment of about 20-22 °C/km. This was probably linked to the ongoing collision and crustal thickening, which led to higher temperatures.

The post-D_2 evolution has been less constrained with respect to the prograde part of the *P-T* paths. However, the retrogression may have followed the same trajectory for the studied samples, starting from the thermal peak in the amphibolite facies towards the greenschist facies. This segment of the *P-T* paths can be ascribed to an additional metamorphic stage which was coeval to the D_3 deformation, affecting the ZMC during early retrograde conditions. It probably was a short-lived stage since a low amount of retrograde minerals, such as chlorite, are observed growing with the S_3 foliation or associated with F_3 microfolds. This might be an indication that

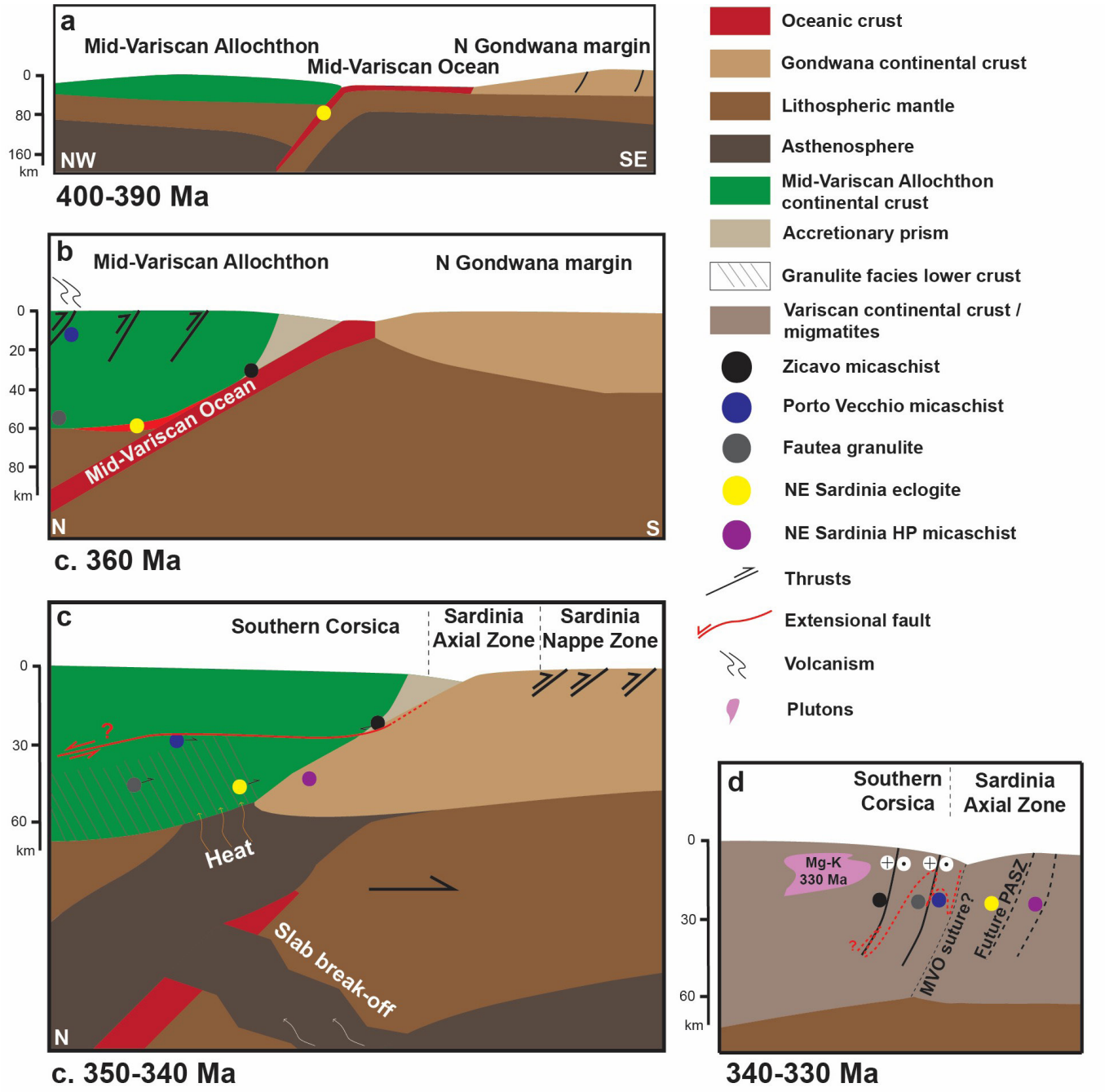

*Figure 4 a-d) Geodynamic evolution from the Devonian **(a)** to the Carboniferous **(d)** for the Corsica and northern Sardinia paleogeographic domains. See details in the text and in Dulcetta et al. (2025).*

there was not enough time to extensively re-equilibrate the rocks according to those conditions. The reason for this apparently short-lived metamorphic stage can be sought in the re-equilibration, after an early retrogression, at high-temperature/low-pressure (HT-LP) conditions during the thermal metamorphism that affected the ZMC at various scales. This thermal metamorphic stage occurred at HT-LP and is well testified by the staurolite-bearing samples (ZIC-157a and ZIC11a,b), which show widespread, post-kinematic andalusite and biotite blastesis. Contact metamorphism occurred at pressures lower than 0.4 GPa (< 13 km in depth) within the andalusite stability field, at 500°C < *T* < 600°C, since K-feldspar was never observed. Lastly, the HT-LP minerals were partly re-equilibrated and overprinted by later phases, linked to the last and final retrogression, which may be related to a final retrograde stage. These include margarite, paragonite and fine-grained muscovite in the schists, white micas on feldspars, chlorite on biotite, and quartz+chlorite on cordierite. As a whole, the post-thermal peak evolution was characterized by a continuous exhumation due to orogenic collapse, during which the high temperature effect was given by the intruding granitoids. The D_4 deformation, characterized by sub-horizontal folds, probably occurred during these last pulses of the orogenic collapse.

Paleotectonic setting

Major and trace/REE whole rock compositions for the orthogneiss Unit and some metavolcanics from the Leptyno-Amphibolite Unit were plotted on tectonic discrimination diagrams and compared to several other similar rocks across Sardinia and Europe.

The ZMC's Orthogneiss Unit was derived from a peraluminous, calc-alkaline to slightly alkali-calcic, magnesian granite of Middle Ordovician age. Based on the paleotectonic affinity, the Zicavo orthogneiss was set within a volcanic arc part of a convergent setting in Middle Ordovician times. This is coherent with the same tectonic environment of formation of the compared orthogneisses from northern Sardinia and Corsica. However, slight yet remarkable differences can be ascribed from both geochemical and geological points of view. A major difference can be seen in the SiO_2 vs Fe* plot, where the Zicavo orthogneiss clearly shows magnesian features, whereas the Sardinia orthogneisses have ferroan characteristics. Secondly, looking at the spider diagrams, the Zicavo suite is always more enriched in incompatible elements and REE. This feature, and the negative anomalies in Nb and Ta, may imply a lower crustal contamination in the generation of the Zicavo magmas.

The Leptyno-Amphibolite Unit represented a bimodal (basic-felsic) volcanic suite emplaced in pre-Variscan times. The analysed metabasite samples are calc-alkaline basalts to basaltic andesites. Concerning the metarhyolites, they are well plotted within the early extension-related fields, *i.e.*, the within plate fields. Regarding metabasites, they mostly plot in two different fields: a first group plots within fields compatible with a convergent setting of formation, while the second group plots in fields associated with extensional settings. These characteristics may be interpreted to represent a tectonic setting's transition during the emplacement of the entire sequence.

A renewed geodynamic scenario

Amongst the several modelled samples, for which the reconstructed *P-T* paths showed a similar metamorphic evolution, the Grt-St micaschist samples ZIC-11 have been chosen for further *P-T* refinement using trace elements thermometry and apatite-in-garnet elastic barometry. The results are shown in Figure 3b. The details of the work are shown in Dulcetta et al. (2025). The other complexes taken into account are the Fautea and Porto Vecchio ones from Corsica (see Giacomini et al., 2008; Massonne et al., 2018; Cruciani et al., 2021) and the Sardinia eclogites and high pressure micaschists (Cruciani et al., 2012, 2022). Figure 4 shows the presented geodynamic model. The evolution begins in the Lower Devonian with the subduction of the Mid-Variscan Ocean (MVO, Martinez-Catalan et al., 2021) below the Mid-Variscan Allochthon (MVA) (Fig. 4a). Between 365-350 Ma, in Corsica, high-pressure metamorphism was recorded coeval with the D_1 deformation by the Fautea septum's felsic granulites, whereas D_1 high-temperature/low-pressure metamorphism was instead documented by the Porto Vecchio micaschists. These latter rocks were metamorphosed at ~25 km in depth at 362 Ma. Massonne et al. (2018) interpreted this *HT-LP* stage as a metamorphic imprint close to a hot volcanic arc. These features may indicate the position of the Porto Vecchio rocks on the upper plate, that is, the MVA (Fig. 4b). On the other hand, the high pressure recorded by Fautea's felsic granulite may be explained by its position at the base of the upper plate. The high-pressure, syn-D_1 metamorphic stage documented by the ZMC's Grt-St micaschists (Fig. 3a, b) might also be coeval with the D_1 metamorphisms in Fautea and Porto Vecchio. In Sardinia, there is no Variscan *s.s.* metamorphic event before 345-340 Ma. The Zicavo high-pressure rocks may be placed either in the deepest portion of the accretionary prism or in fragments accreted to the base of the upper plate. The former environment seems more likely for the Micaschist Unit's protolith.

Between 350-335 Ma, the Variscan collision began (Fig. 4c). The main metamorphic feature in the ZMC was the extensive amphibolite facies re-equilibration after decompression, exhumation and heating experienced by the three units at different degrees. In Fautea, the felsic granulites underwent their second loop in the granulite facies at > 700°C and 1.0 GPa (~30 km), whereas in Porto Vecchio, the Grt micaschist possibly experienced the metamorphic peak. The decompression and heating during the D_2 must have been linked to *i)* a partial exhumation of the units and *ii)* some kind of heat source. The heat source needs to be sought for also for the granulite facies re-equilibration experienced by the Fautea granulites (and Sardinia eclogites). This heat source may have been given by an asthenosphere upwelling below the MVA, consequence of the slab break off of the descending MVO (Fig. 4c). A coupling between slab break off and lithospheric delamination may also be sought for an even higher thermal regime which explains *i)* the strong, ductile, dextral D_2 shearing at 340 Ma in Corsica, *ii)* the large migmatization at 345 Ma, and *iii)* the tectonic juxtaposition of high-grade metamorphic rocks (*i.e.*, the Fautea rocks) on top of lower-grade rocks (*i.e.*, the ZMC rocks), as it is currently observed. This is shown as a crustal scale normal fault caused by a possible lithospheric delamination below Gondwana, which *i)* brought the Zicavo rocks northward of the Fautea and Porto Vecchio ones, and *ii)* juxtaposed the higher-grade, deeper Fautea granulites and migmatites onto the lower grade, shallower Zicavo and Porto Vecchio complexes. Noteworthy, the D_1 phase in Sardinia is coeval or slightly older than the 335-340 Ma D_2 in Corsica, but considerably younger than the D_1 in Corsica, dated at 360 Ma.

Between 330-320 Ma, the Variscan collision was at its climax. Shear zones such as the East Variscan Shear Zone were probably set on main tectonic features such

as suture zones or former shear zones. In Corsica, after the syn-D_2 dextral shearing, further shear deformation accompanied the development of the D_3 phase at 320 Ma. Meanwhile, in Sardina, the same shearing was active during the D_2 deformation and linked to the activity of the well-known PASZ (Carosi et al., 2020). At this time, the Corsica metamorphic complexes were on their way to the surface after the syn-D_2 thermal peak. Coevally, in Sardinia, the syn-D_2 thermal peak and amphibolite facies metamorphism occurred.

Between Corsica and Sardinia, if they were truly divided already prior to the Variscan collision, a suture should then be present. However, currently there are no witnesses of such a suture that can be clearly recognized, as already pointed out by Faure et al. (2014). In this regard, the rather strong shearing activity that characterized the D_2 and D_3 deformation in Sardinia and Corsica, respectively, might help to constrain a hypothetical position of such a suture. The PASZ and other similar structures across the Variscides have all been related to the evolution of the continental-scale EVSZ. Such a structure had to be imposed on a previous, regional-scale, tectonically weak feature, for instance, a suture zone. Following this interpretation, it may be that between Corsica and Sardinia an oceanic suture lies, now erased and obscured mostly by the EVSZ activity. In light of this evidence, the new presented *P-T* data and upon comparing them with other *P-T* constraints from Corsica and Sardinia, it might have been possible that, before the orogenesis took place, the Variscan rocks of southern Corsica and Sardinia could have belonged to two different paleogeographic domains. Further *P-T*-t, geochemical and geochronological data may help, in the future, to better constrain this scenario.

REFERENCES

Carosi, R., Petroccia, A., Iaccarino, S., Simonetti, M., Langone, A., Montomoli, C. (2020) - Kinematics and timing constraints in a transpressive tectonic regime: The example of the Posada-Asinara Shear Zone (NE Sardinia, Italy). Geosciences, 10(8), 288.

Connolly, J.A.D. (1990) - Multivariate phase diagrams: an algorithm based on generalized thermodynamics. Am. J. Sci., 290, 666-718.

Cruciani, G., Franceschelli, M., Groppo, C., Spano, M.E. (2012) - Metamorphic evolution of non-equilibrated granulitized eclogite from Punta de li Tulchi (Variscan Sardinia) determined through texturally controlled thermodynamic modelling. J. Metamorph. Geol., 30(7), 667-685.

Cruciani, G., Franceschelli, M., Massonne, H.-J., Musumeci, G. (2021) - Evidence of two metamorphic cycles preserved in garnet from felsic granulite in the southern Variscan belt of Corsica, France. Lithos, 380-381, 105919.

Cruciani, G., Franceschelli, M., Carosi, R., Montomoli, C. (2022) - P-T path from garnet zoning in pelitic schist from NE Sardinia, Italy: further constraints on the metamorphic and tectonic evolution of the north Sardinia Variscan belt. Lithos, 428-429, 106836.

Dulcetta, L., Faure, M., Rossi, P., Cruciani, G., Franceschelli, M. (2023) - Geology of the Zicavo Metamorphic Complex, southern Corsica (France). J. Maps, 19(1), 2264320.

Dulcetta, L., Zhong, X., Cruciani, G., Vrijmoed, J., Pleuger, J., Franceschelli, M., John, T. (2025) - Coupling Phase Equilibrium Modelling and Apatite-in-Garnet Elastic Barometry to Unravel the P–T Path of the Micaschist Unit From the Zicavo Metamorphic Complex (Corsica, France). J. Metamorph. Geol., *In Press*.

Faure, M., Rossi, P., Gaché, J., Melleton, J., Frei, D., Li, X., Lin, W. (2014) - Variscan orogeny in Corsica: New structural and geochronological insights, and its place in the Variscan geodynamic framework. Int. J. Earth Sci., 103(6), 1533-1551.

Faure, M. & Ferrière, J. (2022) - Reconstructing the Variscan Terranes in the Alpine basement: Facts and arguments for an Alpidic Orocline. Geosciences, 12(2), 65.

Giacomini, F., Dallai, L., Carminati, E., Tiepolo, M., Ghezzo, C. (2008) - Exhumation of a Variscan orogenic complex: Insights into the composite granulitic–amphibolitic metamorphic basement of south-east Corsica (France). J. Metamorph. Geol., 26(4), 403-436.

Holland, T.J.B. & Powell, R. (2011) - An improved and extended internally consistent thermodynamic dataset for phases of petrological interest, involving a new equation of state for solids. J. Metamorph. Geol., 29, 333-383.

Holland, T.J., Green, E.C., Powell, R. (2018) - Melting of peridotites through to granites: a simple thermodynamic model in the system KNCFMASHTOCr. J. Petrol., 59(5), 881-900.

Martínez Catalan, J.R., Schulmann, K., Ghienne, J.F. (2021) - The Mid-Variscan Allochthon: keys from correlation, partial retrodeformation and plate-tectonic reconstruction to unlock the geometry of a noncylindrical belt. Earth Sci. Rev., 220, 1-65.

Massonne, H.-J., Cruciani, G., Franceschelli, M., Musumeci, G. (2018) - Anticlockwise pressure temperature paths ecord Variscan upper-plate exhumation: Example from micaschists of the Porto Vecchio region, Corsica. J. Metamorph. Geol., 36(1), 55-77.

Warr, L.N. (2021) - IMA–CNMNC approved mineral symbols. Mineral. Mag., 85(3), 291-320.

Magma-carbonate interaction under dynamic conditions: experimental insights on crystallization kinetics and multiphase rheology

Gabriele Giuliani
Department of Sciences, University of Roma Tre, L.go San Leonardo Murialdo 1, 00146, Roma
DOI: 10.19276/plinius.2025.01.011

INTRODUCTION

Volcanic systems that develop within carbonate basement rocks represent distinctive geological environments where magma interacts with carbonate-rich lithologies, such as limestone and dolostone. These interactions give rise to a range of complex processes that significantly affect the physicochemical evolution, rheology, and eruptive behavior of the magma (Fig. 1).

Magma-carbonate interaction is a well-documented phenomenon in numerous volcanic systems worldwide (Freda et al., 2008; Gaeta et al., 2009; Mollo et al., 2010; Troll et al., 2012; Jolis et al., 2015). The outcomes of these interactions are observed through various indicators, including the presence of crustal xenoliths in volcanic deposits, variations in mineral assemblages, crystallization patterns, and influences on degassing processes and eruption styles. Evidence of these interactions occurs on multiple timescales, ranging from seconds to days for short-term processes, and from years to thousands of years for long-term processes (Knuever et al., 2023).

When exposed to the heat of magma, carbonate minerals undergo decarbonation, breaking down into their constituent oxides (CaO and MgO) and releasing carbon dioxide (CO_2) gas. The decarbonation process not only dissolves carbonate clasts but also introduces a significant amount of CaO and MgO into the surrounding magma. The diffusion of these oxides is facilitated by thermal gradients between the high-temperature magma and the cooler carbonate rocks, as well as by mechanical processes, such as convective currents within the magma chamber driven by contrasts in magma viscosity and density. The increase of CaO and MgO profoundly affects the physicochemical properties of the magma, as these oxides act as network-modifying agents in silicate melts. The impact of CaO and MgO on magma viscosity extends beyond their effects on the liquid phase; experimental studies highlight that crystallization of minerals rich in these oxides is promoted. Following, the crystallization process involves two simultaneous effects on the system's rheology (lquid+crystal): *i)* chemically, the addition of CaO and MgO to the liquid phase leads to decreased polymerization, as the concentration of network modifiers increases and *ii)* physically, the introduction of crystallizing particles impact magma mobility hindering its flow and increasing its viscosity (Vona et al., 2011; Kolzenburg et al., 2022). As crystal content rises, viscosity increases exponentially, causing the magma to transition from fluid-like to more rigid, solid-like behavior.

At the margins of a magma chamber where assimilation and crystallization are most pronounced and intense, stratified shells rich in mineral assemblages containing CaO and MgO may form. Skarns develop from the reaction of magma-derived fluids with surrounding carbonate rocks, leading to progressive metamorphism and mineralogical transformation. This process is crucial because skarns act as physical barriers at the magma chamber margins, limiting further decarbonation and assimilation of the carbonate host rock. However, skarn recycling introduces fragments of CaO- and MgO-rich crystallized rocks back into the system, which further alters the chemical composition of the evolved magma, promoting further crystallization, thereby enhancing heterogeneity. Simultaneously, convective stirring within the magma chamber and the injection of new magma from deeper parts of the system promote magma mixing. This mixing can be further enhanced by chemical gradients introduced by the decarbonation/assimilation process and differences in crystallization across various parts of the magma chamber. The result is the formation of hybrid magmas, some of which achieve complete homogenization, while others retain evidence of incomplete mixing. Hybrid magmas often exhibit distinct rheological properties due to introduced chemical heterogeneity and variations in crystal content (Morgavi et al., 2022).

Although numerous studies have underscored the key role of magma-carbonate interactions in volcanic dynamics and eruptions, as well as the influence of deformation regimes on crystallization processes and resulting rheology, there remains a notable gap in experi-

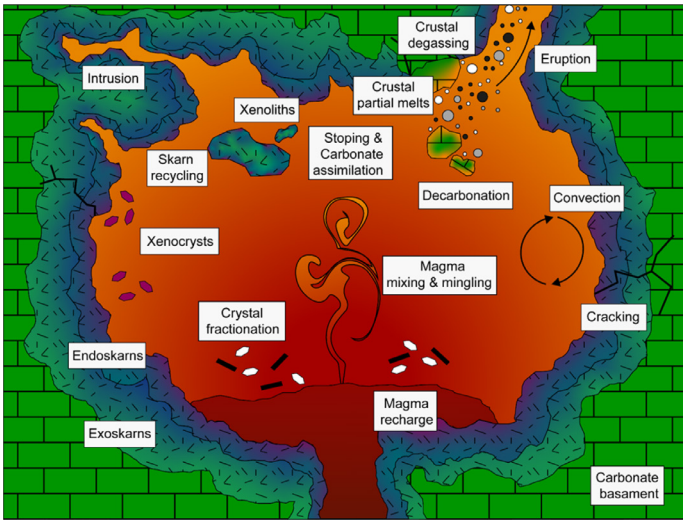

Figure 1 *Schematic sketch showing various magma chamber processes (not to scale). Some of these processes, e.g., endoskarn/exoskarn crystallization, stoping and carbonate assimilation, decarbonation, magma mixing & mingling, cracking and skarn recycling, are examined in detail in the thesis. Sketch modified after Deegan (2010).*

mental investigations that examine the combined effects of stirring and carbonate assimilation. This gap is particularly evident in the context of CaO-MgO-contaminated hybrid magmas, whose rheological properties remain largely unexplored.

Aims of the thesis

The main objective was to address the following questions:

What is the effect of carbonate assimilation on the rheology of single-phase (liquid) melts?

How do dynamic conditions influence crystallization and rheological behavior in multiphase (liquid+crystals) melts affected by carbonate assimilation?

Based on current understanding of magma-carbonate interactions and magma rheology, this project systematically investigated for the first time how carbonate assimilation and deformation regimes affected crystallization kinetics and the rheological evolution of magmas.

Specifically:

For single-phase (liquid) melt, the investigation determined how the addition of CaO and CaO+MgO influenced the crystal-free viscosity across both high- and low-temperature regimes.

For multiphase (liquid+crystals) magmas, the study assessed how these compositional changes, together with deformation regimes, affected rheological behavior under dynamic conditions.

MATERIALS AND METHODS

The research integrated a diverse set of complementary experimental and analytical techniques to provide a comprehensive investigation of magma-carbonate interactions. Experimental petrology and geochemistry were employed to simulate and assess the mechanisms and rates of these interactions in controlled laboratory settings, using natural materials from Somma-Vesuvius (Italy) as representative starting samples. To mimic carbonate assimilation, phonotephrite rock powder from the 472 CE Pollena eruption was doped with varying amounts of CaO and CaO+MgO, obtained from the thermal decomposition of $CaCO_3$ (Fig. 2).

The following techniques were employed:

Major Element Analysis: Electron microprobe analyses of starting and residual glasses were performed at the Bayerisches Geoinstitut (Germany) and the Natural History Museum in London, United Kingdom.

High-Temperature Crystal-Free Viscosity Measurements: Conducted at the EVPLab of the University of Roma Tre using a concentric cylinder apparatus (CC).

Low-Temperature Crystal-Free Viscosity Measurements: Conducted at both the EVPLab of the University of Roma Tre and the GLASS Laboratory of the CNR (Italy), using differential scanning calorimetry (DSC) and micropenetration viscometry (MP).

High-Temperature Crystallization Experiments: Carried out at the EVPLab of the University of Roma Tre, using a CC.

Spectroscopic Techniques: Raman spectroscopy was performed at the EVPLab of the University of Roma Tre, and at the GLASS Laboratory of the CNR (Italy), while Brillouin spectroscopy was carried out at the Bayerisches Geoinstitut (Germany).

Microphotography and Textural Analysis: Microphotographs were taken at the *HP-HT* Laboratory of the National Institute of Geophysics and Volcanology in Rome.

THE EFFECT OF CARBONATE ASSIMILATION AND NANOHETEROGENEITIES ON THE VISCOSITY OF PHONOTEPHRITIC MELT FROM VESUVIUS

This study addressed this gap by presenting novel viscosity data for a leucite-bearing phonotephritic melt from the 472 CE Pollena eruption (Vesuvius, Italy), doped with varying amounts of CaO and CaO+MgO. The chosen compositions closely matched those of melt inclusions and interstitial glasses from skarns at Vesuvius, interpreted as the result of magma mixing with carbonate-derived components (Fig. 2).

Viscosity measurements were conducted across a wide temperature range using concentric cylinder viscometry, differential scanning calorimetry, and micropenetration methods. Specifically, experiments were performed at high temperatures (1150–1400°C) and low temperatures (640–760°C). The integrated approach, which combined Brillouin and Raman spectroscopy with these techniques,

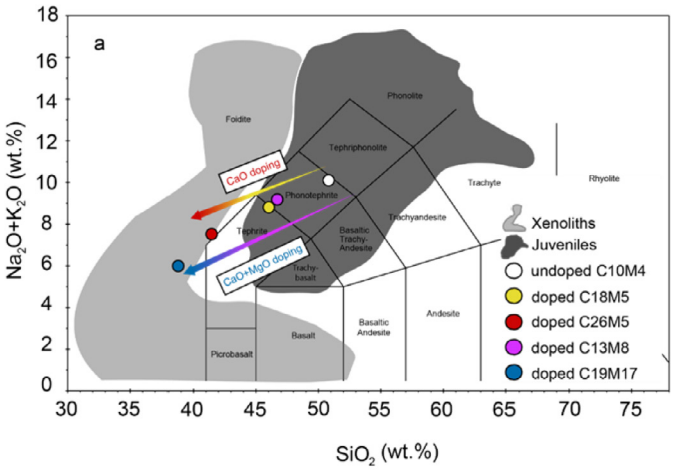

Figure 2 Total alkali vs. silica (TAS) diagram showing the undoped and doped glass compositions used in this study. The undoped material (C10M4) is represented as the white symbol. CaO-doped samples are represented by the yellow (C18M5) and red (C26M5) symbols, whilst purple (C13M8) and blue (C19M17) symbols correspond to samples doped with CaO and MgO. Areas represent the compositional variations of the products erupted from Vesuvius, specifically, the dark grey area represents juvenile materials (Rosi & Santacroce, 1983; Santacroce et al., 2008; Jolis et al., 2015; Macdonald et al., 2016), while the light gray area represents xenoliths (Fulignati et al., 2000, 2004; Del Moro et al., 2001; Jolis et al., 2015).

accurately predicted the viscosity changes induced by carbonate assimilation and identified the formation of nanoheterogeneities during low-temperature viscosity experiments (Fig. 3).

Experimental data revealed a significant viscosity/temperature crossover when CaO and CaO+MgO were added. Above 750°C, the undoped melt exhibited the highest viscosity, whereas doped melts showed substantially lower viscosities. Below this threshold, the trend reversed. Among the doping agents, CaO addition induced a much larger viscosity decrease compared to CaO+MgO addition, underscoring the predominant role of CaO in modifying the viscosity of the silicate liquid (Fig. 3).

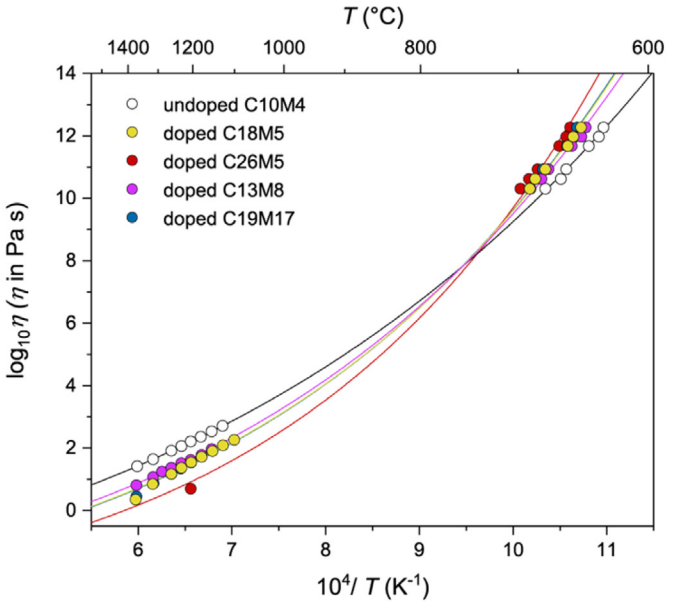

Figure 3 Viscosity data from differential scanning calorimetry and concentric cylinder measurements, and MYEGA fits (Mauro et al., 2009).

Importantly, empirical viscosity models from existing literature (Giordano et al., 2008; Langhammer et al., 2021) failed to reproduce these experimental observations, particularly for highly doped melts and across both temperature regimes, highlighting the limitations of purely chemistry-based models and emphasized the necessity of integrated spectroscopic and experimental approaches for predicting the rheology of carbonate-contaminated magmas.

These results provide new constraints on magma transport properties in volcanic plumbing systems where magma-carbonate interaction occurs. The insights gained into viscosity reduction and the effects of nanoheterogeneities shed light on how carbonate assimilation can promote the mobility, mixing, and hybridization of magmas, ultimately influencing eruption dynamics. Such processes are especially relevant at Vesuvius and similar volcanoes, where carbonate assimilation is well documented and can enhance explosivity through CO_2 release.

THE RHEOLOGICAL EVOLUTION OF A PHONOTEPHRITIC MELT UPON VARIABLE DEGREES OF CARBONATE ASSIMILATION AND DEFORMATION REGIMES

This study presented new insights from isothermal static experiments (ISEs) and isothermal deformation experiments (IDEs), performed at CC, which investigated the rheological evolution of a phonotephritic melt from Somma-Vesuvius (Italy) under varying shear rates (0, 1 and 5 s^{-1}) and doping levels of CaO and CaO+MgO. By examining the interaction between mechanical deformation and melt contamination, the study explored the

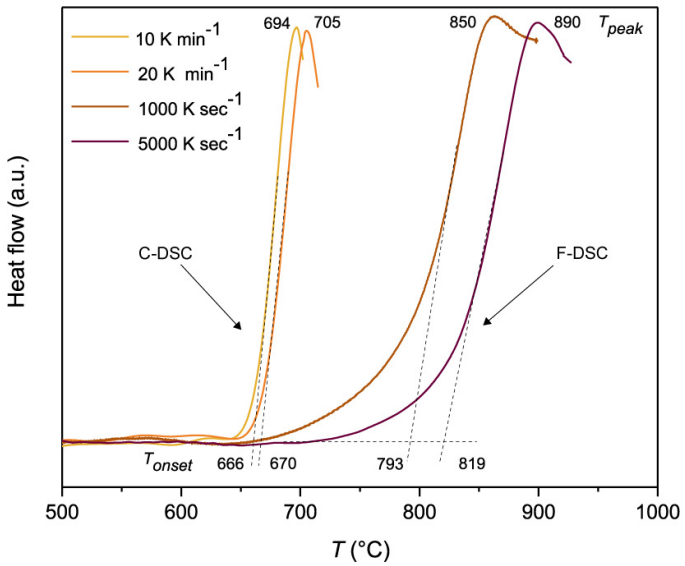

Figure 4 Heat flow of CaO+MgO-doped residual glass measured as a function of temperature using conventional (C-DSC) and Flash (F-DSC) differential scanning calorimetry. Dashed lines correspond to the second upscan during measurements performed at 10 and 20 K min^{-1} and at 1000 and 5000 K s^{-1} using the rate-matching method (Di Genova et al., 2020).

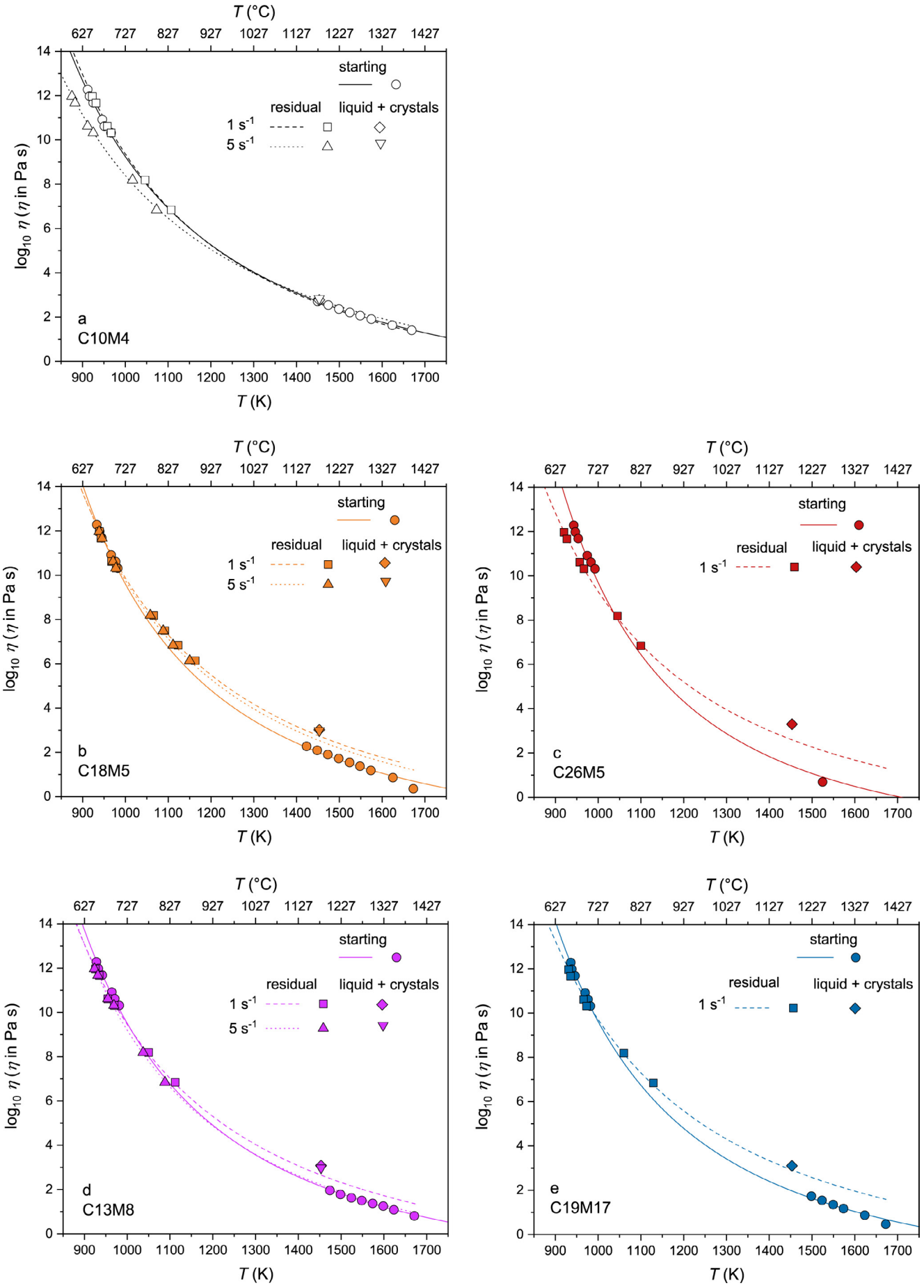

Figure 5 Temperature-dependence of the viscosity measured for starting and residual glasses. The MYEGA fits from the equation of Mauro et al. (2009) refer to viscosity data obtained by C-DSC and F-DSC measurements at low and high temperature regimes. The viscosities of starting melts are displayed as solid lines and circles. The viscosities of residual melts and their modeling are displayed as squares and dashed lines for a shear rate of 1 s^{-1}, and triangles and dotted lines for a shear rate of 5 s^{-1}. The melt+crystal viscosities from IDEs performed at 1180°C are also displayed as diamonds and inverted triangles for shear rates of 1 and 5 s^{-1}, respectively. The panels show the temperature-dependence of the viscosity measured for the undoped sample C10M4 ***(a)****, the low CaO-doped sample C18M5* ***(b)****, the high CaO-doped sample C26M5* ***(c)****, the low CaO + MgO-doped sample C13M8* ***(d)****, and the high CaO + MgO-doped sample C19M17* ***(e)****.*

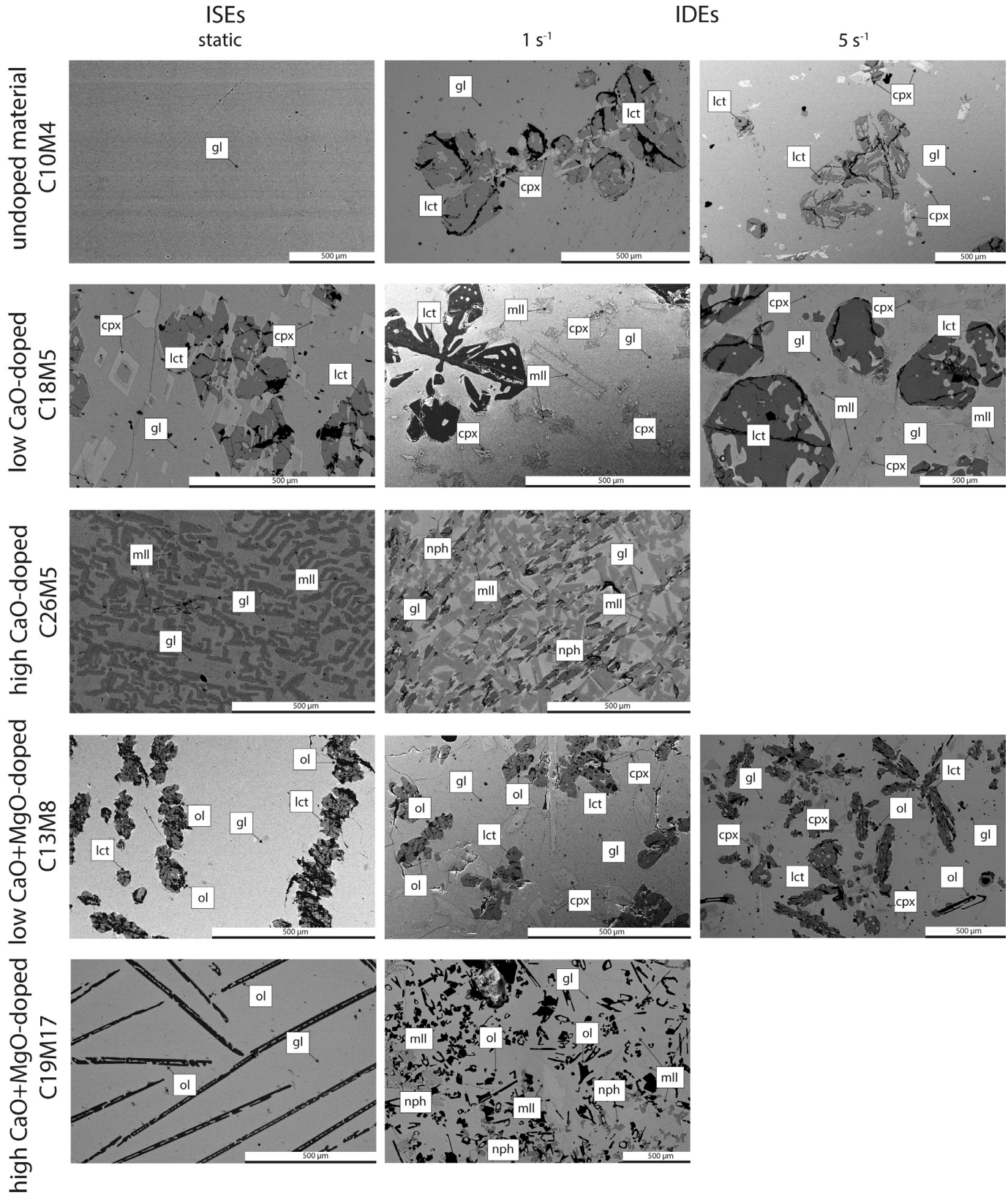

Figure 6 BSE photomicrographs illustrating the phase assemblage and textural features resulting from ISEs and IDEs. Gl: glass, Ol: olivine, Cpx: clinopyroxene, Lct: leucite, Nph: nepheline, Mll: melilite.

processes that governed the nucleation and growth of crystals, as well as the resulting changes in viscosity.

To elucidate the impact of dynamic deformation on the rheological evolution of magmas during crystallization, two interrelated effects were considered: i) changes in crystallinity due to enhanced crystal nucleation and growth process, and ii) compositional evolution of the residual melt as crystallization progressed.

Flash differential scanning calorimetry was employed to directly determine the viscosity of the interstitial melt, enabling the first direct assessment of how crystallization affected melt rheology without relying on empirical models (Fig. 4 and Fig. 5).

IDEs revealed two distinct rheological regimes: (1) viscous deformation characterized by uniform flow, and (2) non-homogeneous deformation marked by shear lo-

calization and viscous or brittle rupture of the magma. With increasing shear rate and carbonate doping, melts displayed non-Newtonian behavior resulting from stress localization and fracturing processes, which were promoted by the formation of a crystal network (Fig. 6). The presence of crystals introduces mechanical heterogeneities that disrupt the uniform flow of the melt, leading to localized stress and premature crack formation.

The measured viscosity range from IDEs was narrower than that predicted by the model (Frontoni et al. 2022) of purely viscous behavior, indicating that shear localization and fracturing processes reduced the resistance to flow in the doped, crystal-rich samples. These observations suggested that the complex rheology of CaO- and CaO+MgO-doped melts, which represent varying degrees of carbonate assimilation, likely reflected the disaggregation of skarn shells at the periphery of magma chambers. This disaggregation favored skarn recycling and enhanced the potential for magma contamination.

Furthermore, the extensive crystallization occurring in skarn-rich environments increased the susceptibility of the system to viscous rupture and brittle failure, thereby influencing the mechanical response of the magmatic system under stress conditions.

Residual melts exhibited nearly isoviscous behavior, facilitating the efficient mixing of magmas during the extraction of interstitial melts from the crystalline framework. This enhanced mixing capability was especially significant at the margins of mature magma chambers in contact with carbonate wall rocks, where CaO- and CaO+MgO-enriched melts maintained high mixing efficiency within solidification fronts.

These findings underscore the critical role of dynamic deformation and carbonate assimilation in controlling the evolution of magmatic rheology and highlight the need for integrated experimental studies to better understand the complex behaviors of contaminated, multiphase magmatic systems.

REFERENCES

Deegan, F.M. (2010) - Processes of Magma-crust Interaction: Insights from Geochemistry and Experimental Petrology. PhD Thesis.

Del Moro, A., Fulignati, P., Marianelli, P., Sbrana, A. (2001) - Magma contamination by direct wall rock interaction: constraints from xenoliths from the walls of a carbonate-hosted magma chamber (Vesuvius 1944 eruption). J. Volcanol. Geoth. Res., 112, 15-24.

Di Genova, D., Zandonà, A., Deubener, J. (2020) - Unravelling the effect of nano-heterogeneity on the viscosity of silicate melts: Implications for glass manufacturing and volcanic eruptions. J. Non-Cryst. Solids, 545, 120248.

Freda, C., Gaeta, M., Misiti, V., Mollo, S., Dolfi, D., Scarlato, P. (2008) - Magma-carbonate interaction: An experimental study on ultrapotassic rocks from Alban Hills (Central Italy). Lithos, 101, 397–415.

Frontoni, A., Costa, A., Vona, A., Romano, C. (2022) - A comprehensive database of crystal-bearing magmas for the calibration of a rheological model. Sci. Data, 9, 1–11.

Fulignati, P., Marianelli, P., Santacroce, R., Sbrana, A. (2000) - The skarn shell of the 1944 Vesuvius magma chamber. Genesis and P-T-X conditions from melt and fluid inclusion data. Eur. J. Mineral., 12, 1025–1039.

Fulignati, P., Marianelli, P., Santacroce, R., Sbrana, A. (2004) - Probing the Vesuvius magma chamber-host rock interface through xenoliths. Geol. Mag., 141, 417–428.

Gaeta, M., Di Rocco, T., Freda, C. (2009) - Carbonate assimilation in open magmatic systems: The role of melt-bearing skarns and cumulate-forming processes. J. Petrol., 50, 361–385.

Giordano, D., Russell, J.K., Dingwell, D.B. (2008) - Viscosity of magmatic liquids: A model. Earth Planet. Sci. Lett., 271, 123–134.

Jolis, E.M., Troll, V.R., Harris, C., Freda, C., Gaeta, M., Orsi, G., Siebe, C. (2015) - Skarn xenolith record crustal CO2 liberation during Pompeii and Pollena eruptions, Vesuvius volcanic system, central Italy. Chem. Geol., 415, 17–36.

Knuever, M., Sulpizio, R., Mele, D., Costa, A. (2023) - Magma–rock interactions: a review of their influence on magma rising processes with emphasis on short-timescale assimilation of carbonate rocks. Geol. Soc. London, Spec. Publ., 520, 101–120.

Kolzenburg, S., Chevrel, M. O., Dingwell, D.B. (2022) - Magma / Suspension Rheology. Rev. Mineral. Geochem., 87, 639–720.

Langhammer, D., Di Genova, D., Steinle-Neumann, G. (2021) - Modeling the Viscosity of Anhydrous and Hydrous Volcanic Melts. Geochem. Geophy. Geosy., 22.

Macdonald, R., Bagiński, B., Rolandi, G., De Vivo, B., Kopczyńska, A. (2016) - Petrology of parasitic and eccentric cones on the flanks and base of Somma-Vesuvius. Mineral. Petrol., 110, 65–85.

Mauro, J.C, Yue, Y., Ellison, A.J., Gupta, P.K., Allan, D.C. (2009) - Viscosity of glass-forming liquids. Proc. Natl. Acad. Sci., 106, 19780–19784.

Mollo, S., Gaeta, M., Freda, C., Di Rocco, T., Misiti, V., Scarlato, P. (2010) - Carbonate assimilation in magmas: A reappraisal based on experimental petrology. Lithos, 114, 503–514.

Morgavi, D., Laumonier, M., Petrelli, M., Dingwell, D.B. (2022) - Decrypting Magma Mixing in Igneous Systems. Rev. Mineral. Geochem., 87, 607–638.

Rosi, M. & Santacroce, R. (1983) - The A.D. 472 "Pollena" eruption: volcanological and petrological data for

this poorly-known, plinian-type event at vesuvius. J. Volcanol. Geoth. Res., 17, 249–271.

Santacroce, R., Cioni, R., Marianelli, P., Sbrana, A., Sulpizio, R., Zanchetta, G., Donahue, D.J., Joron, J. L. (2008) - Age and whole rock-glass compositions of proximal pyroclastics from the major explosive eruptions of Somma-Vesuvius: A review as a tool for distal tephrostratigraphy. J. Volcanol. Geoth. Res., 177, 1–18.

Troll, V.R., Hilton, D.R., Jolis, E.M., Chadwick, J.P., Blythe, L.S., Deegan, F.M., Schwarzkopf, L.M., Zimmer, M. (2012) - Crustal CO2 liberation during the 2006 eruption and earthquake events at Merapi volcano, Indonesia. Geophys. Res. Lett., 39.

Vona, A., Romano, C., Dingwell, D.B., Giordano, D. (2011) - The rheology of crystal-bearing basaltic magmas from Stromboli and Etna. Geochim. Cosmochim. Acta, 75, 3214–3236.

Probing the role of $MgSiO_3$ polymorphs in deep mantle processes

Mattia La Fortezza
Department of Geosciences, University of Padova, Via Giovanni Gradenigo 6, 35131, Padova
DOI: 10.19276/plinius.2025.01.012

This PhD thesis presents a first-principles theoretical study, based on state-of-the-art hybrid DFT calculations, on the thermodynamics and phase stability of magnesium silicates that play a relevant role in determining the mineralogical composition and physico-chemical properties of the Earth's mantle: the polymorphs of $MgSiO_3$, in particular the $MgSiO_3$ pyroxenes. Such minerals display a large stability field that spans the shallower portions of the Earth's mantle, down to the mantle transition zone. In fact, pyroxenes make up as much as 30 vol% of the Earth's upper mantle (Irifune & Tsuchiya, 2007; Frost, 2008) (Fig. 1) and are involved in several geochemical and geophyisical processes that take place in the interior of our planet, such as partial melting and mineralogical phase transitions determining global seismic discontinuities in the mantle. Despite the geochemical, geophysical, and petrological importance of pyroxenes in terrestrial and extraterrestrial bodies, their thermodynamic and thermophysical properties are still affected by large uncertainties, which are poorly defined or even completely lacking, particularly for the high-pressure and high-temperature polymorphs. This hinders the possibility not only to obtain a clearer picture of their phase stability, but also to fully understand their rheological behaviour at mantle conditions, preventing the interpretation of global-scale processes in the Earth.

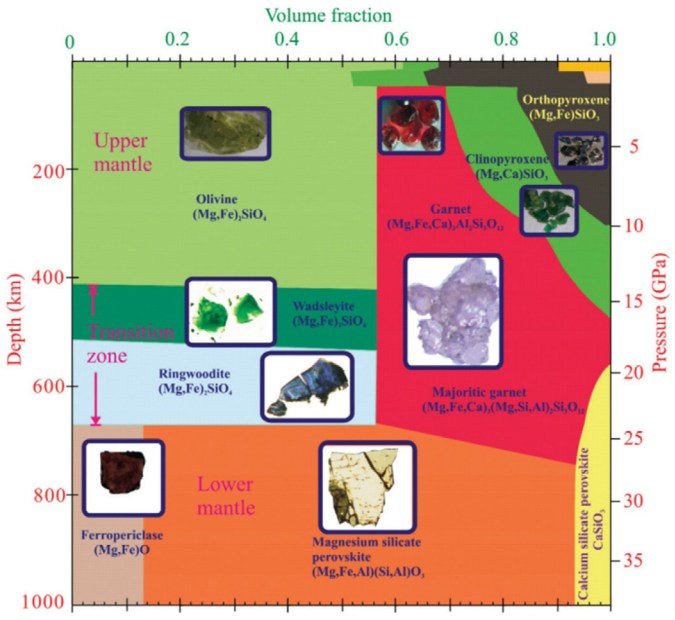

Figure 1 *Mineral volume fractions for the top 1000 km of a pyrolitic mantle. Stability fields of pyroxene phases (ortho- and clino-pyroxene) are represented in dark and light green on the top right of this diagram (after Ringwood, 1991; figure taken from Frost, 2008).*

The thermodynamic stability of the different pyroxene polymorphs depends upon pressure (*P*), temperature (*T*), and chemical composition (*X*). Pyroxenes with $MgSiO_3$ composition are known to exist in at least five different structures and undergo structural phase transitions with increasing *P-T* conditions (Fig. 2).

At low *T* and *P*, monoclinic low-clinoenstatite with space group $P2_1/c$ is the stable phase. A displacive phase transition occurs at high pressure (*i.e.*, P > 6-7 GPa), resulting in high-pressure clinoenstatite with space group *C*2/*c* (Angel et al., 1992). Orthoenstatite (*Pbca*) occurs at high *T* and pressures up to about 7 GPa, whereas protoenstatite (*Pbcn*) and high-*T* clinoenstatite (*C*2/*c*) have small stability fields at high *T* and low *P* according to current phase diagrams in the literature (*e.g.*, Gasparik, 2014). The polymorphism and stability relations of magnesium pyroxene phases are thus a masterpiece of complexity. This is further complicated by the fact that several additional pyroxene phases have been suggested to exist in the Earth's mantle (Thompson & Downs, 2003), some of which may be preserved as metastable phases.

Moreover, stable and metastable pyroxenes are strongly involved in the dynamics of subducting slabs. In fact, the presence of metastable pyroxenes in subducting slabs directly affects the density of the downgoing plate, modifying its buoyancy and favouring slab stagnation at the mantle transition zone (van Mierlo et al., 2013; Agrusta et al., 2014).

This study focused on the theoretical simulation of thermodynamic and thermoelastic properties of $MgSiO_3$ pyroxenes [namely, low-pressure clinoenstatite (LP-

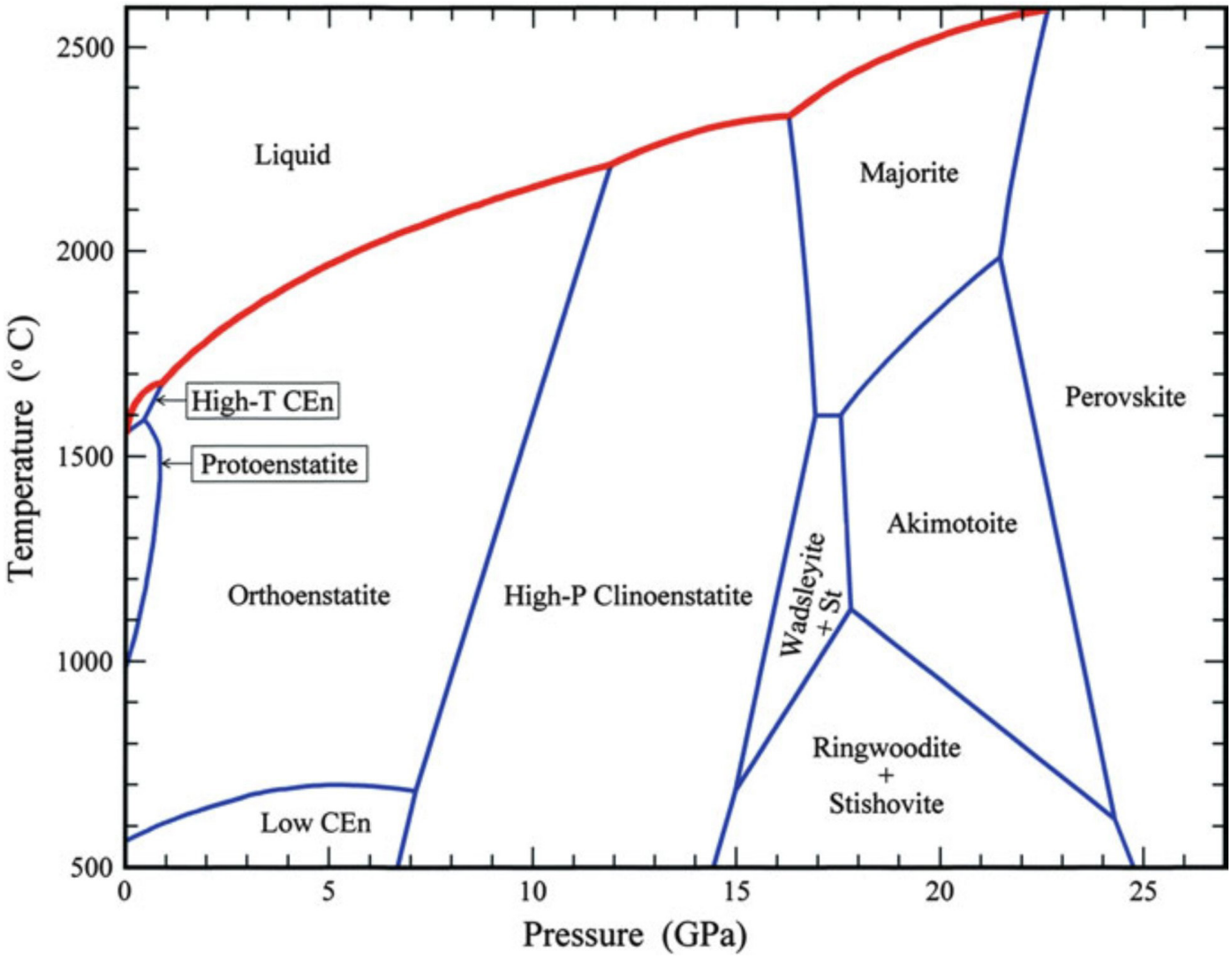

Figure 2 *Temperature – pressure phase diagram for the $MgSiO_3$ system (according to Gasparik, 2014).*

CEn), orthoenstatite (OEn), protoenstatite (PEn), high-temperature clinoenstatite (HT-CEn), high-pressure clinoenstatite (HP-CEn)], performed by *ab initio* DFT calculations up to conditions compatible with their stability in the deep mantle. The *ab initio* thermodynamic data computed in this work represent the first attempt to build up a complete dataset of both physically- and internally-consistent properties for $MgSiO_3$ pyroxenes in a broad range a *P-T* conditions. This first-principles dataset includes all the main thermodynamic properties necessary for the calculation of the Gibbs free energy at high-pressure and high-temperature (*i.e.*, enthalpy, entropy, heat capacity, volume thermal expansion, bulk modulus and its pressure and temperature derivatives elastic moduli and seismic properties), hence to investigate phase stability relations of pyroxenes from subsolidus to liquidus conditions. Gibbs free energy minimisation then provides information on the relative stability of $MgSiO_3$ pyroxenes, allowing the calculation of *P-T-X* phase diagrams. Moreover, thermoelastic properties such as the thermal equation of state and volume thermal expansion are fundamental to predict volume and density changes at mantle conditions, which in turn allows to constrain the rheological role of pyroxenes in mantle processes. Computed data also include the elastic and seismic properties (*i.e.*, the full elastic constant tensor and longitudinal and transverse wave velocities, V_P and V_S), that can be used to infer seismic velocity jumps and seismic impedance contrasts (*i.e.*, $\Delta\rho V_{P,S}$), allowing for a direct comparison with seismological observations on mid-mantle global seismic discontinuities and providing thermodynamic constraints on their origin. In particular, the origin of the so-called X-discontinuity in the mantle, between 270 and 330 km depths, has been tentatively interpreted in the literature as closely related to mineralogical phase transitions that include the OEn to HP-CEn phase transformation as a viable candidate (Woodland, 1998).

The main results, implications and open issues extracted from this Thesis are briefly summarized and described here.

Ab initio hybrid DFT-QHA calculations at the B3LYP level of theory improve the accuracy of the thermodynamic properties of high-pressure magnesium silicates with respect to less sophisticated LDA and GGA

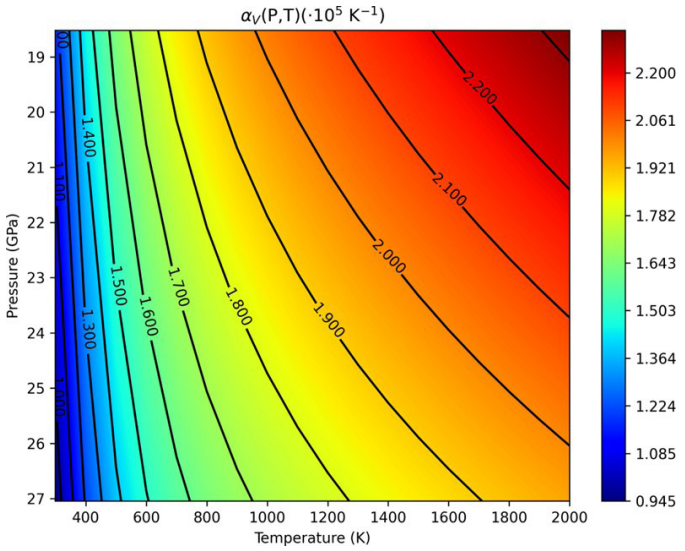

Figure 3 *Contour plot of ab initio volume thermal expansivity of Mg_2SiO_4 ringwoodite at mantle transition zone conditions.*

density functionals. In order to test the performance of B3LYP, a first stage in the development of this PhD project has been dedicated to the theoretical simulation of thermodynamic and thermoelastic properties of γ-Mg_2SiO_4 ringwoodite, using this mineral as a sort of beta test for calculations on more complex crystal structures. The obtained results not only show that *ab initio* B3LYP calculations are able to accurately predict thermodynamic and thermoelastic properties of this fundamental mineral phase up to lowermost mantle transition zone conditions, but clearly demonstrate that empirical extrapolation of thermoelastic data to deep mantle conditions should be taken with care to avoid inaccurate or spurious predictions in phase equilibrium modelling (*cf.*, Belmonte et al., 2022). The most relevant result that came out from this research is represented by the definition of a single (and quite simple) polynomial function that accurately predicts the values of ringwoodite volume thermal expansivity directly at simultaneous high-pressure and high-temperature conditions compatible with the Earth's mantle transition zone (Fig. 3).

Ab initio B3LYP thermodynamic properties of all the pyroxene polymorphs of $MgSiO_3$ (*i.e.*, PEn, OEn, LP-CEn, HP-CEn and HT-CEn) allow to obtain the full phase diagram of $MgSiO_3$, hence providing original insights on the thermodynamic behaviour of such phases at *P-T* conditions compatible with their stability in the Earth's mantle. Despite the lack of experimental results, B3LYP calculations compare favourably with the few experiments available in the literature. *Ab initio* calculations performed in this work help thus to fill the gap in terms of thermodynamic information about some of these unquenchable phases, such as HT-CEn, HP-CEn and PEn. In fact the thermodynamic properties of most of the investigated phases have been determined for the very first time. For instance, the first comprehensive ab initio thermodynamic dataset for high-temperature clinoenstatite (HT-CEn) has been defined in this work, considering that no experimental data exist on this phase and the only information currently available comes from thermodynamic assessments. Thermoelastic properties of protoenstatite (PEn), like volume thermal expansivity and thermal equation of state parameters, were previously almost unknown due to experimental difficulties in the synthesis and characterization of this phase. As a relevant example of the performances of *ab initio* calculations performed in this work, the theoretical isobaric heat capacity of PEn is reported as compared with the only calorimetric data available (Thieblot et al., 1999) and with the polynomial function assessed by Berman (1988) (Fig. 4).

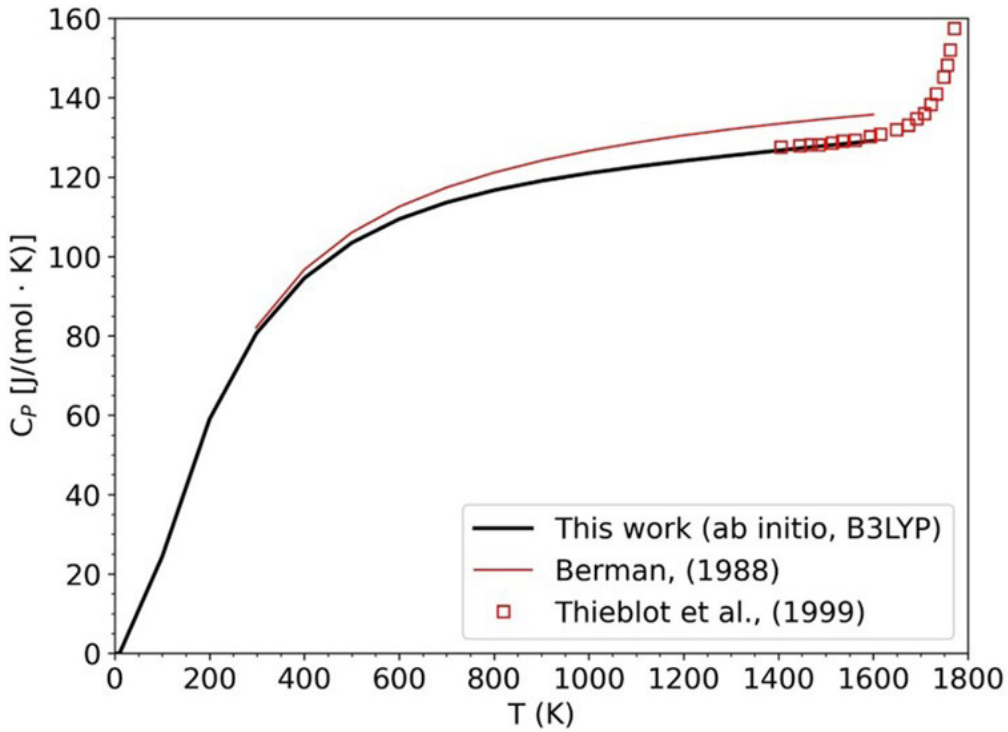

Figure 4 *Ab initio isobaric heat capacity (C_P) for PEn as compared with experimental results and thermodynamic assessment.*

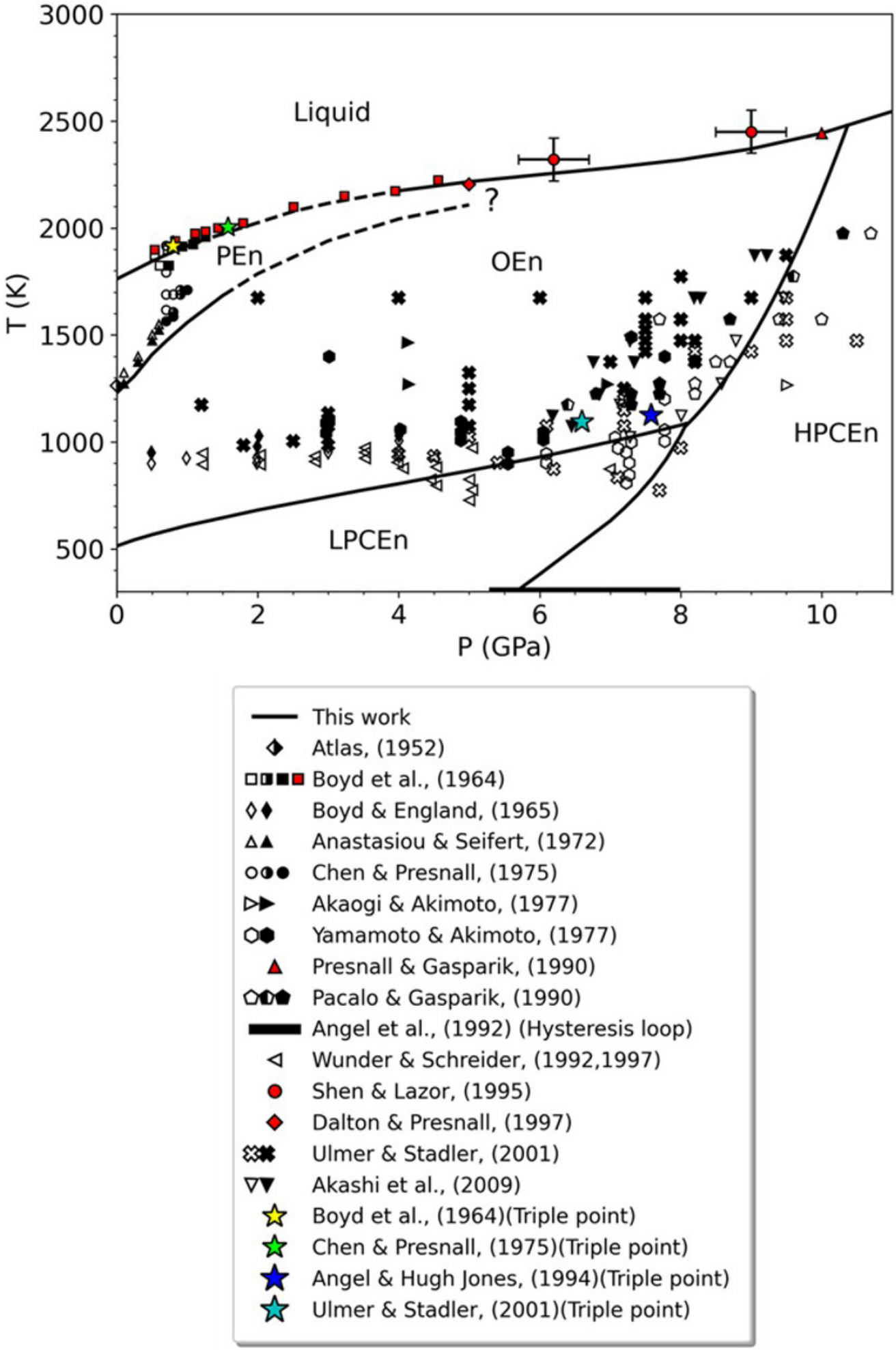

Figure 5 *Ab initio phase diagram for the $MgSiO_3$ system, as compared with literature data. White markers = PEn/LPCEn/HPCEn, black markers = OEn, red markers = liquid.*

All the pyroxene phase transitions occurring in the $MgSiO_3$ system have been investigated and calculated by employing the first-principles thermodynamic dataset obtained in this work. The following univariant equilibria have been determined: $MgSiO_3$ (low-pressure clinoenstatite) = $MgSiO_3$ (orthoenstatite), $MgSiO_3$ (orthoenstatite) = $MgSiO_3$ (protoenstatite), $MgSiO_3$ (protoenstatite) = $MgSiO_3$ (high-temperature clinoenstatite), $MgSiO_3$ (orthoenstatite) = $MgSiO_3$ (high-pressure clinoenstatite), $MgSiO_3$ (low-pressure clinoenstatite) = $MgSiO_3$ (high-pressure clinoenstatite). The investigation of these phase equilibria allowed the obtaining of novel information on the stability of pyroxenes at mantle conditions (Fig. 5).

Moreover, *ab initio* Clapeyron slopes and density contrasts calculated at high temperature and pressure conditions provide physical constraints to numerical modelling of subduction processes. The computational study shows how some of the phase equilibria involving pyroxenes are extremely sensitive to small variations in the Gibbs free energy, thus difficult to reproduce even employing modern DFT-QHA calculations. In particular, some uncertainties still remain in some portions of the $MgSiO_3$ phase diagram, such as the location of the LP-CEn - OEn phase transition boundary at ambient pressure and that of the triple point between PEn, OEn and liquid. These uncertainties seem to be related to a limitation of the DFT-QHA theory in accurately predicting

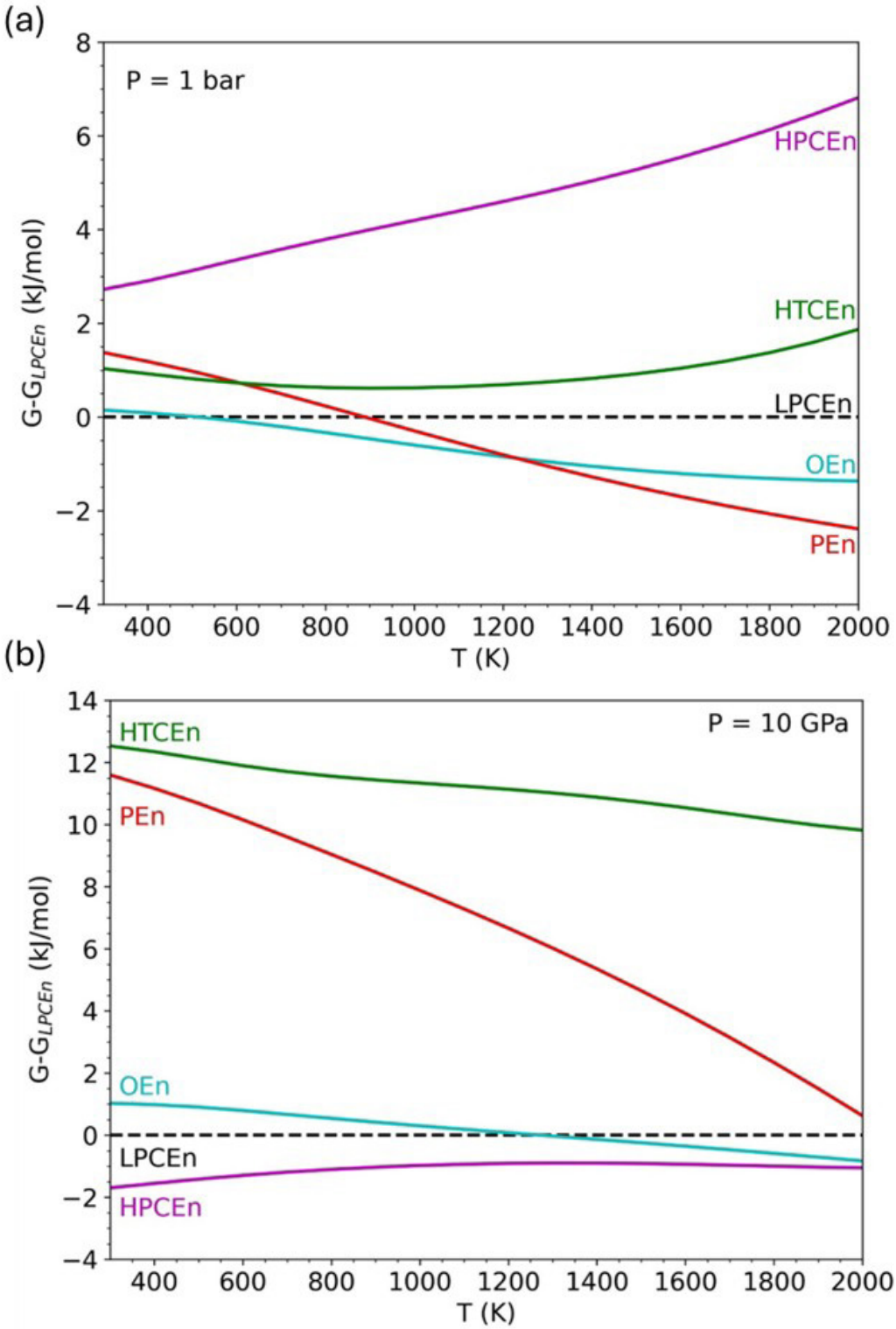

Figure 6 a) *Ab initio Gibbs free energy vs. temperature curves for $MgSiO_3$ pyroxenes at 1 bar and* ***b)*** *10 GPa. HPCEn = high-pressure clinoenstatite, HTCEn = high-temperature clinoenstatite, LPCEn = low-pressure clinoenstatite, OEn = orthoenstatite, PEn = protoenstatite. The Gibbs free energy of all polymorphs is normalised to that of the low-pressure clinoenstatite (i.e., the stable polymorph at T = 0 K and P = 0).*

the thermodynamic properties of orthoenstatite (OEn), which can be explained by the presence of relevant anharmonic effects in this phase (Zucker & Shim, 2009).

High-temperature clinoenstatite (HT-CEn) turns out to be unstable in the whole *T*(-*P*) range according to our investigation (Fig. 6). This result strongly questions the role of this mineral as a stable phase on the liquidus of the $MgSiO_3$ system at low pressures, as claimed by some Authors in the literature on the basis of unphysical thermodynamic data (*e.g.*, Shi et al., 1996; Gasparik, 2014).

The predicted melting curve of the $MgSiO_3$ system, as determined by assessing thermodynamic properties for the liquid phase with a polymeric model that is thermodynamically-consistent with ab initio data for the solid phases, is in excellent agreement with experimental results in the pressure range 0 -10 GPa (Boyd et al., 1964; Presnall & Gasparik, 1990; Dalton & Presnall, 1997). Subsolidus and melting phase relations of pyroxenes in the theoretical phase diagram of $MgSiO_3$ are thus fully consistent with each other.

Finally, predicted *P-T* stability fields of orthoenstatite and high-pressure clinoenstatite in the $MgSiO_3$ phase diagram are compatible with the observed depth range of the seismic X-discontinuity in the mantle (*i.e.*, 250-350 km depths). Nevertheless, the theoretical seismic velocity jumps and impedance contrasts calculated for OEn and HP-CEn at mantle conditions turn out to be much higher than those inferred by global seismological studies, thus disregarding the OEn to HP-CEn phase transition as the only responsible for the origin of the X-discontinuity.

REFERENCES

Agrusta, R., Van Hunen, J., Goes, S. (2014) - The effect of metastable pyroxene on the slab dynamics. Geophys. Res. Lett., 41(24), 8800-8808.

Angel, R.J., Chopelas, A., Ross, N.L. (1992) - Stability of high-density clinoenstatite at upper-mantle pressure. Nature, 358, 322-324.

Belmonte, D., La Fortezza, M., Menescardi, F. (2022) - Ab initio thermal expansion and thermoelastic properties of ringwoodite (γ-Mg_2SiO_4) at mantle transition zone conditions. Eur. J. Min., 34(2), 167-182.

Berman, R.G. (1988) - Internally-consistent thermodynamic data for minerals in the system Na_2O-K_2O-CaO-MgO-FeO-Fe_2O_3-Al_2O_3-SiO_2-TiO_2-H_2O-CO_2. J. Petrol., 29(2), 445-522.

Boyd, F.R., England, J.L., Davis, B.T. (1964) - Effects of pressure on the melting and polymorphism of enstatite, $MgSiO_3$. J. Geophys. Res., 69(10), 2101-2109.

Dalton, J.A., & Presnall, D.C. (1997) - No liquid immiscibility in the system $MgSiO_3$-SiO_2 at 5.0 GPa. Geochim. Cosmochim. Ac., 61, 2367-2373.

Frost, D.J. (2008) - The upper mantle and transition zone. Elements, 4(3), 171-176.

Gasparik, T. (2014) - Phase Diagrams for Geoscientists. An Atlas of the Earth's Interior, 2nd Edition. Springer, New York, 462 pp.

Irifune, T. & Tsuchiya, T. (2015) - Phase transitions and mineralogy of the lower mantle. In: "Treatise on Geophysics, Volume 2: Mineral Physics", 2nd edition, G. Schubert, ed. Elsevier, 33-60.

Presnall, D.C. & Gasparik, T. (1990) - Melting of Enstatite ($MgSiO_3$) From 10 to 16.5 GPa and the Forsteritc (Mg_2SiO_4)-Majoritc ($MgSiO_3$) Eutectic at 16.5 GPa: Implications for the Origin of the Mantle. J. Geophys. Res., 95(B10), 15-771.

Ringwood, A.E. (1991) - Phase transformations and their bearing on the constitution and dynamics of the mantle. Geochim. Cosmochim. Ac., 55, 2083-2110.

Shi, P., Saxena, S.K., Zheru, Z., Sundman, B. (1996) - Re-assessment of the Ca-Mg-Si-O pyroxenes. Calphad, 1(20), 93-94.

Thieblot, L., Tequi, C., Richet, P. (1999) - High-temperature heat capacity of grossular ($Ca_3Al_2Si_3O_{12}$), enstatite ($MgSiO_3$), and titanite ($CaTiSiO_5$). Am. Mineral., 84(5-6), 848-855.

Thompson, R.M. & Downs, R.T. (2003) - Model pyroxenes I: ideal pyroxene topologies. Am. Mineral., 88, 653-666.

van Mierlo, W.L., Langenhorst, F., Frost, D.J., Rubie, D. C. (2013) - Stagnation of subducting slabs in the transition zone due to slow diffusion in majoritic garnet. Nat. Geosci., 6(5), 400-403.

Woodland, A.B. (1998) - The orthorhombic to high-P monoclinic phase transition in Mg-Fe pyroxenes: Can it produce a seismic discontinuity? Geophys. Res. Lett., 25(8), 1241-1244

Zucker, R. & Shim, S.-H. (2009) - In situ Raman spectroscopy of $MgSiO_3$ enstatite up to 1550 K. Am. Mineral., 94, 1638-1646.

Geochemical Background and Baseline values of PTEs (Potentially Toxic Elements) in soils and stream sediments from decommissioned mining areas: the Hg-district of Mt. Amiata (central Italy)

Federica Meloni

Department of Earth Sciences, University of Firenze, Via G. La Pira 4, 50121, Firenze

DOI: 10.19276/plinius.2025.01.013

INTRODUCTION

Throughout history, mining operations have created a complicated challenge between local and global authorities over the use of natural resources in an economic circuit. Italy has a long history of mining, going back to pre-Roman times. The demand increased during the 1800s with industrialization, up to half of the 20th century, when Italy entered the Common European market (the beginning of globalization).

Tuscany, as well as Sardinia, and parts of northern and southern Italy host important ore deposits, and the former region has mineralized areas that have already been exploited since the Etruscan times. Only at the end of the 19th century, the supergiant mercury (Hg) district of Mt. Amiata (between Siena and Grosseto Province) and the large pyrite district of Colline Metallifere were discovered (Dini, 2003). Tuscany had its greatest development for metal ores, including cinnabar, around the 1930s, after which a gradual decline occurred.

The study area regards about 120 km^2 of the eastern portion of the Mt. Amiata Hg-district (Fig. 1a) and includes eight of the most important Hg mines of the area, including that of Abbadia San Salvatore (ASS) mine, which was classified as the third Hg mine in the world. The drastic decrease in HgS extraction occurred in the 1970s due to a decrease in market demand and the

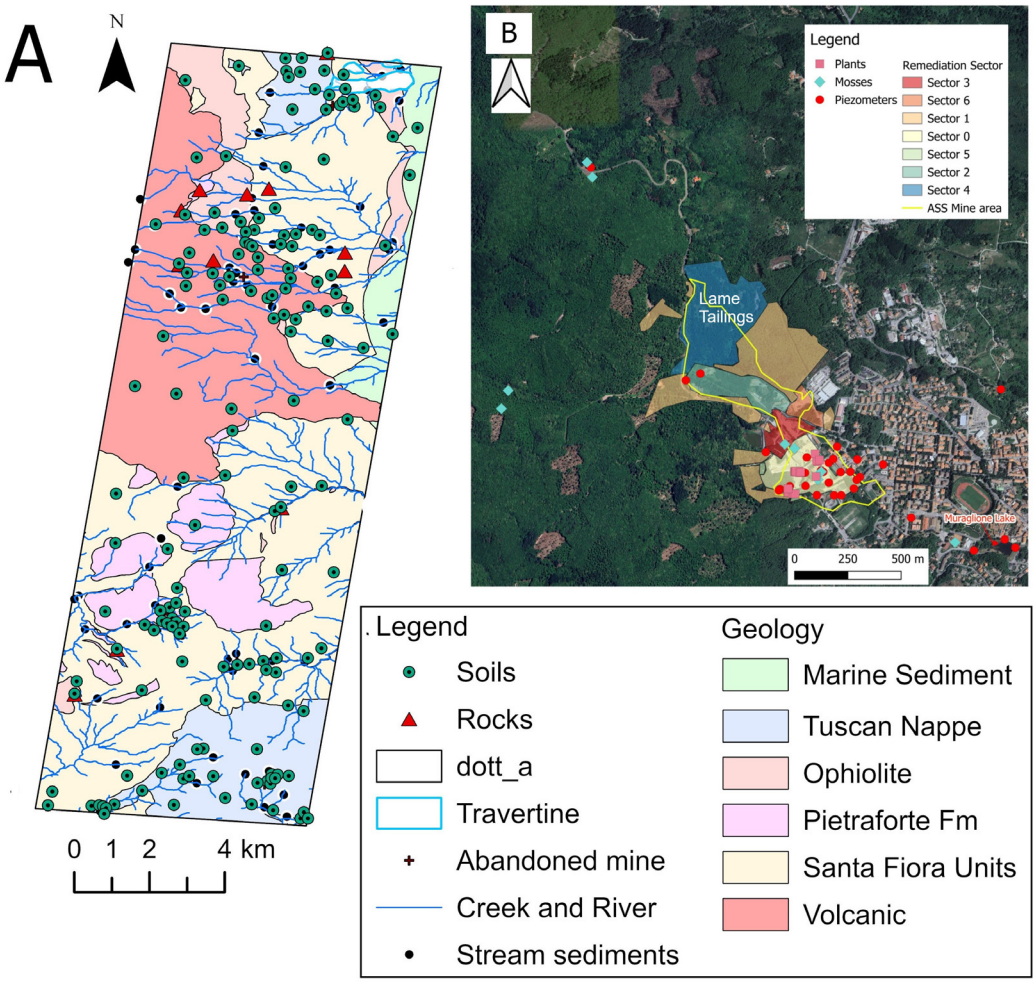

Figure 1 a) *The 120 km^2 geological map of the study area with rocks (red triangles), soils (green circles), and stream sediments (black circles) samples.* ***b)*** *The remediation area of ASS mine subdivides into different sectors according to Hg concentration, the plants samples (pink squares), mosses samples (light blue diamonds), and piezometers (red circles).*

emergence of Hg toxicity after the Minamata (1956) and the Iraq (1971) disasters. The ASS mine was the last mine that ceased its activity in the district in 1982. Mining projects have direct and indirect environmental impacts on the environmental matrices, and any decision is increasingly complex due to the large number of environmental laws that must be followed.

Thus, it becomes important to know the geochemical background value in order to establish reasonable post-mining remediation activities.

This PhD thesis investigated the mercury (Hg) contamination in the Mt. Amiata area by developing methods to assess its speciation and bioavailability in soils and sediments. Environmental matrices (sediments, streams and waters) were investigated during reclamation operations in the ASS mining area (Fig. 1b), identifying zones where further interventions are required. The study also evaluated the Le Lame tailing (Fig. 1b) as a suitable site for storing Hg-contaminated Muraglione lake sediments (Fig. 1b). Ten years of geochemical monitoring surveys were used to model Hg transport and assess mitigation strategies. Lastly, geochemical background values were established to support environmental assessment and policymaking.

MATERIALS AND METHODS

Sampling soils, stream sediments and waters

The geological map was simplified by grouping the main lithologies, *i.e.*, Volcanics, Ophiolitic Unit, Limestones, Sandstone, Mudstone and Travertine. Soil samples were collected from both top- (10-50 cm) and sub- (50-150cm) soils following a two-fold strategy: a) one sample each 2 km^2 and b) 5 to 6 samples each 1 km^2 when approaching the former Hg-mines. The sampling strategy for stream sediments (74 samples) involved the major watercourses present in the area. In addition, 11 rocks, representing the main lithologies, were also sampled. The geographical coordinates (UTM WGS84 - 32N) for all the samples were acquired with a Garmin GPS with an average error of 3 m. Every 4 months, about 29 samples, a water survey (major and minor solutes and trace elements, including Hg, As and Sb) inside and outside the ASS mine area.

Analytical method for solid matrices

The solid geological matrices were oven-dried at 30°C to minimize the release of gaseous mercury (Hg^0). All the rocks were cut to remove any layer of alteration and reduce the sample size. In all samples, XRD analysis, aqua regia digestion (3:1 ratio HCl: HNO_3) for As, Sb, Cr, Co, Cu, Ni, and V determination by ICP-AES, Hg determination by EPA 7473 Method, gravimetric method (550°C) for Organic Matter, Hg speciation by Thermal desorption (TD) technique with Lumex-Pyro 915+, leachates (rock/soil/stream-water 1:10) for As, Sb and Hg analyzed by ICP-MS were carried out.

Additionally, XRF analysis for bulk rocks and bulk streams was carried out. Moreover, Hg in eight different plants and mosses were determined by Lumex-Pyro 915+ and via atomic absorption spectrometric technique with a Hydra-C Mercury Analyzer instrument (Teledyne Instruments Leeman Labs Inc.), respectively. For more information about solid matrices analysis, see Meloni et al. (2023a, b; 2024b, c; 2025).

Analytical method for waters

At each sampling site, four aliquots were collected: *i)* 0.45 µm filtered sample in 125 mL PE bottles equipped with counter-cap for the main anions and NH_4^+; *ii)* 0.45 µm filtered and acidified (1% suprapur HCl) sample in PE 50 mL bottles for main cations; *iii)* 0.45 µm filtered and acidified (1% ultrapure HNO_3) sample in PE 50 mL bottles for trace elements (Al, Fe, Mn, Co, Cr, V, Cu, Ni, Ba, As, Se, Sb, Zn, Rb, Pb, Tl, and Sr); *iv)* 0.45 µm filtered and acidified (1% ultrapure HCl) in 50 mL dark glass bottles for the determination of Hg from piezometers. Additionally, an unfiltered and acidified with 1% ultrapure HCl or ultrapure HNO_3 (in the case that the Hg concentrations in water were > 3 µg/L) in a 50 mL dark glass for Hg for surface waters. Bicarbonates were measured by acidimetric titration, while the main anions and cations were determined by ion chromatography, respectively. Ammonium was measured by molecular spectrophotometry by the Nessler method. Total and dissolved Hg were measured by ICP-MS at the accredited Laboratory of C.S.A. of Rimini until 2021. From 2021 onward, the Hg analysis was performed in the Laboratory of the Department of Earth Science (University of Florence) by a Lumex RA-915M (Lumex Ltd., St. Petersburg, Russia) equipped with an RP-92 device. After the installation of a Lumex-Pyro 915+ in 2022, waters with Hg concentration > 3 µg/L were analyzed with this new instrument.

Statistical methods

Explorative Data Analysis (EDA), *e.g.*, graphical methods and numerical techniques, and multivariate approaches (*e.g.*, Principal Component Analysis-PCA) concerning the compositional nature of geochemical data were carried out using R and RStudio software (R Core Team, 2021). As is well known, geochemical data are compositional data (CoDa) that result in closed data, since they represent a part of a given numerical total, carrying only relative information (Aitchinson, 1986).

To solve this problem, a series of transformations (*e.g.*, centred log-ratio (clr) or isometric log-ratio (ilr)) can be

applied to move the data within the real space called the simplex (Egozcue et al., 2003). Spatial distribution maps of the analyzed PTEs were constructed with Ordinary Kriging using ArcGis-Pro 3.0 software. Before the CoDa transformation, the values of the dataset below the Limit of Quantification (LOQ) were substituted with 2/3 of LOQ according to Gozzi et al. (2020, 2021).

Determination of Geochemical Background and Baseline value

The definition of geochemical background (GBc) and geochemical baseline (GB) values may have different explanations according to the context in which they are applied. According to Cicchella et al. (2022), natural GBc levels of elements vary locally, thus, a single value cannot define them. The concept of "GB" includes both natural and human-influenced contributions and is important for environmental regulations. Italian law (Lgs.D. 152/06) sets fixed thresholds for PTEs but does not account for local geology or element speciation. Therefore, local adjustments are possible through regional authorities. Therefore, in the area of Mt. Amiata, where Hg exploitation began more than 2000 years ago, it may become difficult to distinguish the anthropogenic contribution from the natural one. For this reason, in this research, it will be used the term GB. The GB of the PTEs was defined separately, *i.e.*, top-, sub-soils and stream sediments, by considering the different lithologies present in the area, and by using the ProUCL 5.2.0 software (USEPA, 2022) according to the recommendations of SNPA (2017). The GBs in soils were defined as a range of concentrations (± 10% of analytical uncertainty) and only for the PTEs that had at least one sample with concentrations higher than Lgs.D. 152/06 for residential use. For more details, see Meloni et al. (2023b, 2025).

Hg, As and Sb in aqueous solution speciation and ModFlow modelling

The geochemical code PHREEQC version 3.5.0 (Parkhurst & Appelo, 1999) was used to estimate the aqueous solution speciation of Hg, As and Sb in both water and selected leachate samples. Aqueous phase equilibria were taken into account in the modified *minteq.v4.dat* database. Instead, for the calculation of the groundwater flow distribution and transport, the Modflow 6.4.0 software (Langevin et al., 2024) was used. For more information, see Meloni et al. (2024a). In Figure 2, a schematic workflow is reported.

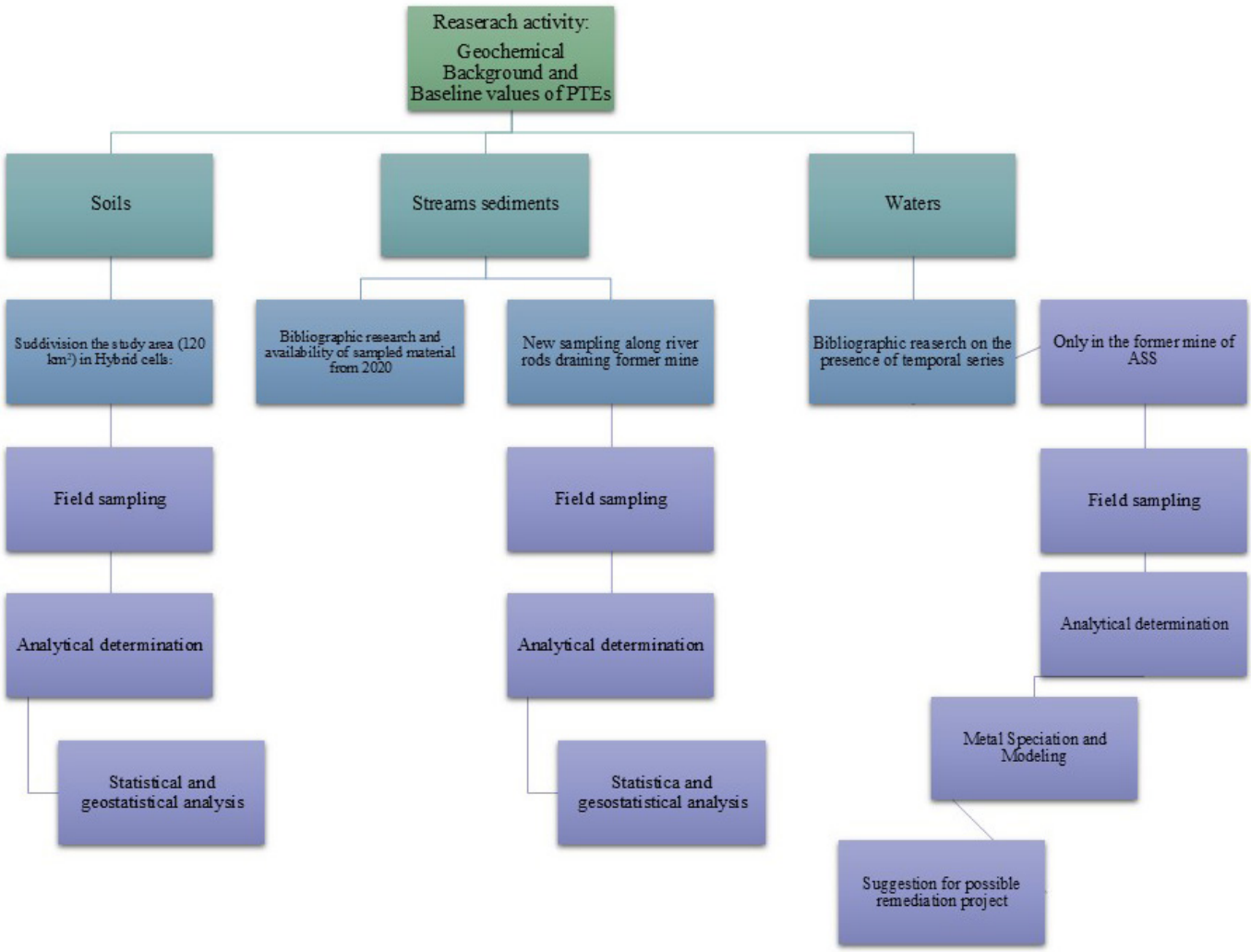

Figure 2 *A Schematic workflow of this research.*

RESULTS AND DISCUSSION

Mercury speciation by thermal desorption and laboratory experiments

Meloni et al. (2024b) have highlighted that the different geological matrices can affect the Hg-speciation in soils and stream sediments by the Thermal Desorption (TD) technique. Therefore, it is important to characterize the Hg compounds by mixing different matrices to understand the correct Hg temperature (*T*) release. According to this assumption, in contaminated soils, it becomes pivotal to know the liquid Hg behavior. In Meloni et al. (2024b), it has been highlighted that after 42 days, all liquid Hg in soils is oxidized in a more stable Hg^{2+} form. Observing the release temperatures of Hg in both silicate- and carbonate-rich soils where the experimental runs were conducted, the resulting form of Hg appears to be metacinnabar (β-HgS). Further studies, however, would be necessary to assess this hypothesis. Taking this experiment and Hg release *T* in silicate and carbonate soils into account, in all soils and river sediments where Hg concentrations were found to be > 5 mg/kg, speciation was carried out. The speciation has allowed us to verify that Hg is mostly hosted as insoluble species, i.e. α-HgS (Cinnabar) and β-HgS and no effects are expected to affect the ecosystem, these minerals being recalcitrant to chemical weathering. Thus, Hg availability is to be regarded as low or even negligible. Only a few samples inside the mine areas showed the presence of Hg_2SO_4 or $HgCl_2$.

Mercury distribution in plants, soils and mosses in the Abbadia San Salvatore mine area

From the eight different plants analysed in the former mining area of ASS, the greatest pathway for Hg accumulation appears to be the leaf system. The *Sambucus nigra* species, however, turns out to be the one that accumulates most Hg from the root system. This plant could be tested to create a pilot site for the extraction of Hg from soil (Meloni et al., 2023a).

In addition, non-indigenous biomonitoring through moss bags was carried out in the same area. This turns out to be an excellent tool for understanding the way Hg can be dispersed, transported, and accumulated. From the Hg analysis in the moss bags, the main Hg emissions were associated with the mining area of ASS and the gas vents. The wet deposition resulted to be a key factor for its accumulation on the uncovered mosses, while dry deposition resulted to be important for the covered samples, especially those located within the mining area (Meloni et al., 2024c).

Total and Leached Arsenic, Mercury and Antimony in the Mining Waste Dumping Area of Abbadia San Salvatore (Mt. Amiata, Central Italy)

Two different soil samplings were carried out in the Le Lame dump (Fig. 2). The characterization of these soils resulted to be important for the reclamation of the former ASS mine. The first sampling was conducted in 2017, and the soils analyzed were concerning the topsoil (0-20 cm), while the second sampling was carried out in 2022 and included both the top- (0.8-1.2 m) and sub-soil (1.2-3 m). In both samplings, Hg, As and Sb resulted in high concentrations (Hg up to 1910 mg/kg, As up to 616 mg/kg and Sb up to 1980 mg/kg). This study showed that the highest concentrations of Hg were found in the highest morphological part of the tailing. This turned out to be because waste materials from the Cermark-Spirek furnaces, which were found to be less efficient than the Gould furnaces, were piled up in this area. On the other hand, the Hg concentrations in the leachates were almost always < 1 µg/L (Italian legal limit), except for three samples, highlighting the fact that Hg occurs as a non-soluble or poorly soluble form. A characterization by TD is necessary to highlight which forms of Hg are present in the landfill soils. Differently, the concentrations of As and, in particular, Sb in the leachates were extremely high. Analysis in PHREEQC, however, showed that these two elements are present in the leachate phase in their less toxic form (As^{5+} and Sb^{5+}), limiting the toxicity of these two PTEs. This is also favored by the fact that in this area, no water course or shallow aquifers are present (Meloni et al., 2021).

Geochemical Surveys of Surface and Ground Waters in the Abandoned Hg-Mine of Abbadia San Salvatore (Central Italy): A Preparatory Investigation before Remediation

According to Bain et al (2001), one of the most important aspects to be considered when dealing with the operation and closure activities of a mining site is related to the presence of contaminated surface and groundwater bodies. In this research, ten years of temporal series of waters were studied inside and outside the former mine of ASS for Hg, As e Sb. Mercury in the outside waters resulted to be always < 0.2 µg/L, and As and Sb < 0.1 µg/L. Inside the mine, the Hg concentrations indeed resulted in being much higher (up to 695 µg/L). On the other hand, the content of As and Sb was lower than those reported in the Lgs.D. 152/2006 (10 and 5 µg/L, respectively), after the construction of the bypass channel (2014) inside the mine (Vaselli et al., 2015; Meloni et al., 2024a). Seasonal variations of the geochemical facies were observed, but they were not apparently associated with seasonality. The PHREEQC modelling, as well as for

Table 1 Baseline values as a range of concentrations of PTEs in stream sediments for cluster 1 and cluster 2.

PTEs	Hg	Sb	As	Cr_{tot}	V	Co pop.1	Co pop.2	Ni pop.1	Ni pop.2	Cu pop.1	Cu pop.2
Baseline value cluster 1	5.2-6.3	8.5-10.5	39.7-48.5	43.0-52.6	31.2-38.1	5.9-7.2	19.0-23.2	9.6-11.6	51.5-62.9	3.71-4.54	72.2-88.2
PTEs	**Hg**	**Sb**	**As**	**Cr_{tot}**	**V**	**Co**	**Ni**	**Cu**	**-**	**-**	**-**
Baseline value cluster 2	20.0-24.3	6.9-8.54	6.3-7.72	51.1-62.5	62.4-76.3	26.3-32.2	52.8-64.6	62.1-75.9	-	-	-

the leachates for the Le Lame Dump, showed As and Sb in the less toxic form, and Hg mostly occurring as Hg^0. The analysis of the reduced sulfur species in some waters highlighted that α-HgS and β-HgS turn out to be at equilibrium or oversaturated, and the presence of Fe-bearing oxy-hydroxides can adsorb Hg, thus representing a possible Hg sink. The groundwater flow modelling suggested that the water flow follows the local topography (W-E oriented), while the Hg transport modelling highlighted that the Hg contamination is mainly limited to the former mining area, where the piezometers mostly pump from water pockets, thus limiting the water flow. Two exceptions are represented by two piezometers from which a Hg-rich plume was evidenced, and migrating to the east (Meloni et al., 2024a).

Mercury contamination in an artificial mining lake: geochemical investigations and remediation strategies at the Lake Muraglione (Mt. Amiata, central Italy)

Between the end of 2021 and 2022, 16 sediments from the artificial Muraglione Lake, located in a public park of ASS, were sampled to characterize and test different remediation strategies: TD test, dewatering test, filter press test, and inertization strategy. It was highlighted that the lake sediments had high Hg concentration (up to 900 mg/kg), and the concentration of Hg was higher in the fine (60 μm) fraction. The sediment granulometry is dominated by sand to silty loam. The high amount of organic material (mostly consisting of small twigs and roots) was the main problem that affected all remediation tests. Better results were obtained when inertization tests were applied, although high Hg concentrations were recovered when leaching tests were performed. Therefore, computing GB values of the Le Lame is of pivotal importance to evaluate whether the Hg concentrations of the lake sediments are lower than those recorded in the soils of the dumping area where these sediments are supposed to be stored. In fact, the lake is to be emptied and the sediments removed to return this area to the population once the lake is reclaimed.

GEOCHEMICAL BACKGROUND/BASELINE VALUES IN STREAM SEDIMENTS AND SOILS

Geochemical characterization of stream sediments from the eastern Hg-district of Mt. Amiata (Siena and Grosseto, central Italy): deciphering sources and interaction processes

After an in-depth geochemical study using XRF analysis of the 74 stream sediments and the 11 rock samples, it was possible to classify them into 4 different groups: 1) volcanic group, 2) volcanic-sedimentary group, 3) sedimentary-volcanic group and 4) sedimentary group. Volcanic sediments are enriched in As (up to 311 mg/kg), and they are mainly distributed on the Mt. Amiata volcano and near the hydrothermal zone and gas vents. Mercury resulted in having a relatively homogeneous distribution with the most remarkable concentrations (up to 850 mg/L) measured in the streams intimately connected with the main former mines, i.e. Cornacchino, Solforate, and Morone mines. Antimony resulted to be enriched in the sedimentary zone and depleted in the volcanics. The higher concentrations were recorded close to or within the Morone mine (the only Sb-Hg mine in the zone), with concentrations up to 84 mg/kg. Mercury and Sb results were not correlated with each other, suggesting a different origin for the two elements and likely linked to two distinct periods of mineralization, as reported by Brogi et al. (2011). For the GB calculation, the four previous groups were considered, and they were further grouped into two clusters: *i)* volcanic + volcanic-sedimentary and *ii)* sedimentary-volcanic + sedimentary (Meloni et al., 2025). The results are summarized in Table 1.

Geochemical Background/Baseline in the eastern sector of Mt. Amiata (Siena, Central Italy) and the case study of Abbadia San Salvatore municipality

After grouping the local formations into macrozones (*e.g.*, Volcanic, Limestone and clay, Jasper, Sandstone), EDA and statistical tests (e.g. Kolmogorov-Smirnov test) to validate the normality of the distribution were performed. Since soils and rocks are CoDa, the ilr transfor-

Table 2 Baseline values as a range of concentrations of soils for the 120 km² of study area subdivided according to the lithologies.

	Volcanic top-soil	Volcanic sub-soil	Clay+ limestone top-soil	Clay+ limestone sub-soil	Clay+ sandstone top-soil	Clay+ sandstone sub-soil	Jasper top-soil	Lgs.D. 152/06
Hg	15.7-19.2	16.1-19.7	1.1-1.3	3.0-3.6	5.4-6.6	3.3-4.0	611.9-747.9	1
As	53.8-65.8	78.8-96.3	Lgs.D. 152/06	Lgs.D. 152/06	-	-	23.5-28.8	20
Sb	-	-	12.6-15.5	8.3-10.1	-	-	12.1-14.7	10
Co	-	-	22.6-27.1	24.5-29.9	-	-	43.4-53.0	20
Cr	Lgs.D. 152/06	Lgs.D. 152/06	162.5-198.6	142.9-174.7	-	-	-	150
Cu	-	-	-	-	-	-	243.3-297.3	120
V	82.4-100.8	83.6-102.2	137-167.4	149.9-183.2	168.4-205.8	192.6-235.4	-	90

mation was performed on the dataset to understand whether top- and sub-soils could have been considered as a unique population, using a non-parametric test called log-contrast homogeneity test (lc-test). This test confirmed that top- and sub-soils represent two different clusters and were studied separately afterwards. With the CoDa analysis, a robust PCA was also performed in both top- and sub-soils to highlight the presence of the outliers (*e.g.*, mineralization).

Robust-PCA confirmed the findings of EDA for both top- and sub-soils, *e.g.*, volcanic lithology is enriched in As while limestone+clay and sandstone+clay groups appear to be enriched in Co, Cr, V, Ni, and Cu. The jasper formation, on the other hand, was found to be anomalous in Hg. Once the outliers (including mineralization) were excluded, the GB value in the top- and sub-soils was defined. The results are shown in Table 2. In addition, a more specific study was carried out within the Municipality of ASS to meet the requirements of the current reclamation project of the former ASS mine. The results are described in detail by Meloni et al. (2023b). When a comparison between the data from this study (Table 3) with those obtained from a larger area is made, Hg and As are characterized by slightly different values with respect to those reported in Table 2. This is because the sampling mesh in the Municipality of ASS is more detailed and therefore, the more the available data the higher the quality of the GB values (*e.g.*, Varrica et al., 2024).

CONCLUSIONS

This PhD study has investigated the environmental matrices (water, plants, soils, and streams) from the former Hg-mining areas of Mt. Amiata, evidencing the main criticalities which are mostly, as expected, related to the contamination of Hg, though Sb and As were also found to be occurring at relatively high contents in soils and streams.

Water contamination appears to be limited to the former mining area of ASS. This is an important result in terms of remediation since, if confirmed, economically speaking, two options can be evaluated:

	Volcanic top-soil	Volcanic sub-soil	SFR top-soil	SFR sub-soil	Lgs.D. 152/06
Hg	17.3-21.2	18.5-22.7	6.8-8.3	6.5-7.9	1
As	69.6-85.1	78.2-95.6	Lgs.D. 152/06	Lgs.D. 152/06	10
Co	-	-	22.3-27.2	23.3-28.5	20
Ni	-	-	Lgs.D. 152/06	Lgs.D. 152/06	120
Cr	Lgs.D. 152/06	Lgs.D. 152/06	160.2-195.8	157.2-192.2	120
V	85.7-104.2	85.9-104.9	149.6-182.8	158.3-193.5	90

Table 3 Baseline values as a range of concentrations of soils for the Municipally of ASS subdivided according to the lithologies: SFR represents the Santa Fiora Units corresponding to the clay+limestone of Table 2.

- no water treatment;

- partial abatement of Hg from the most contaminated water by tested techniques such as MC-TOMAC, Capterall®, or ferrate compounds, which have been successfully used during laboratory tests (Borruguero et al., 2018; Baroni, 2022; Lazzaroni, 2022).

The definition of the GBc and GB values plays a key role when dealing with environmental matrices since they can be used, if accepted as in the case of those computed for ASS, to help the local authorities when new houses, garages or commercial areas are to be built. It was also evidenced by the notable role played by the stream sediments since they could be used as tools for capturing contaminated areas.

The Hg speciation applied to soils and sediments has allowed us to verify that Hg is mostly hosted as insoluble species, *i.e.*, α-HgS and β-HgS, and no effects are expected to affect the ecosystem, as these minerals are resistant to chemical weathering. Thus, Hg availability is to be regarded as low or even negligible.

REFERENCES

Aitchison, J. (1986) - The Statistical Analysis of Compositional Data. In: Monographs on Statistics and Applied Probability. Chapman & Hall Ltd., London.

Bain, J.G., Mayer, K.U., Blowes, D.W., Frind, E.O., Molson, J.W.H., Kahnt, R., Jenk, U. (2001) - Modelling the closure-related geochemical evolution of groundwater at a former uranium mine. J. Contam. Hydrol., 52, 109-135.

Baroni, T. (2022) - Ferrate removal of metal contaminants in the environmental remediation field: synchrotron radiation studies applied to the Hg contaminated waters from Abbadia San Salvatore, Amiata Area. (PhD Thesis). University of Florence, p. 236

Borreguero, A.M., Leura, A., Rodriguez, J.F., Vaselli, O., Nisi, B., Higueras, P.L., Carmona, M. (2018) - Modelling the mercury removal from polluted waters by using TOMAC microcapsules considering the metal speciation. Chem. Engin. J., 341, 308-316.

Brogi A., Fabbrini L., Liotta D. (2011) - Sb-Hg ore deposit distribution Controlled by brittle structures: the case of the Selvena Mining district (Monte Amiata, Tuscany, Italy). Ore Geol. Rev., 41, 35-48.

Cicchella, D., Ambrosino, M., Gramazio, A., Coraggio, F., Musto, M.A., Caputi, A., Avagliano, D., Albanese, S. (2022) - Using multivariate compositional data analysis (CoDA) and clustering to establish geochemical backgrounds in stream sediments of an onshore oil deposits area. The Agri River basin (Italy) case study. J. Expl. Geochem., 238, 107012.

Dini, A. (2003) - Ore deposits, industrial minerals, and geothermal resources. Per. Min., 72, 41–52.

Egozcue, J.J., Pawlowsky-Glahn, V., Mateu-Figueras, G., Barcelo-Vidal, C. (2003) - Isometric log-ratio transformations for compositional data analysis. Math. Geol., 35, 270–300.

Gozzi, C., Sauro Graziano, R., Buccianti, A. (2020) - Part-whole relations: new insights about the dynamics of complex geochemical riverine systems. Minerals, 10 (6), 501.

Gozzi, C., Dakos, V., Buccianti, A., Vaselli, O. (2021) - Are geochemical regime shifts identifiable in river waters? Exploring the compositional dynamics of the Tiber River (Italy). Sci. Total Environ., 785, 147268.

Langevin, C.D., Hughes, J.D., Provost, A.M., Russcher, M.J., Niswonger, R.G., Panday, S., Merrick, D., Morway, E.D., Reno, M.J., Bonelli, W.P., Boyce, S.E., Banta, E.R. (2024) - MODFLOW 6 Modular Hydrologic Model version 6.4.4: U.S. Geological Survey Software Release, 7 February 2024.

Lazzaroni, M. (2022) - Investigating Hg dispersion in the environment: the experience from the abandoned mining area of Abbadia San Salvatore (Tuscany, central Italy) between research and remediation activities of natural and anthropic matrices (PhD Thesis). University of Florence, p. 213.

Meloni, F., Montegrossi, G., Lazzaroni, M., Rappuoli, D., Nisi, B., Vaselli, O. (2021) - Total and leached arsenic, mercury and antimony in the mining waste dumping area of Abbadia San Salvatore (Mt. Amiata, Central Italy). Appl. Sci. 11, 7893.

Meloni, F., Farieri, A., Higueras, P.L., Esbrì, M.J., Nisi, B., Cabassi, J., Rappuoli, D., Vaselli, O. (2023a) - Mercury distribution in plants and soils from the former mining area of Abbadia San Salvatore (Tuscany, Central Italy). Environ. Geochem. Health, 45, 8523–8538.

Meloni, F., Nisi, B., Gozzi, C., Rimondi, V., Cabassi, J., Montegrossi, G., Vaselli, O. (2023b) - Background and geochemical baseline values of chalcophile and siderophile elements in soils around the former mining area of Abbadia San Salvatore (Mt. Amiata, southern Tuscany, Italy). J. Geochem. Explor., 255, 107324.

Meloni, F., Montegrossi, G., Cabassi, J., Bianchi, F., Nisi, B., Rappuoli, D., Vaselli, O. (2024a) - Geochemical Surveys of Ground and Surface Waters in the Abandoned Hg-Mine of Abbadia San Salvatore (Central Italy): A Preparatory Investigation before Remediation. Water, 6, 1210.

Meloni, F., Higueras, P.L., Cabassi, J., Nisi, B., Rappuoli, D., Vaselli, O. (2024b) - Thermal desorption technique to speciate mercury in carbonate, silicate, and organic-rich soils. Chemosphere, 365, 143349.

Meloni, F., Calabrese, S., Vaselli, O., Capecchiacci, F., Brusca, L., Bellomo, S., Daskalopoulou, K., Venturi, S., Nisi, B., Rappuoli, D., Cabassi, J. (2024c) - Active moss biomonitoring of mercury in the mine-polluted area of Abbadia San Salvatore (Mt. Amiata, Central Italy). Toxic, 13(1), 2.

Meloni, F., Dinelli, E., Cabassi, J., Nisi, B., Montegrossi, G., Rappuoli, D., Vaselli, O. (2025) - Provenance and distribution of potentially toxic elements (PTEs) in stream sediments from the eastern Hg-district of Mt. Amiata (central Italy). Environ. Geochem. Health, 47(4), 123.

Parkhurst, D.L. & Appelo, C.A.J. (1999) - User's guide to PHREEQC (Version 2)-A computer program for speciation, batch-reaction, one-dimensional transport, and inverse geochemical calculations: U.S. Geological Survey. Water-Resour. Investig., 312, 99– 4259.

R Core Team (2021) - R: A language and environment for statistical computing. R Foundation for Statistical Computing. Vienna, Austria, Available online: https://www.Rproject.org/ available on-line 15/01/2022.

SNPA (2017) - Linea guida per la determinazione dei valori di fondo per i suoli e per le acque sotterranee (ISBN 978-88-448-0880-8). (In Italian).

USEPA (2022) - ProUCL: Statistical Software for Environmental Applications for Data Sets with and without nondetect Observations. Version 5.2. https://www.epa.gov/landresearch/prouclsoftware.

Varrica, D., Medico, F.L., Zuccolini, M.V., Miola, M., Alaimo, M.G. (2024) - Geochemical baseline values determination and spatial distribution of trace elements in topsoils: An application in Sicily region (Italy). Sci. Tot. Environ., 955, 176951.

Vaselli, O., Nisi, B., Rappuoli, D., Bianchi, F., Cabassi, J., Venturi, S., Tassi, F., Raco, B. (2015) - Geochemical characterization of the ground waters from the former Hg-mining area of Abbadia San Salvatore (Mt. Amiata, central Italy): criticalities and perspectives for the reclamation process. It. J. Geosci., 134, 304-322.

Secondary mineralization processes in pyroclastic rocks of Surtsey, Iceland (ICDP-Sustain Project)

Giovanna Montesano

Department of Earth, Environment and Resource Sciences, University of Napoli - Federico II, Via Cintia 26, 80126, Napoli
DOI: 10.19276/plinius.2025.01.014

INTRODUCTION AND SCIENTIFIC OBJECTIVES

Surtsey is the youngest and the southernmost island of the Vestmannaeyjar archipelago, which marks the seaward extension of Iceland's East Volcanic Zone. First emerging from the ocean surface in 1963, Surtsey was subsequently built up through the interplay of phreatomagmatic and effusive volcanism until 1967. Since it emerged, Surtsey immediately aroused interest among scientists to investigate the formation of a new volcanic island from the very beginning, but only a limited number of them have been permitted to access the island, and, while the eruption was still going on, it has been declared a natural reserve. Consequently, the island is a pristine geological research laboratory. The scientific value of Surtsey was further acknowledged after it became evident that the island would persist, thus providing an exceptional opportunity to study the development of an oceanic island from its origin on the sea floor to the modification of the newly erected structure by hydrothermal processes and wave abrasion. Finally, in 2008, Surtsey was designated a UNESCO World Heritage site. Investigations about the structure and stratigraphy of the volcano, nature of its hydrothermal system, notably thermal conditions, and nature of basaltic tephra hydrothermal alteration and authigenic mineral growth were first carried out in 1979 by a 181-m-deep cored drill hole. During the summer of 2017, three new cores were drilled on the island during the Surtsey Underwater volcanic System for Thermophiles, Alteration processes and Innovative Concretes (SUSTAIN) project, sponsored by the International Continental Drilling Program (ICDP) and funded by several Universities and Research Institutions. The SUSTAIN drilling program was born to sample tephra deposits through a neo volcanic island from the surface to the seafloor, with all the precautions taken to avoid contamination from the surroundings, designating samples as collaborative materials for interdisciplinary research, to trace geological and biological history of Surtsey deposits, the consolidation of freshly erupted tephra and the lithification of the lapilli tuff that currently make up the island. This study aims to investigate hydrothermal water-rock interaction, glass alteration, authigenic and secondary phases formation, taking into account subaerial and submarine samples retrieved during the SUSTAIN program through the volcanic structure of Surtur, the eastern cone of Surtsey island. The samples analyzed in this study come from the three new cores drilled in 2017 in the frame of the SUSTAIN project. All samples were investigated through optical microscopy (OM), X-Ray Powder Diffraction (XRPD) and Field Emission Scanning Electron Microscopy coupled with an Energy Dispersive Spectroscopy (FESEM-EDS), performed at the Department of Earth, Environmental and Resource Sciences (DiSTAR) of the University of Napoli Federico II (Italy). Clay minerals identification was performed at the Institute of Geological Sciences, Polish Academy of Science (Instytut Nauk Geologicznych, Polskiej Akademii Nauk – ING PAN, Kraków, Poland) on representative samples through a clay-fraction separation. Single-crystal analysis was performed on representative samples at the ID15B beamline of the European Synchrotron Radiation Facility (ESRF) in Grenoble (France). The integration of different analytical techniques to describe the suite of samples is pivotal to evaluate the mineralogy and crystal chemistry of authigenic and secondary phases, providing valuable information about their stratigraphic distribution within the subaerial and submarine volcanic structure of Surtur, as well as their paragenetic relationships with glass. Furthermore, this Ph.D. research project represents the first detailed comprehensive petrographic, mineralogical and chemical characterization of primary minerals, authigenic (*i.e.*, palagonite and clay minerals) and secondary (*i.e.*, calcium and aluminium silicates) in Surtsey samples from all the recent 2017 drill cores.

SURTSEY

Named from the name of the giant Surtr, from Norse mythology, and ey (*i.e.*, island), Surtsey Island has become one of the best-monitored volcanic sites on Earth.

Its eruption is the typical example of shallow-to-emergent subaqueous explosive volcanism, demonstrating how magma-water interaction affects fragmentation dynamics to create typical steam-rich tephra jets and fine-grained deposits. Its growth has been thoroughly chronicled by a nearly continuous record of observations, contributing to make it the type example of pyroclastic activity, now recognized as Surtseyan volcanism (Schipper et al., 2015). The Surtsey volcano (Fig. 1) is located in the southernmost sector of the Vestmannaeyjar archipelago, which forms the offshore extension of the Iceland SE rift zone. The island grew from a seafloor depth of ~ 130 m during explosive and effusive basaltic eruptions in 1963–1967 and represents the subaerial portion of the whole Surtsey volcano, which forms a northeast to southwest oriented, mainly submarine ridge approximately 5.8 km long (Jakobsson & Moore, 1986). The main topographical features of Surtsey island are two crescent-shaped cones of tephra and palagonite tuff (Fig. 1), covering an area of 0.72 km^2, named Surtungur (or also Surtur I or Austurbunki) and Surtur (or also Surtur II or Vesturbunki), along with a lava field that caps the southern half of the island. The eastern cone (Surtur) rises to an elevation of 155 m and displays several small lava craters and fissures, whereas the western cone (Surtungur), with a height of 141 m, exhibits slump scars on its western side due to marine abrasion. The constant modification of Surtsey shape is attributed to the challenging weather conditions prevailing in the sea south of Iceland, particularly during the winter season.

Surtsey hydrothermal system, thermal field and palagonitization of Surtsey deposits

Long-term monitoring and mapping have been conducted on the hydrothermal system of Surtsey volcano to gain insight into the rate at which tephra transformed into palagonite tuff, reinforcing volcanic structures and thus enhancing slope stability and fortification against erosion. The first signs of hydrothermal activity, consisting of a zone of anomalous heat exchange, were observed on the island close to the newest lava craters erupted during January 1967 as visible steam rising from the tephra pile (Friedman & Williams, 1970). Since that time, detailed studies have been conducted on the origin and nature of the hydrothermal system in the volcano, as well as the process of tephra alteration, with a thermal survey performed on average every three years (Jakobsson et al., 2000). Evidence from a 181 m-deep drill hole (named SE-01) conducted at Surtsey in 1979 (Fig. 1c) indicates that the heat in the hydrothermal system was most likely generated by the basaltic intrusion that fed the lava flows from 1964 to 1967, which occurred both above and below the sea level at Surtur and Surtungur (Stefánsson et al., 1985). The first temperature measurements were conducted by Jakobsson S.P. in September 1969. He used a traditional mercury thermometer placed at about 5 cm depth in the hottest area of the Surtur vent, where steam was escaping and recorded surficial temperature ranging from 48 to 84°C (Jakobsson, 1978). Between 1969 and 1972, surface temperatures of 40-50°C were observed in the central part of the thermal area. However, in areas with more intense steam emanations, particularly in and around lava craters, temperatures as high as 100°C were measured. This represents the highest temperature recorded on the surface of tephra (Jakobsson, 1978). The monitoring of the surface manifestations of geothermal activity served to understand the changes of the Surtsey thermal field. Overall, the data from these investigations indicate a gradual but noticeable cooling of the eruptive deposits over time (Perez, 2019).

One year after the discovery of the active hydrothermal system, the first signs of palagonitization of basaltic glass were recorded in surficial tephra at the SE of Surtur. Since then, in accordance with the thermal monitoring program established in the same year, the development of palagonite tuff has been monitored and mapped approximately every three years (Perez, 2019). During each geological survey, samples of tephra and tuff have been collected, and a detailed map of the surface of Surtsey was generated to track the growth of the thermal field and palagonite tuff (Jakobsson et al., 2000). Thus, the palagonitization process and evolution were observed in its natural environment for the first time (Jakobsson, 1978).

RESULTS

To obtain a consistent characterization of samples as a function of their depths, the six stratigraphic and hydrothermal zones of Surtur crater (McPhie et al., 2020) were followed. The samples are moderately to strongly vesicular hypo-crystalline lapilli tuffs with inequigranular grain size distributions, except the crystalline basalt (RS-33) collected from the bottom of the HOLE D drill core. In most samples, the larger clastic components, angular to slightly rounded ash- to lapilli-sized pyroclasts, and the fine ash matrix (containing loose-crystals of plagioclase both euhedral and as tiny fragments) appear extensively altered. Pyroclasts show vesicles of variable size and shape, commonly filled with authigenic minerals.

Sideromelane and primary minerals

Translucent sideromelane, pale yellowish-gray at plane-polarized light (PPL) and completely isotropic at cross-polarized light (CPL), occurs in all the hydrothermal zone deposits but not in all samples, and frequently embeds phenocrysts and microphenocrysts of plagi-

oclase and olivine (Fig. 2a-d). Although sideromelane is defined as fresh glass (Peacock & Fuller, 1928), authigenic phases (*e.g.*, clay minerals) can be present at a sub-micrometer scale, so the identification of sideromelane is based here solely on optical petrographic criteria and through FESEM-EDS analysis, not considering the potential occurrence of authigenic phases. SEM-SE images of sideromelane show a typical homogeneous, texturally uniform and smooth surface with abundant rounded, spherical to elliptical vesicles, commonly coalescent (Fig. 2a,b). By contrast, domains of altered glass display a wide range of features reflecting progressive degrees of alteration within the original vesicular morphology, shown in thin section (Fig. 2a–f).

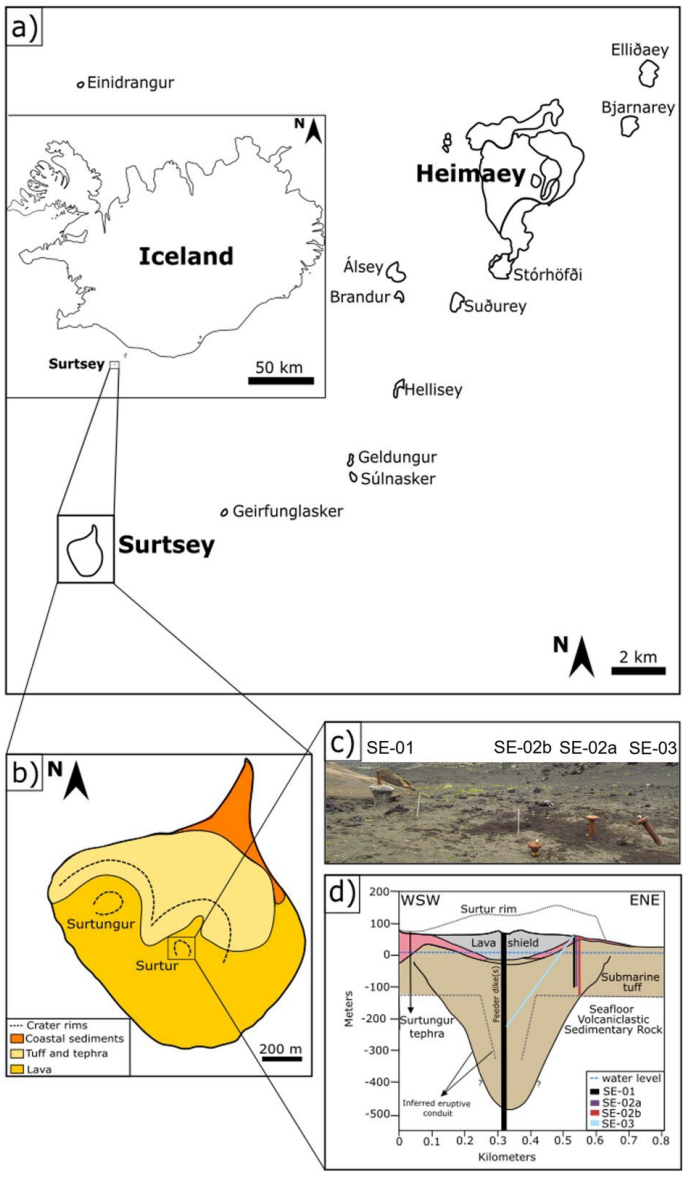

Figure 1 *Surtsey volcano, Iceland.* ***a)*** *Sketch map of the Vestmannaeyjar archipelago with Surtsey at its southwestern tip.* ***b)*** *simplified sketch map of Surtsey showing the main geo-lithological units and crater rims (dashed lines) of Surtur and Surtungur (modified after Prause et al., 2022).* ***c)*** *field photograph showing wellheads of the three 2017 and 1979 boreholes.* ***d)*** *interpretative cross-section of Surtur showing the original crater rim (at the age of its formation; dotted line), 1979 (SE-01) and 2017 (SE-02a, SE-02 b and SE-03) cored drill holes (Jackson, 2017), pyroclastic deposits, lava shield in the central crater, and seafloor volcaniclastic sedimentary rock. The subseafloor inferred eruptive conduit: black solid line (Moore, 1985) and minimum expression (gray dashed line; Jackson et al., 2017).*

Euhedral lath-shaped plagioclase and anhedral to subhedral olivine crystals (Fig. 2a–d) are ubiquitous primary phases. They occur both as phenocrysts and microphenocrysts within the altered fragments of volcanic glass and as loose crystals in the altered fine-ash matrix.

Authigenic alteration

Three principal palagonitic textures (Fig. 2a–c), as previously described by Montesano et al. (2023), are present: *i)* optically isotropic palagonitic rinds (*e.g.*, Fig. 2a), *ii)* fibrous palagonitic type (*e.g.*, Fig. 2b), and *iii)* granular, opaque palagonitic-type (e.g., Fig. 2c).

Olivine crystals can show clay-like alteration rims of variable thickness, either regular, following the original crystal boundaries, or irregular and denticulate, directed towards the interiors of the crystals. Moreover, almost complete pseudomorphic olivine replacement by clay-like secondary minerals (*e.g.*, Fig. 2d) is common. In SEM-SE images, altered basaltic glass appears in globular micro-morphological arrangements (Fig. 2e-f) or as tiny plates with curled edges or feathered "flakes" of randomly intergrown smectite-like clay minerals (Fig. 2g-h). The globules, often agglutinated, are about 3 μm in diameter. Morphological features of the altered glass are highly heterogeneous and may locally display a ragged or sponge-like surface (Fig. 2i-j), or a distinct fibrous appearance, typically with fan or leaf-shaped textures in altered olivine crystals (Fig. 2j).

Chemical composition of authigenic alteration

Regarding the chemical composition, all the investigated sideromelane analyses show a limited compositional spectrum, falling in the basalt field (SiO_2 = 45.16-48.12 wt.%). As regards alteration elements (*i.e.*, palagonitized glass and altered olivine), they show an overall lower Si, Al, Na and Ca content than sideromelane, and higher Fe and Mg. Ti content of several palagonite analyses and of most altered olivine. is lower than the Ti content of sideromelane, approaching zero.

Secondary minerals

Secondary phases occur as zeolite, calcium–aluminium–silicate hydrate, carbonate, and sulphate minerals. They are present as fillings in pyroclast vesicles and pores of the binding fine-ash matrix, as well as surface coatings in large pores of the altered ash matrix (Fig. 3): *i)* euhedral analcime typically forms coatings on the inner walls of vesicles of coarse ash or lapilli or along void spaces in the binding fine-ash matrix (Fig. 3a) and appear through SEM as euhedral and well defined crystals (3f-i); *ii)* phillipsite in vesicles appear as colourless intergrowths and radiating prismatic crystals (Fig. 3b). Phillipsite through

SEM occurs as well-defined crystals filling vesicles and displaying a rosette morphology, or replaced by analcime (3e,g-i); *iii)* tobermorite (3a-b, f, h-i) in vesicles appears as acicular microcrystals arranged in discrete fan-shapes. Tightly bound needles of Al-tobermorite also formed (Fig. 3b). Groups of randomly oriented, sprays of Al-tobermorite appear to postdate analcime and phillipsite (Fig. 3i); *iv)* highly birefringent, microcrystalline calcite forms scattered coatings along the inner walls of matrix pores (Fig. 3c); *v)* colourless, prismatic to fibrous radiating gypsum crystals (3d, j) are also present; *vi)* very few crystals of chabazite occurs as vesicle filling in association with analcime; *vii)* well-defined acicular crystals or massively bound needles associated with analcime and calcite also occur.

Chemical composition of secondary minerals

Chemical composition of secondary minerals, obtained through Energy Dispersive X-ray Spectroscopy (EDS) are the following: *i)* chabazite appears only in the shallowest zones with a Ca- and K-rich composition; *ii)* phillipsite is Ca, Na and K-rich; *iii)* analcime show an overall sodic character; *iv)* Al-tobermorite and clinotobermorite show distinct compositions, both containing Ca as prevalent cation along with K and Na, but the former also contain Al; *v)* xonotlite consists mainly of Ca and Al; *vi)* a Si-rich phase, containing almost completely Si with lesser amount of Al, Fe, Ca and alkali.

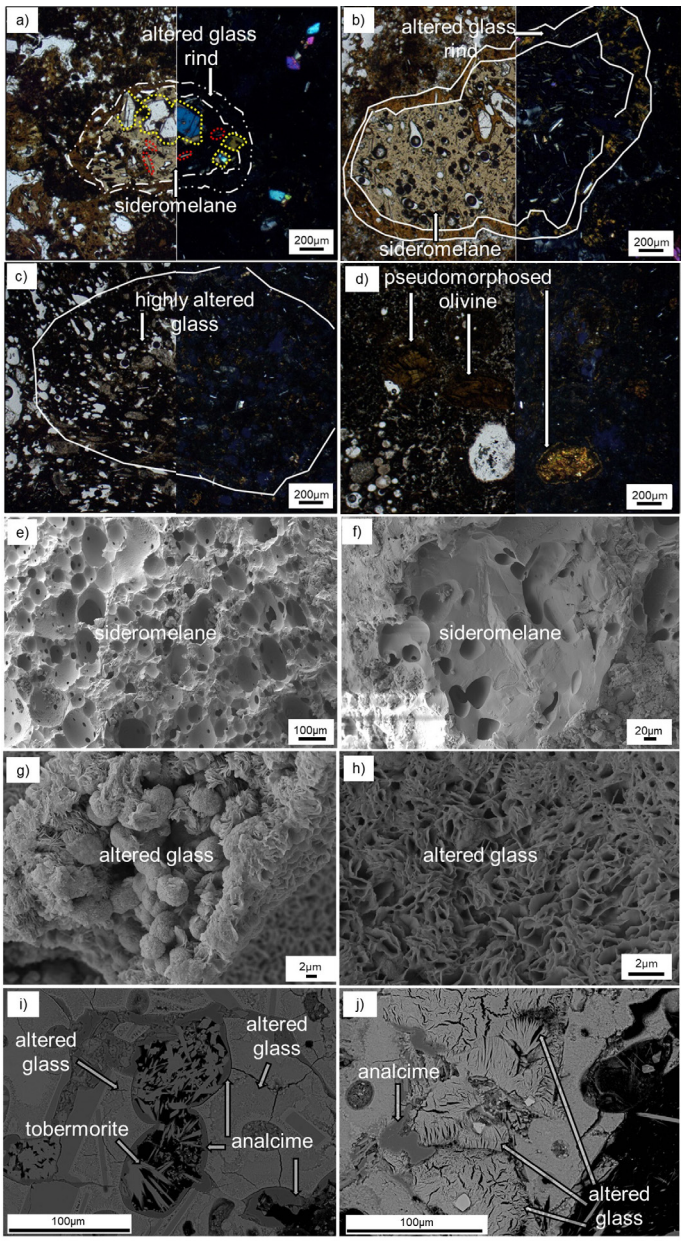

Figure 2 *Petrographic images [PPL plane-polarized light (left) and CPL cross-polarized light (right)] showing the three different types of glass fabrics:* ***a)*** *apparent sideromelane,* ***b)*** *altered glass rinds,* ***c)*** *highly altered glass and* ***d)*** *complete pseudomorphic olivine replacement by clay-like phases; SEM-SE images showing* ***e-f)*** *sideromelane;* ***g-j)*** *SEM-BSE images showing altered glass, along with tobermorite and analcime.*

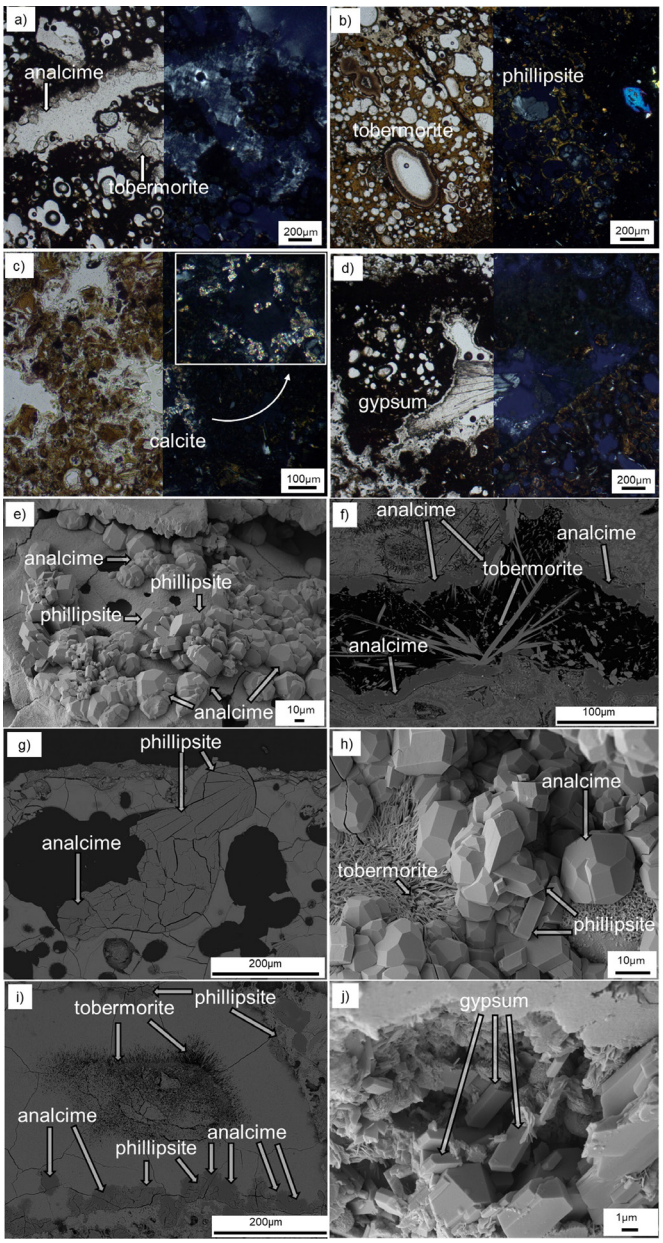

Figure 3 *Petrographic and SEM images showing secondary mineral growth.* ***a-d)*** *Petrographic images [PPL plane-polarized light (left) and CPL cross-polarized light (right)] showing* ***a)*** *analcime and tobermorite,* ***b)*** *phillipsite and tobermorite,* ***c)*** *calcite and* ***d)*** *gypsum.* ***e,h)*** *SEM-SE and* ***f,g,i)*** *SEM-BSE images showing phillipsite, analcime and tobermorite;* ***j)*** *SEM-SE image showing gypsum crystals.*

Structural characterization

Structural characterization performed through single-crystal X-ray diffraction analysis proved necessary to corroborate the presence of the very fine-grained secondary minerals. The selection of the crystals focused on pores and vesicle fillings. According to the cell parameters obtained through this analysis, the crystal selected as phillipsite to be analyzed is actually merlinoite, a rare zeolite morphologically identical to phillipsite (Gatta et al., 2015). Moreover, this analysis confirmed the presence of xonotlite, very similar to tobermorite, and also revealed the presence of a phase whose identification is still controversial.

X-Ray Powder Diffraction - mineralogical characterization of bulk samples and one-dimensional modelling of separated clay fractions

From each of the investigated rock samples, powders have been prepared for qualitative and quantitative mineralogical investigations, reported in Figure 4 and Table 1. X-ray powder diffraction analysis performed on the bulk samples detected the presence of peaks in the low-angle part of the patterns ascribable to the presence of clay minerals. For this reason, representative samples were subjected to a clay fraction separation following the procedure of Jackson (1969). The separated fractions $\phi < 0.2$ µm were acquired both at air-dried conditions (AD) and after ethylene glycol treatment (EG). The presence swelling smectites is dominant in the mineralogical assemblages of the analyzed samples, along with chlorite and serpentine (Fig. 5a). To further confirm the presence of the abovementioned phases in the separated fraction $\phi < 0.2$ µm, the acquired patterns were analyzed also through the software Sybilla (Fig. 5b), a software which help to discriminate between the various clay species (Chevron™, Zeelmaekers et al., 2007). According to the modelling through Sybilla, almost all the calculated patterns fit well with trioctahedral smectite, trioctahedral chlorite and serpentine.

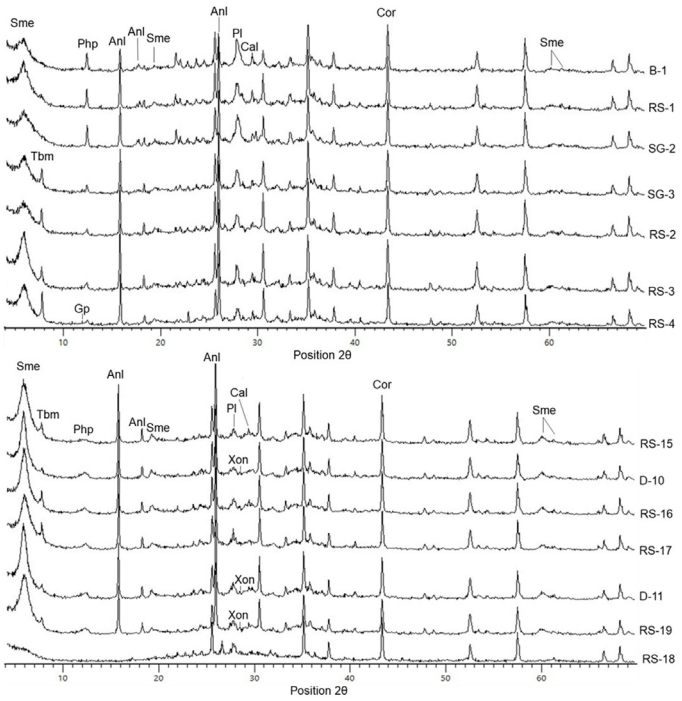

Figure 4 *Representative XRPD patterns of untreated powders of Surtsey samples.*

DISCUSSION AND CONCLUSIONS

The progressive hydrothermal alteration within the Surtsey subaerial and submarine system is recorded by two main processes: alteration of fresh basaltic glass (sideromelane) and primary minerals (mainly olivine and plagioclase), and precipitation of secondary phases as pyroclasts pores and vesicles fillings or in void spaces in the matrix. and precipitation of secondary phases as pyroclasts pores and vesicles fillings, or in void spaces in the matrix.

The presence of clinopyroxene can be explained by embracing the "pyroxene paradox" hypothesis, considering clinopyroxene as present only in the

Sample	Depth (m)	Pl	Ol	Cpx	Anl	Cal	Php	Gp	Tbm	AC
RS-1	22.6	11	3	3	12	2	10	0	2	57
RS-3	43.7	11	3	4	17	2	2	1	4	56
RS-5	65.3	6	2	5	17	2	6	0	4	58
RS-6	78.2	6	1	4	17	2	6	1	5	58
RS-8	92.6	4	1	7	21	2	4	1	5	55
RS-9	101.5	5	1	7	24	2	1	1	5	54
RS-10	110.9	6	1	7	22	2	1	1	5	55
RS-12	128	4	1	8	26	2	1	1	4	53
RS-14	148.7	12	2	4	12	2	8	0	3	57
RS-17	176.1	6	2	5	17	2	6	0	4	58

Table 1 *Representative quantitative XRPD analysis.*

Abbreviations: AC: amorphous content and disordered clay minerals; pl: plagioclase; cpx; clinopyroxene; ol: olivine; php: phillipsite; anl: analcime; tbm: Al-tobermorite; cal: calcite; gp: gypsum.

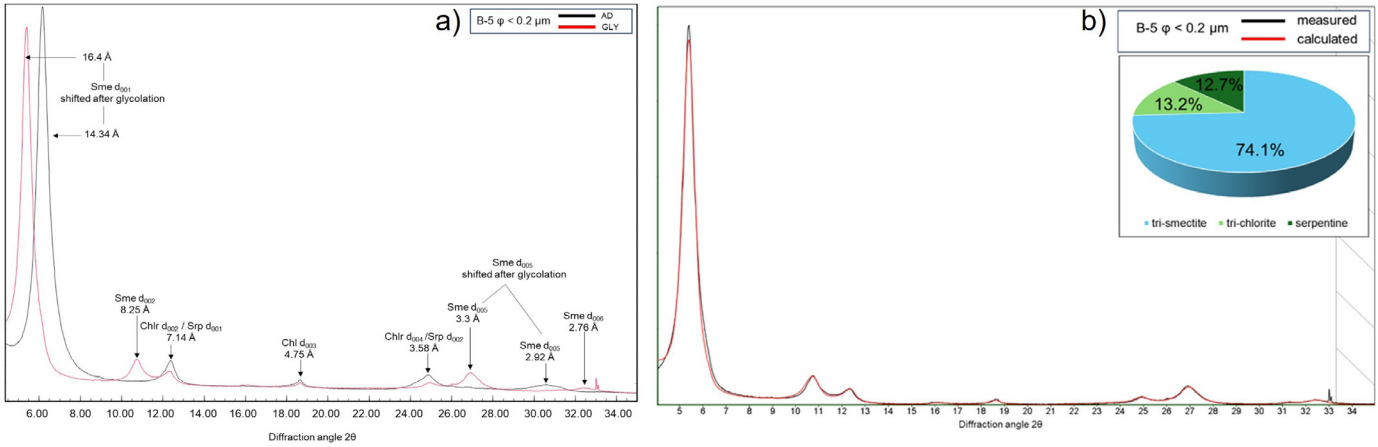

Figure 5 a) *Representative XRPD pattern of the oriented clay aggregate (ϕ < 0.2 μm) of sample B-5 acquired at air-dried conditions (AD, black line) and after ethylene-glycol solvation (EG, red line).* ***b)*** *One-dimensional modelling of EG pattern of the oriented clay aggregate (ϕ < 0.2 μm) of sample B-5. Striped areas have been excluded from modelling because they contained residual non-clay minerals. Pie chart shows the percentages of the phases used for the modelling.*

groundmass or considering that hydration reactions can lead to the transformation of pyroxene to smectite (Velbel et al., 2008). Sideromelane undergoes hydration and extensive alteration; nonetheless, significant variations in the mineralogical assemblages can be recognized in both subaerial and submarine Surtsey deposits. Different generalized temperature domains can be recognized in the Surtsey deposits basing on temperature measurements: *i)* a low temperature domain, in which temperature is lower than 90-100°C (0-65 m and 130-300 m b.s.), *ii)* a high-temperature domain, in which temperature is higher than 100-125°C (65-165 m b.s.), and *iii)* a thermal bulge where temperature reaches 140°C (80-145 m b.s.). Sideromelane in pyroclasts is still preserved in the low-temperature domain deposits, while it is almost completely altered in the high-temperature domain deposits. However, some sideromelane is still preserved where the temperature is higher. The results of this research suggest that the microenvironment (*i.e.*, fine-scale conditions related to direct glass-fluid interactions) may be just as influential as macroenvironment (*i.e.*, physical parameters of the system, such as temperature) in controlling the development of alteration products and each sample shows its own alteration history, with specific fluid–glass–crystal interactions, such that the fluid compositions in vesicles (or pores) change over time to form phases and to precipitate crystals with different and evolving compositions. Figure 6 shows a schematic representation of this process: the first element to undergo alteration is sideromelane, from which chemical elements are mobilized. The mobilization of some chemical elements entails, on one side, the *in situ* alteration (*i.e.*, authigenic alteration or palagonitization) of sideromelane, on the other, the precipitation of secondary phases. The maturation of palagonite entails the formation of clay phases. The comparison of patterns of the separated fractions ϕ < 0.2 μm acquired at air-dried conditions and after ethylene-glycol treatment and through the modelling by using Sybilla software (Chevron™, Zeelmaekers et al., 2007) displayed the presence of tri-octahedral smectite, tri-octahedral chlorite and serpentine.

As regards secondary phases, zeolites appear to be early alteration products in the crystallization sequence. Crystallization of phillipsite and analcime is mirrored as they correlate negatively with each other, and at higher temperatures, he more favourable crystallization of analcime strongly influences the presence of phillipsite. This is in accordance with the stability field proposed by Apps (1983), according to which phillipsite is stable at lower temperatures than analcime. However, they can form contemporaneously depending on the composition of the solution. Also, chabazite has been identified in the shallowest zones of lower temperature, in accordance with the zonation proposed by Apps (1983) for hydrothermally altered basalts from Iceland. Zeolites form before acicular tobermorite and xonotlite.

According to single-crystal diffraction experiments, the possible concomitant occurrence of merlinoite along with phillipsite can explain the extremely variable composition of Surtsey phillipsite. Structural characterization also confirmed the presence of xonotlite. The identification of the hydrated Si-rich crystals is still controversial.

The systematic petrographic, mineralogical and chemical analyses of sideromelane altered glass and secondary minerals of the 50-year-old pyroclastic deposits at Surtsey volcano recorded compositional variations that

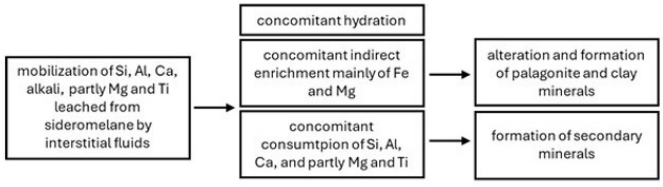

Figure 6 *Schematic explanation of authigenic and secondary phase formation in Surtsey deposits.*

provide new insights into processes that produce mineral growth in young oceanic basalts. The description of the finely resolved, spatial frameworks of mineralization in the young, active and well-monitored hydrothermal system of Surtsey volcano offers new insights into the structural organization of the alteration process and secondary mineral growth in oceanic basalt. The alteration path along the analysed subaerial and submarine sequences was identified through the integrated results, trying to develop a minerogenetic model to explain their genesis. This model would provide a reference framework for assessing the mineralogical evolution not only in other Surtseyan-type volcanoes but also in both modern and ancient different basaltic environments.

REFERENCES

Apps, J.A. (1983) - Hydrothermal evolution of repository groundwaters in basalt. In NRC Nuclear Waste Geochemistry '83, U.S. Nuclear Regulatory Commission Report NUREG/CP-0052, 14-51.

Friedman, J.D. & Williams, R.S. (1970) - Changing Patterns of Thermal Emission from Surtsey, Iceland between 1966 and 1969. U.S. Geol. Survey 700-D, 116-124.

Gatta, G.D., Rotiroti, N., Bersani, D., Bellatreccia, F., Della Ventura, G., Rizzato, S. (2015) - A multi-methodological study of the (K,Ca)-variety of the zeolite merlinoite. Mineral. Mag., 79, 1755-1767.

Jackson, M.L. (1969) - Soil chemical analysis. Advanced course. 2nd ed. published by the author. University of Wisconsin. Madison. USA.

Jackson, M.D. (2017) - Petrographic and material observations of basaltic lapilli tuff, 1979 and 2017 Surtsey drill cores, Iceland. Surtsey Res., 14, 47–62.

Jakobsson, S.P. (1978) - Environmental factors controlling the palagonitization of the Surtsey tephra, Iceland. Bull. Geol. Soc. Denmark, 27, 91–105.

Jakobsson, S.P. & Moore, J.G. (1986) - Hydrothermal minerals and alteration rates at Surtsey volcano, Iceland. Geol. Soc. Am. Bull., 97, 648–659.

Jakobsson, S.P., Guðmundsson, G., Moore, J.G. (2000) - Geological monitoring of Surtsey, Iceland, 1967-1998. Surtsey Res., 11, 99-108.

McPhie, J., White J.D.L., Gorny, C., Jackson, M.D., Guðmundsson, M. T., Couper, S. (2020) - Lithofacies from the 1963- 1967 Surtsey eruption in SUSTAIN drill cores SE-2a, SE-2b and SE-03. Surtsey Res., 14, 19-32.

Montesano, G., Rispoli, C., Petrosino, P., Jackson, M. D., Weisenberger, T.B., Guðmundsson, M.T., Cappelletti, P. (2023) - Authigenic mineralization in Surtsey basaltic tuff deposits at 50 years after eruption. Sci. Rep., 13.

Moore, J.G. (1985) - Structure and eruptive mechanism at Surtsey Volcano, Iceland. Geol. Mag., 122, 649–661.

Peacock, M.A. & Fuller, R.E. (1928) - Chlorophaeite, sideromelane, and palagonite from the Columbia River Plateau. Am. Mineral., 13, 360–382.

Perez, V. (2019) - Fifty Year Evolution of Thermal Manifestations at Surtsey Volcano 1968 - 2018, master's thesis, Faculty of Earth Science, University of Iceland, 92.

Prause, S., Weisenberger, T.B., Kleine, B.I., Monien, P., Rispoli, C., Stéfansson, A. (2022) - Alteration of basaltic glass within the Surtsey hydrothermal system, Iceland - Implication to oceanic crust seawater interaction. J. Volcanol. Geoth. Res., 429, 107581.

Schipper, C.I., Jakobsson, S.P., White, D.L., Palin, J.M., Marcinowski, T.B. (2015) - The Surtsey Magma Series. Sci. Rep., 5, 11498.

Stefánsson, V., Axelsson, G., Sigurdsson, O., Gudmundsson G., Steingrimsson, B. (1985) - Thermal condition of Surtsey. J. Geodyn., 4, 91–106.

Velbel, M.A. & Barker, W.W. (2008) - Pyroxene weathering to smectite: conventional and Cryo-field Emission Scanning Electron Microscopy, Koua Bocca ultramafic complex, Ivory Coast. Clay Miner., 56, 112-127.

Zeelmaekers, E., McCarty, D., Mystkowski, K. (2007) - 'SYBILLA user manual', Chevron proprietary software, Texas, USA.

Reconstructing Phoenician pottery production in Sardinia: a multi-analytical characterization of samples from the site of Pani Loriga (8-7th century BC) and Monte Sirai (6-5th century BC)

Giulia Morabito

Department of Earth Sciences "A. Desio", University of Milano, Via Luigi Mangiagalli 34, 20133, Milano
DOI: 10.19276/plinius.2025.01.015

INTRODUCTION

Pottery represents one of the earliest materials created by humans as an expression of the cultural background (Rice, 2015). As one of the most complex and ubiquitous archaeomaterials, ceramics offer invaluable insights into past societies. Their analysis is essential for understanding the diverse cultures and functions they served, as well as the variety of materials and manufacturing technologies employed (Maritan, 2004; Hunt, 2017). However, the complexity of pottery's chemical and mineralogical composition requires a multi-analytical approach to fully understand its history. This approach combines physical and chemical analyses to determine raw material sources, explore technological aspects of pottery production, and define firing conditions, while also investigating post-burial processes (Cultrone et al., 2001; Barone et al., 2002; Belfiore et al., 2010; Hunt, 2017).

The present PhD thesis aimed to perform a multi-analytical archaeometric study on 53 pottery samples from two archaeological sites in Sardinia: Pani Loriga (7th-8th century BCE) and Monte Sirai (5th-6th century BCE), both from the Phoenician period. These sites are located in the South-West of the Sardinian region (Italy). Studying the history and the culture of these sites helps to reconstruct the extent of cultural interactions between the indigenous Nuragic people and the incoming Phoenician settlers, who played a crucial role in the exploitation of resources from the Sulcis inland area, establishing their control over the territory (Botto, 2016).

The main goal of this research was to explore the chemical, microstructural and mineralogical complexities of archaeological ceramics, providing specific guidelines for developing research strategies and formulating anthropological questions. The focus was to gather exhaustive information about the raw materials, provenance, and manufacturing techniques of the ceramics, with particular attention to firing temperatures and atmospheric conditions. This approach allowed a comprehensive characterization of the production processes involved.

METHODS

The samples were examined with petrographical, mineralogical, chemical and archaeomagnetic approaches, and all the data gathered were crucial for understanding and reconstructing the cultural context of the Phoenician-Punic population. This study is particularly significant because the pottery from the Pani Loriga site had never been analysed using an archaeometric approach. The characterization protocol began analysing the mineralogical and microstructural composition of Monte Sirai samples, defining the best analytic procedure later applied to a wide set of samples from Pani Loriga.

RESULTS

Macroscopic observations of the shards were initially performed to assess their features, including form, colour, texture, surface treatment, and visible inclusions. These observations were essential for ensuring a comprehensive understanding of the samples' morphology and other macroscopic characteristics. Based on these analyses, five fabric groups were identified. Two of these groups, encompassing most of the samples, are characterized by coarse inclusions, suggesting minimal processing or purification of raw materials during the ceramic body preparation (Fig. 1). In contrast, the other three groups display purified clay, with minimal inclusions (Fig. 2). Optical petrography, combined with X-ray diffraction analysis, provided insights into the mineralogical associations, firing temperatures, and rock inclusions.

X-ray diffraction analyses further identified three distinct mineralogical groups based on their assemblages (Fig. 3). In the most populated groups, the presence of minerals such as quartz, plagioclases, feldspars, and hydro-silicates, compatible with igneous rocks from pyroclastic and epiclastic deposits (including dacites and rhyolites), suggests the local production of these samples. Conversely, a high calcite content, along with microfossils observed in thin sections, indicates that some samples were likely imported. The third group is charac-

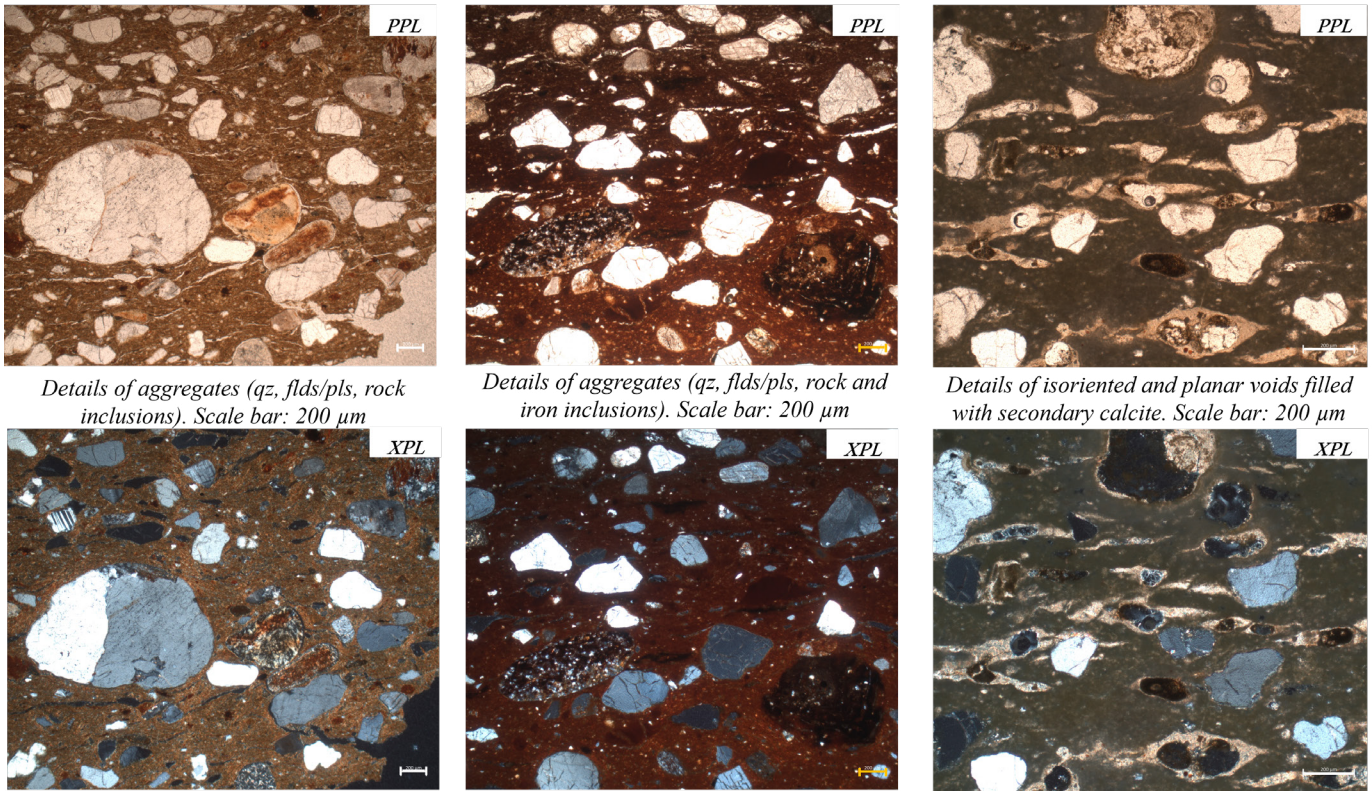

Figure 1 *Details of inclusions, matrix and voids of samples with a coarse matrix.*

terized by a pronounced presence of diopside and gehlenite. The identification of minerals such as hydro-silicates, (primary) calcite, gehlenite, and diopside reflects different firing conditions and allows the estimation of firing temperature ranges. Such temperature ranges are further supported by archaeomagnetic analyses, which provided additional insights into the thermal history of the pottery, offering additional data for their characterisation and confirming the firing process reconstructions based on XRD data (and the mineral stability fields).

After the first characterization of the ceramic samples, Scanning Electron Microscopy analysis was employed to perform micromorphological analyses in order to describe the textural and morphometric features of non-plastic inclusions, and SEM-EDS was used to perform microchemical analysis and maps, which allow describing the chemical variation within the ceramic body. To examine in depth the bulk chemical composition of the samples, elemental analyses were performed using a portable XRF instrument. All the ceramic bodies turned

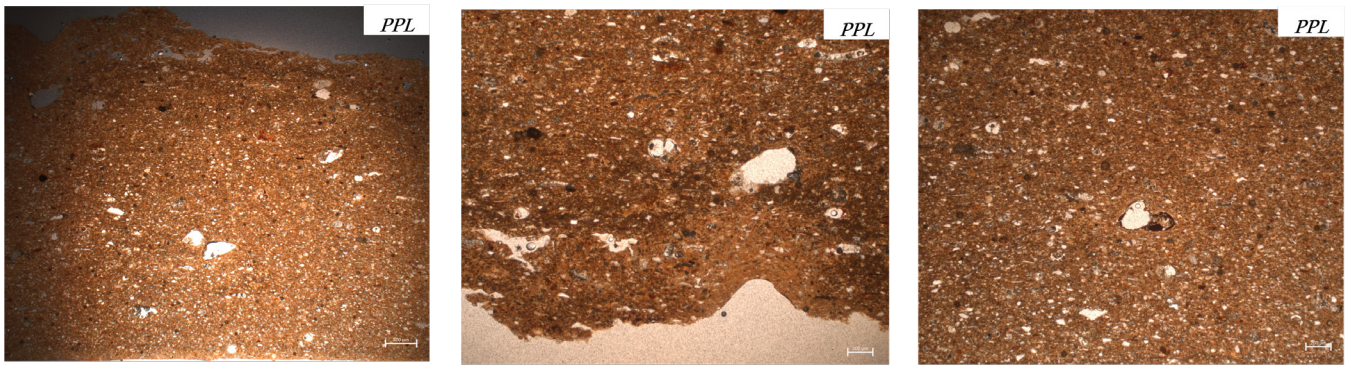

Details of matrix, vesicles pores and silt siliceous inclusions (2.5x and 5x). Scale bar: 500 µm in the first left image and 200 µm in the others

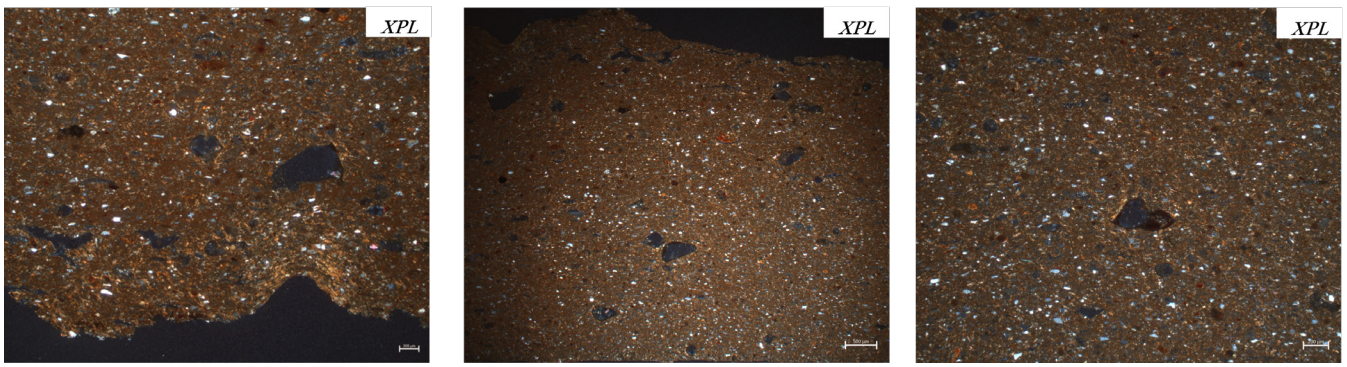

Figure 2 *Details of matrix and voids of the sample with a purified matrix.*

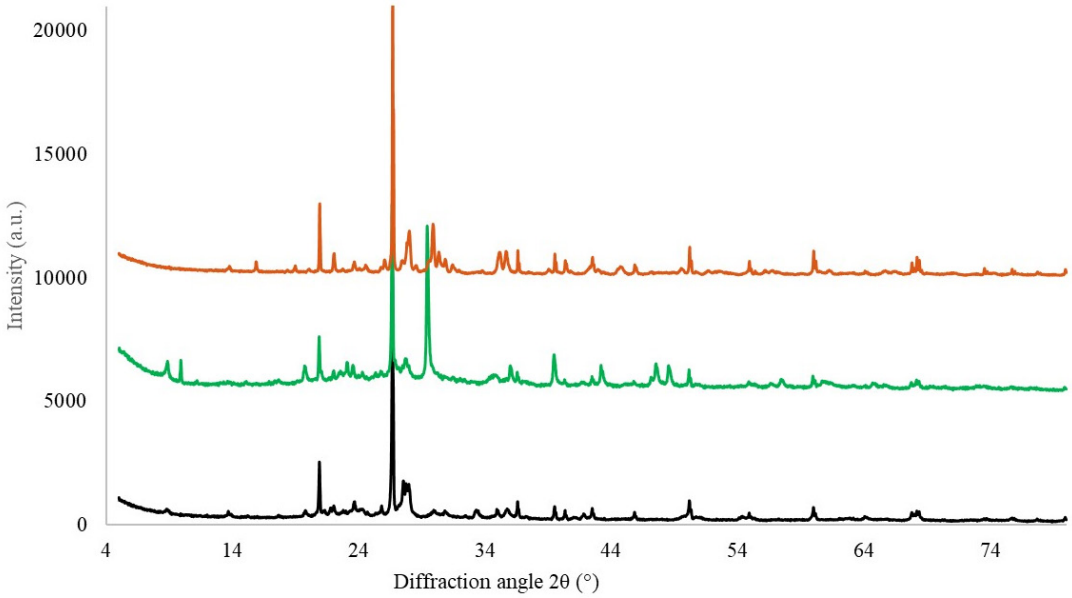

Figure 3 XRD patterns of three different samples representative of each of the three different mineralogical associations.

out to be composed mainly of Si, Al, K, Ca, Fe and Ti, a typical elemental composition expected in ceramic materials. This approach also provided experimental evidence for distinguishing locally produced ceramics from potential imports, as the chemical data plotted in the diagrams clustered into two distinct groups: one characterized by silica as the primary component, and the other diverging due to a higher calcium content (Fig. 4).

DISCUSSION

Petrographic analysis revealed significant variations among the different groups, offering insights into production techniques, raw material sources, and firing conditions. The first observations focused on the sherds' matrix composition, leading to a division into two main categories: silicate and carbonate matrices. In potteries with a silicate matrix, there is a high presence of quartz, feldspars/plagioclases, and notably dacites and rhyolites, demonstrating the local provenance, as proved by the geological setting (Assorgia et al., 1992; Barca et al., 2009). Conversely, samples with a carbonate matrix exhibit very low inclusions, primarily consisting of microfossils, suggesting a significant use of limestone or marl in the raw material. The different sources of raw material and the different manufacturing techniques of these sherds suggest they come from places where different production techniques were used.

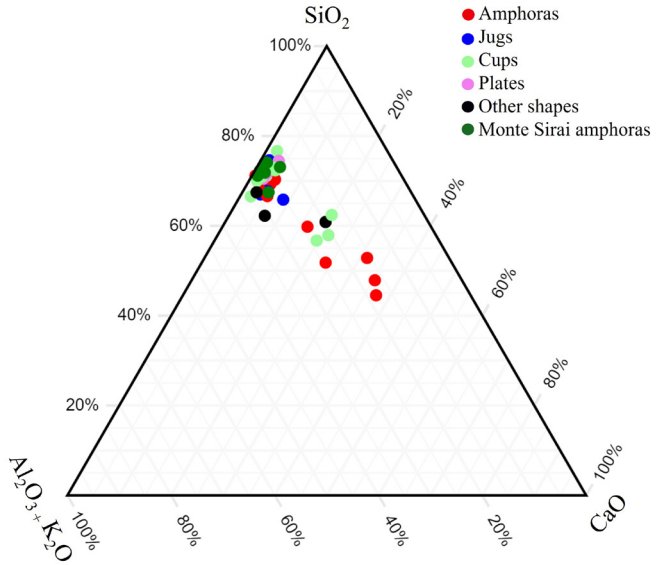

Figure 4 XRF ternary diagram showing the relationship between SiO_2, Al_2O_3+K_2O, and CaO weight fraction (%).

The void arrangement also differs between these identified fabrics. Planar and iso-oriented voids are indicative of pottery manufactured using a pottery wheel. On the other hand, the absence of iso-oriented voids suggests that this sample was likely produced without a pottery wheel, which prevented the formation of planar and iso-oriented voids. The matrix optical properties, mainly governed by the hydrosilicate behaviour, can reveal the temperature range at which the pottery was fired. If the matrix is optically active and shows birefringence, it indicates that the pottery was fired at temperatures below 800-850°C, a range at which the clay matrix generally loses its birefringence. In contrast, when samples display an optically inactive matrix, it suggests that the firing temperature was above 800-850°C (Gosselain, 1992; Ferrara et al., 2016; Amicone et al., 2021; Quinn, 2022). For carbonate samples, the firing temperature was determined by examining the structure of microfossils, which are not completely destroyed by the firing process, and well-formed traces of the shells are clearly visible. The microfossil degradation *status* can thus support the hypothesis of a firing temperature not above 900°C. Another group contains samples which exhibit a fully vitrified matrix, where optical activity has disappeared. This particular matrix appearance suggests that these samples were likely fired at a temperature around 1000-1200°C (Gosselain, 1992; Ferrara et al., 2016; Amicone et al., 2021; Quinn, 2022). The XRD mineralogical analyses also suggest different firing conditions between the samples, which range from low-temperature (maximum

temperature T_{max} < 850-900°C), as shown by the co-presence of hydro-silicates (group one) and carbonates (group two), to high-temperature firing conditions (T_{max} > 1000°C), with newly-formed phases such as Ca-(Mg,Fe)-pyroxenes and gehlenite (group three). Archaeomagnetic analysis allowed refining the firing temperature estimation, adding precision to the XRD interpretation. The hysteresis cycle of the three samples investigated, each representing a different mineralogical group, was measured at increasing firing steps, up to 700°C, and changes in magnetic behaviour were analysed to determine thermal alteration thresholds. The sample belonging to the silicate low-firing group begins to change its magnetic behaviour after heating to 500°C, suggesting an original firing temperature lower than the maximum one estimated by X-ray diffraction. In contrast, the behaviour of the carbonate-rich sample displayed a slight alteration of its hysteresis curves above 300°C, but this change was not pronounced enough to conclusively determine the original firing temperature (Rasmussen et al., 2012; Matau et al., 2013; Vaknin et al., 2023). A different pattern was observed for the over-fired sample, where the hysteresis curves remained unchanged throughout the heating process, indicating that the material had already been subjected to higher temperatures.

Pottery samples with slips were then analysed by SEM-EDS, which provided interesting results. Micro-chemical analyses revealed that the slip is more iron-rich if compared to the body of the samples analysed. Despite this slight variability, no other significant differences were found in the chemical compositions between the body and the slip. Additionally, from a morphological point of view, no visible differences between the clay grains of the slip and the body are detectable. This variation in iron content could be related to the addition of hematite in the slip.

Chemical analyses performed using portable XRF provided further confirmation of the sample composition observed with other analytical techniques. Most of the samples are characterised by the predominance of SiO_2, Al_2O_3 and K_2O, which is a common feature in ceramic as these elements are correlated to the abundance of detrital quartz grains and other silicate minerals or rock fragments. In addition, SiO_2 is also present in the clay minerals composing the finer groundmass. However, a relevant compositional differentiation is observable in the distinct group, which is characterised by a high calcium content, which suggests, again, the use of different clay sources. The consistency in the composition, even from a chemical perspective, suggests a standardized production technique and common raw material sources among most of the pottery samples. Conversely, the outliers may represent different sources, indicating the existence of trade and pottery exchanges.

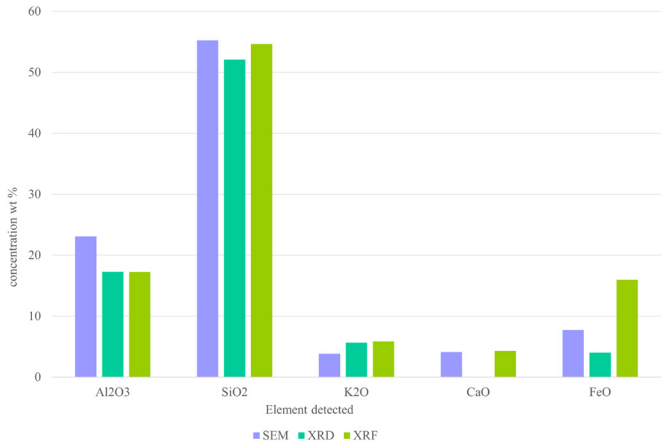

Figure 5 Graphic representation of the chemical content of one silicatic sample, as obtained by SEM-EDS, XRD and XRF. Ca-bearing phases were not here detected by XRD.

XRF data also acquire additional strength when directly compared to the results obtained by SEM and XRD analyses, as they offer compelling insights into the reliability and consistency of the methods employed and underscore their complementary nature. The convergence across different methodologies is significant, as it suggests that despite the inherent differences in how each technique operates—SEM and XRF providing direct chemical data, while XRD Rietveld analysis the mineralogical phases—they can offer a reliable characterisation of the material composition (Fig. 5). Moreover, the possibility of comparing chemical and mineralogical analyses opens new possibilities for estimating also the raw material composition.

CONCLUSIONS

In this research project, we addressed several challenges in archaeometry with the aim of expanding our understanding of the Phoenician-Punic archaeological world of Sardinia. A multi-analytical approach was employed to disclose hidden details about these ceramic shards. As a first step, the combination of XRD and optical microscopic analysis was essential for understanding the mineralogical content and structural features of these samples, thereby defining their main characteristics. By combining microtextural features and mineralogical assemblages, the samples were divided into three groups based on their phase content, which was influenced both by the raw materials and the firing environment. Some phases, such as hydro-silicates and carbonates, indicated lower heating (below 800°C), while the presence of pyroxenes and gehlenite suggested higher firing temperatures (over 950°C). Additionally, techniques such as SEM and XRF provide further information about point and bulk chemical composition of the samples. While macroscopic observations did not allow a robust distinction of the samples, the instrumental analysis indicated the presence of two distinct production groups. The first group, characterized by the occurrence of dacites and rhyolites, suggested the use of local raw materials from the Sulci

region. The second group, with a carbonate-rich composition, pointed to different sources. The manufacturing techniques further distinguished the two groups: one group had an abundance of coarse temper, indicating a rougher production process, while the other showed a higher degree of purification, suggesting a more refined and controlled manufacturing technique. The presence of planar and oriented voids in the coarse-matrix group suggested the use of a pottery wheel, whereas the more purified samples, which lacked such orientation, likely indicated handcrafting methods. Chemical analysis, particularly p-XRF, corroborated the data obtained by other methodologies, reinforcing the division of the samples into two main compositional groups.

The analyses on the shards suggest that the Phoenician-Punic population of Sardinia predominantly produced their utilitarian ceramics locally, using basic production processes with minimal purification and under less controlled firing conditions. However, some samples, particularly those rich in carbonates and microfossils, indicate trade and commerce with other Mediterranean regions. These higher-quality, highly purified ceramics likely represent luxury goods exchanged with other colonies, as evidenced by the different raw materials.

REFERENCES

Amicone, S., Forte, V., Solard, B., Berthold, C., Memmesheimer, A., Mirković-Marić, N. (2021) - Playing with fire: Exploring ceramic pyrotechnology in the Late Neolithic Balkans through an archaeometric and experimental approach. J. Archaeol. Sci. Rep., 37, 102878.

Assorgia, A., Brotz, P., Callegari, E., Fadda, A., Lonis, R., Ottelli, L., Ruffini, R., Abrate, T. (1992) - Geological map of the Cenozoic volcanic district of Sulcis (south-western Sardinia). Scale 1: 50.000. S. El. Ca., Firenze: Geological Society of Italy.

Barca, S., Serri, R., Rizzo, R., Farci, A., Calzia, P., Pertusati, P. C. (2009) - Notes on the Geological Map of Italy - Sheet 565 Capoterra, Cagliari. Geological Society of Italy.

Barone, G., Ioppolo, S., Majolino, D., Migliardo P., Tigano, G. (2002) - A multidisciplinary investigation on archaeological excavation in Messina (Sicily). Part I a comparison of pottery findings in "the Strait of Messina area". J. Cul. Her., 3, 145–53.

Belfiore, C.M., Di Bella, M., Triscari, M., Viccaro, M. (2010) - Production technology and provenance study of archaeological ceramics from relevant sites in the Alcantara River Valley (North-eastern Sicily, Italy). Mat. Charact., 61, 440–51.

Botto, M. (2016) - The Punic settlement of Pani Loriga in the light of recent discoveries. J. Fasti Online, 1-19.

Cultrone, G., Rodriguez-Navarro, C., Sebastian, E., Cazalla, O., De La Torre, M.J. (2001) - Carbonate and silicate phase reactions during ceramic firing. Eur. J. Mineral, 13, 621–34.

Ferrara, E., Tema, E., Beatrice, C. (2016) - Estimating the equivalent firing temperature of ancient baked clay artifacts through magnetic measurements. Proceedings of the IMEKO International conference on Metrology for Archaeology and Cultural Heritage. IMEKO, 265-269.

Gosselain, O.P. (1992) - Bonfire of the enquiries. Pottery firing temperatures in archaeology: What for? J. Archaeol. Sci., 19, 243–59.

Hunt, A.M.W. (2017) - The Oxford handbook of archaeological ceramic analysis. Oxford University Press.

Maritan, L. (2004) - Archaeometric study of Etruscan-Padan type pottery from the Veneto region: petrographic, mineralogical, and geochemical-physical characterization. Eur. J. Mineral., 16, 297–307.

Matau, F. & Salaoru, T.A. (2013) - Cucuteni Culture: A Systematic Physical Study of Pottery Shards. J. Adv. Res. Phys., 4.1.

Quinn, P.S. (2022) - Thin section petrography, geochemistry & scanning electron microscopy of archaeological ceramics. Archaeopress Archaeology.

Rasmussen, K.L., De La Fuente, G.A., Bond, A.D., Mathiesen, K.K., Vera, S.D. (2012) - Pottery firing temperatures: A new method for determining the firing temperature of ceramics and burnt clay. J. Archaeol. Sci., 39, 1705–16.

Rice, P.M. (2015) - Pottery analysis: a sourcebook. 2nd ed. University of Chicago Press, 3.

Vaknin, Y., Shaar, R., Lipschits, O., Behar, A.E., Maeir, A.M., Ben-Yosef, E. (2023) - Applying thermal demagnetization to archaeological materials: A tool for detecting burnt clay and estimating its firing temperature. PLOS One, 18.

Volcanology and petrology of Middle Triassic magmatism of the Dolomites (Southern Alps): Insights on architecture, dynamics and timescales of plumbing systems

Nicolò Nardini

Department of Physics and Earth Sciences, University of Ferrara, Via Saragat 1, 44122, Ferrara

DOI: 10.19276/plinius.2025.01.016

INTRODUCTION, GEOLOGICAL SETTING AND AIMS

Ancient magmatic systems offer crucial insights into processes typically hidden beneath active volcanoes. The Dolomites (Southern Alps, Italy) provide an exceptional case study, where both volcanic and plutonic rocks are well exposed and spatially connected. This rare preservation makes the region ideal for reconstructing the full architecture of a magmatic plumbing system. The Middle Triassic magmatic event, dated between ~237–242 Ma (Storck et al., 2019), shaped the NW Adria margin through the emplacement of volcanic and plutonic rocks across the South Alpine–Austroalpine domains, extending into the Dinarides and Hellenides (Sloman, 1989; Bonadiman et al., 1994; Pamić et al., 1998; Casetta et al., 2018a, b, 2019, 2021). In the Dolomites, extensive exposures of lava flows, plutons, volcaniclastic units, and dyke swarms are exceptionally well-preserved. The region was marked by high sedimentation rates in shallow marine carbonate platforms and intense localised extension (Doglioni, 1987). Despite this tectonic regime, the magmas exhibit orogenic geochemical characteristics, including LILE enrichment and depletion of Nb, Ta, and Ti. Various models have been proposed to explain this, such as inherited metasomatism from Variscan subduction (Sloman, 1989; Bonadiman et al., 1994).

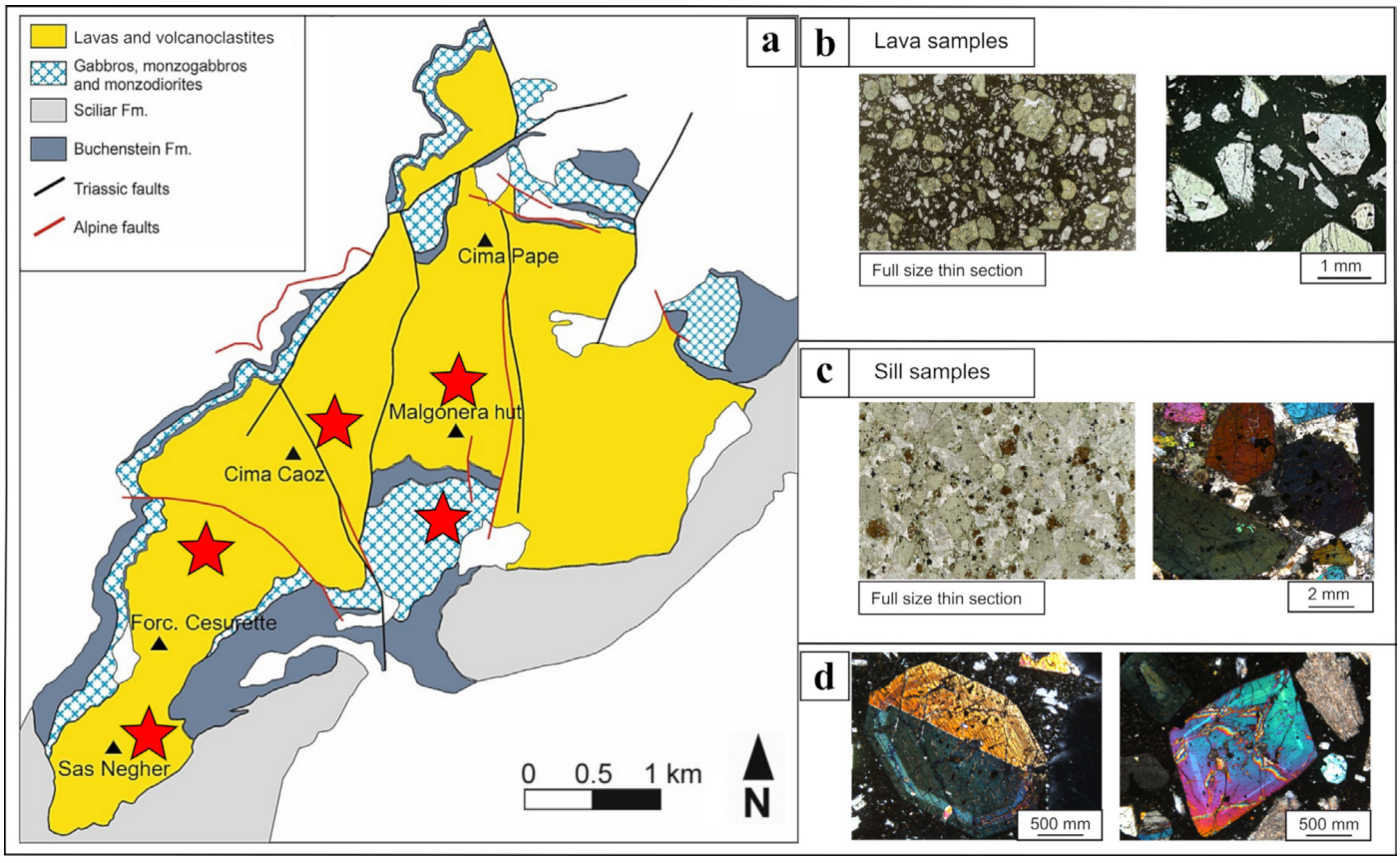

Figure 1 a) *Simplified geological map of the Cima Pape complex. Red stars indicate the sampling areas (modified from Nardini et al., 2022).* ***b)*** *Thin section scan and microphotograph of a representative lava sample.* ***c)*** *Thin section scan and microphotograph of a representative sample from the sill.* ***d)*** *Crossed-polar photomicrographs of clinopyroxene individuals showing high-Mg# and high-Cr intermediate band.*

This thesis aimed to reconstruct the geometry and dynamics of the main Dolomites' magmatic plumbing systems (*i.e.*, Predazzo, Mt. Monzoni, Cima Pape) by focusing on underexplored volcanic and subvolcanic rocks. Using tools typically applied to active volcanoes, the study treats the Dolomites as a natural-scale laboratory for volcanological research. The exceptional exposure of volcanic and intrusive rocks allows for direct comparison between surface and deep-crustal products, providing insights into magma storage and contributing to models of active systems. Additional objectives of the work were to define the petrology and geochemistry of the less-studied areas (*e.g.*, Cima Pape Complex, Sciliar) and improve the timeline of the magmatic pulses that composed the Middle Triassic occurrence in the Dolomites.

ANALITYCAL METHODS

Whole-rock major and trace element analyses of magmatic rocks considered were conducted at the Department of Physics and Earth Sciences, University of Ferrara (Italy), using an ARL Advant-XP automated wavelength-dispersive X-ray fluorescence spectrometer (WDXRF) and a Thermo Series X inductively coupled plasma mass spectrometer (ICP-MS). Major element analyses of mineral phases from representative samples were performed at the Department of Lithospheric Research, University of Vienna (Austria), using a CAMECA SXFive FE electron microprobe equipped with five WD and one ED spectrometers. Whole-rock $^{87}Sr/^{86}Sr$ and $^{143}Nd/^{144}Nd$ analyses were made at the Scottish Universities Environmental Research Centre (SUERC) by thermal ionisation mass spectrometry (TIMS). Trace element concentrations of clinopyroxene were measured at the CNR - Istituto di Georisorse of Pavia by laser ablation inductively coupled plasma-mass spectrometry (LA-ICP-MS), while LA-ICP-MS element mapping of clinopyroxene was undertaken in the Imaging and Analysis Centre (IAC) at the Natural History Museum in London (NHM) using a Teledyne Iridia 193 nm system coupled to an Agilent 8900 ICP-MS. Detailed back-scattered electron (BSE) images for the diffusion chronometry calculations were acquired with the Jeol IT500 FEG-SEM and the FEI QUANTA 650 FEG-SEM, at the IAC at the NHM. Titanite crystals were analysed for U–Pb dating and simultaneous trace element analysis by laser ablation-inductively coupled-mass spectrometry (LA-ICP-MS) at the Institute of Geochemistry and Petrology, ETH Zurich, Switzerland, using a RESOlution S-155 (ASI/Applied Spectra) 193-nm ArF excimer laser ablation system connected to an Element XR (Thermo) sector-field ICP-mass spectrometer. Zircon separates were dated at Purdue University (Indiana, USA) through Isotope Dilution Thermal Ionisation Mass Spectrometry (ID-TIMS).

RESULTS AND DISCUSSION

The Cima Pape Complex

A comprehensive sampling campaign targeted both intrusive and effusive lithologies, including trachybasaltic to basaltic trachyandesitic lava flows, pillow breccias, and a 50–300 m thick gabbroic to monzodioritic sill (Fig. 1). The volcanic rocks are highly porphyritic (PI up to 50%) and dominated by clinopyroxene phenocrysts displaying complex zoning: augitic cores, concentric high-Mg# (up to 91) and Cr-rich diopsidic bands (up to 1.2 wt.%), and LILE- and LREE-enriched augitic rims. In contrast, clinopyroxenes in the sill are largely homogeneous and unzoned, reflecting slower cooling conditions.

Whole-rock geochemistry confirmed a SiO_2-saturated, shoshonitic affinity typical of orogenic magmatism (Peccerillo and Taylor, 1975), and Sr-Nd isotopic signatures ($^{87}Sr/^{86}Sr_i$ = 0.7045–0.7050; $^{143}Nd/^{144}Nd_i$ = 0.51223–0.51228) highlighted derivation from an enriched lithospheric mantle source (Bonadiman et al., 1994; Lustrino et al., 2019). Thermobarometric and hygrometric modelling (Putirka, 2008; Perinelli et al., 2016) revealed a vertically zoned plumbing system: augitic cores crystallised at 7–14 km depth from evolved, H_2O-rich melts (T = 1035–1075°C; H_2O = 2.6–3.8 wt.%), followed by the injection of hotter, more primitive basaltic magmas (T = 1130–1150°C; H_2O = 2.1–2.8 wt.%) responsible for the formation of high-Mg#, Cr-rich diopsidic bands. Rim re-equilibration with hybrid magmas occurred during later stages of ascent, while microphenocrysts and outer rims crystallised under shallow conditions (50–150 MPa; T = 975–1010°C). The zoned clinopyroxene population observed for the first time in the Dolomitic area is similar to those reported in the products of active volcanoes such as Stromboli and Etna which is consistent with similar processes among plumbing systems (Giacomoni et al., 2014, 2016; Petrone et al., 2018; Di Stefano et al., 2020). These findings provide the first investigation into the pressure and temperature conditions of magma storage in the ancient Cima Pape volcano alongside the first evidence of recharge and mixing dynamics in the Dolomites, captured through crystal-scale zoning. The study underscored the utility of clinopyroxene zoning as a tool for reconstructing magmatic processes and highlights how fossil systems like Cima Pape can serve as analogues for modern volcanism, advancing our understanding of Mid-Triassic magmatism and crustal evolution in the Southern Alps.

Magma mixing in the Dolomites: dynamics and timescales

Starting from the outcomes of the investigation on the Cima Pape complex, this study aimed to reconstruct the architecture and dynamics of ancient magma plumbing

systems in all the main Middle Triassic volcano-plutonic complexes of the Dolomites (Southern Alps). The set of magmatic rocks investigated for this study involved only volcanic and subvolcanic (*i.e.*, dykes) samples from Predazzo, Mt. Monzoni, Cima Pape and Sciliar, all exhibiting transitional to alkaline basaltic to trachybasaltic compositions and porphyritic textures (Pl 30-55%). The zoning pattern observed in the clinopyroxene population hosted by the rocks from Cima Pape is also present in the other centres. Augitic cores (Mg# 67–78) are typically mantled by high-Mg#, Cr-rich diopsidic bands (Mg# 77–91; Cr_2O_3 up to 1.2 wt.%) and overgrown by augitic rims with or without oscillatory zoning. However, the zoning pattern became more complex: Textural types include diopsidic, resorbed to highly resorbed and/or patchy cores, as well as sector-zoned varieties, along with aggregates or glomerocrysts that share zoning histories, indicating complex crystallisation environments (Fig. 2). To codify this diversity, a classification of the clinopyroxene has been made: Type A crystals with augitic cores (subtype A0 = unzoned augite; A1 = augitic core with one diopsidic band; A2 = augitic core with multiple diopsidic bands), Type B crystals with diopsidic cores (B0 = no bands; B1 = one diopsidic band; B2 = multiple bands), and Type C crystals showing sector zoning (C0 = sector-zoned augite; C1 = sector-zoned with diopsidic band).

The compositions of resorbed and patchy diopsidic cores are mirrored by diopside in clinopyroxenitic xenoliths from the Latemar area, which is in equilibrium with a trachybasaltic melt. Diopsidic cores in lava and dyke samples, likely representing fragments of a deeper reservoir subsequently cannibalised during mafic recharge events. Whole-rock and melt inclusion chemistry confirms a shoshonitic signature, consistent with mantle-derived magmas metasomatised during earlier Variscan subduction (Bonadiman et al., 1994; Casetta et al., 2021), and supports prior interpretations

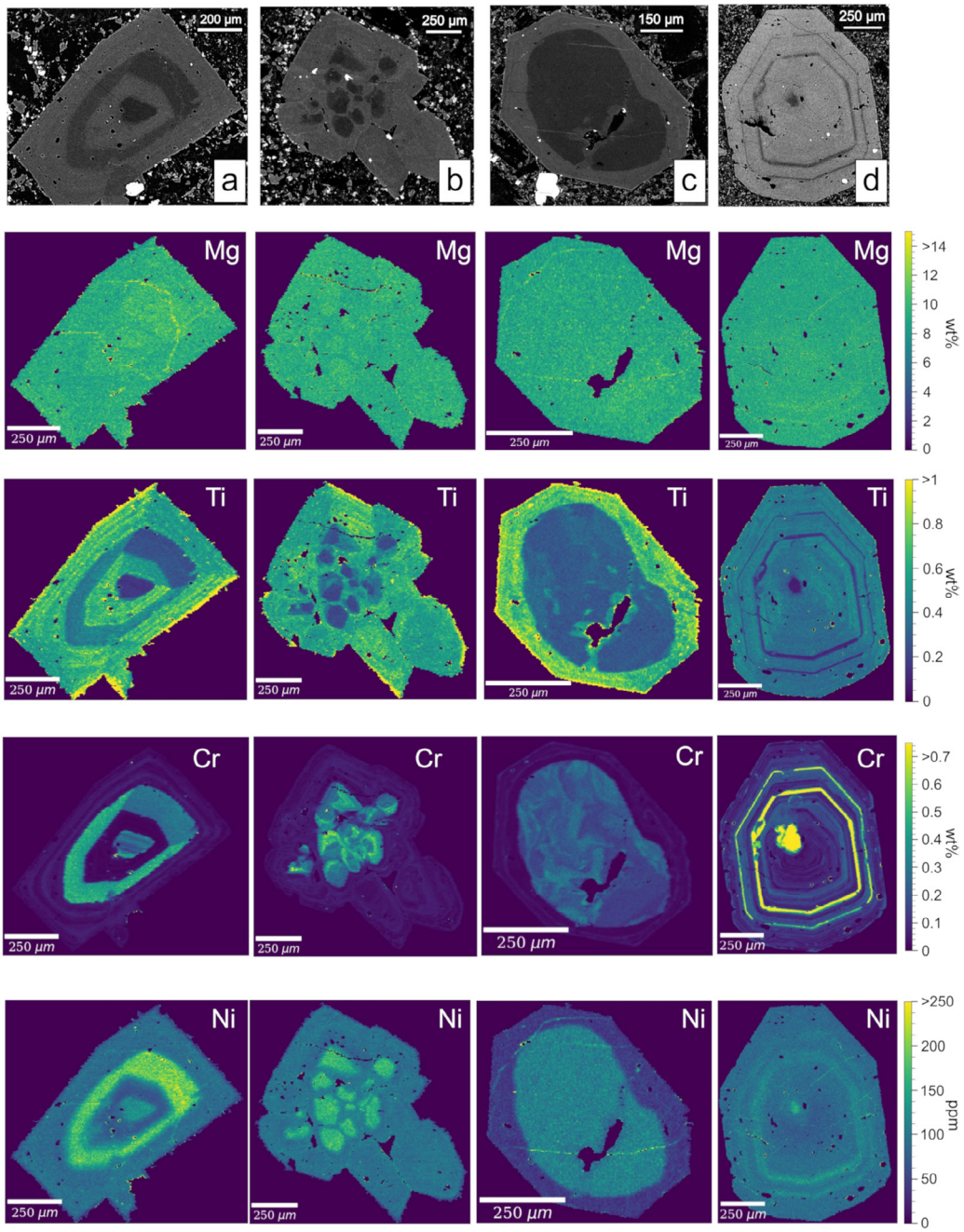

Figure 2 *Major and trace element chemical mapping of clinopyroxene crystals from the Dolomites. BSE images (top) and quantitative chemical mapping of Mg, Ti, Cr and Ni for four representative clinopyroxene crystals.* ***a)*** *Type B1,* ***b)*** *and* ***c)*** *Type B0 (mottled core and resorbed diopsidic) and* ***d)*** *B2 (highly resorbed diopsidic core) from left to right (from Nardini et al., 2024).*

of calc-alkaline magmatism in an extensional regime. Thermobarometric modeling using clinopyroxene-only formulations (Wang et al., 2021; Higgins et al., 2022) combined with clinopyroxene-based melt hygrometry (Perinelli et al., 2016) reveals that augitic domains crystallised at mid-crustal levels (5–8.5 km, 150–250 MPa) from trachyandesitic melts (T = 1044–1118°C, H_2O ≈ 2.8 wt.%), while the diopsidic zones record injection of more primitive, hotter trachybasaltic magmas (T = 1056–1170°C). The deepest pressures (300–500 MPa; 10–17 km) are associated with patchy-zoned and highly resorbed diopsidic cores, indicating crystal storage and recycling from a lower crustal mush (Fig. 3).

Diffusion chronometry using Fe–Mg interdiffusion profiles through the NIDIS model (Petrone et al., 2016) resolved magma recharge and mixing timescales from weeks to decades, with differences between the centres (Fig. 4).

Type B0 clinopyroxenes from Mt. Monzoni suggested rapid pre-eruptive ascent (< 1 year), whereas Types A1–A2 and B1–B2 crystals from Cima Pape and Predazzo indicated prolonged residence (up to 80 years), likely reflecting differing thermal regimes and conduit connectivity (Fig. 4). The occurrence of double plateaux in diopsidic bands and anomalous diffusion gradients further testifies to instant growth rates and incomplete melt mixing. Sector zoning and Ti-enrichment in lavas indicate variable undercooling rates, reinforcing the interpretation of dynamic, convective magmatic systems with evolving physical conditions. Overall, the study provided compelling evidence for episodic magma recharge, antecryst recycling, and polybaric crystallisation within the Middle Triassic vertically-extended plumbing systems in the Dolomites. The consistent patterns of clinopyroxene chemistry and zoning across different centres suggest regionally coherent magma dynamics, while local differences in zoning style, diffusion rates, and undercooling reflect individual reservoir histories.

Timing and Evolution of Predazzo Magmatism

The Middle Triassic magmatism in the Predazzo area is marked by the emplacement and eruption of compositionally diverse magma batches within a short time frame. New geological surveys documented the presence of phonolite dykes cutting across Middle Triassic volcanic sequences. These phonolites have porphyritic texture (PI 5-10%) and are sodalite- and aegirine-bearing, with titanite, apatite, and magnetite as accessory phases. Geochemically, they retain a distinct orogenic-like trace element signature, with enrichment in LILE and LREE and depletion in Nb–Ta–Ti, in line with other

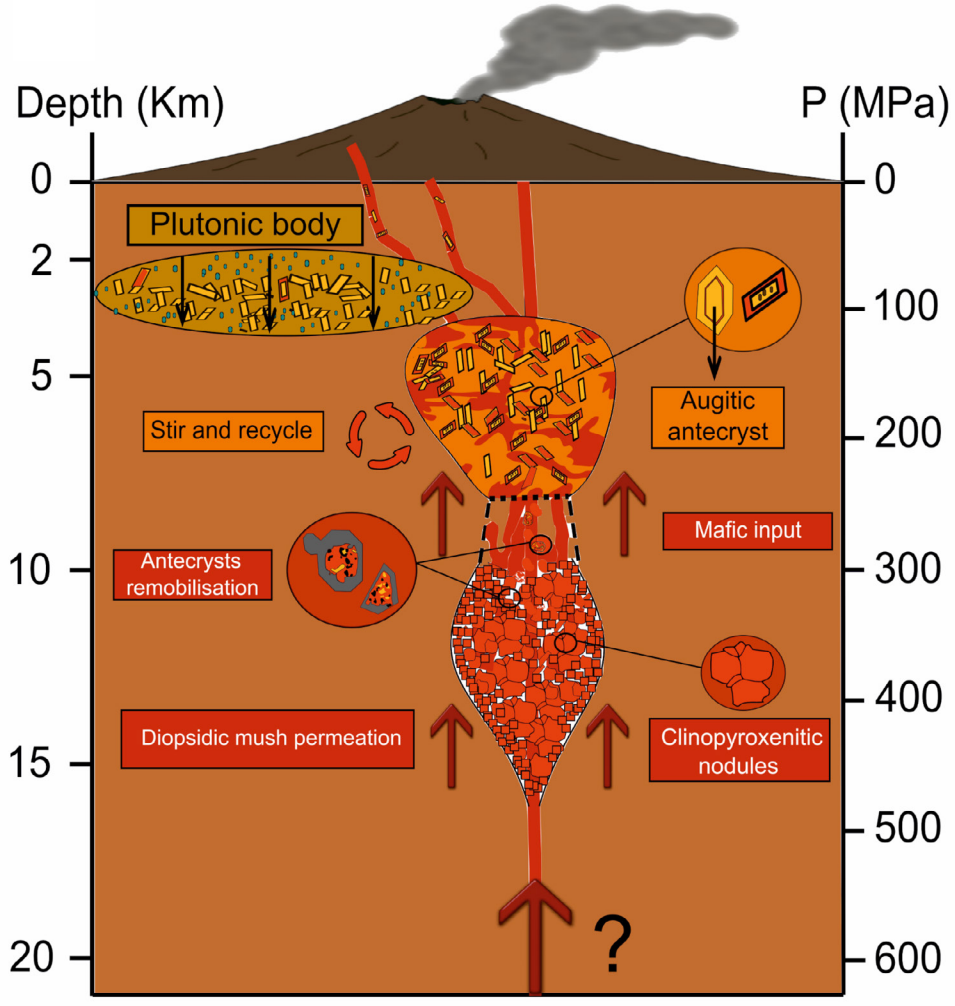

Figure 3 *Sketch of a general feeding system beneath the Mid-Triassic volcanoes in the Dolomites. The mafic input recycles diopsidic antecrysts permeating the diopsidic mush (witnessed by clinopyroxenitic nodules) in the shallower trachyandesitic magma reservoir (Type B crystals) and mantle the augitic antecrysts (previously formed in the more evolved reservoir) with diopsidic bands (Type A1 and A2 crystals) (modified from Nardini et al., 2024).*

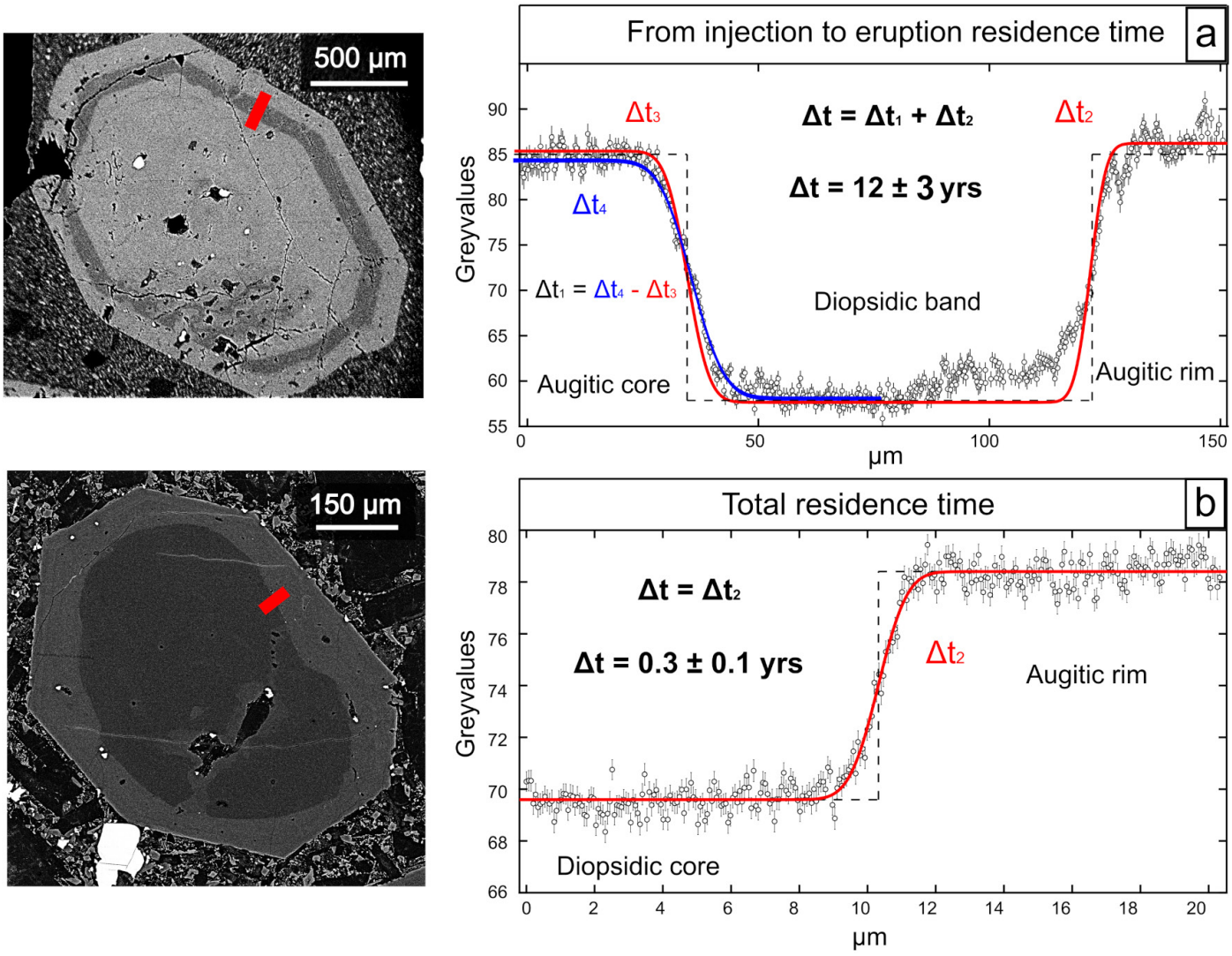

Figure 4 *Grey value diffusion profiles of two representative clinopyroxene crystals from the Dolomites calculated inside the red area of the associated BSE-SEM images.* ***a)*** *Diffusion profile of a crystal from Cima Pape; the computation expresses the timescale from mafic injection to the eruption.* ***b)*** *Diffusion chronometry on a crystal from Mt. Monzoni expressing the total residence time of the diopsidic antecryst in the evolved magma (at the evolved magma conditions of T), which corresponds to the time from the mafic input to the eruption (modified from Nardini et al., 2024). For the explanation of* Δt_1, Δt_2, Δt_3 *and* Δt_4, *the reader is referred to Petrone et al. (2016) or Nardini et al. (2024).*

Mid-Triassic magmas of the region and in contrast to other alkaline subvolcanic manifestations present in the area (*i.e.*, lamprophyres; Casetta et al., 2019).

Titanite and zircon U–Pb geochronology on phonolite dykes and representative samples from every magmatic suites of the Predazzo pluton (Silica Saturated suite (SS); Silica Undersaturated suite (SU) and Granitic Unit (GU); see Casetta et al., 2018a, b) represented the first complete chronological framework for the Predazzo volcano-plutonic complex. Zircon dating of the plutonic units yields crystallisation ages between 237.97 ± 0.15 Ma and 238.31 ± 0.13 Ma, while titanite dating from phonolitic dykes indicates emplacement between 233.8 ± 3.1 Ma and 238.1 ± 4.5 Ma (Fig. 5). These overlapping age ranges, coupled with the presence of sodalite as phenocryst, confirmed that both silica-saturated and -undersaturated magmas were emplaced in a geologically brief interval during the Middle Trias, consistent with earlier studies (Casetta et al., 2018a, b). Additionally, phonolite dykes age is coherent with those of volcanic and plutonic manifestations documented in literature (Storck et al., 2020). Mineral-based thermometry and hygrometry indicate that the phonolites represent volatile-rich (H_2O = 8 ± 0.6 wt.%), REE-enriched, highly differentiated melts, emplaced at relatively low temperatures (752–868°C), potentially driving associated Cu–W mineralisation. Comparison with subvolcanic rocks from the Central (Edolo) and Western Alps (Finero) highlights the regional persistence of this signature across the Southalpine domain before the opening of the Alpine Tethys.

Volcano-Plutonic Link and Evidence of Magma Recharge in Plutonic Rocks

Clinopyroxene crystals from mafic intrusive rocks in the Dolomites (Predazzo, Mt. Monzoni, and Cima Pape) have been selected to investigate their texture (if any) in response to the plumbing system dynamics studied in lava and dyke samples. Only the most mafic rocks have been chosen (augite-bearing clinopyroxenites, gabbros and monzogabbros) based on two main

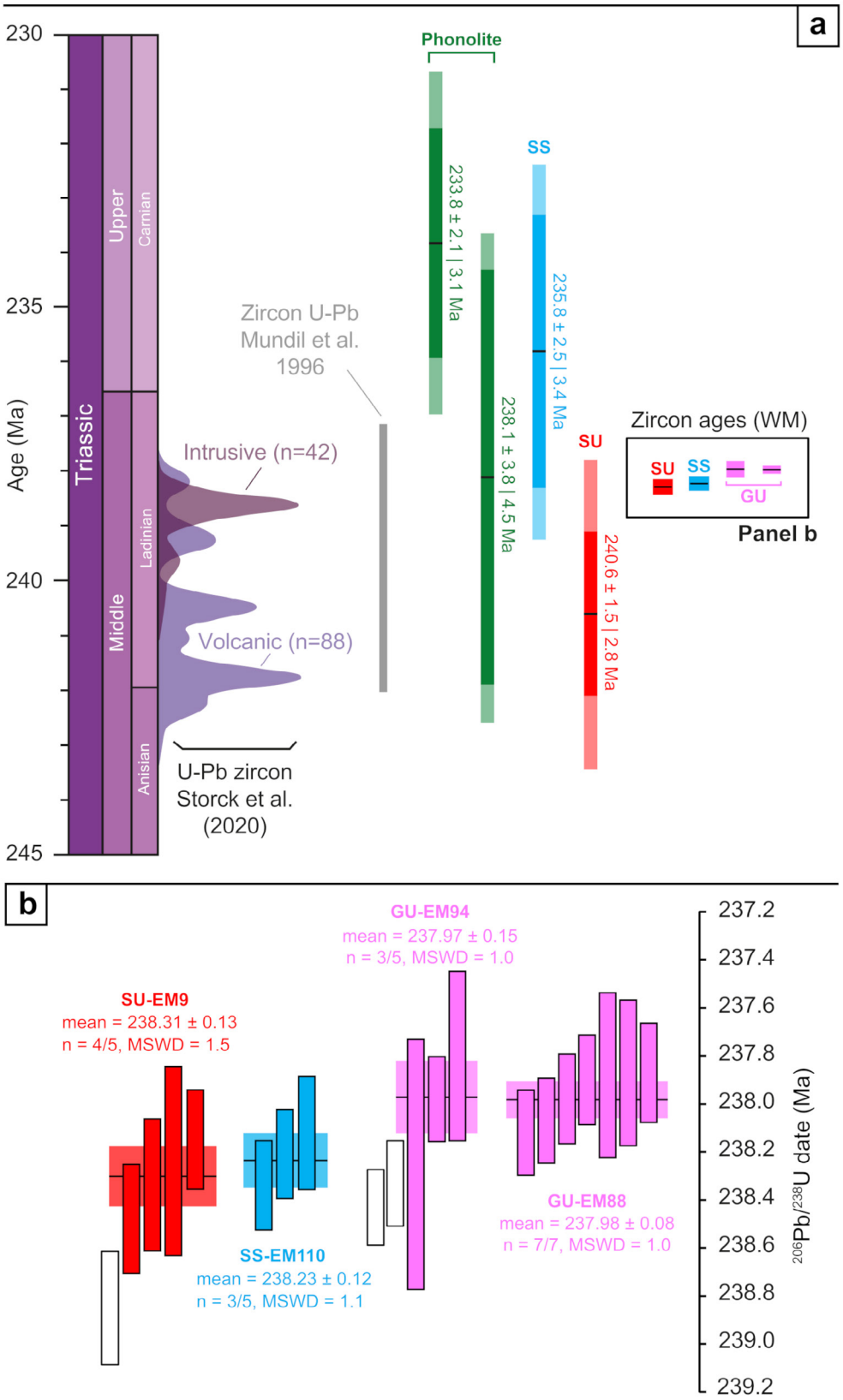

Figure 5 a) *U-Pb ages on titanites obtained in this work compared to literature studies on the same area (Storck et al., 2020).* ***b)*** *Rank-order plot of CA-ID-TIMS zircon dates. Coloured bars represent Th-corrected ID-TIMS $^{206}Pb/^{238}U$ dates of individual zircon crystals with their 2σ uncertainty (from Nardini et al., 2025).*

reasons: *i)* to compare effusive rocks with their intrusive equivalents–gabbros and clinopyroxenites were selected because the effusive rocks are primarily basalts to basaltic trachyandesites; *ii)* the most mafic plutonic rocks are richest in clinopyroxene, which consistently serves as the dominant primary cumulus mineral. Textural and compositional studies on clinopyroxene populations reveal compelling evidence for magma mixing. As already observed in lavas and dykes clinopyroxene population (Nardini et al., 2024), two distinct compositional domains, augitic and diopsidic, were identified across all intrusions, with diopsidic zones marked by higher Mg# (79-90) and Cr_2O_3 (up to 0.6 wt.%) contents compared to augite (Mg# 62-77; Cr_2O_3 < 0.1 wt.%). Zoning patterns, including diopsidic cores and bands, indicate the periodic intrusion of more primitive melts into crystallising magma bodies, mirroring patterns observed in volcanic rocks from the same region (Nardini et al., 2022, 2024). Pressure estimations on clinopyroxene significantly refined the depth of the main, more evolved

ponding zone, indicating shallower levels (1.5 and 5.5 km) than previously calculated within the volcanic rocks. Additionally, it is now possible to distinguish between different formation pressures of the diopsidic cores and bands. The diopsidic cores appear to have formed at greater depths than the associated bands, a difference not observed in the volcanic equivalents. This discrepancy provides further evidence in support of the model developed through textural and compositional analysis of clinopyroxenes in effusive rocks.

The newly acquired pressure data for diopsidic cores crystallisation closely match the pressure estimates for the Latemar nodules (Nardini et al., 2024). This supports the interpretation that these cores are older diopside crystal fragments from the Latemar nodules, entrained by the mafic input and transported to shallower levels of the magmatic plumbing system. Ultimately, these nodules became incorporated into lavas and dykes, leading to their present-day exposure.

The preservation of compositional zoning, despite the expected diffusive re-equilibration in plutonic settings, supports earlier inferences of rapid cooling for the Predazzo and Mt. Monzoni plutons (Bonadiman et al., 1994; Casetta et al., 2018a). The connection between these intrusive textures and coeval volcanic counterparts strengthens the volcano-plutonic link and reveals the geometry of vertically structured magma storage zones. Furthermore, the presence of diopsidic rims and bands unique to intrusive rocks suggests crystallisation events not preserved in surface products, offering direct insight into processes often inferred in active systems.

CONCLUSIONS AND FUTURE PERSPECTIVES

This thesis makes a comprehensive contribution to the understanding of Middle Triassic magmatism in the Southern Alps, providing enhancements in both the fine-scale dynamics of magma systems and the broader geological framework of the region.

At the small scale, detailed petrological and geochemical analyses of clinopyroxene crystals from key volcano-plutonic complexes like Predazzo, Mt. Monzoni, Cima Pape, and pivotal magmatic manifestations near the Sciliar and Lateman carbonate platforms have allowed the reconstruction of magma plumbing systems with unprecedented resolution. The results indicate that volcanism in these centres was governed by episodic magma recharge events from deep-seated mafic inputs that remobilised mid-crustal mush zones before feeding shallower reservoirs, with crystallisation sequences and convection processes revealing complex magmatic interactions. Tectonic processes, particularly trans-tensive regimes, were shown to play a pivotal role in facilitating magma ascent and eruption, especially in centres like Predazzo and Cima Pape, where diffusion chronometry on clinopyroxene crystals revealed years to decades of injection to eruption timescales. These interpretations were further refined through complementary studies on intrusive and ultramafic rocks, offering new insight into the deeper magmatic roots of these systems and proposing a refined methodology for plumbing system reconstruction, exploring the volcano-plutonic link.

At the large scale, this work has provided the first integrated petrological, geochemical, and isotopic characterisation of the Cima Pape volcano-plutonic complex in recent literature, establishing a clearer picture of its magmatic evolution and emplacement history. Additionally, the first documentation and dating of phonolitic dykes within the Predazzo complex have expanded the known compositional diversity of its subvolcanic units. Zircon and titanite U-Pb geochronology on phonolite dykes and coeval intrusive rocks has refined the timeline of magmatism at the Predazzo complex, highlighting a prolonged orogenic-like magmatism lasting into the Upper Triassic and distinguishing it from later rift-related lamprophyric events.

Altogether, this research significantly enhances our knowledge of Middle Triassic volcanic and plutonic processes in the Dolomites. It not only documents new magmatic episodes and reservoir dynamics but also establishes an innovative framework for the study of ancient and active volcanic systems. The approaches and results outlined here have the potential to inform future investigations into magma storage, transport, and eruption triggering, critical elements in both academic research and volcanic hazard assessment.

REFERENCES

Bonadiman, C., Coltorti, M., Siena, F. (1994) - Petrogenesis and T-fθ2 estimates of Mt. Monzoni complex (Central Dolomites, Southern Alps): a Triassic shoshonitic intrusion in a transcurrent geodynamic setting. Eur. J. Mineral., 6, 943–966.

Casetta, F., Coltorti, M., Ickert, R.B., Bonadiman, C., Giacomoni, P.P., Ntaflos, T. (2018a) - Intrusion of shoshonitic magmas at shallow crustal depth: T–P path, H2O estimates, and AFC modeling of the Middle Triassic Predazzo Intrusive Complex (Southern Alps, Italy). Contrib. Mineral. Petrol., 173, 57.

Casetta, F., Coltorti, M., Marrocchino, E. (2018b) - Petrological evolution of the Middle Triassic Predazzo Intrusive Complex, Italian Alps. Int. Geol. Rev., 60, 977–997.

Casetta, F., Ickert, R.B., Mark, D.F., Bonadiman, C., Giacomoni, P.P., Ntaflos, T., Coltorti, M. (2019) - The Alkaline Lamprophyres of the Dolomitic Area (Southern Alps, Italy): Markers of the Late Triassic Change from Orogenic-like to Anorogenic Magmatism. J. Petrol., 60, 1263–1298.

Casetta, F., Ickert, R.B., Mark, D.F., Giacomoni, P.P., Bonadiman, C., Ntaflos, T., Zanetti, A., Coltorti, M. (2021) - The Variscan subduction inheritance in the Southern Alps Sub-Continental Lithospheric Mantle: Clues from the Middle Triassic shoshonitic magmatism of the Dolomites (NE Italy). Lithos, 380–381, 105856.

Di Stefano, F., Mollo, S., Ubide, T., Petrone, C.M., Caulfield, J., Scarlato, P., Nazzari, M., Andronico, D., Del Bello, E. (2020) - Mush cannibalism and disruption recorded by clinopyroxene phenocrysts at Stromboli volcano: New insights from recent 2003–2017 activity. Lithos, 360–361, 105440.

Doglioni, C. (1987) - Tectonics of the Dolomites (southern alps, northern Italy). J. Struct. Geol., 9, 181–193.

Giacomoni, P.P., Coltorti, M., Bryce, J.G., Fahnestock, M. F., Guitreau, M. (2016) - Mt. Etna plumbing system revealed by combined textural, compositional, and thermobarometric studies in clinopyroxenes. Contrib. Mineral. Petrol., 171, 34.

Giacomoni, P.P., Ferlito, C., Coltorti, M., Bonadiman, C., Lanzafame, G. (2014) - Plagioclase as archive of magma ascent dynamics on "open conduit" volcanoes: The 2001–2006 eruptive period at Mt. Etna. Earth-Sci. Rev., 138, 371–393.

Higgins, O., Sheldrake, T., Caricchi, L. (2022) - Machine learning thermobarometry and chemometry using amphibole and clinopyroxene: a window into the roots of an arc volcano (Mount Liamuiga, Saint Kitts). Contrib. Mineral. Petrol., 177, 10.

Lustrino, M., Abbas, H., Agostini, S., Caggiati, M., Carminati, E., Gianolla, P. (2019) - Origin of Triassic magmatism of the Southern Alps (Italy): Constraints from geochemistry and Sr-Nd-Pb isotopic ratios. Gondwana Res., 75, 218–238.

Nardini, N., Casetta, F., Ickert, R.B., Mark, D.F., Ntaflos, T., Zanetti, A., Coltorti, M. (2022) - From the Middle Triassic Cima Pape complex (Dolomites; Southern Alps) to the feeding systems beneath active volcanoes: Clues from clinopyroxene textural and compositional zoning. J. Volcanol. Geoth. Res., 422, 107459.

Nardini, N., Casetta, F., Petrone, C.M., Buret, Y., Ntaflos, T., Coltorti, M. (2024) - Modelling ancient magma plumbing systems through clinopyroxene populations: a case study from Middle Triassic volcanics (Dolomites, Italy). Contrib. Mineral. Petrol., 179, 22.

Nardini, N., Casetta, F., Ickert, R.B., Tavazzani, L., Okhai, D.C., Peres, S., Dellantonio, E., Ntaflos, T., Coltorti, M. (2025) - The timing of the Middle Triassic magmatism in the Dolomites area (Southern Alps, Italy): U-Pb geochronology of zircon and titanite hosted in plutonic rocks and phonolite dykes. Lithos, 494–495, 107894.

Pamić, J., Gušić, I., Jelaska, V. (1998) - Geodynamic evolution of the Central Dinarides. Tectonophysics, 297, 251–268.

Peccerillo, A. & Taylor, S.R. (1975) - Geochemistry of upper cretaceous volcanic rocks from the Pontic Chain, Northern Turkey. Bull. Volcanol., 39, 557–569.

Perinelli, C., Mollo, S., Gaeta, M., De Cristofaro, S.P., Palladino, D.M., Armienti, P., Scarlato, P., Putirka, K. D. (2016) - An improved clinopyroxene-based hygrometer for Etnean magmas and implications for eruption triggering mechanisms. Am. Mineral., 101, 2774–2777.

Petrone, C.M., Bugatti, G., Braschi, E., Tommasini, S. (2016) - Pre-eruptive magmatic processes re-timed using a non-isothermal approach to magma chamber dynamics. Nat. Commun., 7, 12946.

Petrone, C.M., Braschi, E., Francalanci, L., Casalini, M., Tommasini, S. (2018) - Rapid mixing and short storage timescale in the magma dynamics of a steady-state volcano. Earth Planet. Sc. Lett., 492, 206–221.

Putirka, K.D. (2008) - Thermometers and Barometers for Volcanic Systems. Rev. Mineral. Geochem., 69, 61–120.

Sloman, L.E. (1989) - Triassic shoshonites from the dolomites, northern Italy: Alkaline arc rocks in a strike-slip setting. J. Geophys. Res., 94, 4655–4666.

Storck, J.-C., Brack, P., Wotzlaw, J.-F., Ulmer, P. (2019) - Timing and evolution of Middle Triassic magmatism in the Southern Alps (northern Italy). J. Geol. Soc. London, 176, 253–268.

Storck, J-C., Wotzlaw, J-F., Karakas, Ö., Brack, P., Gerdes, A., Ulmer, P. (2020) - Hafnium isotopic record of mantle-crust interaction in an evolving continental magmatic system. Earth Planet. Sc. Lett., 535, 116100.

Wang, X., Hou, T., Wang, M., Zhang, C., Zhang, Z., Pan, R., Marxer, F., Zhang, H. (2021) - A new clinopyroxene thermobarometer for mafic to intermediate magmatic systems. Eur. J. Mineral., 33, 621–637.

Characterization of H_2 and hydrocarbons trapped in exhumed metamorphic rocks: origin and fluxes of energy sources in subduction zones

The petrology of hidden deep energy sources

Orlando Sébastien Olivieri

Department of Biological, Geological, and Environmental Sciences, University of Bologna, Via Zamboni 67, 40126, Bologna
DOI: 10.19276/plinius.2025.01.017

INTRODUCTION

Methane (CH_4) and molecular hydrogen (H_2) are small volatile compounds with a huge impact on Earth's habitability. These reduced molecules are well known for being key energy sources for microbial life in the deep subsurface, potentially comprising one of Earth's largest biospheres (Whitman et al., 1998; Colman et al., 2017; Magnabosco et al., 2018).

Recent studies suggested that fluid-rock interactions in subduction zones can generate deep metamorphic CH_4- and H_2-rich fluids, offering essential ingredients for sustaining deep microbial life at forearc regions (Mottl et al., 2003; Ohara et al., 2012; Plümper et al., 2017; Vitale Brovarone et al., 2020; Peverelli et al., 2024).

However, the extent to which metamorphic processes can generate deep energy sources at convergent margins and their isotopic fingerprints is largely unconstrained. This scientific gap leads to large uncertainties in other fields of research, such as the study of the redox-state of metamorphic fluids, the production of greenhouse gas, CH_4, and strategic carbon-neutral fuel, H_2, through metamorphic processes.

PETROLOGY AND FLUID INCLUSION ANALYSIS TO UNVEIL UNCONVENTIONAL DEEP ENERGY SOURCES

Petrology is fundamental in order to understand the origin and fluxes of terrestrial volatiles. The investigation of fluid-rock interactions and fluid inclusions (hereafter FIs) preserved in the rock record represents a powerful tool to reconstruct geologic processes and their impact on the evolution of life on our planet.

The aim of this PhD project is to foster our understanding of metamorphic hydrocarbons and H_2, through the petrographic, spectroscopic and isotopic characterisation of FIs trapped in exhumed metamorphic rocks from different geologic settings across the globe. To reach these goals, this PhD project required:

- The selection of a global-scale set of target samples of exhumed ultramafic, metabasic, metasomatic, and metasedimentary rocks, including two field sites for detailed characterisation and more than 17 exhumed metamorphic terranes worldwide, spanning from the Paleoproterozoic to the Eocene.
- The detailed petrographic characterisation of FIs from the micro to the nanoscale, combining optical microscopy, scanning and transmission electron microscopy, micro-Raman spectroscopy and energy dispersive X-ray spectroscopy.
- The development of FIs extraction protocols for the analysis of volatiles abundance and isotopic fingerprints in metamorphic rocks.

DEVELOPMENT OF FLUID INCLUSION EXTRACTION PROTOCOLS FOR $\delta^{13}C_{CH_4}$ AND $\delta^{13}C_{CO_2}$ CAVITY RING-DOWN SPECTROSCOPY (CRDS) ANALYSIS

Despite being a powerful tool to assess the nature and origin of paleo-geologic fluids, the isotopic characterisation of volatiles extracted from FIs can be hampered by a number of analytical artifacts (Salvi & Williams-Jones, 2003, and references therein) and is commonly based on expensive, and complicated extraction and purification systems, usually not available on the market.

This research project addressed these issues through the development of robust protocols for FIs extraction and $\delta^{13}C_{CH_4}$ and $\delta^{13}C_{CO_2}$ analysis through Cavity Ring-Down Spectroscopy (CRDS), a recently developed analytical technique that does not require gas separation and ensures high accuracy while maintaining a compact size and cost compared to conventional systems like Gas Chromatography Isotope Ratio Mass Spectrometry (GC-IRMS).

Blank, isotopic labelling, interlaboratory, and inter-technique comparison experiments highlighted the

benefits and drawbacks of two off-line mechanical extraction techniques, namely ball milling and crushing in stainless steel tubes. The protocols developed in this study allowed to replicate previously measured $\delta^{13}C_{CH4}$ values within 1 ‰ (Fig. 1) and could be applied to gas samples with CH_4 and CO_2 concentrations above 10 and 1000 ppm, respectively.

These protocols in combination with petrological FIs characterisation could be exploited on a broad range of geological samples, providing insights into the nature and origin of terrestrial and extraterrestrial volatiles, and could answer extremely relevant scientific questions. For instance, these analytical techniques could be applied in geo-astrobiology to identify evidence of biotic CH_4 and past extraterrestrial life activity, preserved within FIs in Martian rock samples.

However, the results of this study underscore the importance of properly addressing the analytical limitations of mechanical/thermal fluid inclusion extraction techniques, and, in particular, blank CH_4 production, which could be easily misinterpreted as natural biotic CH_4 extracted from the sample.

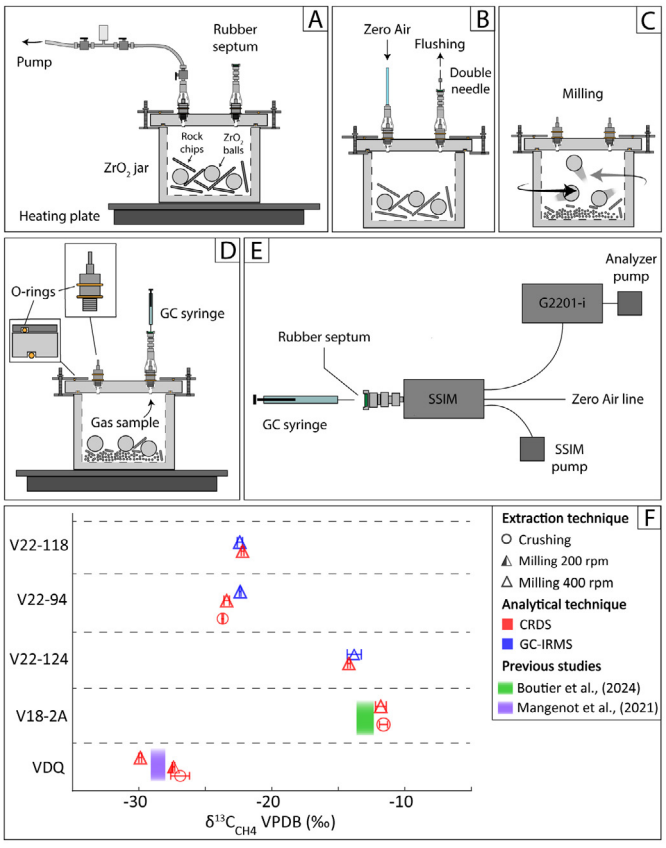

Figure 1 a-e) Graphical representation of the ball milling extraction protocol steps, including sample loading and jar evacuation ***(a)****, flushing and pumping with N_2-O_2 (Zero-Air)* ***(b)****, milling and fluid inclusion mechanical extraction* ***(c)****, gas extraction* ***(d)*** *and injection in the CRDS analyser with a GC syringe* ***(e)****.* ***f)*** *Results of interlaboratory and inter-technique comparison tests highlighting the reproducibility of the $\delta^{13}C_{CH4}$ VPDB (expressed in ‰) values within 1 ‰.*

CATCH AND RELEASE OF DEEP ENERGY SOURCES

Fluid inclusions within minerals may trap substantial amounts of energy sources, such as CH_4 and H_2, which, upon mechano-chemical release, may generate fluxes large enough to sustain microbial life at hydrothermal systems (McDermott et al., 2015; Klein et al., 2019; Grozeva et al., 2020).

Despite the increasing documentation of CH_4-H_2 FIs in crustal and mantle rocks exhumed from great depths (Vitale Brovarone et al., 2020; Peng et al., 2021; Spranitz et al., 2022; Zhang et al., 2023; Boutier et al., 2024; Peverelli et al., 2024), their evolution, residence time, and impact on volatile fluxes in the deep Earth remain unassessed.

This research project explored a novel approach to the study of deep CH_4-H_2, combining a high-resolution, 0.7 km^2-scale mapping of FIs petrographic-spectroscopic characterisation, and bulk CH_4 concentration and isotope composition measurement from 67 mafic, ultramafic, metasedimentary, and metasomatic rocks from the Belvidere Mountain Complex (BMC), Northern Vermont, USA (Fig. 2).

This allowed reconstructing multiple events of CH_4-H_2 catch and release in/from FIs (Fig. 2), opening a new perspective on the migration and residence time of volatile species and energy sources, such as CH_4, H_2, and NH_3, in deep metamorphic environments.

The FIs trapped in metamorphic/metasomatic rocks of the BMC acted as a sink for deep volatiles, isolating them from active fluid flow for geologic timescales.

The fate of these energy "vessels" – storage and transportation to shallower crustal levels vs. release at depth – was determined by mineralogical transformations and redox reactions throughout their exhumation history towards habitable environments.

The isotopic characterisation of CH_4 extracted from FIs provided a powerful tool to track the origin and reactivity of deep energy sources throughout the BMC tectono-metamorphic history (Fig. 2). This revealed an increasing input of metasediment-derived CH_4 driving pervasive carbonation of the ultramafic-mafic rocks during their exhumation.

THE HIDDEN DIVERSITY OF SERPENTINISATION-DERIVED HYDROCARBONS

The study of CH_4-H_2 FIs trapped in orogenic peridotites represents a powerful tool to understand the potential of different serpentinisation environments to generate energy sources, such as abiotic hydrocarbons and H_2 (Zhang et al., 2021; Boutier et al., 2024).

However, deciphering the serpentinisation and

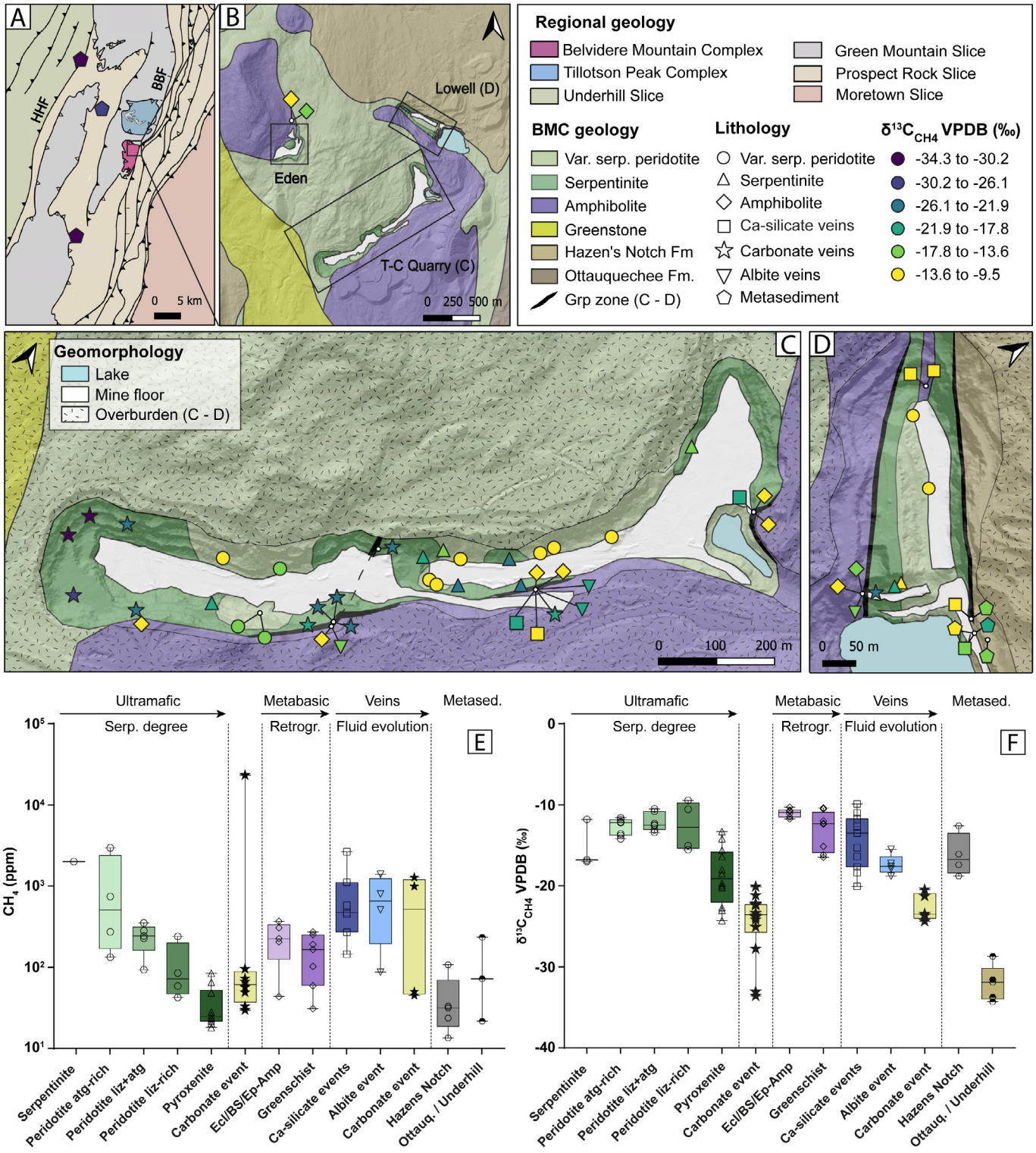

Figure 2 a-d) *Mapping of CH_4 distribution and isotopic fingerprints in the BMC area. Geological maps are modified after Gale (2007), Ratcliffe et al. (2011), and Honsberger (2023). Symbols represent samples analyzed for bulk fluid inclusion isotope analysis. The symbol shape indicates the type of lithology. Symbol colors refer to the bulk $\delta^{13}C_{CH_4}$ value (see the legend for color scale).* ***e)*** *Boxplots of bulk CH_4 concentrations expressed in ppm (logarithmic scale) measured on gas samples extracted from different rock types, highlighting a correlation between the CH_4 content and the serpentinisation degree of ultramafic and retrogression and metabasic host rocks and mineralogical transformation of FIs-hosting minerals.* ***f)*** *Boxplots of bulk $\delta^{13}C_{CH_4}$ expressed in permill relative to the VPDB measured on gas samples extracted from different rock types depicting multiple CH_4 generation/migration events characterised by distinct isotopic fingerprints. Abbreviations: Atg = Antigorite. BBF = Burgess Brach Fault Zone; BMC = Belvidere Mountain Complex; Liz = Lizardite. GMS = Green Mountain Slice; Grp = Graphite; HHF = Honey Hollow Fault Zone; Metased. = Metasediment. MTS = Moretown Slice; Ottauq. = Ottauquechee. PRS = Prospect Rock Slice; Retrogr. = Retrogression. Serp = Serpentinisation. TPC = Tillotson Peak Complex; UHS = Underhill Slice; Var. serp. = Variably serpentinised.*

energy source generation history of exhumed ophiolites can be extremely challenging. Subducted mantle lithosphere can preserve evidence of multi-stage fluid-rock interaction, from the subseafloor down to the serpentine-out reaction in subduction zones (Debret et al., 2013; Padrón-Navarta et al., 2013; Scambelluri et al., 2014; Vitale Brovarone et al., 2020; Ressico et al., 2024), leading to the entrapment of multiple fluid inclusion populations and CH_4-H_2 generation events (Zhang et al., 2021).

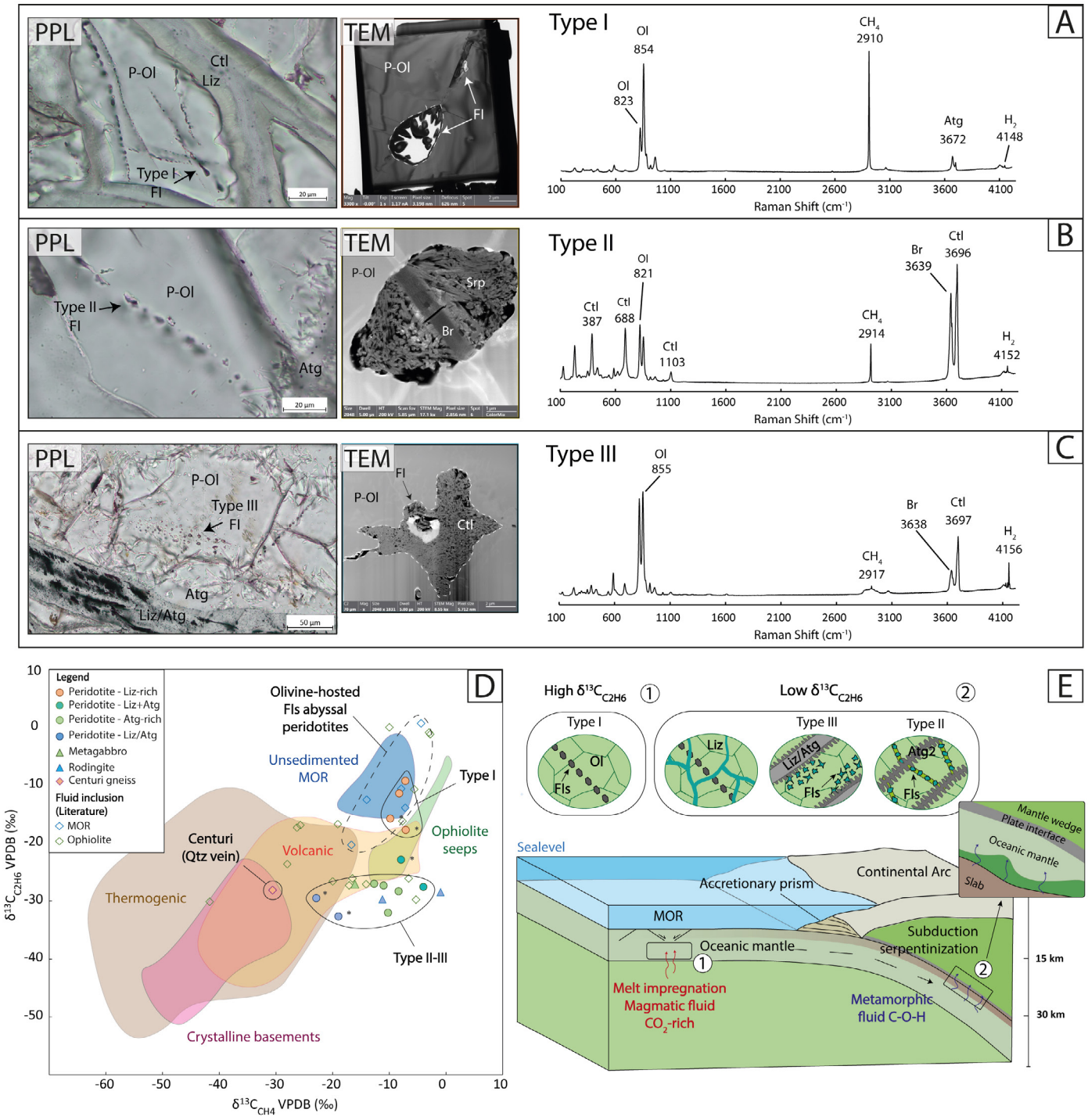

Figure 3 a-c) *The three main populations of multiphase olivine-hosted fluid inclusions (Type I, II, and III) trapped in the Monte Maggiore orogenic peridotite imaged at the optical microscope under plane polarised light (PPL) and through transmission electron microscopy (TEM), and representative micro-Raman spectra highlighting changes in the composition of trapped solid phases and CH_4-H_2 gas mixtures.* ***d)*** *$\delta^{13}C_{CH4}$ vs. $\delta^{13}C_{C2H6}$ diagram of mechanically extracted FIs in the Monte Maggiore massif, highlighting a clear difference between Type I FIs and Type II-III FIs populations. The diagram also displays FIs literature data of C_1 and C_2 alkanes (symbols) and terrestrial surface and submarine emissions (coloured regions). Asterisks highlight samples with low C_2H_6 concentrations.* ***e)*** *Reconstructed model of the fluid-rock interaction history experienced by the Monte Maggiore peridotite, associated microstructures, and events of hydrocarbon-H_2 genesis from a mid-ocean-ridge setting (1) to the Alpine subduction (2). Abbreviations: Atg = antigorite; Br = brucite; Ctl =chrysotile; FI = fluid inclusion; Liz = lizardite; MOR = mid-ocean-ridge; P-Ol = primary olivine; Qtz = quartz.*

The micro- and nanoscale FIs petrographic-spectroscopic study and CH_4-C_2H_6 isotope analysis on 42 samples of ultramafic rocks, meta-gabbros, and rodingite from the Monte Maggiore orogenic peridotite, Northern Corsica, demonstrates that subducted and exhumed oceanic lithosphere can retain a diverse record of energy sources.

The nanostructure, mineral assemblages, and CH_4-H_2 gas mixtures preserved within olivine-hosted multiphase FIs highlighted different generations of olivine-hosted multiphase FIs characterised by distinct CH_4-C_2H_6 isotopic patterns (Fig. 3).

The $\delta^{13}C$-enriched C_2H_6 component points to the preservation of abiotic hydrocarbons formed in a

mid-ocean-ridge setting, while the $\delta^{13}C$-depleted C_2H_6 component is related to multiple high-pressure serpentinisation events in the Alpine subduction zone. These results highlight possible differences in the hydrocarbon sources occurring in different geo-dynamic settings, or relevant changes in the C_1-C_2 carbon isotope fractionation during abiotic polymerisation reactions.

This study underlines the potential of CH_4-C_2H_6 isotope analysis combined with micro to nanoscale FIs characterisation to distinguish between different hydrocarbon sources and geodynamic settings of deep energy production, which could be otherwise hindered by long-lived and complex fluid-rock interaction histories.

The complex CH_4-C_2H_6 isotopic patterns preserved in the Monte Maggiore FIs underscore our limited understanding of abiotic low-molecular-weight hydrocarbons generation through fluid-rock interactions, which could provide valuable tools in the identification of biotic vs. abiotic hydrocarbons on Earth, and in extraterrestrial environments.

TOWARDS A GLOBAL INVENTORY OF METAMORPHIC HYDROCARBONS

For the first time, petrographic-spectroscopic analysis of FIs from several exhumed metamorphic terranes across the globe revealed the widespread presence

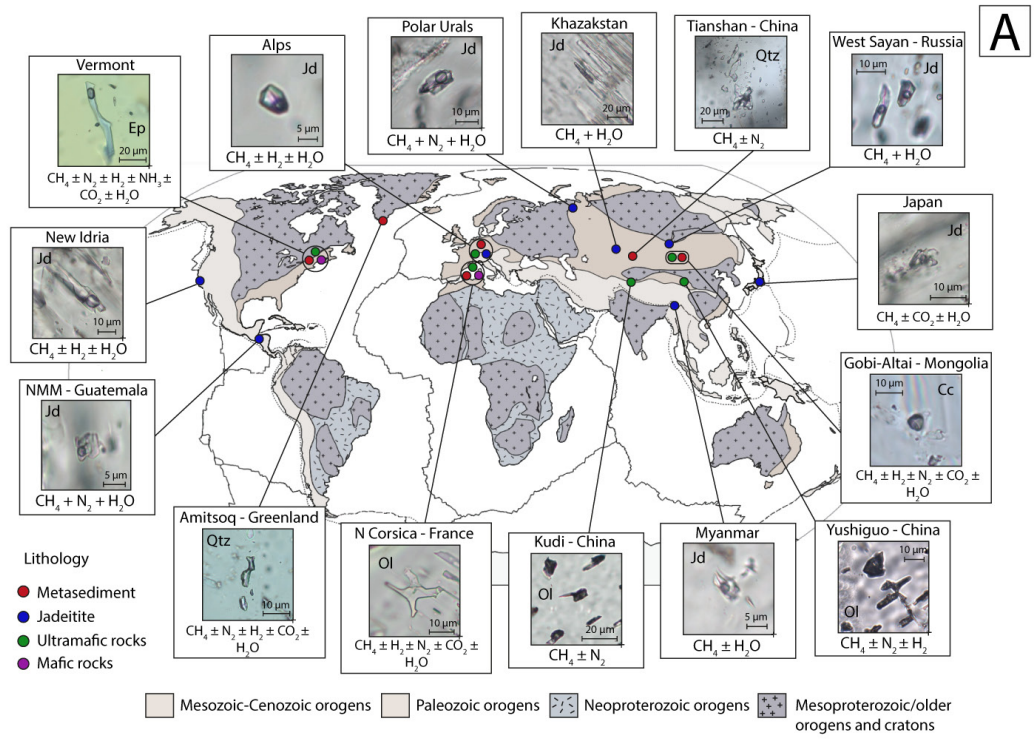

Figure 4 a) *Worldwide distribution of energy sources, i.e., CH_4, H_2, and NH_3, in metasediments (red circle), jadeitites (blue circle), ultramafic (green circle), and mafic (purple circle) rocks from exhumed metamorphic terranes, and orogens from, the Mesoproterozoic to the Cenozoic. Each locality investigated in this study is associated with a photomicrograph of representative fluid inclusions, and the list of fluid species identified through micro-Raman spectroscopy. The base map is after Tsujimori and Harlow (2012).* ***b)*** *The $\delta^{13}C_{CH4}$ vs. δD_{CH4} diagram, expressed in ‰ relative to the VPDB and VSMOW, respectively. The color-filled symbols show the isotopic composition of the CH_4 extracted FIs from this study, including variably metamorphosed and metasomatised mafic-ultramafic rocks (triangles), a jadeitite sample (rhomb), and metasediments (squares). Data from the literature are represented by empty symbols. The coloured regions represent the CH_4 isotopic composition from terrestrial surface and submarine emissions from the literature.*

of life essential ingredients, *i.e.*, CH_4, C_2H_6, NH_3, and H_2, in FIs trapped in a wide variety of lithologies (Fig. 4a,b), including a vast collection of jadeitites from Guatemala, USA, Russia, Alps, and Japan spanning the entire Phanerozoic (results published in Peverelli et al., 2024); metasediments, including Cambrian dolomitic marbles from the Chandman massif (Mongolia), Carboniferous graphitic schists from Western Tianshan, and Paleoproterozoic graphitic schists from Amitsoq (Southern Greenland); ultramafic rocks, including Alpine de-serpentinisation veins from the Zermatt Saas Fee unit, in the Western Alps, and metasomatic diopside veins from the Negru Shear Zone, in Alpine Corsica (results published in Dobe et al., 2025).

The petrology and isotope analysis of fluid inclusions trapped in exhumed metamorphic rocks allowed to open a new window into the distribution, nature, and isotopic fingerprints of deeply sourced metamorphic CH_4 from the Paleoproterozoic to the Eocene, and from various geodynamic contexts. Figure 4b provides a first insight into the preliminary global distribution of metamorphic CH_4 isotopic signatures, combining the results obtained throughout this PhD project, with other fluid inclusion isotope studies from different localities and lithologies (Suzuki et al., 2017; Zhang et al., 2023).

Developing a global dataset of metamorphic CH_4 distribution, isotopic fingerprints, and abundance in rocks could provide answers to fundamental scientific questions such as the extent to which metamorphic processes influenced the climate and habitability of our planet in the past and at present.

Exploring the petrology and geochemistry of deep unconventional energy sources preserved in the rock record could change dramatically our understanding of the link between plate tectonics and life emergence and evolution on Earth.

REFERENCES

Boutier, A., Martinez, I., Sissmann, O., Agostini, S., Daniel, I., Van Baalen, M., Mana, S., Vitale Brovarone, A. (2024) - Complexity of graphite formation in response to metamorphic methane generation and transformation in an orogenic ultramafic body. Geochim. Cosmochim. Ac., 364, 166-183.

Colman, D.R., Poudel, S., Stamps, B.W., Boyd, E.S., Spear, J.R. (2017) - The deep, hot biosphere: Twenty-five years of retrospection. P. Natl. Acad. Sci. USA, 114, 6895–6903.

Debret, B., Nicollet, C., Andreani, M., Schwartz, S., Godard, M. (2013) - Three steps of serpentinization in an eclogitized oceanic serpentinization front (Lanzo Massif – Western Alps). J. Metamorph. Geol., 31, 165–186.

Dobe, R., Giuntoli, F., Olivieri, O.S., Siron, G., Viola, G., Menegon, L., Vitale Brovarone, A. (2025) - Tracking molecular hydrogen migration along a subduction shear zone. Geol. Soc. Am. Bull.

Gale, M.H. (2007) - Bedrock Geologic Map of the Hazens Notch and Portions of the Eden and Lowell Quadrangles, Vermont.

Grozeva, N.G., Klein, F., Seewald, J.S., Sylva, S.P. (2020) - Chemical and isotopic analyses of hydrocarbon-bearing fluid inclusions in olivine-rich rocks. Philos. T. R. Soc. A, 378, 20180431.

Honsberger, I.W. (2023) - Newly recognized blueschist-facies metamorphism (glaucophane-omphacite-garnet), Belvidere Mountain Complex, northern Appalachians. Geosphere, 19, 645–653.

Klein, F., Grozeva, N.G., Seewald, J.S. (2019) - Abiotic methane synthesis and serpentinization in olivine-hosted fluid inclusions. P. Natl. Acad. Sci., 116, 17666–17672.

Magnabosco, C., Lin, L.-H., Dong, H., Bomberg, M., Ghiorse, W., Stan-Lotter, H., Pedersen, K., Kieft, T.L., van Heerden, E., Onstott, T.C. (2018) - The biomass and biodiversity of the continental subsurface. Nature Geosci., 11, 707–717.

McDermott, J.M., Seewald, J.S., German, C.R., Sylva, S.P. (2015) - Pathways for abiotic organic synthesis at submarine hydrothermal fields. P. Natl. Acad. Sci., 112, 7668–7672.

Mottl, M.J., Komor, S.C., Fryer, P., Moyer, C.L. (2003) - Deep-slab fluids fuel extremophilic Archaea on a Mariana forearc serpentinite mud volcano: Ocean Drilling Program Leg 195. Geochem. Geophys. Geosyst., 4.

Ohara, Y., Reagan, M.K., Fujikura, K., Watanabe, H., Michibayashi, K., Ishii, T., Stern, R.J., Pujana, I., Martinez, F., Girard, G., Ribeiro, J., Brounce, M., Komori, N., Kino, M. (2012) - A serpentinite-hosted ecosystem in the Southern Mariana Forearc. P. Natl. Acad. Sci., 109, 2831–2835.

Padrón-Navarta, J.A., Sánchez-Vizcaíno, V.L., Hermann, J., Connolly, J.A.D., Garrido, C.J., Gómez-Pugnaire, M.T., Marchesi, C. (2013) - Tschermak's substitution in antigorite and consequences for phase relations and water liberation in high-grade serpentinites. Lithos, 178, 186–196.

Peng, W., Zhang, L., Tumiati, S., Vitale Brovarone, A., Hu, H., Cai, Y., Shen, T. (2021) - Abiotic methane generation through reduction of serpentinite-hosted dolomite: Implications for carbon mobility in subduction zones. Geochim. Cosmochim. Ac., 311, 119–140.

Peverelli, V., Olivieri, O.S., Tsujimori, T., Giovannelli, D., Shi, G., Cannaò, E., Piccoli, F., Vitale Brovarone, A. (2024) - Cold-subduction biogeodynamics boost deep energy delivery to the forearc. Geochim. Cosmochim. Ac., 138, 195-207.

Plümper, O., King, H.E., Geisler, T., Liu, Y., Pabst, S., Savov, I.P., Rost, D., Zack, T. (2017) - Subduction zone forearc serpentinites as incubators for deep microbial life. P. Natl. Acad. Sci., 114, 4324–4329.

Ratcliffe, N.M., Stanley, R.S., Gale, M.H., Thompson, P.J., Walsh, G.J., With contributions by Hatch Jr.,

N.L., Rankin, D.W., Doolan, B.L., Kim, J., Mehrtens, C.J., Aleinikoff, J.N., McHone, J.G., Cartography by Masonic, L.M. (2011) - Bedrock geologic map of Vermont (Report No. 3184), Scientific Investigations Map. Reston, VA.

Ressico, F., Cannaò, E., Olivieri, O.S., Pastore, Z., Peverelli, V., Malaspina, N., Vitale Brovarone, A. (2024) - Behaviour of fluid-mobile elements across a high-pressure serpentinization front (Monte Maggiore unit, Alpine Corsica). Chem. Geol., 662, 122228.

Salvi, S. & Williams-Jones, A. (2003) - Bulk analysis of volatiles in fluid inclusions. In: "Fluid Inclusions: Analysis and Interpretation", I. Samson, A. Anderson, D. Marshall, eds. Mineralogical Association of Canada.

Scambelluri, M., Pettke, T., Rampone, E., Godard, M., Reusser, E. (2014) - Petrology and Trace Element Budgets of High-pressure Peridotites Indicate Subduction Dehydration of Serpentinized Mantle (Cima di Gagnone, Central Alps, Switzerland). J. Petrol., 55, 459–498.

Spránitz, T., Padrón-Navarta, J.A., Szabo, C., Szabó, Á., Berkesi, M. (2022) - Abiotic passive nitrogen and methane enrichment during exhumation of subducted rocks: Primary multiphase fluid inclusions in high-pressure rocks from the Cabo Ortegal Complex, NW Spain. J. Metamorph. Geol., 40, 1291-1319.

Suzuki, N., Saito, H., Hoshino, T. (2017) - Hydrogen gas of organic origin in shales and metapelites. Int. J. Coal Geol., 173.

Tsujimori, T. & Harlow, G. (2012) - Petrogenetic relationships between jadeitite and associated high-pressure and low-temperature metamorphic rocks in worldwide jadeitite localities: A review. Eur. J. Mineral., 24, 371-390.

Vitale Brovarone, A., Sverjensky, D.A., Piccoli, F., Ressico, F., Giovannelli, D., Daniel, I. (2020) - Subduction hides high-pressure sources of energy that may feed the deep subsurface biosphere. Nat. Commun., 11, 3880.

Whitman, W.B., Coleman, D.C., Wiebe, W.J. (1998) - Prokaryotes: the unseen majority. P. Natl. Acad. Sci., 95, 6578–6583.

Zhang, L., Wang, Q., Ding, X., Li, W.-C. (2021) - Diverse serpentinization and associated abiotic methanogenesis within multiple types of olivine-hosted fluid inclusions in orogenic peridotite from northern Tibet. Geochim. Cosmochim. Ac., 296, 1–17.

Zhang, L., Zhang, L., Tang, M., Wang, X., Tao, R., Xu, C., Bader, T. (2023) - Massive abiotic methane production in eclogite during cold subduction. Natl. Sci. Rev., 10, nwac207.

Development of multiscale hyperspectral sensing for integrated remote and proximal characterization of mineralized districts

Anna Sorrentino

Department of Earth, Environment and Resource Sciences, University of Napoli - Federico II, Via Cintia 26, 80126, Napoli
DOI: 10.19276/plinius.2025.01.018

INTRODUCTION AND AIMS

Since its advent, hyperspectral remote sensing has been widely used in Earth observation for various geological applications, enabling the detection and quantitative analysis of surface materials through calibrated reflectance spectra acquired as images in hundreds of narrow, contiguous spectral bands, typically within the Visible Near-Infrared (VNIR; 400–1300 nm) and Shortwave-Infrared (SWIR; 1300–2500 nm) regions (Bedini, 2017) (Fig. 1). Solar radiation interacting with an exposed surface causes absorption at specific wavelengths. The resulting reflectance spectra contain spectral signatures, or "fingerprints," that enable the identification of rock-forming minerals.

Notably, it has proven to be a powerful and cost-effective tool for mineral exploration of vast and remote areas, allowing the detection of hydrothermal and supergene alteration minerals, which serve as key vectors for identifying potential mineral deposits (Bedini & Chen, 2020).

Despite the widespread use of satellite- and airborne-based hyperspectral imaging for regional-scale exploration (*e.g.*, Laukamp et al., 2011; Sorrentino et al., 2024), close-range investigations using drones and tripod-mounted systems remain limited but crucial for understanding ore deposit formation and associated physicochemical gradients (Cudahy et al., 2008).

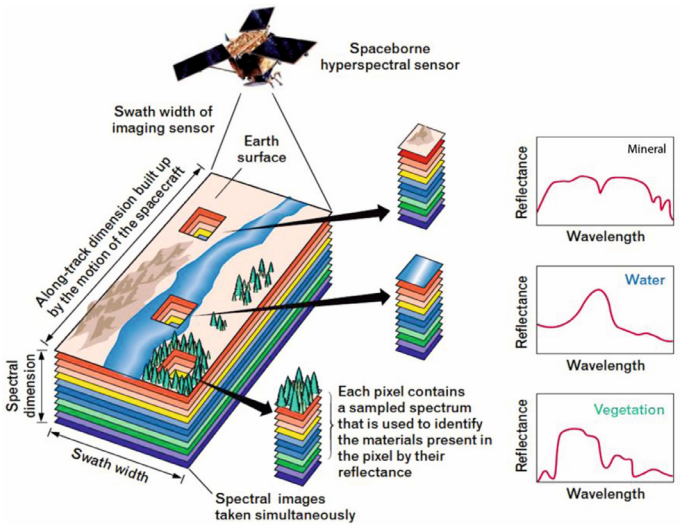

Figure 1 Schematic concept of hyperspectral sensing (from Bedini, 2017).

This PhD research aimed to bridge the scale gap by testing multi-scale hyperspectral sensing with new-generation satellite data, tripod-based imaging, and high-resolution sample-based point and imaging spectroscopy, across various mineralized areas worldwide, including porphyry-Cu and epithermal systems, Iron Oxide-Copper-Gold (IOCG) deposits, nonsulfide Zn mineralizations, and orogenic gold deposits (Fig. 2).

This approach enabled the detection and mapping of several ore-bearing and host-rock minerals, both well-documented phases (*e.g.*, Al-sheet silicates, alunite, carbonates; Laukamp et al., 2021) and previously un-characterized Zn-silicates.

VNIR-SWIR ABSORPTION FEATURES OF ROCK-FORMING MINERALS

Mineral species and groups exhibit diagnostic absorption features over the VNIR-SWIR spectral range (Clark et al., 1990; Laukmap et al., 2021).

In the VNIR region, absorption mainly results from electronic transitions of unfilled d-electron shells of transition metals and ligand-to-cation charge transfer, as observed in Fe-oxy-hydroxide minerals (Cudahy & Ramanaidou, 1997). In the SWIR range, vibrational modes dominate, due to bond stretching and bending in oxygen-bearing species, such as Al-OH in phyllosilicates, and C-O in carbonates (Laukamp et al., 2021).

The analysis of absorption features enables the estimation of key physicochemical properties of minerals, including: *i)* relative abundance, which is assumed to be proportional to the band depth (Clark et al., 1990); *ii)* chemical composition or mineral mixing, resulting in shifts in the wavelength position (Vedder & McDonald,

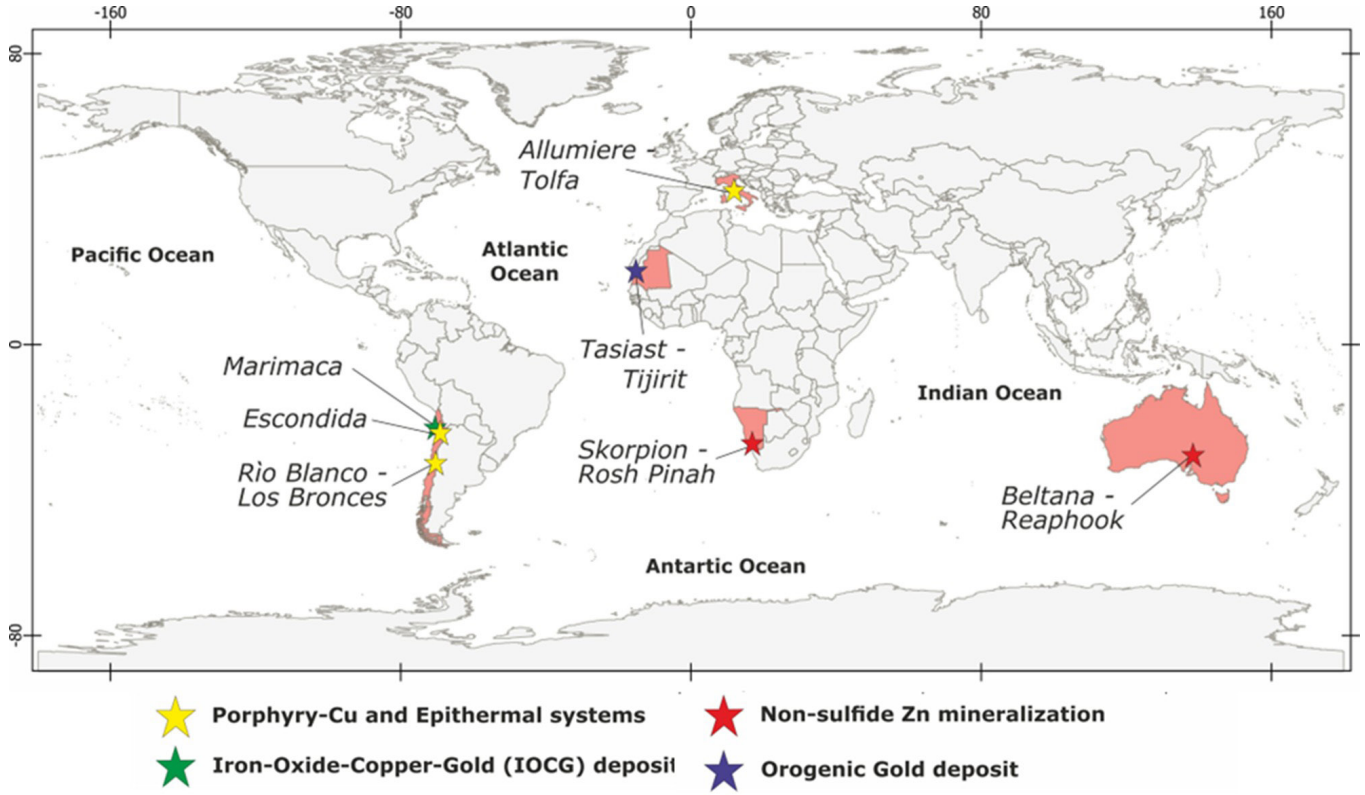

Figure 2 Global distribution of investigated study areas.

1963); *iii)* crystallinity degree, which decreases as the absorption width increases due to bond length variability in disordered structures (Murray & Lyons, 1955).

SPECTRAL MINERAL MAPPING AND HYPERSPECTRAL DATASET

In this thesis, spectral data were analyzed and processed to extract the previously mentioned spectral parameters and to identify VNIR-SWIR active minerals forming the investigated rocks. A multiple feature-guided workflow was employed, based on a combination of band ratios and minimum wavelength mapping methods.

The band ratio technique (Fig. 3a) involves constructing ratios to estimate relative abundance and chemical composition. For the former, it is calculated by dividing the sum of the shoulder reflectance values by that at the minima of a target absorption, while in the second case, it is calculated as the ratio between two specific bands (Laukamp et al., 2011). These analyses were performed using the Band Algebra Tool in ENVI software.

Minimum wavelength mapping (Fig. 3b) was instead employed using the open-source HyLite script in Python, as developed by Thiele et al. (2021). This method fits the absorption feature with a polynomial function of variable degree, within a specified range, allowing simultaneous extraction of all spectral parameters for each pixel.

At the regional scale, hyperspectral data were acquired from the Italian Space Agency's PRISMA and the German Aerospace Centre's EnMAP satellites, providing images of 30x30 km with a 30 m spatial resolution (for more specifics, see Chabrillat et al., 2024; Cogliati et al., 2021).

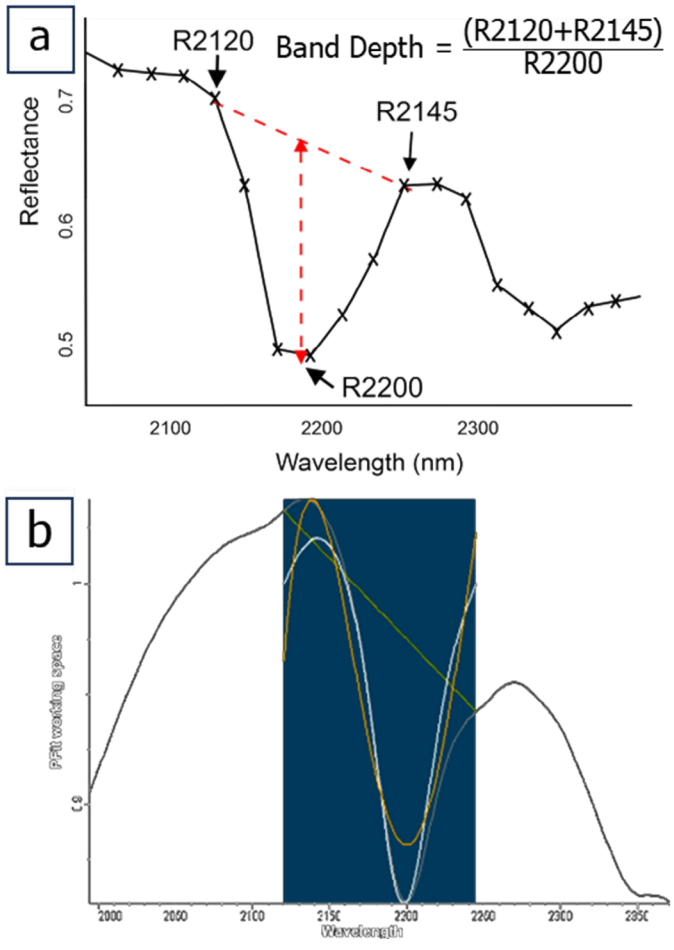

Figure 3 a) Band ratio and *b)* Minimum wavelength mapping methods (from CSIRO Mineral Resources).

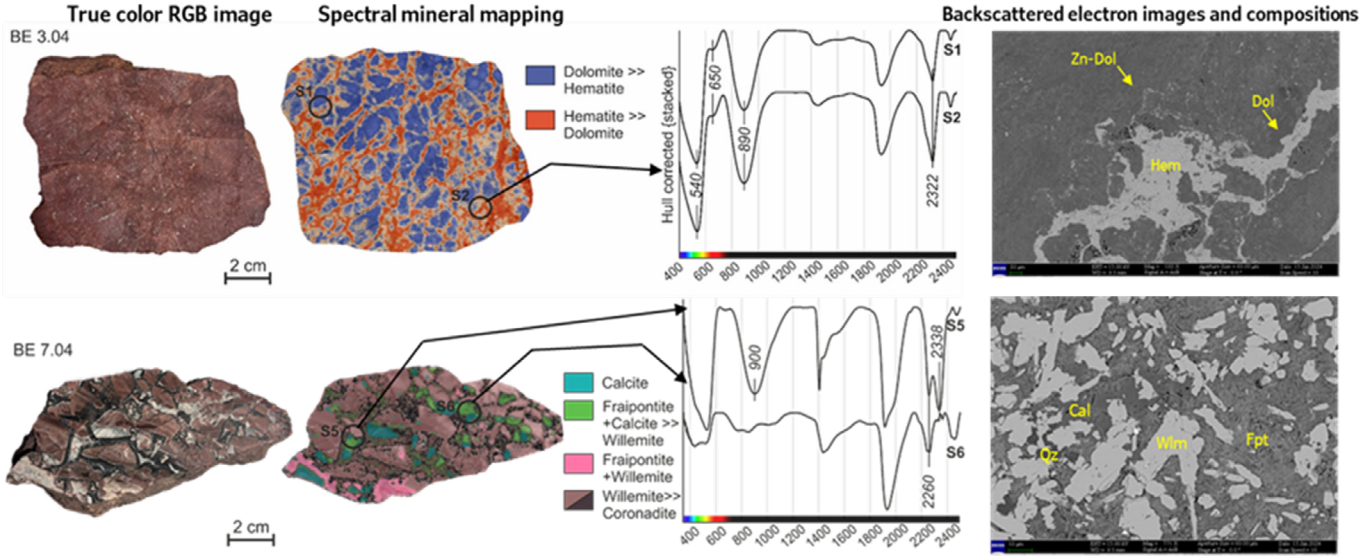

Figure 4 True-color and VNIR-SWIR hyperspectral images of altered and mineralized Beltana samples. Reflectance spectra from marked points are shown with the main absorption features. Backscattered electron images are depicted on the right.

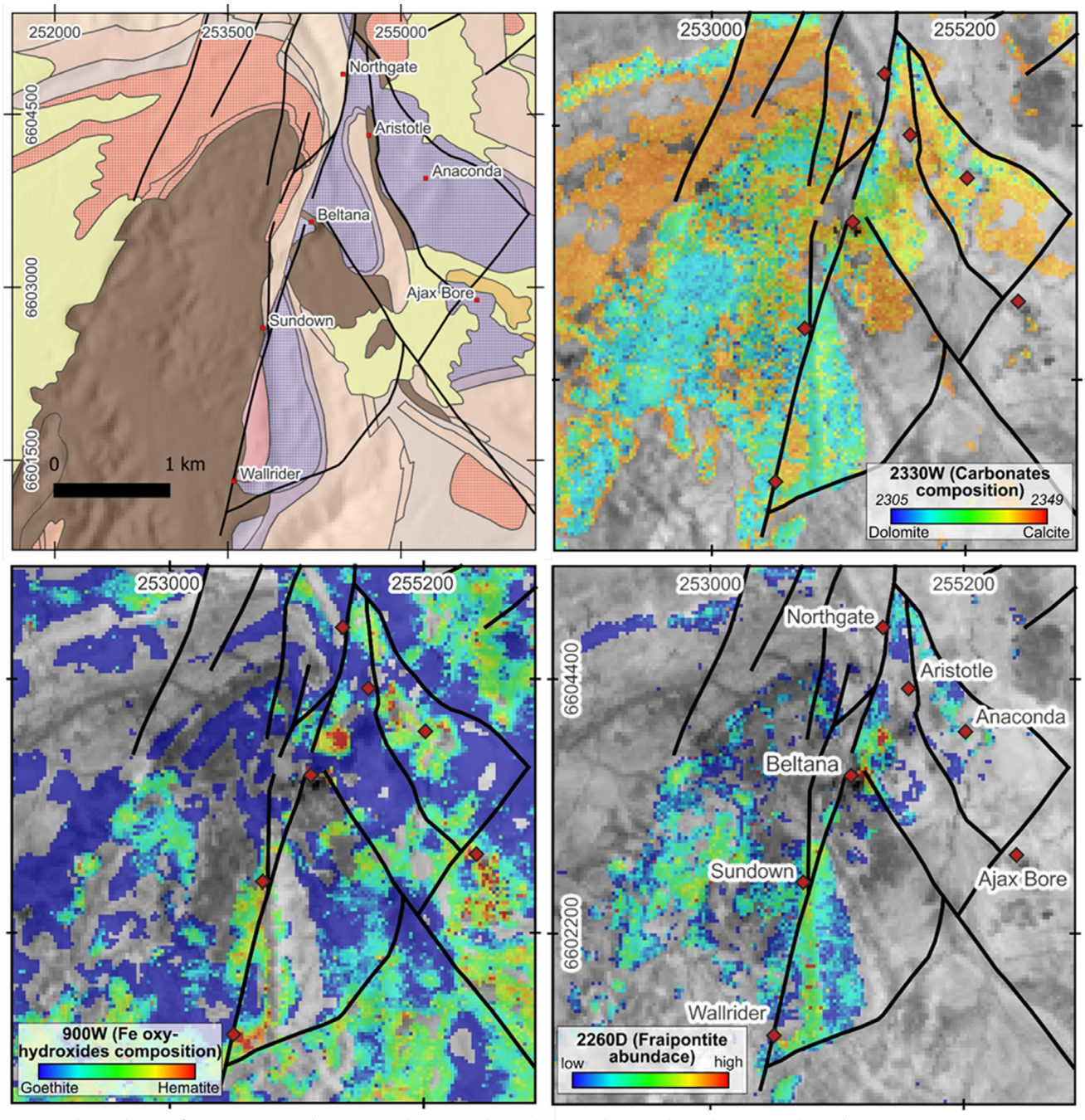

Figure 5 Geological map (from Groves et al., 2003) and EnMAP-derived spectral mineral products over the Beltana mining area.

At the outcrop and sample scales, hyperspectral data were collected using Headwall Photonics Micro- and Nano-Hyperspec cameras (supplied by the Department of Geosciences, University of Padua), mounted on tripods and in a laboratory setting. Moreover, high-resolution sample-based data were obtained at GFZ Potsdam with HySpex VNIR-1600 and SWIR-320m-e sensors, as well as the ASD FieldSpec-4 spectroradiometer.

The spectral results were further validated through mineralogical analyses on ground samples (*e.g.*, XRD, SEM, and optical microscopy).

MAIN RESULTS

Non-sulfide Zn mineralizations

The first case study is represented by the Beltana structurally-controlled Zn mineralized district located in the Flinders Ranges in South Australia. The Zn mineralization in this area is hosted by Lower Cambrian lithologies and contains significant willemite and fraipontite, associated with extensive hematite- and dolomite-bearing hydrothermal alteration (Groves et al., 2003).

Ten ground samples were analyzed through laboratory spectroscopy and mineralogical-petrographic methods (Fig. 4). Altered samples revealed the presence of hematite (absorption at ~870 nm) and dolomite (absorption at 2320 nm), which constitute the main pervasive alteration in the area. Spectral analyses of mineralized samples enabled the identification of spectral signatures of willemite (broad absorption feature between 900–1200 nm) and fraipontite (absorption at 2260 nm), previously unreported in the literature.

The same mineral phases were mapped at the regional scale using EnMAP satellite data (Fig. 5). Spectral mineral maps, representative of the relative abundance and chemical composition of alteration and ore minerals, were prepared by applying a multiple-feature extraction methodology based on polynomial fitting and band ratio.

The spectral products revealed the highest concentrations of fraipontite at the Beltana mining area, spatially associated with hematite and surrounded by dolomite. This also highlights the controlling effects of fault structures on mineralization and associated alteration haloes so that mineralized zones are punctually located at intersections between interacting faults or in the proximity of lateral fault terminations.

This work demonstrated the effectiveness of remote and proximal hyperspectral sensing for characterizing oxidized Zn mineralization, providing insights into the spectral behavior of several Zn-bearing minerals to support regional prospecting.

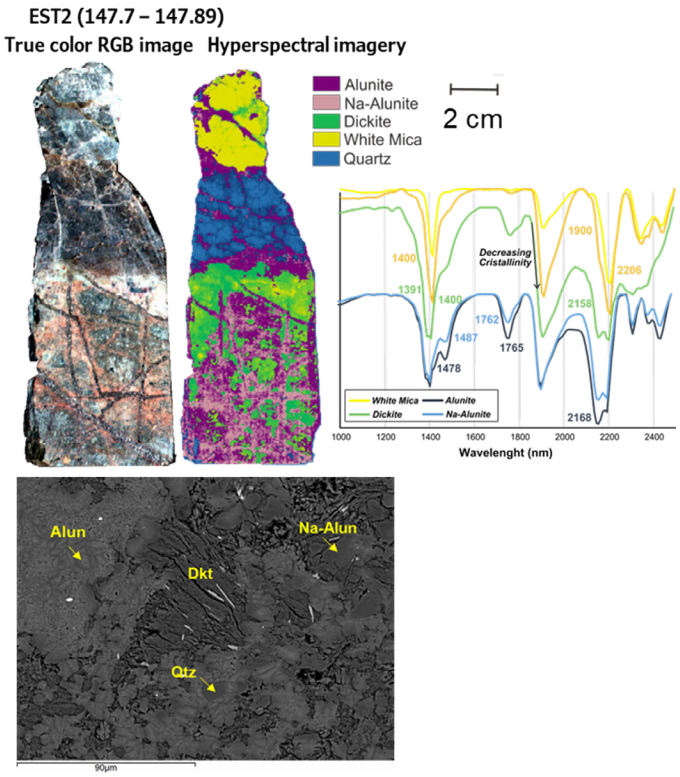

Figure 6 True-color and hyperspectral image of an Escondida sample. Reflectance spectra with the main absorption features are shown on the right. Backscattered electron images are reported at the bottom.

Porphyry copper deposits

The second case study is represented by the porphyry-Cu deposit of Escondida (Antofagasta Region, Northern Chile). The Escondida deposit, located in the Middle Eocene–Early Oligocene porphyry copper belt within the Domeyko Cordillera, hosts several orebodies centred on multiphase monzonitic-granodioritic-porphyry stocks (Hervé et al., 2012).

PRISMA and EnMAP satellite images were integrated with spectroscopic and mineralogical analyses (*i.e.*, optical and electron-scanning microscopy) conducted on forty-eight drill-core samples, to characterize the mineralogy of the wall-rocks in open pit areas.

Hyperspectral images of drill-core hyperspectral images were processed through the minimum wavelength mapping method, detecting several optically active mineral phases such as Fe oxy-hydroxides, chlorite and epidote, di-octahedral phyllosilicates (*i.e.*, white mica, pyrophyllite, kaolinite and dickite) and sulfates (*i.e.*, alunite, natroalunite, jarosite) minerals (Fig. 6).

At the district scale, the spatial distribution of alunite and kaolinite was mapped using the 2160 nm absorption feature in both PRISMA and EnMAP data. The PRISMA-derived map highlights higher concentrations in the eastern sector, with small spots in the northern and southern sectors. EnMAP results show a similar trend but outline a broader area in the northern sector (Fig. 7).

Notably, zones exhibiting higher concentrations of advanced argillic alteration minerals correspond to

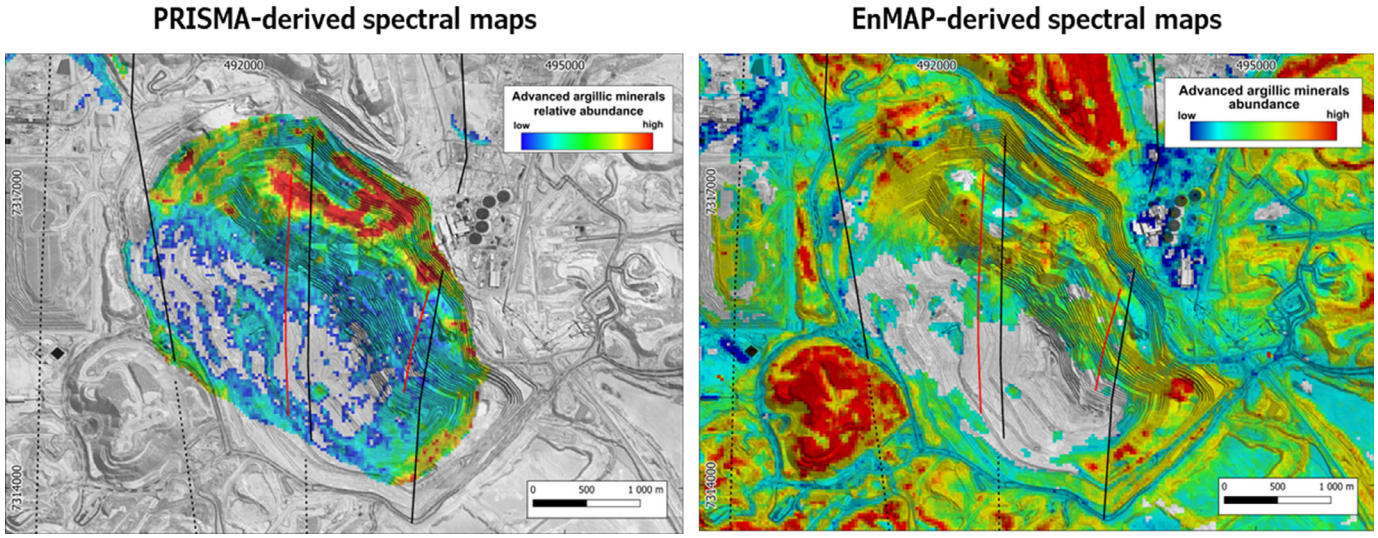

Figure 7 PRISMA- and EnMAP-derived mineral maps over the Escondida district.

domains of increased bench instability, consistent with sample-based observations.

The integration of multi-scale spectral data provides critical support for evaluating the bench stability across different domains of the pit. Moreover, these areas are progressively exposed due to ongoing exploitation processes, making this approach a rapid and cost-effective tool to be implemented along the mining value chain to provide real-time information on ore value and geotechnical evaluations.

High-sulfidation epithermal systems

As the third case study, the lithocap zone of the Allumiere epithermal system, north of Rome, was selected. The area is characterized by volcanic rocks, affected by widespread, structurally-controlled hydrothermal alteration, spanning from residual silica, to advanced argillic, to intermediate argillic zones, overprinted by supergene alteration (Marchesini et al., 2024).

Hyperspectral data were acquired at the Allumiere open pit mine, using tripod-mounted cameras and validated through laboratory imaging spectroscopy on 24 ground samples.

Mineral identification was performed using polynomial fitting and band ratios.

Sample-based analyses allowed to define the mineral assemblages associated with the distinct alteration zones typifying lithocap bodies, including sulfates (*i.e.*, alunite and natroalunite), kaolinite-group minerals (*i.e.*, kaolinite and dickite), Al- and Fe-rich smectites, opaline silica, and Fe-oxy-hydroxides (Fig. 8). These high-resolution data are crucial for defining outcrop-scale spectral targets and for cross-validation.

At the outcrop scale, hyperspectral images effectively mapped the relative abundances and compositional variations of these mineral phases (Fig. 9).

The spatial distribution of Fe oxides and hydroxides is likely associated with the presence of goethite, due to the Fe^{3+}- related absorptions (at ~ 900 nm). This mineral phase is rather widespread throughout the quarry, with the highest values predominantly concentrated

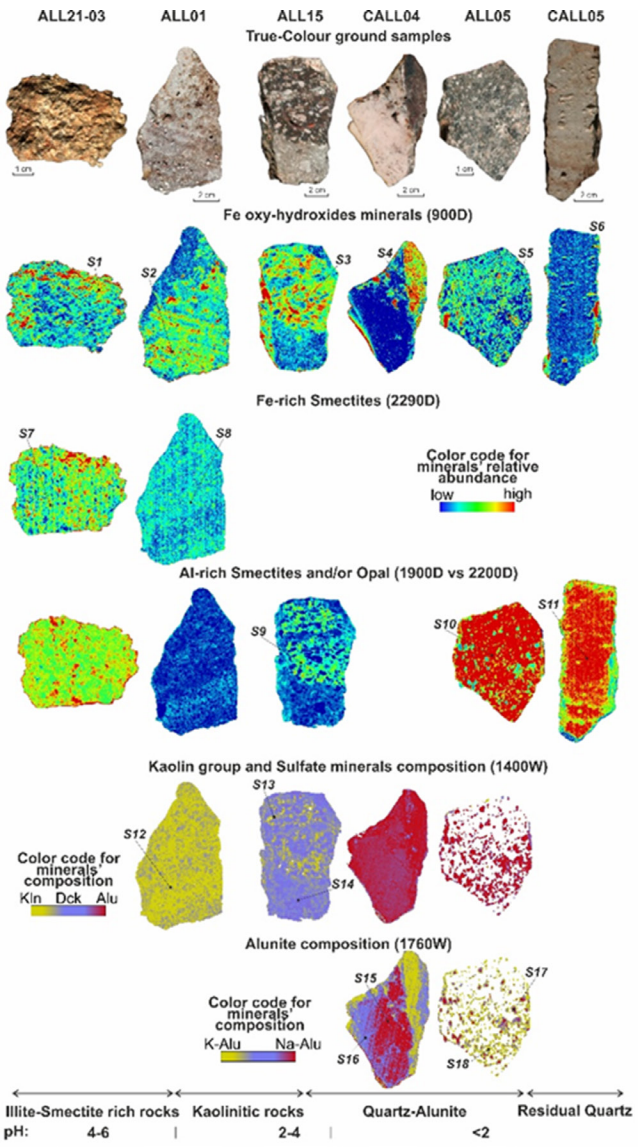

Figure 8 Hyperspectral imaging analysis conducted on six samples collected from the Allumiere quarry.

in the southeastern sector of the area, as well as in the uppermost benches.

Towards the southeastern sector, the high 900D values are coupled with medium to high relative abundances of the subtle feature at ~ 2290 nm, indicative of the presence of Fe-smectites. This portion of the quarry is also distinguished by deepest values of 2200D, which is mainly associated with the occurrence of Al-rich smectites and, to a lesser extent, opaline silica. The lowest values of this feature are found in the upper and inner part of the quarry, as well as towards the northwest in an area enclosed between faults.

The dominant mineral phases within the quarry, covering more than 80% of the area, consist of minerals belonging to the kaolin (*i.e.*, kaolinite and dickite) and sulfate groups, sharing the main absorption at ~ 2160 nm. These minerals display medium to high abundances, as highlighted by green to red colours, across the entire quarry area. Notably, the distribution of the highest values closely follows the trend of the main faults.

This approach provided significant insights into the geometry of the alteration mineral assemblages and their spatial relationship with the ore-controlling tectonic structures.

DISCUSSIONS AND CONCLUSIONS

This thesis demonstrates the potential of multi-scale hyperspectral imaging for ore deposit characterization. The research allowed developing advanced techniques for processing multi-scale spectral data. PRISMA and

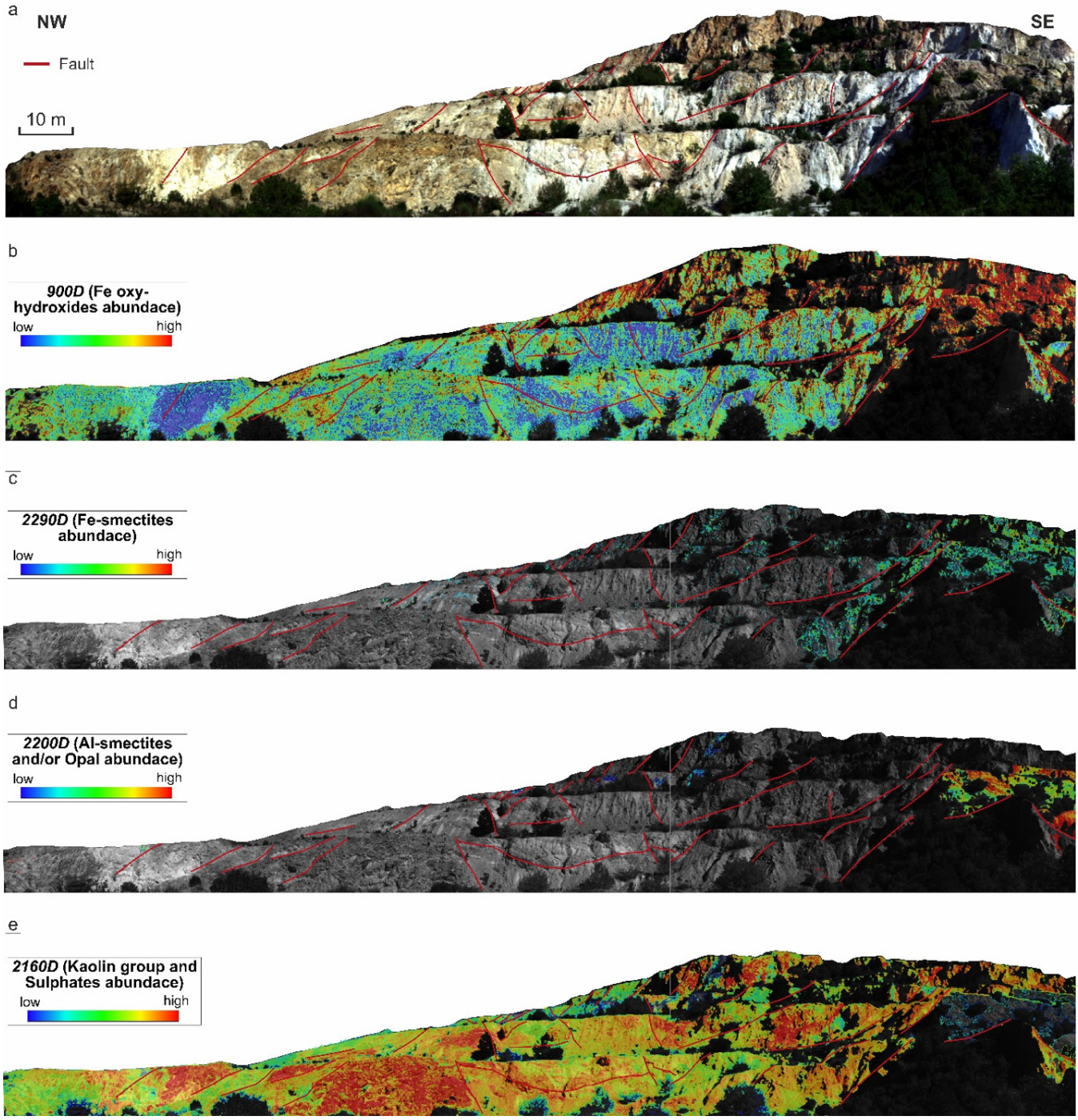

Figure 9 *Spectral mineral maps of the Allumiere quarry.*

EnMAP satellite data were integrated with high-resolution outcrop-scale scanning and image- and point-based analyses on samples. The adopted approach provided both a large-scale overview and detailed insights into the investigated mineralized areas.

Hyperspectral investigations, conducted across various geological settings, enabled the identification and detection of a wide range of mineral phases, such as Fe-oxy-hydroxides, phyllosilicates, sulfates, carbonates, and Zn-bearing minerals. The spectral data were successfully validated with common mineralogical analyses.

The feature extraction workflow based on band ratios and polynomial fitting allowed for a critical assessment of their advantages and limitations. The band ratio method is simple and fast, but less accurate for detecting subtle compositional variations (<10 nm spectral shift) or mineral mixing. Polynomial fitting is more precise but requires higher computational effort and careful parameter selection to avoid noise overfitting.

Overall, the results obtained highlight the effectiveness of integrating multiscale spectral datasets, enabling critical evaluations for exploration purposes with reduced costs and times, providing deposit-scale vectors toward mineralized centres to facilitate drilling, and supporting real-time ore evaluation and geotechnical assessment along the mining value chain.

REFERENCES

Bedini, E. (2017) - The use of hyperspectral remote sensing for mineral exploration: A review. J. Hyperspec. Remote Sens., 7, 4, 189–211.

Bedini, E. & Chen, J. (2020) - Application of PRISMA satellite hyperspectral imagery to mineral alteration mapping at Cuprite, Nevada, USA. J. Hyperspec. Remote Sens., 10, 2, 87–94.

Chabrillat, S., Foerster, S., Segl, K., Beamish, A., Brell, M., Asadzadeh, S., Milewski, R., Ward, K.J., Brosinsky, A., Koch, K. (2024) - The EnMAP spaceborne imaging spectroscopy mission: Initial scientific results two years after launch. Remote Sens. Environ., 114379.

Clark, R.N., King, T.V., Klejwa, M., Swayze, G.A., Vergo, N. (1990) - High spectral resolution reflectance spectroscopy of minerals. J. Geophys. Res-Solid Ea., 95, 8, 12653–12680.

Cogliati, S., Sarti, F., Chiarantini, L., Cosi, M., Lorusso, R., Lopinto, E., Miglietta, F., Genesio, L., Guanter, L., Damm, A. (2021) - The PRISMA imaging spectroscopy mission: Overview and first performance analysis. Remote Sens. Environ., 262, 112499.

Cudahy, T. & Ramanaidou, E. (1997) - Measurement of the hematite: goethite ratio using field visible and near-infrared reflectance spectrometry in channel iron deposits, Western Australia. Aust. J. Earth Sci., 44, 4, 411–420.

Cudahy, T., Jones, M., Thomas, M., Laukamp, C., Caccetta, M., Hewson, R., Rodger, A., Verrall, M. (2008) - Next generation mineral mapping: Queensland airborne HyMap and satellite ASTER surveys 2006–2008. CSIRO Report, 2007/364.

Groves, I.M., Carman, C.E., Dunlap, W.J. (2003) - Geology of the Beltana willemite deposit, Flinders Ranges, south Australia. Econ. Geol., 98, 4, 797–818.

Hervé, M., Sillitoe, R.H., Wong, C., Fernández, P., Crignola, F., Ipinza, M., Urzúa, F. (2012) - Geologic overview of the Escondida porphyry copper district, northern Chile. In: "Geology and Genesis of Major Copper Deposits and Districts of the World: A Tribute to Richard H. Sillitoe", J.W. Hedenquist, M. Harris, F. Camus, eds. Soc. Econ. Geol. Spec. P.

Laukamp, C., Cudahy, T., Thomas, M., Jones, M., Cleverley, J., Oliver, N. (2011) - Hydrothermal mineral alteration patterns in the Mount Isa Inlier revealed by airborne hyperspectral data, Aust. J. Earth Sci., 58, 8, 917–936.

Laukamp, C., Rodger, A., LeGras, M., Lampinen, H., Lau, I.C., Pejcic, B., Stromberg, J., Francis, N., Ramanaidou, E. (2021) - Mineral physicochemistry underlying feature-based extraction of mineral abundance and composition from shortwave, mid and thermal infrared reflectance spectra. Minerals, 11, 4, 347.

Marchesini, B., Tavani, S., Mercuri, M., Mondillo, N., Pizzati, M., Balsamo, F., Aldega, L., Carminati, E. (2024) - Structural control on the alteration and fluid flow in the lithocap of the Allumiere-Tolfa epithermal system. J. Struct. Geol., 179, 105035.

Murray, H.H. & Lyons, S.C. (1955) - Correlation of Paper-Coating Quality with Degree of Crystal Perfection of Kaolinite. Clay Clay Miner., 4, 31–40.

Sorrentino, A., Chirico, R., Corrado, F., Laukamp, C., Di Martire, D., Mondillo, N. (2024) - The application of PRISMA hyperspectral satellite imagery in the delineation of distinct hydrothermal alteration zones in the Chilean Andes: The Marimaca IOCG and the Río Blanco-Los Bronces Cu-Mo porphyry districts. Ore Geol. Rev., 105998.

Thiele, S.T., Lorenz, S., Kirsch, M., Acosta, I.C.C., Tusa, L., Herrmann, E., Möckel, R., Gloaguen, R. (2021) - Multi-scale, multi-sensor data integration for automated 3-D geological mapping. Ore Geol. Rev., 136, 104252.

Vedder, W. & McDonald, R.S. (1963) - Vibrations of the OH ions in muscovite. J. Chem. Phys., 38, 7, 1583–1590.

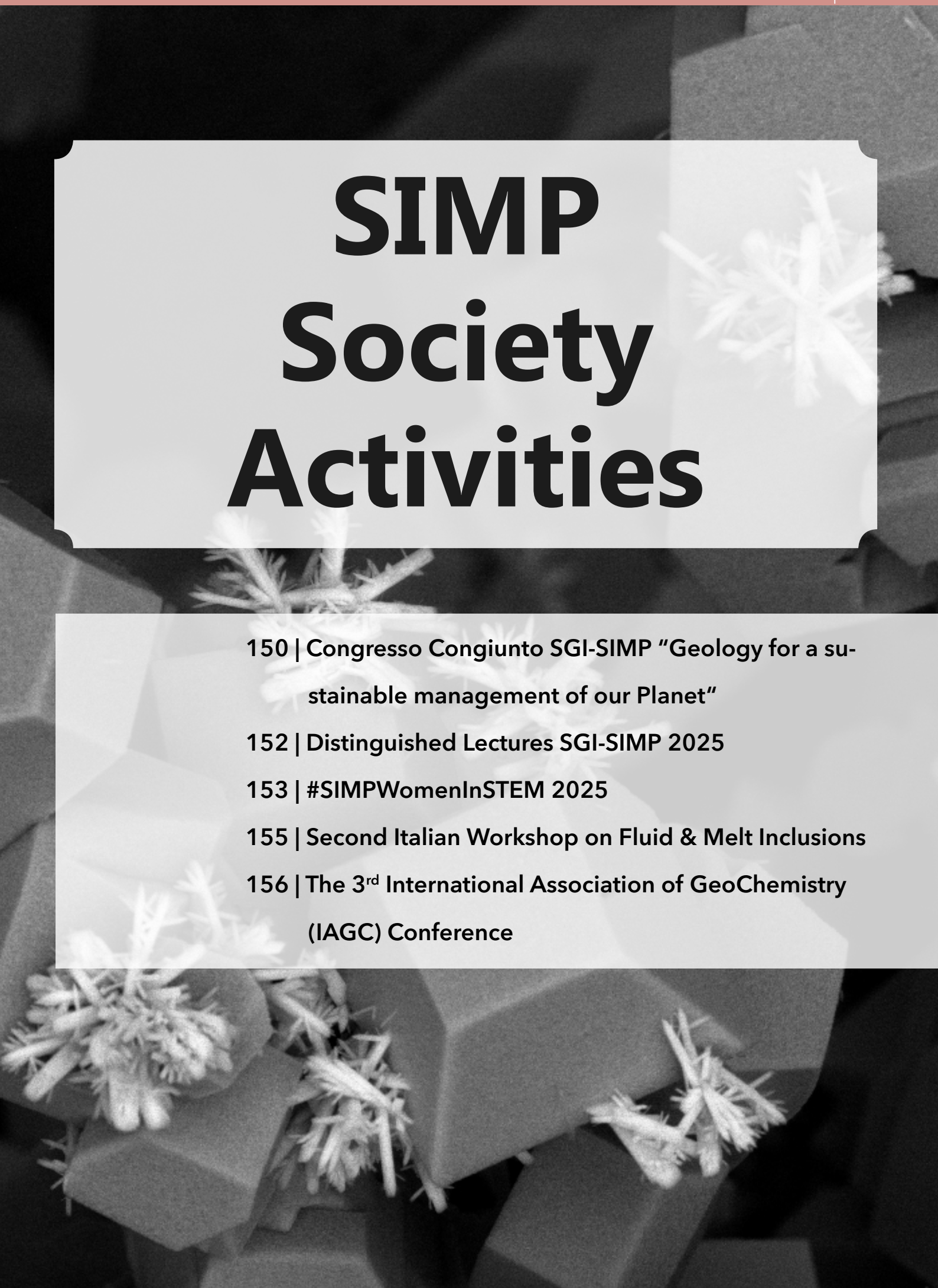

SIMP Society Activities

CONGRESSO CONGIUNTO SGI-SIMP "GEOLOGY FOR A SUSTAINABLE MANAGEMENT OF OUR PLANET"

Dates: 3-5 September 2024
Event link:
https://www.geoscienze.org/bari2024/

The Joint SGI-SIMP Congress 2024 was held at the University Campus of Bari from September 3 to 5. An opening event dedicated to public outreach, titled "GEOLOGY FOR SOCIETY: The importance of communication, so difficult, so necessary," featured Christopher Jackson, Ozlem Adiyaman Lopes, Luigi Bignami, and Emilio Casalini. The congress focused on the contribution of the geosciences to sustainable planetary management through research, communication, and education.

Speakers for the opening ceremony.

The congress hosted 1,099 participants, with over 1,200 abstracts and 53 parallel scientific sessions across 20 thematic areas, including tectonics, mineralogy, volcanology, geochemistry, palaeontology, and geohazards. The program featured plenary lectures by internationally recognized scholars, panel discussions, workshops, and a dedicated PhD Day for early-stage researchers.

SIMP Society meeting during the second day of the Congress.

SIMP prizes awarded to junior members.

The Italian Society of Mineralogy and Petrology (SIMP) co-organized the event together with the Italian Geological Society (SGI), contributing to the scientific program and the coordination of thematic sessions, with particular attention to mineralogical and petrological topics.

Ten SIMP grants were awarded to young researchers for participation in the congress. The grant recipients were: Roberto Conconi, Maria Cristina Di Carlo, Irene Luconi, Sara Monico, Thomas Nanni, Francesca Natali, Alessandro Petroccia, Sarah Scarani, Lorenzo Sedda, Jhonnathan Sieber, Mattia Sisti, Anna Sorrentino, Kevin Gabriele Terranova, Alice Tomassini and Sabrina Elettra Zafarana.

The SIMP Society meeting was an occasion for discussing many topics. Among these, the SIMP prizes and grants were awarded to junior members, and the upcoming issue of Plinius (volume 50/2024) was presented to the community.

Presentation of the upcoming Plinius volume 50/2024.

DISTINGUISHED LECTURES SGI-SIMP 2025

Dates: January-May 2025
Event link: https://www.socminpet.it/N251/x-ciclo-di-conferenze-itineranti.html
Video link on the SIMP Youtube Channel: https://www.youtube.com/watch?v=RPf9Wv6s0m0

The Distinguished Lectures are a series of traveling lectures organized by the Italian Society of Mineralogy and Petrology (SIMP) and the Italian Geological Society (SGI), where topics are examined from different perspectives by speakers presenting their innovative and critically provocative research. SIMP and SGI have organized this joint initiative since 2012, aiming to stimulate critical interdisciplinary debate on topics in the Geosciences by touring the Distinguished Lectures across Italy.

The theme of the Distinguished Lectures 2025 is: "Le geoscienze per l'archeologia: il caso di Pompei" (Geosciences for Archaeology: The Case of Pompeii). The speakers have visited seven departments/research institutions between January 2025 and May 2025: Benevento, Chieti, Camerino, Urbino, Napoli, Milano, and Pavia. The conferences are held jointly and are aimed at students, PhD students, postdocs, and researchers.

During the Distinguished Lectures 2025, Claudio Scarpati (University of Napoli "Federico II") contributed a lecture titled "The Vesuvian eruption of 79 AD and the destruction of Pompeii" presenting recent stratigraphic and volcanological analyses of the 79 AD eruption. Based on field observations from excavations in Regions V and IX of Pompeii, the lecture illustrated how eruptive phases impacted the city and its inhabitants. The sequence of events revealed fatalities from roof collapses during the Plinian phase, followed by trauma and asphyxiation during subsequent pyroclastic flows. Celestino Grifa (University of Sannio) presented "Pompeii: a treasure trove of geological discoveries – the contribution of mineralogy and petrology", focused on the insights provided by petrographic and mineralogical studies on materials from key archaeological contexts. These analyses shed light on raw material procurement and production techniques of Roman artisans, including potters and painters, offering new perspectives on technological practices and material culture in Pompeii.

Message from Claudio and Celestino to the Plinius Editorial Board: "We were welcomed warmly and enthusiastically everywhere, which allowed us to engage in fruitful exchanges with students and colleagues from diverse disciplinary backgrounds. We hope our contributions have sparked genuine interest. In truth, it was the participants' enthusiasm during these encounters that offered us a valuable source of engagement and scientific inspiration.

Claudio Scarpati (left) and Celestino Grifa (right), the two lecturers for the Distinguished Lectures 2025.

#SIMPWomenInSTEM 2025

Dates: February 2025
Video links:
https://fb.watch/APBU4XhL63/
https://fb.watch/APBWrB4lnD/
https://fb.watch/APBXPc-ObZ/
https://fb.watch/APBZ2g6yXx/
https://fb.watch/APB_Sa7Qxe/
https://fb.watch/APC0kU1Ymw/
Access to the videos is also possible by using the QR codes.

In continued alignment with its commitment to the International Day of Women and Girls in Science, the Società Italiana di Mineralogia e Petrologia (SIMP) once again presents its #SIMPWomenInSTEM initiative. This activity aims to give voice to female geoscientists, illustrating their professional activities and dedication within academia. Interviews with six talented geoscientists from the SIMP community offer a glimpse into their contributions to the field of geosciences.

Covers of the video interviews.

Roberta Spellanzani is a dedicated researcher at Saint-Gobain Italia, where she applies her geological expertise to the development of cement-based products. Her academic journey in geology started in Modena, leading her to specialize in volcanology in France and pursue a PhD in experimental mineralogy, petrology, and volcanology in Germany. Following a research year in the USA, she returned to Italy. Her initial encounter with geosciences sparked from a high school collaboration with the University, where she discovered her passion for explaining the intricacies of geological specimens. This early fascination naturally progressed into a deep interest in volcanology during her university studies.
To young female geoscientists: *The valuable thing is not to compare your academic and student path with that of other people because everyone's journey is unique. Try to broaden your horizons and not get stuck in a single direction; keep an open mind to all the possibilities that life gives.*

Francesca Innocenzi is a highly accomplished post-doctoral researcher in petrology and geochemistry at the University of Padova, recognized with the SIMP 2024 award for her doctoral thesis. Her current research focuses on the intricate world of stable isotopes, particularly in nominally anhydrous mantle minerals and diamonds, aiming to unravel the mysteries of Earth's deep-water cycle and its origins within a European research project. Her fascination with the Earth's power and hidden secrets motivated her to pursue geosciences, a decision that has yielded significant personal and professional growth. She attributes her journey to the inspiring guidance of female mentors, Prof. Sara Ronca and Prof. Martha Pamato.
To young female geoscientists: *Tenacity and perseverance will always be rewarded, as will commitment.*

Francesca Corrado, a promising PhD student at the University of Naples "Federico II," is immersed in the study of mineral deposits and remote sensing techniques. Her research leverages spectral analysis to identify the spectral signatures of minerals, a crucial tool for pinpointing potentially economic zones during mineral exploration activities. Her pursuit of geosciences was ignited by an inherent curiosity about the Earth and the natural world. Her undergraduate studies in mineralogy and mineral deposits deeply captivated her, shaping her academic trajectory through her master's and current doctoral research.
To young female geoscientists: *The important thing is to gain practical experience, both in the lab and in the field. Being a constantly developing science, it would also be important to have knowledge or study how software and programming languages work. Continue with your passion and believe in your skills.*

Covers of the video interviews.

Maria Camila Lopez Suarez, a geologist from Colombia currently undertaking her PhD at the University of Pavia, has been driven by an insatiable curiosity about the workings of our planet and the universe since childhood. Her strong aptitude for science paved the way for her pursuit of geology, supported by a scholarship for her Master's degree in Saudi Arabia. Her research experience spans mafic and ultramafic complexes, ophiolites for mineral exploration, and carbon sequestration. Her doctoral research in Pavia investigates the chemical and physical parameters governing the transition between the Earth's crust and mantle in the Sulphur Alps. ***To young female geoscientists:*** *Science is a good try if you are curious and have an open mind to keep asking questions. Be proactive, get out of your comfort zone, and be persistent. Try to respect and love the process, look for guidance and mentors, because science is really life changing.*

Maura Mancinelli is a dedicated post-doctoral researcher at the University of Ferrara, holding a PhD in Mineralogy and Crystallography. Her research focuses on the characterization and application of advanced materials for environmental and industrial solutions. She investigates microporous zeolites for removing emerging contaminants like PFAS from various environmental matrices and explores metal oxides for advanced sensing technologies. Her lifelong fascination with nature sparked her initial interest in natural processes. Discovering geological sciences through an aptitude test proved to be a perfect alignment with her inclinations. ***To young female geoscientists:*** *The advice is to follow your passion and curiosity. Geology and related environmental issues are increasingly relevant and offer the possibility of combining theory and practice for a sustainable future. Choosing a path that resonates with your inner interests is very satisfying and allows you to overcome difficulties with greater motivation and make a significant contribution.*

Patrizia Onnis, an esteemed researcher at the University of Cagliari, specializes in mineralogy. Her academic career began at the University of Cagliari, where an international research group aroused her interest and led her to pursue research opportunities abroad, including the USA, France, and England, where she obtained her doctorate and held a research grant. She returned to Italy to continue her research on the formation of primary and secondary minerals in different environments, using advanced analytical techniques such as synchrotron analysis. She describes herself as an "accidental geologist" at first unaware of the scope and importance of the geosciences, but this coincided with her concern about the environment and her desire to understand the processes that shape the world. ***To young female geoscientists:*** *Young geoscientists, me included, must learn to believe in themselves. Validate your own opinions and stand firm. It is important to explore this part of awareness of our potential. Believe in yourself and go ahead with the things you think are important.*

As part of the campaign, an feedback survey was introduced for the first time, designed to gather SIMP members' insights to improve future initiatives.

SECOND ITALIAN WORKSHOP ON FLUID & MELT INCLUSIONS

Dates: 12-14 November 2024
Event link: https://www.socminpet.it/N236/second-italian-workshop-on-fluid-melt-inclusions.html

The "Second Italian Workshop on Fluid and Melt Inclusions", organized by the University of Palermo, University of Milano-Bicocca, INGV and SIMP, took place in the beautiful setting of the Botanical Garden of Palermo. After the success of the first edition, the event once again brought together the Italian community working on fluid and melt inclusions, with the addition of new collaborations, including the National Institute of Geophysics and Volcanology (INGV) and the Editorial Board of Plinius.

The workshop brought together a diverse audience of students, PhD candidates, researchers, university lecturers, and professionals from the commercial and gemmological sectors, both from Italy and abroad. Held over three days, the event unfolded through thematic sessions introduced by leading experts, with the aim of fostering discussion on approaches, methodologies, advantages, and challenges linked to the use of fluid and melt inclusions in Earth Sciences. Particular emphasis was placed on encouraging collaboration between academia and the gemmological-commercial world. Sixteen abstracts were presented and collected in an abstract book published on Plinius with DOI.

As in the first workshop held in 2023, SIMP sponsored the event, providing funds for junior members through grants and offering logistical and organisational support while maintaining constant dialogue with the organizing committee. Clarissa Quaranta (UNIPA), Master's student and junior member of SIMP, received a grant.

Thirty-four participants attended the event, following four main thematic areas: 1) fluid and melt inclusions as tracers of geodynamic processes; 2) fluid and melt inclusions in deep and shallow magmatic processes; 3) resources and reserves – inclusions as an exploration tool; 4) fluid inclusions in gemmological materials and cultural heritage.

Abstract book published as a Special Issue of Plinius 50/2024.

The organizing committee (Lo Forte F. M., Maffeis A., Costa S., Romano P.) declared to the Plinius Editorial Board that is delighted with the success of the event, which, for the second year in a row, confirmed its value as an opportunity for exchange and scientific growth. The new ideas generated open promising prospects for future editions, which we plan to enhance further and, in all likelihood, host at new venues. Special thanks go to SIMP, which believed in the initiative from the outset, first supporting it on thematic grounds, then providing logistical help and, finally (chronologically, though no less importantly), financial backing.

Group photo of some of the participants during the coffee break.

THE 3RD INTERNATIONAL ASSOCIATION OF GEOCHEMISTRY (IAGC) CONFERENCE

Dates: 16-21 June 2025
Event link:
https://www.unica-wri-18.it/

The third IAGC International Conference "Water Rock Interaction-18 & Applied Isotope Geochemistry-15" was held at the University Citadel in Monserrato, Cagliari, Sardinia. The event was organized by the Department of Chemical and Geological Sciences of the University of Cagliari, with the support of a team of over twenty young researchers. The General Secretary of the Congress was Prof. Giovanni De Giudici. The event gathered from the international scientific community working on water–rock interaction and isotope geochemistry, providing a crucial platform to present and discuss the latest advancements, findings, and innovations in these dynamic fields. Sardinia offered a unique geological and hydrological context, enriching discussions and learning opportunities.

The congress welcomed approximately 300 registered participants from 22 countries across five continents, highlighting its international significance. A total of 308 scientific contributions were submitted and compiled into a digital volume published by UNICAPRESS, accessible at the following link: https://unicapress.unica.it/index.php/unicapress/catalog/view/978-88-3312-187-1/978-88-3312-187-1/941-1

The conference featured a comprehensive program of 22 thematic sessions, 7 plenary lectures, 3 pre-congress thematic workshops, 1 pre-congress field excursion to Mount Etna, 1 post-congress excursion to the Larderello–Amiata geothermal area, 7 mid-conference scientific excursions.

The Organizing Committee wishes to express sincere gratitude to the Italian Society of Mineralogy and Petrology (SIMP) for its patronage and for the active involvement of its members as organizers, convenors, and speakers. Special thanks also go to SIMP for awarding two grants (each €1000) to young SIMP members, which were conferred to Salvatore Guerrieri and Lisa Tagliacollo, in support of their participation in the congress. This contribution underscores SIMP's dedication to supporting early-career researchers and advancing international collaboration in geosciences. The Organizing Committee extends its heartfelt appreciation to SIMP for the unwavering support provided from the earliest stages of planning. The scientific program was developed with the contribution of both a national and an international scientific committee, including representatives from academic institutions, research centres, and professional associations from Italy and abroad.


Photo
Contest
Submissions

Here are all the submissions of the SIMP members to the photo contest, with the theme "***Minerals dress code on the SIMP Red Carpet***" held to decide the image that is being featured on the cover of this issue.
A commission of experts has appointed "**Abito lungo con cappello nero, stilista Madre Natura**" by **Matteo Chinellato** as the winner of the contest.

From here onward, the photos are displayed according to the submission order.

Abito gessato

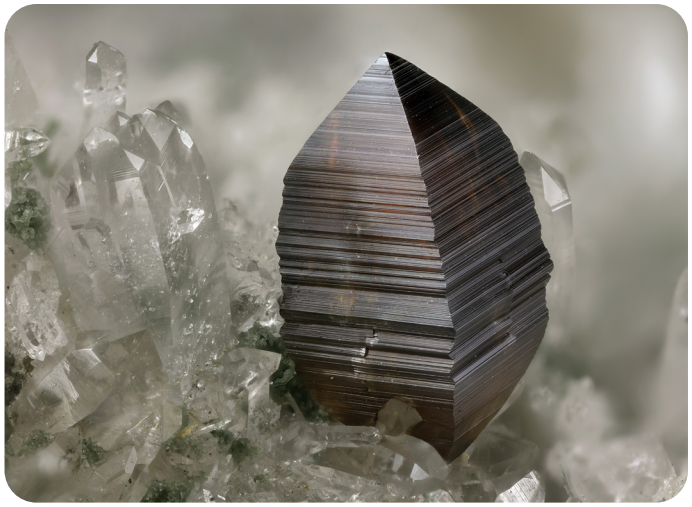

#1 Matteo Chinellato

Abito a righe azzurro

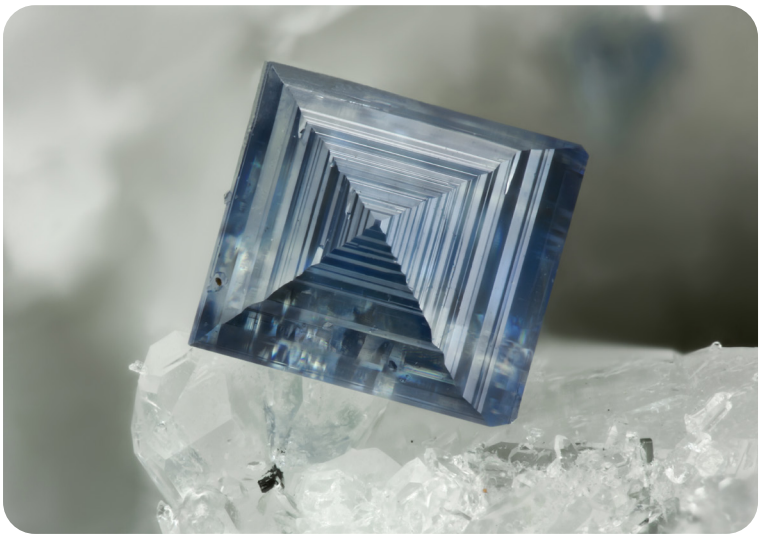

#2 Matteo Chinellato

Abito Zig Zag

#3 Matteo Chinellato

Abito a triangolo blu, stilista Madre Natura

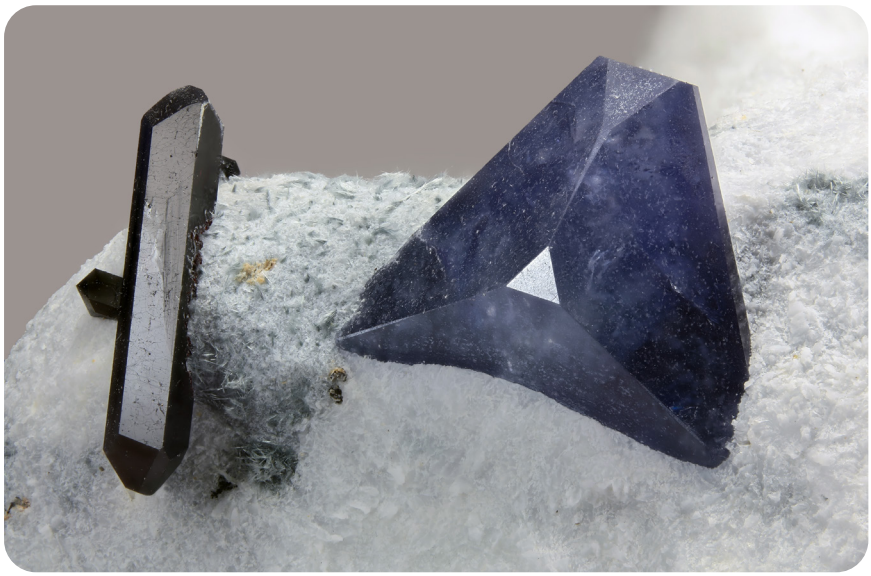

#4 Matteo Chinellato

Abito lungo con cappello nero, stilista Madre Natura

#5 Matteo Chinellato

Quarzo in Smoking

#6 Giulia Tumaini

Scultorea e radiosa, questa pegmatite di Minas Gerais, Brasile, sfila in passerella con un abito scolpito dal tempo

#7 Maria Camila Lopez Suarez

L'anima gialla della Sicilia - Il Mistero dello Zolfo

#8 Maria Camila Lopez Suarez

Una Fetta di Brasile - Il Dolce Fascino della Tormalina Acqua di Anguria da Minas Gerais

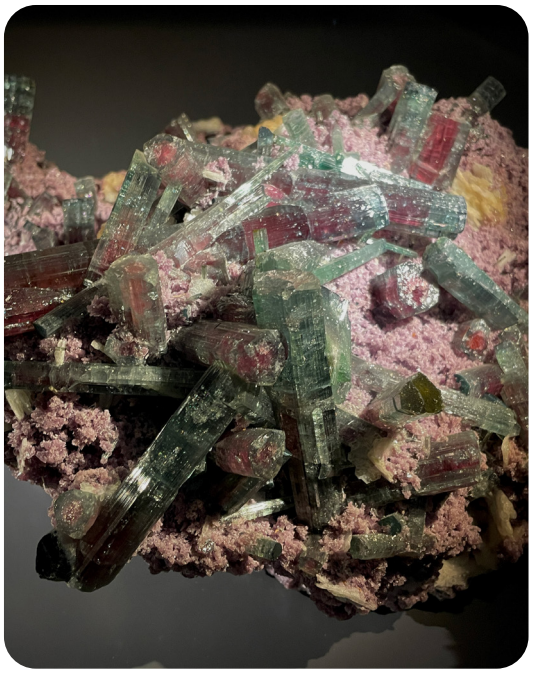

#9 Maria Camila Lopez Suarez

Splendore Siberiano - La Perfezione Octaedrica della Fluorite di Dalnegorsk”

#10 Maria Camila Lopez Suarez

Il Segreto dell’Isola – Cristalli di Tormalina Bosco Scuro dalla Grotta d’Oggi, Isola d’Elba, Italia

#11 Maria Camila Lopez Suarez

A clinopyroxene in tree's clothing

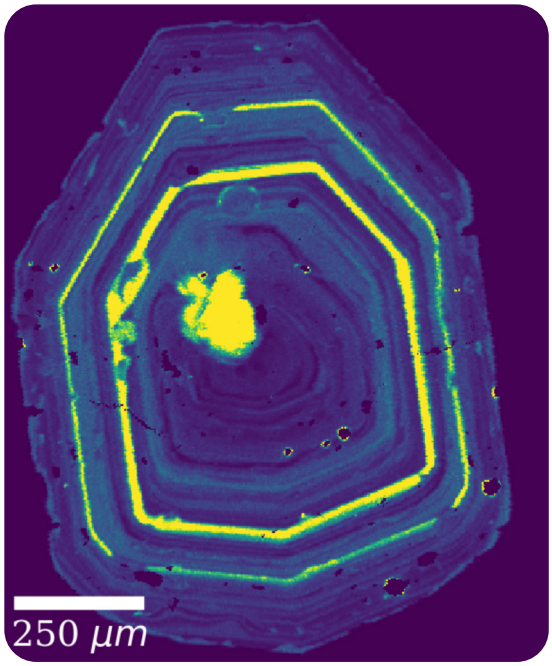

#12 Nicolò Nardini

Crystalline garden

#13 Giovanna Montesano

Graticcio di Cristalli di Nioboaeschynite-(Y)

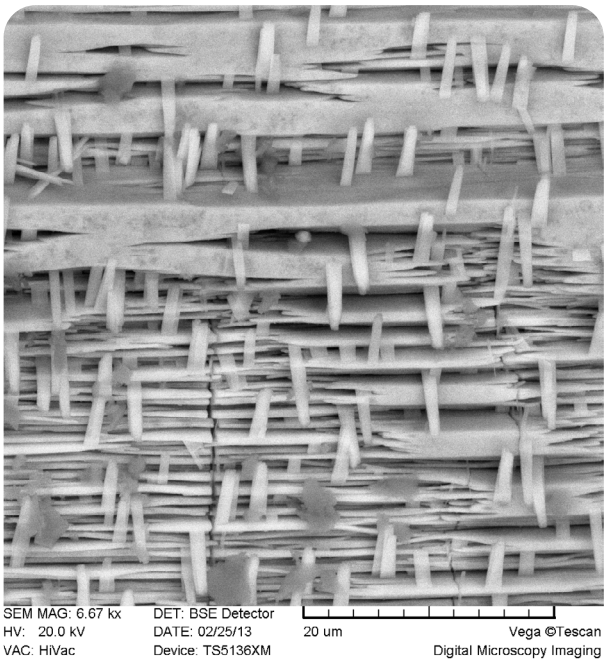

#14 Paolo Gentile

Agardite-(Nd)

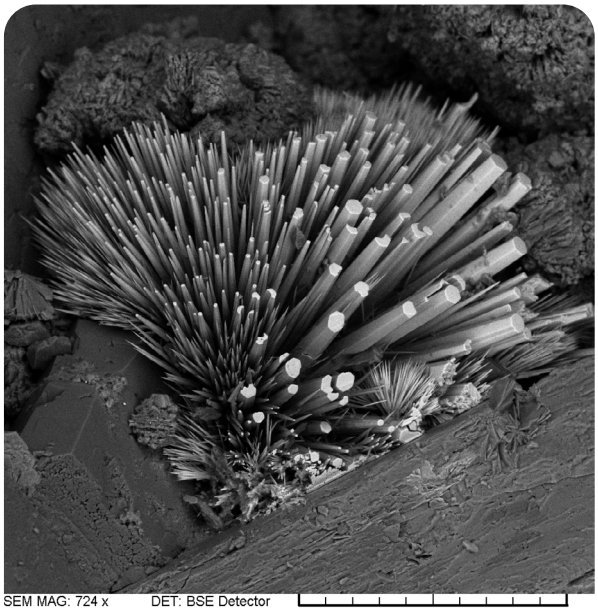

#15 Paolo Gentile

Mimetite

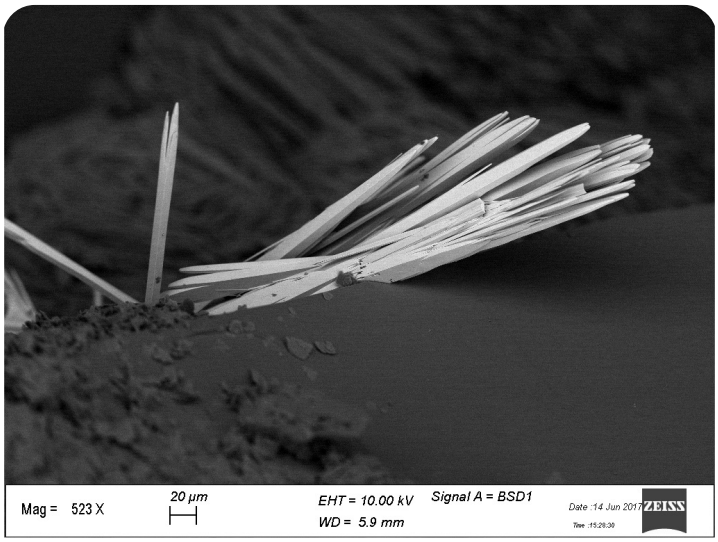

#16 Paolo Gentile

Nioboaeschynite-(Y) su anatasio

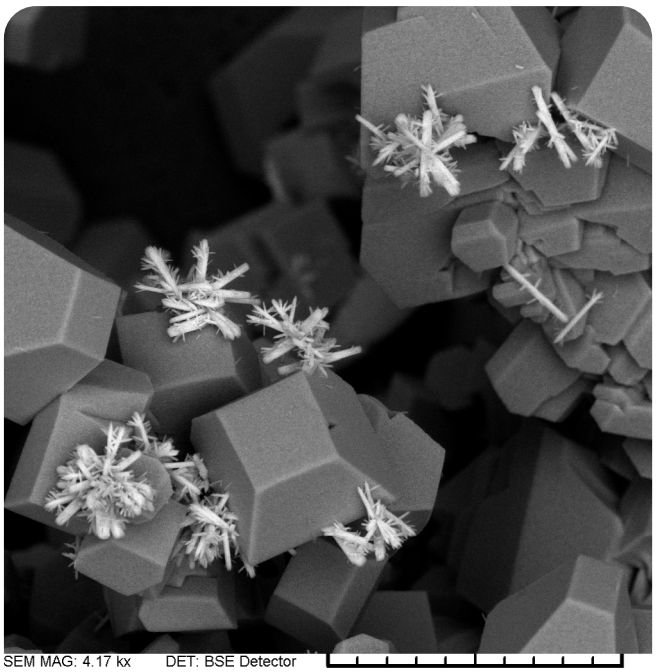

#17 Paolo Gentile

Segnitite

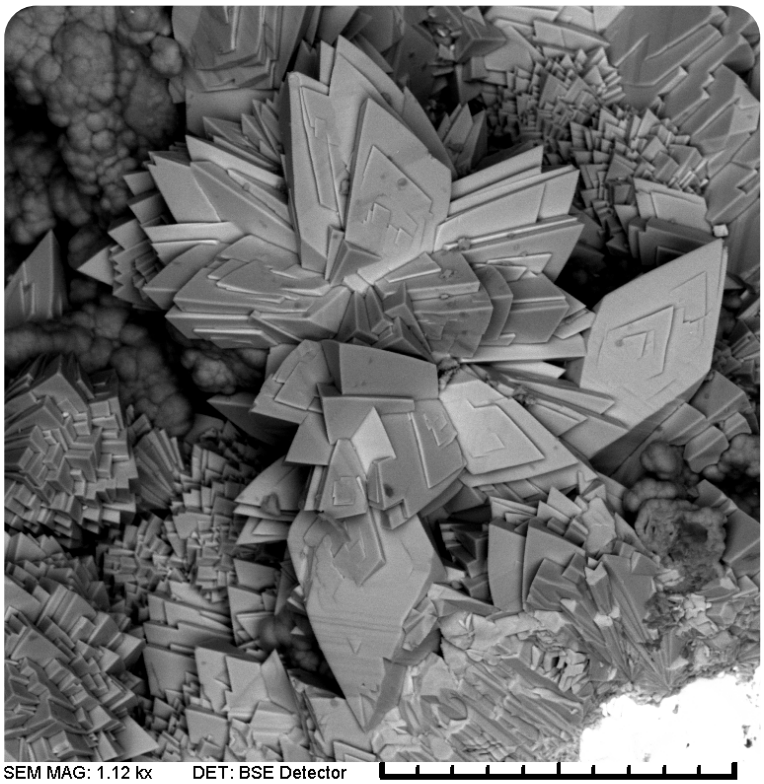

#18 Paolo Gentile

Senarmontite su stibnite

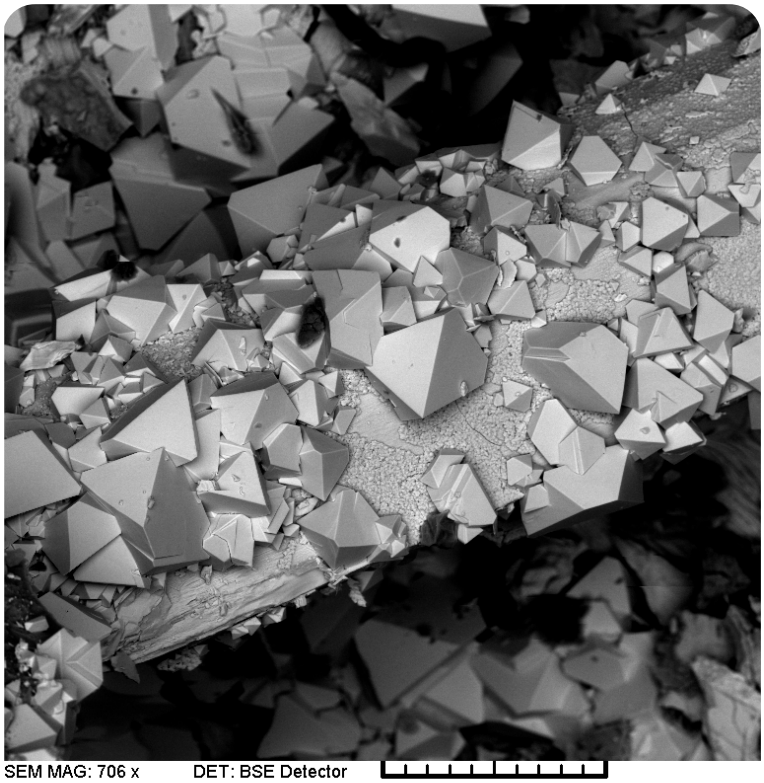

#19 Paolo Gentile

Matteo Chinellato (*GML Lombardia*) - **Abito gessato** - Anatasio - Cristallo di Anatasio rosso-scuro di 3,77 mm proveniente da Corni di Boden, Valle Toggia. Ex Collezione Micheli Paolo ritrovato il 16/09/1986. Collezione e foto Matteo Chinellato.

Matteo Chinellato (*GML Lombardia*) - **Abito a righe azzurro** - Anatasio - Val di Susa (Valle di Susa), Città metropolitana di Torino (Provincia di Torino), Piemonte, Italia - Cristallo di Anatasio blu di 0,8 mm. Collezione e foto Matteo Chinellato.

Matteo Chinellato (*GML Lombardia*) - **Abito Zig Zag** - Bixbyite-(Mn) - Thomas Range, Juab County, Utah, USA - Cristallo di Bixbyite di 7,94 mm. Collezione e foto Matteo Chinellato.

Matteo Chinellato (*GML Lombardia*) - **Abito a triangolo blu, stilista Madre Natura** - Benitoite, Neptunite - California State Gem Mine, Santa Rita Peak, San Benito County, California, USA - Cristallo di Benitoite di 12x11 mm. Foto e Collezione Chinellato Matteo.

Matteo Chinellato (*GML Lombardia*) - **Abito lungo con cappello nero, stilista Madre Natura** - Elbaite - Grotta d'Oggi (Cava di Grotta d'Oggi), San Piero in Campo, Campo nell'Elba, Isola d'Elba, Livorno, Toscana, Italia - Esemplare storico di Elbaite con terminazione "testa di moro" di 12,48 mm su quarzo fumé. Ex Collezione Gernot Smolle Foto e collezione Matteo Chinellato.

Giulia Tumaini (*University of Trieste*) - **Quarzo in Smoking** - Quarzo fumé su matrice, Ghiacciaio di Triolet - Val Ferret (AO). Quartz is the quintessential mineral – familiar even to those outside the world of geology. With its clean geometry and timeless charm, smoky quartz elevates elegance through simplicity. In this image, I wanted to celebrate the natural symmetry and simple elegance of a crystal that wears its "evening dress" with effortless style. The title "Quarzo in Smoking" is a play on words: it refers both to the variety of the mineral – smoky quartz – and to the idea of the crystal dressed in a tuxedo ("smoking" in Italian), ready to walk the Science catwalk.

Maria Camila Lopez Suarez (*University of Pavia*) - **Scultorea e radiosa, questa pegmatite di Minas Gerais, Brasile, sfila in passerella con un abito scolpito dal tempo** - Minas Gerais, Brasile.

Maria Camila Lopez Suarez (*University of Pavia*) - **L'anima gialla della Sicilia- Il Mistero dello Zolfo** - Zolfo, Sicilia.

Maria Camila Lopez Suarez (*University of Pavia*) - **Una Fetta di Brasile - Il Dolce Fascino della Tormalina Acqua di Anguria da Minas Gerais** - Watermelon tourmailine, Minas Gerais, Brazil.

Maria Camila Lopez Suarez (*University of Pavia*) - **Splendore Siberiano - La Perfezione Octaedrica della Fluorite di Dalnegorsk"** - Flluorite, Dalnegorsk, Siberia.

Maria Camila Lopez Suarez (*University of Pavia*) - **Il Segreto dell'Isola – Cristalli di Tormalina Bosco Scuro dalla Grotta d'Oggi, Isola d'Elba, Italia** - Tormaline, Grotta d'Oggi, Isola d'Elba.

Nicolò Nardini (*Univesity of Ferrara*) - **A clinopyroxene in tree's clothing** - Mappa composizionale in Laser Ablation della concentrazione in Cromo di un clinopirosseno zonato. Le zone gialle sono zone ricche in cromo (fino a 1.2 wt.%), mentre le zone blu sono zone povere in cromo (< 0.1 wt.%). La mappa mostra la fitta zonatura oscillatoria in un clinopirosseno dovuta a movimenti di convezione all'interno del sistema di alimentazione. Questo rende la sua mappa composizionale in cromo simile ai cerchi degli alberi. Inoltre, le zone molto ricche in cromo corrispondono a composizioni primitive del clinopirosseno, dovute a ricariche mafiche all'interno del sistema, che hanno portato alla formazione di bande diopsidiche primitive e il riciclo di nuclei diopsidici antecristici poi riassorbiti (come si vede nel nucleo del cristallo).

Giovanna Montesano (*University of Chieti-Pescara*) - **Crystalline garden** - Erionite crystals in zeolitic tuff from the Basin and Range Province. Erionite crystals are homogenously distributed forming dense and radiating bundles. The fibers tend to split easily into thinner fibrils giving the aggregate a fluffy appearance.

Paolo Gentile (*University of Milano-Bicocca - Piattaforma di Microscopia*) - **Graticcio di Cristalli di Nioboaeschynite-(Y)** - Nioboaeschynite-(Y): (Y,REE,Ca,Th,Fe)(Nb,Ti,Ta)$_2$(O,OH)$_6$. Località: Cava Subalpina - Cuasso al Monte (VA).

Paolo Gentile (*University of Milano-Bicocca - Piattaforma di Microscopia*) - **Agardite-(Nd)** - Agardite-(Nd): $NdCu_6(AsO_4)_3(OH)_6 \cdot 3H_2O$. Località: Greisen di Cave Puricelli - Quasso al Monte (VA).

Paolo Gentile (*University of Milano-Bicocca - Piattaforma di Microscopia*) - **Mimetite** - Mimetite: $Pb_5(AsO_4)_3Cl$. Località: Greisen di Cave Puricelli - Quasso al Monte (VA).

Paolo Gentile (*University of Milano-Bicocca - Piattaforma di Microscopia*) - **Nioboaeschynite-(Y) su anatasio** - Nioboaeschynite-(Y): (Y,REE,Ca,Th,Fe)(Nb,Ti,Ta)$_2$(O,OH)$_6$. Località: Cava Subalpina Quasso al Monte (VA).

Paolo Gentile (*University of Milano-Bicocca - Piattaforma di Microscopia*) - **Segnitite** - Segnitite: $PbFe^{3+}{}_3AsO_4(AsO_3OH)(OH)_6$. Località: Valbona - Valbiandino (LC).

Paolo Gentile (*University of Milano-Bicocca - Piattaforma di Microscopia*) - **Senarmontite su stibnite** - Senarmontite: Sb_2O_3. Località: Miniera dei Salati.

MEMORIAL BOX

A small message from outgoing Editorial Board members

Three intense years filled with layout drafts, last-minute edits, countless emails and messages… and lots of satisfaction. Being part of the Plinius editorial board has truly been a wonderful journey. From the very beginning, I tried to contribute to the journal's visual renewal of the bulletin and its logo, always with the idea of giving Plinius a coherent and recognisable identity, true to the spirit of our scientific community.

Plinius gave me the chance to get to know the Italian geoscience landscape more deeply – especially in mineralogy, petrology, and geochemistry – and, more importantly, to connect with passionate, generous, and brilliant people. Most of all, Plinius has been a space where design and science meet, and where I've found both creative fulfilment and a sense of belonging in our community.

My adventure with the Plinius editorial board began in 2022. With each issue, we've aimed to reflect the spirit of SIMP and its role in the scientific community. To me, SIMP has always been more than just a society; it's a true family. It's a place where young, aspiring researchers like me are supported, inspired, and guided as we take our first steps into the world of science, chasing our dreams and believing in our potential.

This experience has enriched me both personally and professionally, becoming a journey of passion and collaboration. Now it's time to "pass the torch" and make space for new voices, fresh perspectives and the kind of energy that drives progress.

To my incredible fellow board members: thank you!! Thank you for the conversations, the shared vision, the laughter, and the hard work. Thank you for everything this experience has given me.

I will continue to follow Plinius, this time as a reader, because I believe deeply in its mission and values, and because it has given me the precious gift of belonging to something truly meaningful.

A brief but very involving visit!

That's how I'd describe my experience on the Plinius editorial board. I had the chance to contribute to volumes 50 and 51: the first full of questions, the second with greater clarity… and it's already time to pass the torch!

In these two years, I learned about the complexity of the editorial process, had fun creating new images for social media, and realized that, even in a new context, what truly matters is stepping in and learning along the way.

I'm leaving feeling enriched, especially thanks to my extraordinary colleagues, who made this task manageable and, dare I say, enjoyable! I look forward to seeing you again at future events!

In the meantime, I wish the very best to those who will continue and those who will join the board, while I'll keep following Plinius... this time as a reader!

Plinius is the official SIMP Bulletin

Follow SIMP on social media

For any communication and news write to
comunicazione@socminpet.it
plinius@socminpet.it